Title	バイオマス由来糖類の高度活用に向けた高機能層状複水酸化物固体触媒の開発
Author(s)	城取，万陽
Citation	
Issue Date	2017-03
Type	Thesis or Dissertation
Text version	ETD
URL	http://hdl.handle.net/10119/14258
Rights	
Description	Supervisor:海老谷　幸喜，マテリアルサイエンス研究科，博士

Development of Layered Double Hydroxide-based Highly Functionalized Solid Catalysts for Utilization of Biomass Derived Saccharides

Japan Advanced Institute of Science and Technology

MAHIRO SHIROTORI

Doctoral Dissertation

Development of Layered Double Hydroxide-based Highly Functionalized Solid Catalysts for Utilization of Biomass Derived Saccharides

MAHIRO SHIROTORI

Supervisor: Dr. Kohki Ebitani

School of Materials Science

Japan Institute of Science and Technology

March 2017

Supervisor:	**Professor**	**Dr. Kohki Ebitani**
Referees:	**Professor**	**Dr. Tatsuya Shimoda**
	Professor	**Dr. Masayuki Yamaguchi**
	Associate Professor	**Dr. Kazuaki Matsumura**
	Associate Professor	**Dr. Yusuke Yoshinaga**

Development of Layered Double Hydroxide-based Highly Functionalized Solid Catalysts for Utilization of Biomass Derived Saccharides

Mahiro Shirotori

Ebitani Laboratory, School of Materials Science, JAIST

Introduction

From the 19th century, the development of catalysis science and chemical industry, especially petrochemical industry, has enriched our lives by enabling mass production of energy and chemical products. Recently, catalytic conversion of biomass derived materials into value-added chemicals including furfural has been attracted much attention because biomass has potential to substitute for fossil resources as the only renewable carbon source. The main objectives of this dissertation are the development of highly functionalized solid catalysts and apply them to transformation of biomass derived saccharides. I basically focused on high functionality of layered double hydroxide (LDH), one of a layered solid base catalyst which has Brønsted base site. Some strategies to develop highly functionalized LDH-based catalysts, preparation methods, results of characterizations, activity for chemical reactions including biomass derived saccharides as well as outlook based on my research are summarized in this doctoral thesis.

Results and Discussion

The one-pot transformation of xylose, one of the main components of hemicellulose, into furfural or furfural derivatives by combined use of Brønsted base Mg-Al LDH and solid acid resin Amberlyst-15 was conducted and described in **Chapter 2**. The effective synthesis of (2-furanylmethylene)malononitrile (FMM), the Knoevenagel product of furfural with malononitrile, was progressed *via* three elemental reactions; (i) aldose-ketose isomerization of xylose into xylulose over LDH, (ii) dehydration of xylulose into furfural over Amberlyst-15 and (iii) the Knoevenagel condensation of furfural with malononitrile over LDH, with FMM yield of 21% in a one-pot manner. To facilitate the aldose-ketose isomerization, rate-determining step in the one-pot synthesis, I synthesized two types of bi-functional Lewis acid – Brønsted base catalyst, Cr/Mg-Al LDH and Ni^{2+}-modified Al_2O_3 catalyst, and found that the bi-functional acid-base sites effectively promote the aldose-ketose isomerization. In **Chapter 3**, study of the detailed local structure and the optimized surface structure on the bi-functional acid-base Cr/Mg-Al LDH was conducted. The results of various characterizations and investigation of catalytic activities revealed that (i) below 1 wt%, a part of a Lewis acidic Cr^{3+} oxide monomer is trapped by peripheral defect sites of Mg-Al hydroxide layer, and others are immobilized onto LDH surface, (ii) Lewis acidic Cr^{3+} oxide dimer or trimer is generated on the LDH surface with covering LDH surface up to 5 wt%, (iii) above 5 wt%, excess Cr^{3+} species form Mg-Cr and/or Mg-Al-Cr LDH-like composite. Above 0-15 wt%, the 5 wt%Cr/Mg-Al LDH surface that comprises LDH carrier and covering layer of Cr^{3+} oxide possesses the most effective interaction between Lewis acidic Cr^{3+} oxide and basic Mg-Al LDH surface to generate abundant bi-functional Lewis acid – Brønsted base sites, leading to the best catalytic activity with 59% yield of furfural and FMM. Description of **Chapter 4** is the development of immobilized fine-crystallized SiO_2@LDH catalyst for improvement of basicity on LDH. Various SiO_2@LDHs were prepared by co-precipitation method with coexistence of spherical SiO_2(40nm). They have smaller LDH crystallite compared with conventional LDHs and showed highly base catalysis for the Knoevenagel condensation. For instance, in the case of Mg-Al type LDH with Mg/Al ratio of 3, the reaction rate over optimized SiO_2@LDH was 2.2 times higher than that of conventional LDH. Based on the results of ^{29}Si CP-MAS NMR and STEM-EDS, I concluded that dispersion of starting points of LDH crystal growth on SiO_2 surface lead to generate fine crystalline LDH which exhibits highly base catalysis.

Conclusion

In conclusion, I discovered the preparation methods of the LDH-based highly functionalized solid catalysts such as Lewis acid – Brønsted base bifunctional catalysts and immobilized fine-crystallized LDH catalysts. I also demonstrated that the multifunctional solid catalytic system composed of bifunctional Lewis acid-Brønsted base LDH-based catalysts effectively catalyzed one-pot synthesis of pentoses to furfurals. These achievements described in this doctoral thesis give catalytic science new strategies to design the multi-functionalized supported catalysts and to increase the original function of the layered catalysts for the development of noble modern organic synthesis including biomass-derived saccharides transformations.

Keywords: Layered Double Hydroxide, Solid Surface, Heterogeneous Bi-functional Acid – Base Catalysis, Control of Crystalline, Biomass Transformation

Preface

From the 19th century, catalyst has supported industry and sometimes it has been a driving force of revolution in chemical industry and our lives. The development of catalysis science and chemical industry, especially petrochemical industry, has enriched our lives by enabling mass production of energy and chemical products. However, it has led to benefits as well as serious problems including environmental destruction and concerns about the depletion of fossil resources. Recently, the renewable resources have attracted much attention as sustainable resources substituted for fossil resources. Among them, biomass resources have potential to supply not only energies but also various chemical materials and fuels as the only renewable carbon source. Thus, catalytic conversion of biomass into value-added chemicals has been accepted worldwide as one of the important and challenging task. Moreover, development of highly functionalized catalyst is indispensable for realization of next generation advanced substance conversion technology.

The main objectives of this dissertation are the development of highly functionalized solid catalysts and apply them to transformation of biomass derived saccharides. I basically focused on high functionality of layered double hydroxide (LDH), one of a layered solid base catalyst which has Brønsted base site. Some strategies to develop highly functionalized LDH-based catalysts, preparation methods, results of characterizations, activity for chemical reactions including biomass derived saccharides as well as outlook based on my research are summarized in this doctoral thesis,

The studies presented in this thesis are collection of the author’s studies which have been performed at School of Materials Science, Japan Advanced Institute of Science and Technology from 2012 to 2017 under the supervision of Prof. Kohki Ebitani.

I wish to express my sincere gratitude to my supervisor Prof. Dr. Kohki Ebitani, whose exact guidance, productive discussions and valuable comments. He has never forced my research policy and given me the opportunity to conduct research under freewheeling thinking. His guidance brought me not only the achievement of my studies described in present thesis but also the ability and confidence to accomplish a research independently. It has been a great honor to be able to do my doctoral research in his laboratory.

My heartfelt appreciation goes to Asst. Prof. Dr. Shun Nishimura for his instructive discussions, precise insight and warmhearted encouragement. He has continuously provided me the unconditional support and research environment, and has sometimes given me effective advices breakthrough against the difficulties. This study could not have been done without his support.

I also would like to thank the members of my reading committee, Prof. Dr. Tatsuya Shimoda, Prof. Dr. Masayuki Yamaguchi and Assoc. Prof. Dr. Kazuaki Matsumura for their valuable comments and remarks.

I am deeply grateful to Assoc. Prof. Dr. Yusuke Yoshinaga at Tokyo Gakugei University, who was my supervisor when I studied in Tokyo Gakugei University, for his precise guidance, beneficial suggestions and kind encouragement. I learned many things including approach to research and researcher’s way from him. I thank him for all his teaching and support.

This work described in present thesis was supported by a Grant-in-Aid from Japan Society for the Promotion of Science (JSPS) Fellows (No. 15J10050). I am grateful for their financial support.

I would like to thank sincerely to my lab members Dr. Duangta Tongsakul, Dr. Pham Anh Son, Dr. Hemant Choudhary, Dr. Jaya Tuteja, Mr. Yotaro Ohmi, Mr. Naoya Ikeda, Mr. Takamasa Takahashi, Ms. Saumya Dabral, Mr. Mujahid Mohammad, Mr. Jia Jixiang, Mr. Ryo Sato, Mr. Takuma Shimura, Mr. Shinpei Fujiwara, Mr. Nao Yoshida, Mr. Jatin Sharma, Ms.

Kanishika Gaur, Mr. Naoto Ozawa, Mr. Ryosuke Matsuzawa, Mr. Kunihiko Mizuhori, Ms. Pooja Tomar, Mr. Ravi Tomar, Mr. Yuuhei Umehara, Mr. Shuusuke Miyazaki, Mr. Souta Yuuki, Ms. Sari Tomita, Mr. Yuuoh Nozoe, Mr. Hongrong Yin, Mr. Shintaro Ohmatsu, Mr. Le Dinh Son and Mr. Atsuki Shibata for their kind encouragements, supports and friendly behaviors.

Finally, I deeply thank my parents, Hiroshi and Yuki, and my grandfather Shinji for their understandings, kind supports and encouragements. I wish to express my sincere gratitude to my brother Satoki for his moral support.

Mahiro Shirotori

Ishikawa,

December, 2016

CONTENTS

Chapter 1

General Introduction

Current Situation and Importance of Solid Acid-Base Catalyst

Catalysis was first recognized in the end of 18^{th} by Joseph Priestley, an English natural philosopher. He observed a phenomenon that when ethyl alcohol passed through natural clay, it converted into another gas. In 1836, A Swedish chemist Jöns Jacob Berzelius designated such phenomenon as “Katalyse” in German; the meaning of Katalyse (denoted as “Catalysis” in English) is equivalent to “Dissolution”. He defined “Catalyst” as a substance that causes the chemical reaction without itself being affected. In 1896, a Deutsch-Balten chemist Friedrich Wilhelm Ostwald defined catalyst as a substance that speeds up a chemical reaction, but do not change equilibrium without its consumption. This definition gave researchers recognition that “Acid” and “Base” are catalyst. Early 1900s was one of the times when the chemical industry and catalyst chemistry were progressing greatly; a German physicochemist Fritz Haber initiated the research for ammonia synthesis from nitrogen molecule using catalyst and equilibrium theory in 1904. He collaborated with Carl Bosch, a German chemist who belonged to BASF Corporation, to implement development of an iron catalyst for ammonia synthesis and the practical application of ammonia production, Haber-Bosch process, in 1912. It had great effect on the world because mass production of ammonia by Haber-Bosch process enhanced not only production of gunpowder and explosive but also generation of chemical fertilizer to lead a population explosion. Although this is an example that chemical industry made rapid progress by generation of a novel catalyst, chemical industry and catalysis chemistry are deeply involved even now. Presently, catalyst assumes important roles in not only chemical industry but also converting petroleum, exhaust gas purification of automobile and factories, energy conversion, organic chemistry, medicinal chemistry and fine chemistry.[1-3]

Catalyst is broadly classified into two types: homogeneous catalyst and heterogeneous catalyst. Homogeneous catalyst includes typical liquid acid and base such as H_2SO_4 and NaOH, as well as metal complex catalyst. Homogeneous catalyst is used for many liquid phase reactions especially in organic synthesis because liquid catalyst generally shows higher selectivity at low temperature, lower investment and better flexibility than heterogeneous catalyst. On the other hand, homogeneous catalytic system has toxicity and requires a large amount of solvent, and is difficult to separate catalyst from the solution as well as to reuse a catalyst. Solid catalyst, such as metal catalyst and metal oxide or hydroxide catalyst including zeolite and layered double hydroxide (LDH), belong to heterogeneous catalyst. Although it is relatively difficult to develop selective catalytic system using heterogeneous catalyst, solid catalyst can be applied to a reaction at high temperature and is easily removed from reactor and reused. Thus, solid catalyst is widely used in chemical industry, and further development of highly active and selective solid catalysts is desirable.

Catalytic reaction over a solid catalyst is initiated by adsorption of substrate onto catalyst surface. Therefore, active site of solid catalyst is mainly considered to be solid surface, especially at corner and edge because of low coordination state and high reactivity of corner and edge atom (Figure 1). Basically, an activity of solid catalyst is dependent on the elements that form a catalyst. For instance, Fe, Co, Ni, Cu and platinum group catalysts show activity for

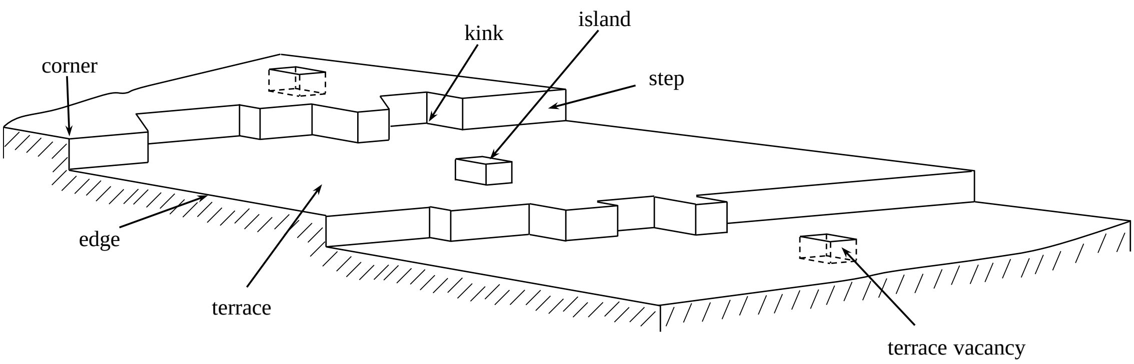

Figure 1 Structural model of solid surface.

hydrogenation following dissociation of hydrogen molecules whereas platinum group, Ag and Au catalysts show activity for oxidation by molecular oxygen activation. On the other hand, the local structure around active site on solid catalyst also affects significant effect on catalysis. Niwa *et al.* investigated acidity on H-Y zeolite, which is composed from SiO_2 and Al_2O_3 framework, using infrared-mass spectrometry / temperature programmed desorption (IRMS-TPD) of ammonia. Although considering Tanabe's hypothesis, homogeneously metal oxide catalysts possess same active sites if they have same compositions, they found that H-Y zeolite possess four kinds of acidic hydroxyl regions at super cage, sodalite cage, and hexagonal cage.[4] These four kinds of acid sites have different Si-OH-Al angles and Al-O bond length to lead a generation of different acid site on same catalyst surface. Roeffaers *et al.* "observed" crystal-face-dependent catalysis on Li-Al LDH followed by real time monitoring of the chemical transformation of individual organic molecules by fluorescence microscopy. They reported that although transesterification occurs on the {0001} plane of Li-Al LDH where the basal surface of the LDH crystal, ester hydrolysis is mainly catalyzed over $\{10\bar{1}0\}$ faces where the exchanged OH^- ions at the entrance of the galleries.[5]

Solid acid catalysts are widely used in many important processes in petroleum refining and the production of petrochemicals such as naphtha cracking, xylene isomerization, alkylation of aromatics, etc. Thus, an enormous number of studies have been devoted to solid acid catalysts. In contrast with extensive studies on solid acid catalysts, fewer efforts have been devoted to heterogeneous basic catalysts.[2] One of the reasons that had inhibited the promotion of solid base catalyst studies is that generation of base catalysis on solid surface is more difficult than generation of acid catalysis on solid surface because most of base site on solid surface are easily poisoned by moisture and carbon dioxide in atmosphere.[6] The first study on the heterogeneous base catalyst was reported by Pines and Haag in 1958. They found that sodium metal dispersed on alumina was an effective catalyst for double-bond isomerization of alkenes.[7] In 1972, Tanabe *et al.* reported that CaO and MgO exhibited highly catalytic activities for 1-butene isomerization when the catalysts were pretreated under vacuum.[8-9] Since then, various kinds of solid base catalysts such as metal oxides, mixed oxides, alkali or alkaline earth oxides on support, amides, imines on support, alkali metals on support, anion exchangers, zeolites, phosphates and crays have been developed and investigated.

When homogeneous liquid acid and base are purged into the same reactor, neutralization will occur immediately to produce water molecule and salt. On the other hand, neutralization does not occur in the case of heterogeneous solid acid-base system even solid acid and solid base are present in the same reaction solution. Because acid and base site on solid catalyst is stabilized on the solid surface, these conflicting active sites can act independently without physical encounter each other. Such a characteristic is called “site isolation”, and is applied to one-pot synthesis. One-pot synthesis continuously conducts a plural reaction to lead a synthesis of chemical product in a one reactor. In contrast with conventional multistep reaction, sequential one-pot reaction can reduce consumption of energy, reagent and time by excluding separation and purification process of intermediate.[10]

One-pot synthesis using solid catalysts was reported by Avnir *et al.* in 2000. They physically entrapped Wilkinson’s complex and ethylenediamine derivative in SiO_2-sol-gel matrices and found that these two active species performed independently.[11] Corriu *et al.* designed a bifunctional mesoporous material containing two antagonist functions, that is, an acidic group in the framework and a basic one in the channel pores.[12] One-pot synthesis conducted by combined use of solid acid and base were presented by Motokura *et al.*[13-14] and Ebitani *et al*.[15-19] Motokura and coworkers reported that the combined use of layered clay Ti^{4+}-exchanged montmorillonite (Ti^{4+}-mont) and hydrotalcite (HT) showed high activities for tandem Aldol reaction followed by deacetalization and aldol condensation, and tandem Michael reaction and acetalization. In this system, Ti^{4+}-mont and HT respectively act as solid Brønsted acid and base catalysts (Figure 2).[13] Ebitani and coworkers reported that the combined use of basic HT and Brønsted acidic sulfonated resin shows activity for one-pot synthesis of furfurals from aldose *via* aldose-ketose isomerization over HT and successive dehydration over sulfonated resin.[15, 19]

Most of fine chemicals are currently synthesized by multistep process. In addition, several processes in chemical industry are required to be improved; (i) processes with the mass generation of wastes, (ii) processes that use hazardous materials and (iii) processes with the mass consumption of energies. One-pot synthesis using heterogeneous solid acid—base catalytic systems promises to serve development of environment-friendly low energy chemical process from the viewpoint of green chemistry.

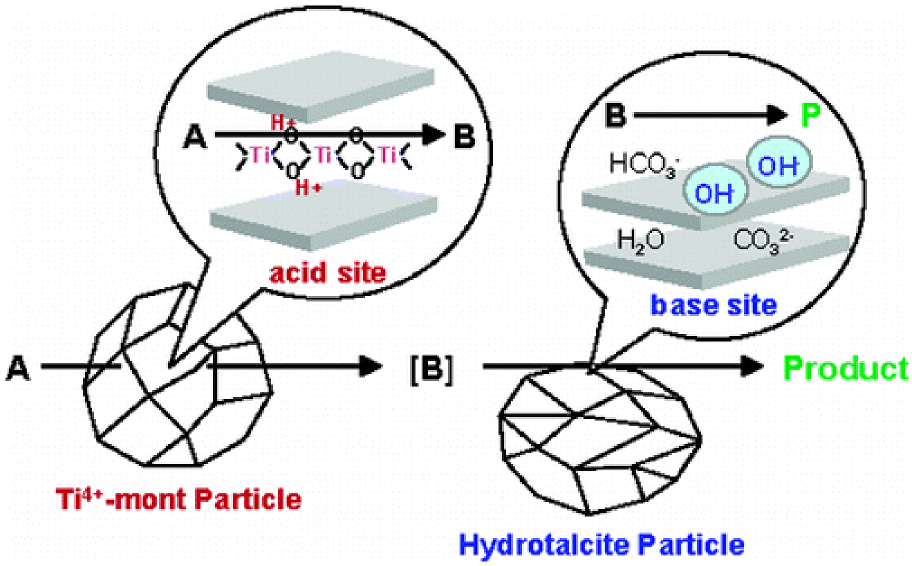

Figure 2 One-pot reaction using acidic Ti^{4+}-exchanged motmorillonite and basic hydrotalcite.[13]

Characteristic, Function and Application for Layered Double Hydroxide

Layered double hydroxide, "LDH", is one of the well-known layered clay mineral which is composed of two-dimensional brucite-like sheets and interlayer anion. The chemical formal of LDH is denoted as $[M^{2+}_{1-x}M^{3+}_{x}(OH)_2]^{x+}A^{n-}_{x/n}\cdot mH_2O$, where M^{2+} and M^{3+} are di- and tri- valent metal ions, such as Mg^{2+}, Mn^{2+}, Fe^{2+}, Co^{2+}, Ni^{2+}, Zn^{2+}, and Al^{3+}, Cr^{3+}, Fe^{3+}, Co^{3+}, Ga^{3+}, respectively, and where A^{n-} is the interlayer anion.[20-22] The two dimensional sheet, $[M^{2+}_{1-x}M^{3+}_{x}(OH)_2]^{x+}$, possesses positive charge derived from partially substituted M^{3+} ion for M^{2+} ion in hydroxide layer. The positive charge over hydroxide layer is compensated by insertion of molecular water and anion A^{n-}, such as CO_3^{2-}, NO_3^-, F^- and Cl^-, to interlayer of hydroxide sheets (Figure 3). The interlayer distance is related to the size of interlayer anions, for instance, 2.8, 2.9 and 4.1 Å for CO_3^{2-}, Cl^- and NO^{3-} type LDHs, respectively. The most famous Mg-Al-CO_3 type LDH, $Mg_6Al_2(OH)_{16}CO_3 \cdot nH_2O$, is called hydtoralcite (HT).

The LDH has been investigated its utilities in various fields because of simplicity and variety of synthesis, and interesting characteristics.

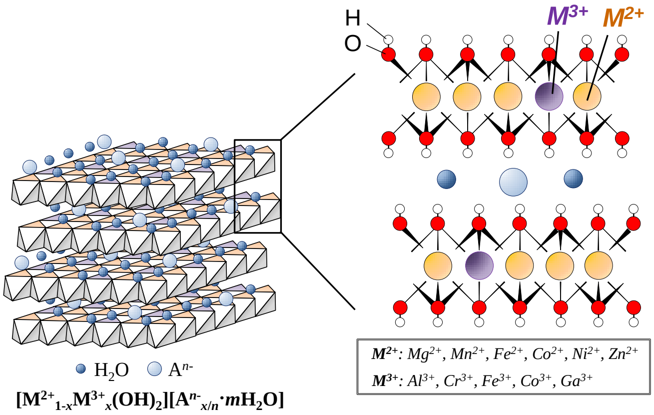

Figure 3 Structural model of LDH.

Synthesis. One of the most general methods to prepare the LDH is the co-precipitation method, where a mixed solution of M^{2+} and M^{3+} ions is precipitated by an alkali source such as sodium hydroxide and ammonia (Figure 4(A)). The pH range is commonly adjusted between 7 and 10 to avoid formation of an impurity; for instance, in the case of Mg-Al LDH, aluminum precipitates and magnesium hydroxide respectively generates at lower and higher pH values.[23] The crystallite of LDH can be controlled by changing pH, solvent as mother solution, aging time and temperature as well as metal concentration. The high crystalline LDH can be synthesized by homogeneous nucleation and crystal growth by using hydrolysis of urea instead of sodium hydroxide and ammonia,[24-27] called as urea co-precipitation method (Figure 4(B)). For instance, Sasaki *et al.* prepared well-crystalline Co-Al LDH with a mean lateral size as large as 4 μm and a thickness of about 30 nm by urea co-precipitation method as follows; $CoCl_2 \cdot 6H_2O$, $AlCl_3 \cdot 6H_2O$, and urea were dissolved in 1dm^3 of deionized water to give the final concentrations of 10, 5, and 35 mM, respectively. Then, the mixed solution was heated at the refluxing temperature under continuous stirring for 2 days. The resulting product was filtered, washed with deionized water and anhydrous ethanol several times, and finally air-dried at room temperature.[26]

LDH also can be obtained by various techniques: a simple dissolution-reprecipitation mechanism of MgO and Al_2O_3,[28-29] immediate nucleation process using a colloid mill rotating,[30] an in-line dispersion-precipitation method,[31] sol-gel method,[32-35] microwave irradiation,[33, 36] solvothermal[37] and hydrothermal method.[37-41] As advanced research studies, two-dimensional LDH nanosheet materials has been released by Adachi *et al.* in 2000.[42] To date, LDH nanosheet has widely been investigated[26, 43-47] because delamination of LDH will lead to a novel generation of LDH-based materials in which total surface of layered compound can be rendered accessible for chemical reactivity.[42] Fabrication of nano-sized LDH by combination with other nano-materials has also been presented. Winter *et al.* and Li *et al.* respectively synthesized LDH nano-platelets in the pore carbon nanofibers (Figure 4(C))[48] and silica mesopores (SBA-15).[49] Several immobilized nano-LDH materials onto SiO_2 sphere which possess core-shell, yolk-shell or hollow-shell structure have been demonstrated[50-55] as shown in Figure 4(D). A typical structure generally denoted as SiO_2@LDH is one of a hierarchial core-shell material which promises strategy to avoid *ab*-face stacking aggregation.[55]

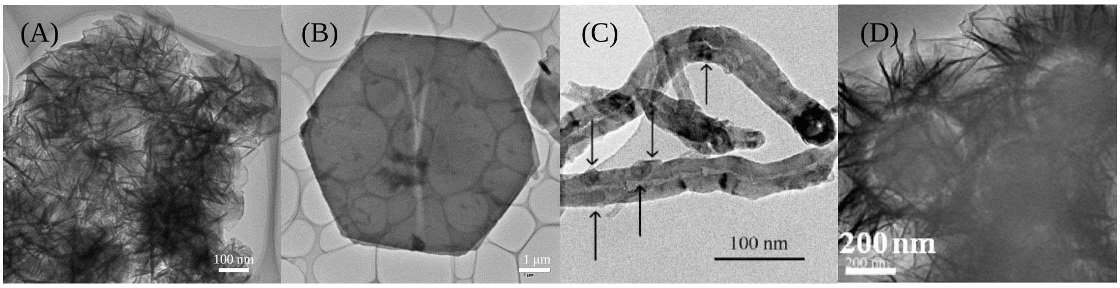

Figure 4 TEM images of LDHs prepared by various methods. (A) co-precipitation, (B) urea co-precipitation, (C) hydrotalcite/carbon[48] and (D) SiO_2@LDH core-shell.[51]

Characteristic and application. Typical characteristics of LDH are (i) phase transformation *via* thermal decomposition and recover the original lamellar structure by hydration, (ii) adsorption capacity, (iii) anion-exchange ability of the interlayer space, and (iv) tunable basicity of the surface.[22, 37]

The mixed hydroxide LDH transforms to mixed oxide through thermal decomposition, involving dehydration, decomposition of interlayer anions, and dehydroxylation of layer hydroxide groups.[56] The detailed dehydration and dehydroxylation mechanism of hydrotalcite-like compounds were investigated by Jia *et al.* in 2010 using the themogravimetry / differential thermal analysis / mass spectrometry (TG-DTA-MS); First, dehydration of crystalline water molecules starts on the surface and edge, second, continues to the interlayer water, third, mixed hydroxide layer undergo dehydroxylation, followed by or overlapping with decomposition of interlayer anions.[57] The dehydroxylation temperature is related to the type of hydroxyl groups in the LDH lattice, *i.e.* OH-(M(II)$_3$) and OH-(M(II)$_2$M(III)), and the thermal stability of hydroxyl groups in LDHs is OH-(Ca$_3$) (~480 ºC) > OH-(Mg$_2$Al) (~410 ºC) > OH-(Mg$_2$Fe) (~350 ºC) ≈ OH-(Mg$_3$) (300—370 ºC) ≈ OH-(Ca$_2$Al) (~330 ºC) > OH-(Ca$_2$Fe) (~290 ºC).[57] Interestingly, mixed oxide derived by thermal decomposition of LDH can be retransformed to LDH form by hydration process. This characteristic, called as memory effect, is applied to one of an intercalation technique and designs for functionalized LDH-based catalysts.[58-60]

It is known that pretreated LDH at > 500 ºC acts as adsorbent of CO_2.[61-64] LDH transforms to an amorphous M^{2+}-M^{3+} mixed solid oxide with a large surface area and good stability at high temperature *via* thermal treatment. The obtained mixed oxide is a viable material for CO_2 sorption.

Anionic species located within the interlayer of LDH can be exchanged with inorganic or organic anions[20, 65-66] as well as organic molecules.[67-69] Intercalation of LDH promises utilities for anions removal, drug delivery system, and preparation of nano-scale organic/inorganic hybrid materials such as bio-composite and biosensor.

Catalytic Reactions using LDH as Solid Base Catalyst

Base sites on most of metal oxide and mixed oxide are Lewis basic site which is derived on the unsaturated coordinative O^{2-} ion. These typical solid Lewis acid catalysts usually required a pretreatment with high temperature to generate the basic O^{2-} anion because these Lewis base sites are easily poisoned by CO_2 and H_2O in the atmosphere.[6] On the other hand, LDH is known as a unique solid which can be stored in an air atmosphere and exhibits basic character without pretreatment.[22] Base sites on LDH are mainly considered to be identical Brønsted basic OH^- and HCO_3^- anions which are adsorbed onto LDH surface. There are many reports of catalytic activities of LDH as base catalyst for various reactions. Kaneda *et al.*[29, 70] and Pârvulescu *et al.*[71] respectively presented that Mg-Al LDH-based solid catalyst effectively promoted epoxidation of *α,β*-unsaturated ketones and styrene with aqueous hydrogen peroxide. Typical basic reactions such as Aldol and Knoevenagel condensations are also catalyzed by LDH.[72-74] Ebitani *et al.* found that reconstructed Mg-Al LDH, obtained by treating the Mg-Al mixed oxide with water, efficiently catalyzed Aldol condensation of carbonyl compounds. They also considered that the reconstructed Mg-Al LDH provide a unique acid—base bifunctional surface capable of promoting the Knoevenagel condensation and Michael reactions of nitriles with carbonyl compounds.[60] Transesterification of dimethyl carbonate is a conventional method for polycarbonate production. Guangxing *et al.* reported that Mg-Al LDH facilitated the transesterification of dimethyl carbonate with phenol. Recently, LDH has been investigated its utility for biomass derived saccharides transformation. Ebitani *et al.* applied LDH to one-pot synthesis of furfurals from mono- and/or polysaccharides with solid acid catalyst.[15-19] In these systems, LDH acts as an isomerization catalyst for aldose-ketose isomerization. They also revealed that LDH catalyst effectively promotes formic acid synthesized from monosaccharides by using aqueous H_2O_2 as an oxidant in ethanol.[75] Synthesis of lactic acid from glucose over LDH catalyst *via* reverse Aldol reaction is also reported by Onda *et al.*[76] Tanaka *et al.* studied photocatalytic activity of LDH for CO_2 conversion in aqueous solution and found that Ni-Al LDH exhibited the large amount of CO evolved among the various kinds of LDHs.[77-79]

Brønsted basic LDH transforms to mixed metal oxide which possesses a pair of a bifunctional Lewis acid—Lewis base sites. Lewis acid and Lewis base sites are respectively generated on coordinatively unsaturated metal cations and an oxide anion. These acid and base sites are also known to act as highly active sites for various organic reactions, such as epoxidation,[70-71] Aldol condensation,[80] Knoevenagel condensation,[81] transesterification,[82-84] saccharides transformations[75-76] and Meerwein-Ponndorf-Verley reduction.[85]

Various metal species such as metal salts and metal clusters can be immobilized on LDH surface *via* adsorption. Thus, LDH has been widely used as not only base catalyst but also support for metal catalyst such as Ru, Pd, Ag, Au and Pt.[22, 86-93] The most important character of the LDH as a metal support is its basicity which promotes the abstraction of protons from organic molecules, especially from alcohols even after metal immobilization.[22] Kaneda *et al.* presented that Au nanoparticles immobilized on the Mg-Al LDH (Au/HT) surface efficiently catalyze the deoxygenation of epoxides into the corresponding olefins using alcohols. In this system, the Au nanoparticles and basic sites of LDH surface cooperatively work for the deoxygenation of the epoxides as follows; First, base site of HT abstracts proton of the alcohol to generate $[H\text{-}HT]^+$ and a $[Au\text{-}Alcoholate]^-$ species at the Au nanoparticles—HT interface. The Au-alcoholate species then under goes β-hydride elimination to give an $[H\text{-}Au]^-$ species. Lastly, protonation from the $[H\text{-}HT]^+$ species opens the epoxide, and subsequent attack of $[H\text{-}Au]^-$ species and dehydration of the surface intermediates provide the olefins.[92]

If support itself possesses one active site, immobilization of another active species onto support surface generates at least three kinds of active sites; (i) an active site originated from support, (ii) an active site originated from immobilized species and (iii) a cooperative active site between support and immobilized species where is located at cross boundary. Although the combined catalytic system of first and second active sites can be served by physical mixing of two different solid catalysts, the third active site cannot be served by physical mixing. Thus, immobilization of active species on LDH surface enables design of novel multi-functional catalyst to lead generation of novel functionalized solid catalyst.

Biomass as Sustainable Carbon Resources

Fossil resources such as petroleum, coal and natural gas are important resources to our life to supply energy and chemicals. The primary energy usage compositions of 2013 (Figure 5[94]) shows that fossil resources account for most of the primary energy usage on a global scale. However, continuously usage of fossil resources has several problems. First problem is that there is a great difference between consumption rate and reproduction rate of fossil resources; millions of years are required for its production while its consumption rate is quite high.

Another problem is the environmental pollution including air pollution, acid rain, water pollution, soil pollution, ozone layer depletion and global warming caused by release of exhaust gas such as CO_2, SO_x and NO_x, and waste from factory and/or automobile. To overcome these problems, development and practical realization of sustainable resources such as sunlight, wind power, geothermal heat and biomass are desired. Above all, biomass resource has attracted much attention because it can serve as a sustainable source of not only renewable fuels but also chemicals in a carbon-neutral fashion.[95-97]

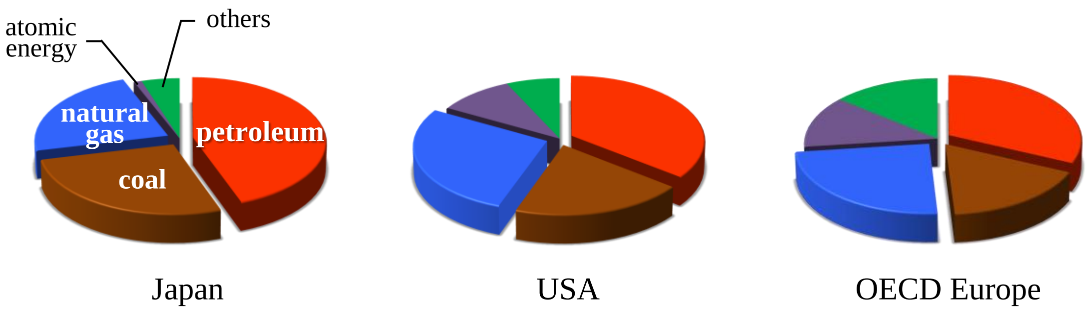

Figure 5 The primary energy usage compositions of 2013.[95]

Definition, assortment and potential of biomass. Biomass is defined as all organic material that stems from plants (including algae, trees and crops) or living organisms (animal and microorganism).[98] Corn stover and sugarcane derived from a cultivated plant are called first-generation biomass. At first, production of bioethanol from first-generation biomass was energetically conducted in USA and Brazil, while it has been pointed out that the usage of cultivated plant competes with food supply. Currently, inedible biomass has been investigated its usage for energy source and substrate of chemical production, as a second-generation biomass. There are a wide variety of inedible biomass, such as wood, agriculture, non-edible portion of crops, black liquor and municipal solid waste (MSW).

Through the world, biomass can be considered as the best option and has the largest potential, which meets these requirements and could insure fuel supply in the future.[99] Hall *et al.* reported the potential of biomass that the production amount of biomass is calculated to about 220 billion tons per year.[100] In terms of energy, this corresponds to 4500 EJ which is comparable to sunlight. Although all these cannot be utilized for energy production, and in fact it only covers 10-15% of the current world primary energy usage, several scenario studies suggest potential market share of modern biomass till year 2050 of about 10-50%.[98-99]

Lignocellulosic biomass. Lignocellulosic biomass, which is mainly composed of monosaccharides in the form of cellulose, hemicellulose, and lignin, is the most abundant woody biomass.[98] Although the composition ratio differs depending on the type of lignocellulosic biomass, for instance it consists of 33-40% of cellulose, 20-25% of hemicellulose and 15-20% of lignin in the case of wheat straw (Figure 6).

Cellulose is the major biopolymer synthesized by nature that generates secondary cell wall of plant. It is composed of a long chain of linked glucose units *via* β-1,4-glycisidic bonds with degree of polymerization of *ca.* 500 to 25,000. Cellulose is very stable and resistant to acid and alkali reagents.

Hemicellulose is a polysaccharide which has more branched structure than cellulose. It is a heteropolysaccharide composed of pentose unit such as xylose, arabinose and hexose unit including glucose, mannose and galactose. It is more soluble than cellulose because of lower

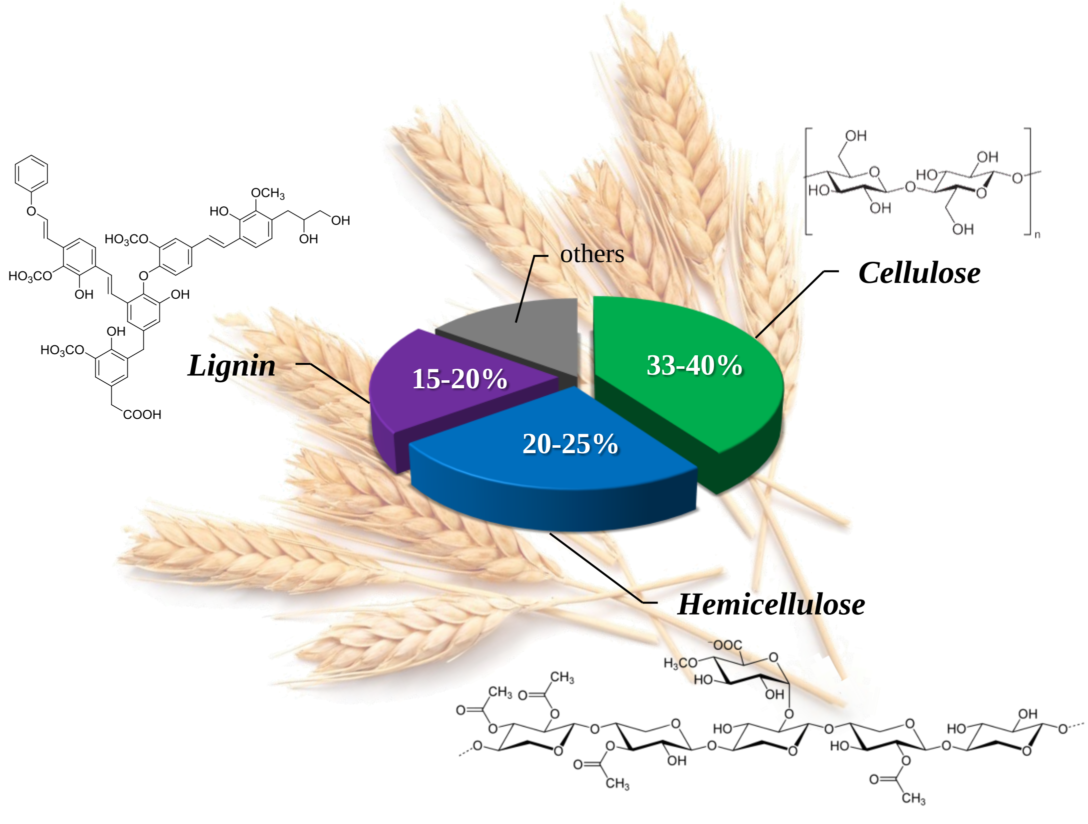

Figure 6 Lignocellulose composition: cellulose, hemicellulose and lignin.

degree of polymerization.

Lignin is a complex polymer which has a highly irregular and insoluble cross-link built of substituted phenols. Although lignin possesses the potential to be converted into fuels and high valuable chemicals because it is the only source of aromatic compounds from biomass, the complexity of its structure and non-uniformity of its composition makes it more difficult to utilize.

Catalytic Transformation of Biomass-derived Materials

Plant-derived biomass is broadly classified into storage ingredient (sugar, starch, fat and oil) and cell wall component (cellulose, hemicellulose and lignin). Among storage ingredient, sugar and starch are used as a substrate for fermentative ethanol synthesis, while fat and oil are converted to biodiesel fuel (BDF) *via* transesterification. Because this transesterification make a glycerol as a bi-product, development of effective utilization method of glycerol is also required. In recent years, many researchers have reported catalytic conversion of glycerol to various chemical compounds such as alcohols, glycerol carbonate and acrylic acid (Figure 7). Acrolein is a synthetic raw material for medicine, allyl alcohol, 1,3-propanediol and crosslinking agent and can be synthesized from glycerol using heteropoly acid as a solid catalyst.[101-102] Plant scale

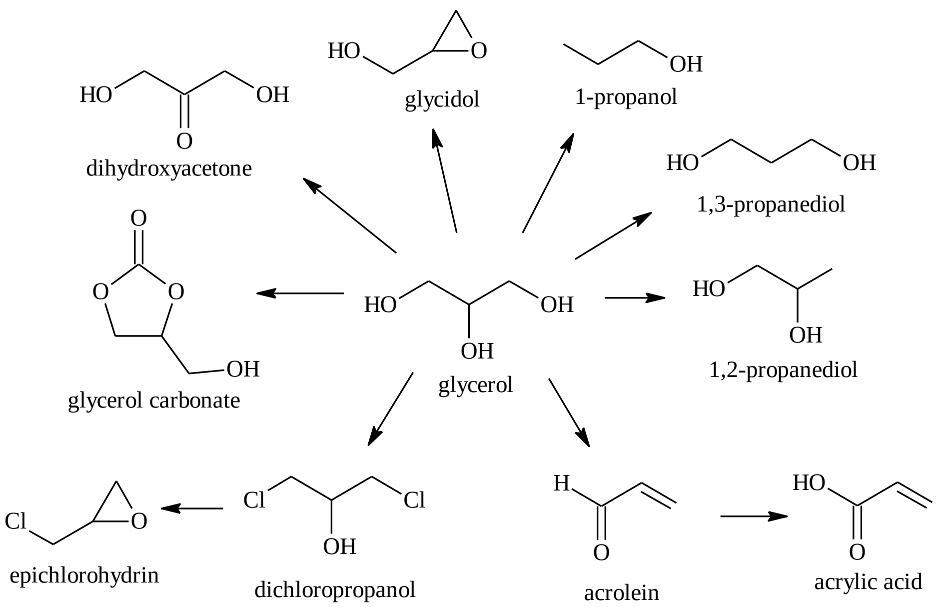

Figure 7 Scheme of various chemical synthesis from glycerol.

1,2-propanediol production from glycerol over Cu catalyst was developed by Suppes *et al.* and was started up with annual production of 35,000 tons by Senergy Chemical Ltd. from 2008. DuPont company has conducted operation of 1,3-propanediol production from glycerol using genetically engineered Escherichia coli since 2006. Recently, catalytic synthesis of 1,3-propanediol from glycerol was investigated using solid catalyst such as $Pt/WO_3/ZrO_2$[103] and $Cu\text{-}H_4SiW_{12}O_{40}/SiO_2$.[104]

Among cell wall component, cellulose and hemicellulose are decomposed to mono- or polysaccharides, and then obtained saccharides are converted into fuels and chemical products by catalytic transformation. The hydrolysis of cellulose and hemicellulose into monosaccharides, the first step in biorefinery operations, has been conducted with enzyme and chemical catalysts such as homogeneously liquid acid (H_2SO_4 and HCl) and solid acid,[105-107] acidic carbons[108-111] and sulfonated carbons.[112-114] As an advanced study, Fukuoka *et al.*[115] has recently reported that biomass-derived carbon-based material exhibits high activity for hydrolysis of woody biomass

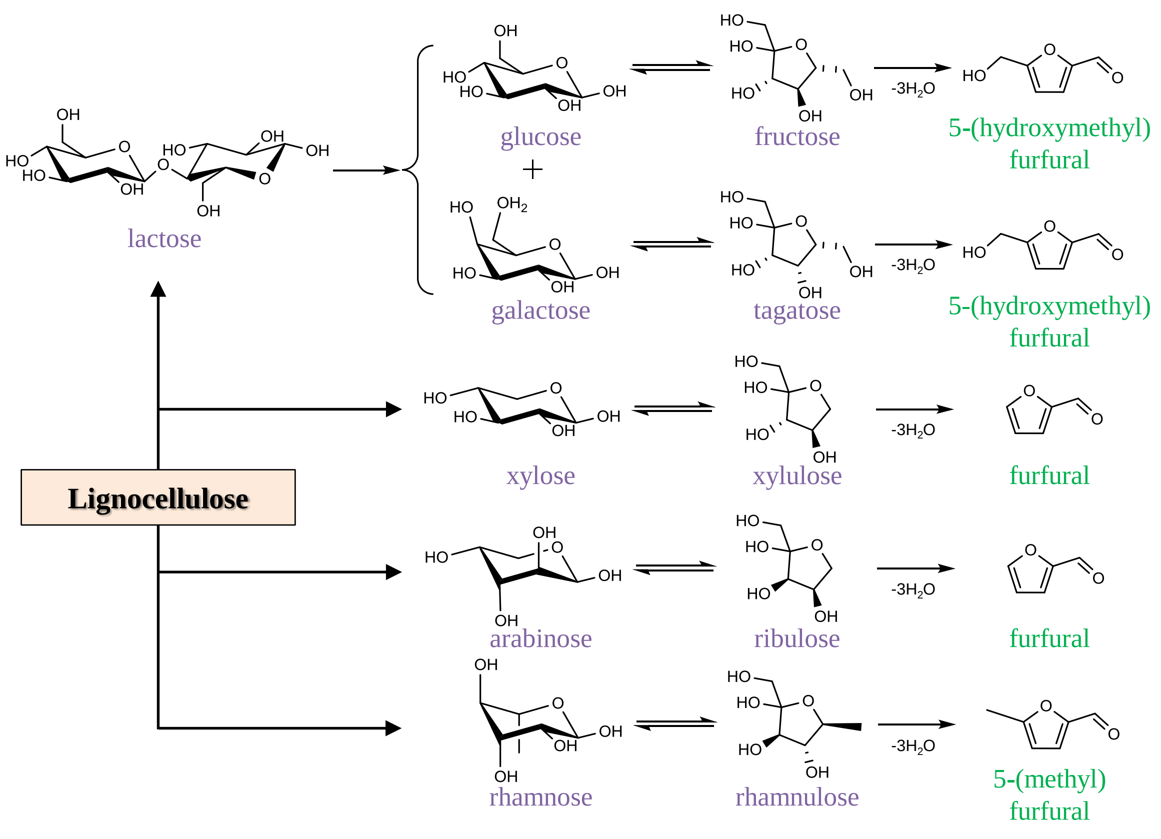

Figure 8 Scheme of furfurals synthesis from saccharides

in trace HCl aq. with glucose and xylose yield of >78% and >89%, respectively. They also described; "This is a self-contained system using woody biomass as both the catalyst source and substrate for realizing facile catalyst preparation and recycling."[115]

The successive conversion of saccharides into furans such as 5-(hydroxymethyl)furfural (HMF), 5-methylfurfural and furfural (Figure 8) have been attracted much attention because they have great potential as non-petroleum substrates in production of biofuels, polymers, pharmaceuticals, and fine chemicals.[18, 116-119]

Previous studies on furfural synthesis. Furfural is produced around 300,000 ~ 500,000 tons a year in the world. Furfural and furfural derivatives are one of the biomass-derived versatile chemicals which can be used as solvent and substrate of biofuels, polymers and fine chemistry. Generally, furfural is obtained by thermal treatment of lignocellulose and/or xylose with homogeneous liquid acid. According to Montana and coworker's report,[120] furfural can be synthesized with >50% yield by the hydrolysis of olive stones in dilute sulfonic acid at high temperature (220-240 ºC) and short reaction time. Kottke reported that in the high reaction temperature condition, sulfonic acid is not essential because acetic acid in cellulose acts as a dehydration catalyst.[121] Dehydration of xylose into furfural in trace liquid acid were also reported.[122-123] However, these processes have several problems such as pollution of apparatus and environmental with large amount of acidic wastewater, and these require neutralization of reaction solution. Thus, development of a new furfural production process which implement not only high productivity but also low environmental impact.

Furfural synthesis over heterogeneous solid catalyst has recently been focused as a clean process with reduced environmental impact. Many researchers have reported dehydration of xylose into furfural using various solid acid catalysts as shown in Table 1. Moreau *et al.*[124] found that H-form fajasite zeolite with a Si/Al ratio of 10 effectively dehydrate xylose into furfural in toluene/water co-solvent with 34% yield. They also described that xylose conversion and furfural selectivity depend on both acidic and structural properties, and the use of HY faujasite with Si/Al ratio of 15 gave higher furfural selectivity (96%). Catalytic dehydrations of xylose into furfural in toluene/water co-solvent were also reported by Dias *et al.* They prepared

MCM-41-SO_3H solid acid catalyst which has anchored sulfonic acid groups and applied it to xylose dehydration. The MCM-41-SO_3H with the highest sulfonic acid groups displayed high selectivity for furfural (83%) at high xylose conversion (91%).[125] They also examined exfoliated titanate, niobate and titanoniobate nanosheets as solid acid catalysts for dehydration of xylose, and found that $HTiNbO_5$-MgO catalyst achieved 55% yield of furfural after 4 h of reaction time.[126] Sulfonated resins are also known to act as Brønsted acid catalyst for xylose dehydration.[127] Jeong *et al.* presented that sulfonic acid modified mesoporous shell silica bead (MSHS-SO_3H) effectively synthesizes furfural from xylose even in water solvent.[128] Recently, highly active and stable arenesulfonic SBA-15 catalyst was prepared by incorporation of the arenesulfonic precursor on SBA-15 support, and was released by Agirrezabal-Telleria *et al.* They found that prepared arenesulfonic SBA-15 catalyst can achieve furfural yield of 86% at 99% conversion on reactions at 433 K. They mentions that this was mainly attributed to the high hydrothermal stability of the arenesulfonic-sites and to the porous structure.[129] These catalytic process of furfural synthesis solve the pollution of the equipment and environmental, however, direct dehydration of xylose over single Brønsted acid site need high reaction temperature (>423 K) as well as high thermal stability of active site on catalyst surface. Thus, low energy consumption type efficient dehydration method with low reaction temperature has been sought as advanced research studies.

Table 1 Previous reports of dehydration of xylose to furfural using solid acid catalysts.

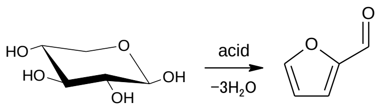

xylose furfural

Catalyst	Solvent	Temp. / K	Time / h	Yield (Selec.) /%	Ref.
HY faujasite	toluene/water	443	0.5	34 (70)	124
MCM-41-SO_3H	toluene/water	413	24	76 (83)	125
$HTiNbO_5$-MgO	toluene/water	433	4	55 (60)	126
Nafion 117	DMSO	423	2	60	127
MSHS-SO_3H	water	463	1	43 (68)	128
arenesulfonic SBA-15	toluene/water	433	20	86 (87)	129

The most important reason that dehydration of xylose on single Brønsted acid catalyst requires high energy is that the structure of aldose type xylose is too stable. To overcome this problem, one approach merging the isomerization of xylose (aldose) into unstable xylulose (ketose) intermediate before the dehydration was generated.[17, 130] Some researchers calculated activation barrier for dehydration of saccharides, and reported that activation barrier can be reduced from 30-32 kcal/mol[131-132] to 23.1 kcal/mol[133] by isomerizing xylose to xylulose. In fact, several studies on two-step transformations of xylose into furfural *via* aldose-ketose isomerization and dehydration of ketose under mild condition (373 K) have been reported as shown in Table 2. It is known that aldose-ketose isomerization is catalyzed on both Lewis acid sites and Brønsted base sites *via* hydride shift and proton shift, respectively.[134] Two-step dehydration of xylose composed of aldose-ketose isomerization over Lewis acid and successive dehydration at 373 K were reported by Binder *et al.*[130] and Suzuki *et al.*[135] Binder *et al.* used various chromium species as homogeneously Lewis acid catalysts. They confirmed that aldose-ketose isomerization over chromium species follows hydride shift mechanism by deuterium-labeling experiment, and found that use of $CrCl_2$ with LiBr in DMA solvent achieves 56% yield of furfural.[130] Suzuki *et al.* tested various sulfonated metal oxides as heterogeneous solid acid catalyst. They found that sulfonated tin oxide (SO_4^{2-}/SnO_2) which possesses both Lewis acid sites and Brønsted acid sites derived from tin oxide and sulfonic acid group,

Table 2 Previous reports of dehydration of xylose to furfural at 373 K *via* aldose-ketose isomerization.

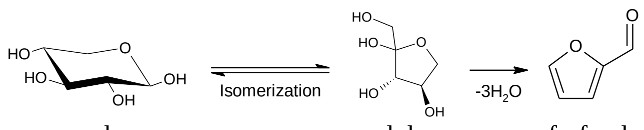

xylose xylulose furfural

Catalyst		Solvent	Time / h	Yield (Selectivity) /%	Ref.
Isomerization (active site)	Dehydration				
$CrCl_2$ (Lewis acid)	$CrCl_2$	DMA (Additive: LiBr)	4	56	130
SO_4^{2-}/SnO_2 (Lewis acid)	SO_4^{2-}/SnO_2	toluene/water	48	29 (47)	135
Mg-Al LDH (Brønsted base)	Amberlyst-15	DMF	3	37 (51)	17

respectively, exhibited the highest catalytic activity. In this system, Lewis acid sites and Brønsted acid sites act independently for isomerization and dehydration, respectively.[135] Ebitani *et al.* developed two-step dehydration process by combined use of solid acid and base catalyst. They selected Mg-Al LDH and Amberlyst-15 as solid base and solid Brønsted acid catalyst, respectively, and simultaneously applied two solid catalysts to the reaction. They confirmed that solid acid and base catalysts independently act in the same reactor to lead furfural production with 37% yield in 3 h. In this system, xylose is isomerized to xylulose by solid base Mg-Al LDH and obtained xylulose is successively dehydrated into furfural.[17] Although these reports are epoch-making examples of realizing dehydration of xylose under mild conditions, each has some problems to be solved. Because Binder's report uses homogeneous catalyst, the separation of catalyst from solution is difficult even it exhibits high activity. A heterogeneous SO_4^{2-}/SnO_2 catalyst released by Suzuki *et al.* is easy to handle, however, it gives a lower furfural yield relative to take a long reaction time. In the case of Ebitani's report, although furfural production amount is higher than Suzuki's report, the maximum furfural yield is still less than 40%. This is mainly attributed to low reaction rate of isomerization step over Mg-Al LDH and proceeding of side reaction over Mg-Al LDH to lead decrease of furfural selectivity. Although various studies on efficient production of furfural from pentoses have been conducted, an ideal catalytic system has not yet been developed.

Outline of the Present Thesis

Based on the previous reports described above, I studied development of layered double hydroxide (LDH)-based highly functionalized solid catalysts for utilization of biomass derived saccharides, especially for one-pot synthesis of furfural from xylose. LDH possesses Brønsted basicity on its surface as adsorbed anions. As a solid base catalyst, LDH can promote various organic reactions such as Aldol condensation, Knoevenagel condensation, transesterification and epoxidation as well as aldose-ketose isomerization. Ebitani *et al.* have recently found that the combined use of LDH and Brønsted acid resin effectively synthesize furfurals from aldoses *via* aldose-ketose isomerization over LDH and successive dehydration of ketose over Brønsted acid in a one-pot manner. Because furfurals are one of the key chemicals as substrates for production of bio-fuels and various chemical compounds, development of catalytic system for furfurals from saccharides has been accepted as one of the important reactions to utilize renewable resources. However, application of LDH as a solid base catalyst to furfurals synthesis from saccharides has several problems as follows; (i) because aldose-ketose isomerization over LDH is a static rate determining step in furfural synthesis, the total reaction rate decreases, (ii) aldose-ketose isomerization over LDH causes frequent side reactions such as decomposition and polymerization of substrates or products to lead decrease in selectivity and (iii) since the anions in the interlayer space of LDH cannot participate in the chemical reaction, bare LDH catalyst cannot exhibit its potential. Thus, discovery of a highly functionalized LDH-based catalyst has been regarded as a crucial theme for development of catalytic utilization of biomass derived saccharides.

In this doctoral thesis, I applied two strategies to design novel LDH-based catalysts. First strategy is development of bifunctional acid—Brønsted base sites on same catalyst surface by immobilization of active species. One of the important advantages on heterogeneous solid catalyst is that different active sites can be generated on one catalyst surface. For instance, most of metal oxide catalysts possess a pair of Lewis acid—Lewis base site at surface M-O-M bonding regardless of strength and amount, and immobilization of functional groups such as sulfonic acid groups and amine groups easily give catalyst surface Brønsted acidity and Lewis basicity, respectively. However, the acid base bifunctional catalyst which has *Brønsted base sites* as base site has hardly been studied. In this doctoral thesis, I designed several novel bifunctional Lewis acid—Brønsted base LDH-based catalysts by joining Lewis acidic metal oxide domain and Brønsted basic complex metal hydroxide domain. The catalytic activity for biomass derived saccharides transformation and detailed local structure of bifunctional Lewis acid—Brønsted base sites were investigated and have been summarized in this doctoral thesis.

Second strategy is development of highly active layered catalyst by controlling its crystal size. This strategy comes from a simple notion that is “fine crystallization of material lead to more exposure of active site where located on the surface”. Although LDH is one of the well-known solid base catalysts and is applied to various organic reactions, the active site actually precipitating to the chemical reaction is limited to only surface sites. Thus, inhibition of *ab*-face stacking is required to utilize all LDH hydroxide layers. Moreover, number of unsaturated coordinative atoms which are located at edge and corner is also important to increase the amount of active site. To overcome these problems, I designed a novel immobilized LDH catalyst with inhibition of excess crystal growth, and investigated the change of base catalysis and structural property on prepared catalyst.

In this doctoral thesis, I discovered (i) some LDH-based acid—base bifunctional catalysts show high activity for one-pot synthesis of aldopentoses into furfurals and (ii) immobilized LDH catalysts prepared with coexistence of SiO_2 sphere exhibit highly base catalysis.

Chapter 2 describes “Development of Acid-Base Catalytic System for One-pot Synthesis of Furfural Derivatives from Pentoses”. I found that LDH promotes not only the Knoevenagel condensation of furfural with various active methylene compounds but also one-pot synthesis of furfural derivatives from aldopentoses by combined use of solid Brønsted acid. The author also revealed that some Lewis acidic metal oxide supported LDH catalysts and LDH—γ-Al_2O_3 composite catalysts evolve bifunctional Lewis acid—Brønsted base site at the solid surface, and these bifunctional sites effectively catalyze aldopentoses transformation.

In Chapter 3, “Genesis of Bi-functional Acid-Base Site on Cr-supported Layered Double Hydroxide Catalyst Surface for One-pot Synthesis of Furfural from Xylose with Solid Acid Catalyst” is described. Correlation between catalytic activity for aldopentoses transformation and surface property on a highly active acid-base bifunctional Cr supported LDH catalysts were investigated with various Cr loading amounts. The results of structural characterization such as X-ray diffraction patterns (XRD), X-ray photoelectron spectroscopy (XPS), X-ray absorption spectra (XAS), electron spin resonance (ESR) and nitrogen adsorption measurement suggested that Lewis acidic Cr^{3+} oxides are supported on LDH surface as two-dimensional monolayer domains of monomer or small cluster. The author concluded that the cross boundary between supported Cr^{3+} oxide and LDH surface generates Lewis acid—Brønsted base bifunctional site that are highly active sites for aldose-ketose isomerization.

Description in Chapter 4 is "Development and Evaluation of Base Catalysis of Layered Double Hydroxide Prepared with Coexistence of SiO_2 Spheres." I developed a novel LDH catalyst by *in-situ* growth of LDH crystal on the spherical SiO_2 surface (SiO_2@LDH). Obtained SiO_2@LDH catalysts show higher activity for the Knoevenagel condensation than conventional LDH. The crystallite property and morphology are investigated by XRD, ^{29}Si cross polarization magic angle spinning nuclear magnetic resonance (^{29}Si CP-MAS NMR), transmission electron microscopy (TEM) and energy-dispersive X-ray spectrometry (EDS). Results indicated that small LDH crystals are immobilized onto SiO_2 surface with Si-O-M covalent bond, and more metal hydroxide layer was exposed to the surface compared with conventional LDH. I concluded that dispersion of starting points of LDH crystal growth on SiO_2 surface lead to generate fine crystalline LDH which has highly base catalysis.

Finally, some concluding remarks, possible contributions of this work to catalytic science and scope have been given based on the preceding chapter's achievement.

References

1. M. Misono and Y. Saito, *Syokubai Kagaku*. Maruzen, Tokyo, 2009.
2. Y. Ono and H. Hattori, *Solid Base Catalysis*. Springer-Verlag Berlin Heidelberg / Tokyo Institute of Technology Press, Tokyo, 2011.
3. E. Kikuchi, Y. Imizu, K. Segawa, A. Tada and H. Hattori, *Atarashii Syokubai Kagaku New ed.*, Sankyo Syuppan, Tokyo, 2013.
4. K. Suzuki , N. Katada and M. Niwa, *J. Phys. Chem. C*, 2007, **111**, 894.
5. M. B. Roeffaers, B. F. Sels, I. H. Uji, F. C. De Schryver, P. A. Jacobs, D. E. De Vos and J. Hofkens, *Nature*, 2006, **439**, 572.
6. H. Hattori, *Appl. Catal. A*, 2001, **222**, 247.
7. H. Pines and W. O. Haag, *J. Org. Chem.* 1958, **23**, 328.
8. K. Tanabe, N. Yoshii and H. Hattori, *Chem. Commun.* 1971, 464.
9. H. Hattori, N. Yoshii and K. Tanabe, *Proceedings of the 5th International Congress on Catalysis*, 1972, Miami Beach, p.233.

10. B. Voit, *Angew. Chem. Int. Ed. Engl.*, 2006, **45**, 4238.
11. J. Blum, F. Gelman., R. Abu-Reziq, I. Miloslavski, H. Schumann and D. Avnir, *Polyhedron*, 2000, **19**, 509.
12. J. Alauzun , A. Mehdi, C. Reyé and R. J. P. Corriu, *J. Am. Chem. Soc.*, 2006, **128**, 8718.
13. K. Motokura, N. Fujita, K. Mori, T. Mizugaki, K. Ebitani and K. Kaneda, *J. Am. Chem. Soc*,. 2005, **127**, 9674.
14. K. Motokura, M. Tada and Y. Iwasawa, *J. Am. Chem. Soc.*, 2009, **131**, 7944.
15. A. Takagaki, M. Ohara, S. Nishimura and K. Ebitani, *Chem. Commun.*, 2009, 6276.
16. M. Ohara, A. Takagaki, S. Nishimura and K. Ebitani, *Applied Catalysis A*, 2010, **383** 149.
17. A. Takagaki, M. Ohara, S. Nishimura and K. Ebitani, *Chem. Lett.*, 2010, **39**, 838.
18. A. Takagaki, M. Takahashi, S. Nishimura and K. Ebitani, *ACS Catal.*, 2011, **1** 1562.
19. J. Tuteja, S. Nishimura and K. Ebitani, *Bull. Chem. Soc. Jpn.*, 2012, **85**, 275.
20. S. Miyata, *Clays Clay Miner.*, 1980, **28**, 50.
21. P. J. Sideris, U. G. Nielsen, Z. Gan and C. P. Grey, *Science*, 2008, **321**, 113.
22. S. Nishimura, A. Takagaki, K. Ebitani, *Green Chem.*, 2013, **15**, 2026.
23. H. Tamura, J. Chiba, M. Ito, T. Takeda, S. Kikkawa, Y. Mawatari and M. Tabata, *J Colloid. Interface Sci.*, 2006, **300**, 648.
24. U. Costantino, F. Marmottini, M. Nocchetti and R. Vivani, *Eur. J. Inorg. Chem.*, 1998, 1439.
25. J.-M. Oh, S.-H. Hwang and J.-Ho Choy, *Solid State Ionics.*, 2002, **151**, 285.
26. Z. Liu, R. Ma, M. Osada, N. Iyi, Y. Ebina, K. Takada and T. Sasaki, *J. Am. Chem. Soc.*, 2006, **128**, 4872.
27. Y. Yang, X. Zhao, Y. Zhu and, F. Zhang, *Chem. Mater.*, 2012, **24**, 81.
28. Y. Yanmin, Z. Xiaofei, Z. Yue and Z. Fazhi, *J. Mater. Chem*,. 2000, **10**, 2754.
29. T. Honma, M. Nakajo, T. Mizugaki, K. Ebitani and K. Kaneda, *Tetrahedron Lett.*, 2002, **43**, 6229.
30. Y. Zhao, F. Li, R. Zhang, D. G. Evans and X. Duan, *Chem. Mater.*, 2002, **14**, 4286.
31. S. Abelló, S. Mitchell, M. Santiago, G. Stoica and J. Pérez-Ramírez *J. Mater. Chem.*, 2010, **20**, 5878.
32. M. A. Aramendía, V. Borau, C. Jiménez, J. M. Marinas, J. R. Ruiz and F. J. Urbano, *J.Solid State Chem.*, 2002, **168**, 156.

33. S. P. Paredes, G. Fetter, P. Bosch and S. Bulbulian, *J. Mater. Sci.*, 2006, **41**, 3377.
34. M. R. Othman and J. Kim, *J. Sol-Gel Sci. Technol.*, 2008, **47**, 274.
35. F. Puoci, F. Iemma, G. Cirillo, M. Curcio, O. I. Parisi, U. G. Spizzirri and N. Picci, *Eur. Polym. J.*, 2009, **45**, 1634.
36. D. Tichit, A. Rolland, F. Prinetto, G. Fetter, M. J. Martınez-Ortız, M. A. Valenzuela and P. Bosch, *Mater. Chem.*, 2002, **12**, 3832.
37. M. R. Othman, Z. Helwani, Martunus and W. J. N. Fernando, *Appl. Organomet. Chem.*, 2009, **23**, 335.
38. F. Kooli, V. Rives and M. A. Ulibarri, *Inorg. Chem.*, 1995, **34**, 5114.
39. M. del Arco, P. Malet, R. Trujillano and V. Rives, *Chem. Mater.*, 1999, **11**, 624.
40. U. Olsbye, D. Akporiaye, E. Rytter, M. Ronnekleiv and E. Tangstad, *Appl. Catal. A*, 2002, **224**, 39.
41. F. Kovanda, T. Grygar, V. Dorničák, T. Rojka, P. Bezdička and K. Jirátová, *Appl. Clay Sci.*, 2005, **28**, 121.
42. M. Adachi-Pagano, C. Forano and J.-P. Besse, *Chem. Commun.*, 2000, 91-92.
43. E. Gardner, K. M. Huntoon and T. J. Pinnavaia, *Adv. Mater.*, 2001, **13**, 1263.
44. S. O'Leary, D. O'Hare and G. Seeley, *Chem. Commun.*, 2002, 1506-1507.
45. T. Hibino, *Chem. Mater.*, 2004, **16**, 5482.
46. W. Chen, L. Feng and B. Qu, *Chem. Mater.*, 2004, **16**, 368.
47. H. Kang, Y. Shu, Z. Li, B. Guan and S. Peng, *Carbohydr. Polym.*, 2014, **100**, 158.
48. F. Winter, A. J. van Dillen and K. P. de Jong, *Chem. Commun.*, 2005, 3977.
49. L. Li and J. Shi, *Chem. Commun.* 2008, 996.
50. M. Shao, F. Ning, J. Zhao, M. Wei, D. G. Evans and X. Duan, *J. Am. Chem. Soc.*, 2012, **134**, 1071.
51. M. Shao, F. Ning, Y. Zhao, J. Zhao, M. Wei, D. G. Evans and X. Duan, *Chem. Mater.*, 2012, **24**, 1192.
52. C. Chen, P. Wang, T.-T. Lim, L. Liu, S. Liu R. Xu, *J. Mater. Chem. A*, 2013, **1**, 3877.
53. S. D. Jiang, Z. M. Bai, G. Tang, L. Song, A. A. Stec, T. R. Hull, Y. Hu and W. Z. Hu, *ACS Appl. Mater. Interfaces.*, 2014, **6**, 14076.
54. J. Wang, R. Zhu, B. Gao, B. Wu, K. Li, X. Sun, H. Liu and S. Wang, *Biomaterials*, 2014, **35**, 466.
55. C. Chen, R. Felton, J. C. Buffet and D. O'Hare, *Chem. Commun.*, 2015, **51**, 3462.

56. J. S. Valente, J. Prince, A. M. Maubert, L. Lartundo-Rojas, P. Angel, G. Ferrat, J. G. Hernandez and E. Lopez-Salinas, *J. Phys. Chem. C*, 2009, **113**, 5547–5555.
57. J. Zhang, Y. F. Xu, G. Qian, Z. P. Xu, C. Chen and Q. Liu, *J. Phys. Chem. C*, 2010, **114**, 10768.
58. T. Shishido, M. Sukenobu, H. Morioka, R. Furukawa, H. Shirahase and K. Takehira, *Catal. Lett.*, 2001, **73**, 21.
59. T. Shishido, M. Sukenobu, H. Morioka, M. Kondo, Y. Wang, K. Takaki and K. Takehira, *Appl. Catal. A*, 2002, **223**, 35.
60. K. Ebitani, K. Motokura, K. Mori, T. Mizugaki and K. Kaneda, *J. Org. Chem.*, 2006, **71**, 5440.
61. N. D. Hutson, *Chem. Mater.*, 2004, **16**, 4135.
62. M. K. Ram Reddy, Z. P. Xu, G. Q. (Max) Lu, and J. C. Diniz da Costa, *Ind. Eng. Chem. Res.*, 2006, **45**, 7504.
63. M. R. Othman, N. M. Rasid and W. J. N. Fernando, *Chem. Eng. Sci.*, 2006, **61**, 1555.
64. N. D. Hutson and B. C. Attwood, *Adsorption*, 2008, **14**, 781-789.
65. N. Iyi, T. Matsumoto, Y. Kaneko and K. Kitamura, *Chem. Mater.*, 2004, **16**, 2926.
66. Y. F. Lung, Y. S. Sun, C. K. Lin, J. Y. Uan and H. H. Huang, *Sci. Rep.*, 2016, **6**, 32458.
67. J.-H. Choy, S.-Y. Kwak, J.-S. Park, Y.-J. Jeong and J. Portier, *J. Am. Chem. Soc.*, 1999, **121**, 1399.
68. S. Aisawa, H. Hirahara, K. Ishiyama, W. Ogasawara, Y. Umetsu and E. Narita, *J. Solid State Chem.*, 2003, **174**, 342.
69. J. H. Lee, S. W. Rhee and D.-Y. Jung, *Chem. Mater.*, 2004, **16**, 3774.
70. K. Yamaguchi, K. Mori, T. Mizugaki, K. Ebitani, and K. Kaneda, *J. Org. Chem.*, 2000, **65**, 6897.
71. O. D. Pavel, B. Cojocaru, E. Angelescu and V. I. Pârvulescu, *Appl. Catal. A*, 2011, **403**, 83.
72. M. J. Climent, A. Corma, S. Iborra, K. Epping and A. Velty, *J. Catal.*, 2004, **225**, 316.
73. H. C. Greenwell, P. J. Holliman, W. Jones and B. V. Velasco, *Catal. Today*, 2006, **114**, 397.
74. D.-G. Crivoi, R.-A. Miranda, E. Finocchio, J. Llorca, G. Ramis, J. E. Sueiras, A. M. Segarra and F. Medina, *Appl. Catal. A*, 2016, **519**, 116.
75. R. Sato, H. Choudhary, S. Nishimura and K. Ebitani, *Org. Process Res. Dev.*, 2015, **19**, 449.
76. A. Onda, T. Ochi, K. Kajiyoshi and K. Yanagisawa, *Catal. Commun.* 2008, **9**, 1050.

77. K. Teramura, S. Iguchi, Y. Mizuno, T. Shishido and T. Tanaka, *Angew. Chem. Int. Ed. Engl.*, 2012, **51**, 8008.

78. S. Iguchi, K. Teramura, S. Hosokawa and T. Tanaka, *Catal. Today*, 2015, **251**, 140.

79. S. Iguchi, S. Kikkawa, K. Teramura, S. Hosokawa, T. Tanaka, *Phys. Chem. Chem. Phys.*, 2016, 13811.

80. L. Hora, V. Kelbichová, O. Kikhtyanin, O. Bortnovskiy and D. Kubička, *Catal. Today* 2014, **223**, 138.

81. E. Angelescu, O. D. Pavel, R. Bîrjega, R. Zăvoianu, G. Costentin and M. Che, *Appl. Catal. A*, 2006, **308**, 13.

82. M. Fuming, P. Zhi and L. Guangxing, *Org. Process Res. Dev.*, 2004, **8**, 372.

83. E. Li, Z. P. Xu and V. Rudolph, *Appl. Catal. B*, 2009, **88**, 42.

84. J. Nowicki, J. Lach, M. Organek and E. Sabura, *Appl. Catal. A*, 2016, **524**, 17.

85. J. R. Ruiz, C. Jiménez-Sanchidrián and J. M. Hidalgo, *Catal. Commun.*, 2007, **8**, 1036.

86. K. Kaneda, T. Yamashita, T. Matsushita and K. Ebitani, *J. Org. Chem.*, 1998, **63**, 1750.

87. N. Kakiuchi, Y. Maeda, T. Nishimura and S. Uemura, *J. Org. Chem.*, 2001, **66**, 6620.

88. K. Motokura, D. Nishimura, K. Mori, T. Mizugaki, K. Ebitani and K. Kaneda, *J. Am. Chem. Soc.*, 2004, **126**, 5662.

89. T. Mitsudome, Y. Mikami, H. Funai, T. Mizugaki, K. Jitsukawa and K. Kaneda, *Angew. Chem. Int. Ed. Engl.*, 2008, **47**, 138.

90. T. Mitsudome, A. Noujima, T. Mizugaki, K. Jitsukawa and K. Kaneda, *Green Chem.*, 2009, **11**, 793.

91. W. Fang, Q. Zhang, J. Chen, W. Deng and Y. Wang, *Chem. Commun.*, 2010, **46**, 1547.

92. T. Mitsudome, A. Noujima, Y. Mikami, T. Mizugaki, K. Jitsukawa and K. Kaneda,. *Angew. Chem. Int. Ed. Engl.*, 2010, **49**, 5545.

93. A. Tsuji, K. T. V. Rao, S. Nishimura, A. Takagaki and K. Ebitani, *ChemSusChem*, 2011, **4**, 542.

94. Ministry of Economy, Trade and Industry, *Japan's Energy White Paper 2016*, Agency for Natural Resources and Energy, 2016.11.9.

95. G. W. Huber, J. N. Chheda, C. J. Barrett and J. A. Dumesic, *Science*, 2005, **308**, 1446.

96. R. Karinen, K. Vilonen and M. Niemelä, *ChemSusChem*, 2011, **4**, 1002.

97. P. Gallezot, *Chem. Soc. Rev.*, 2012, **41**, 1538.

98. P. McKendry, *Bioresour. Technol.*, 2002, **83**, 37.

99. M. F. Demirbas, M. Balat and H. Balat, *Energ. Conver. Manage.*, 2009, **50**, 1746.

100. D.O. Hall and F. Rosillo-Calle, *World Energy Council*, London, 1998.

101. E. Tsukuda, S. Sato, R. Takahashi and T. Sodesawa, *Catal. Commun.* 2007, **8**, 1349.

102. H. Atia, U. Armbruster and A. Martin, *J. Catal.*, 2008, **258**, 71.

103. T. Kurosaka, H. Maruyama, I. Naribayashi and Y. Sasaki, *Catal. Commun.*, 2008, **9**, 1360.

104. L. Huang, Y. Zhu, H. Zheng, G. Ding, Y. Li, *Catal. Lett.*, 2009, **131**, 312.

105. T. Lloyd and C. E. Wyman, *Appl. Biochem. Biotechnol.*, 2003, **105**, 53.

106. H. Kobayashi and A. Fukuoka, *Green Chem.*, 2013, **15**, 1740.

107. J. S. Luterbacher, D. M. Alonso and J. A. Dumesic, *Green Chem.*, 2014, **16**, 4816.

108. H. Kobayashi, M. Yabushita, T. Komanoya, K. Hara, I. Fujita and A. Fukuoka, *ACS Catal.*, 2013, **3**, 581.

109. P.-W. Chung, A. Charmot and O. A. Olatunji-Ojo, *ACS Catal.*, 2014, **4**, 302.

110. P.-W. Chung, M. Yabushita, A. T. To, Y. Bae, J. Jankolovits, H. Kobayashi, A. Fukuoka, and A. Katz, *ACS Catal.*, 2015, **5**, 6422.

111. A. T. To, P.-W. Chung and A. Katz, *Angew. Chem. Int. Ed.*, 2015, **54**, 11050.

112. S. Suganuma, K. Nakajima, M. Kitano, D. Yamaguchi, H. Kato, S. Hayashi and M. Hara, *J. Am. Chem. Soc.*, 2008, **130**, 12787.

113. X. Zhao, J. Wang, C. Chen, Y. Huang, A. Wang and T. Zhang, *Chem. Commun.*, 2014, **50**, 3439.

114. P. Dornath, H. J. Cho, A. Paulsen, P. Dauenhauer and W. Fan, *Green Chem.*, 2015, **17**, 769.

115. H. Kobayashi, H. Kaiki, A. Shrotri, K. Techikawara and A. Fukuoka, *Chem. Sci.*, 2016, **7**, 692.

116. J. N. Chheda, G. W. Huber and J. A. Dumesic, *Angew. Chem. Int. Ed. Engl.*, 2007, **46**, 7164.

117. C. H. Zhou, X. Xia, C. X. Lin, D. S. Tong and J. Beltramini, *Chem. Soc. Rev.*, 2011, **40**, 5588.

118. H. Choudhary, S. Nishimura and K. Ebitani, *Chem. Lett.*, 2012, **41**, 409.

119. B. Danon, G. Marcotullio and W. de Jong, *Green Chem.*, 2014, **16**, 39.

120. D. Montané, J. Salvadó, C. Torras and X. Farriol, *Biomass and Bioenergy*, 2002, **22**, 295.

121. R. H. Kottke, *Kirk-Othmer Encyclopedia of Chemical Technology, 4th ed.*, John Wiley and Sons, New York, 1999, **23**.

122. M. J. Antal Jr., T. Leesomboon, W. S. Mok and G. N. Richards, *Carbohydr. Res.*, 1991, **217**, 71.

123. H. D. Mansilla, J. Baeza, S. Urzúa, G. Maturana, J. Villaseñor and N. Durán, *Bioresour. Technol.*, 1998, **66**, 189.

124. C. Moreau, R. Durand, D. Peyron, J. Duhamet and P. Rivalier, *Ind. Crops. Prod.*, 1998, **7**, 95.

125. A. Dias, M. Pillinger and A. Valente, *J. Catal.*, 2005, **229**, 414.

126. A. Dias, S. Lima, D. Carriazo, V. Rives, M. Pillinger and A. Valente, *J. Catal.*, 2006, **244**, 230.

127. E. Lam, E. Majid, A. C. W. Leung, J. H. Chong, K. A. Mahmoud and J. H. T. Luong, *ChemSusChem*, 2011, **4**, 535.

128. G. H. Jeong, E. G. Kim, S. B. Kim, E. D. Park and S. W. Kim, *Microporous and Mesoporous Mater.*, 2011, **144**, 134.

129. I. Agirrezabal-Telleria, J. Requies, M. B. Güemez and P. L. Arias, *Appl. Catal. B*, 2014, **145**, 34.

130. J. B. Binder, J. J. Blank, A. V. Cefali and R. T. Raines, *ChemSusChem*, 2010, **3**, 1268.

131. R. Weingarten, J. Cho, Wm. C. Conner, Jr. and G. W. Huber, *Green Chem.*, 2010, **12**, 1423.

132. M. J. Climent, A. Corma and S. Iborra, *Green Chem.*, 2011, **13**, 520.

133. V. Choudhary, S. I. Sandler and D. G. Vlachos, *ACS Catal.*, 2012, **2**, 2022.

134. Y. Roman-Leshkov, M. Moliner, J. A. Labinger and M. E. Davis, *Angew. Chem. Int. Ed. Engl.*, 2010, **49**, 8954.

135. T. Suzuki, T. Yokoi, R. Otomo, J. N. Kondo and T. Tatsumi, *Appl. Catal. A*, 2011, **408**, 117.

Chapter 2

Development of Acid-Base Catalytic System for One-pot Synthesis of Furfural Derivatives from Pentoses

Chapter 2-1

One-pot Synthesis of Furfural Derivatives from Pentoses using Solid Acid and Base Catalysts

Abstract

One-pot synthesis of (2-furanylmethylene)malononitrile, a Knoevenagel product of furfural with malononitrile, from xylose efficiently proceeded by combined use of acid Amberlyst-15 and acid-base Cr/hydrotalcites in 44% yield. Structural characterization was carried out using X-ray diffraction (XRD), X-ray photoelectron spectroscopy (XPS), X-ray absorption spectroscopy, and nitrogen adsorption measurements. The Lewis acidic properties of the highly active Cr/HT were investigated using the Meerwein–Ponndorf–Verley (MPV) reaction. It was confirmed that the prepared Cr/HT possessed the Lewis acid Cr_2O_3 on the HT surface. Thus, combined use of the dispersed Lewis acid Cr_2O_3 and the Brønsted base HT facilitated the isomerization step of aldose into ketose and strongly promoted activity for the synthesis of furfural derivatives from aldoses through isomerization, dehydration and Knoevenagel condensation reactions in a one-pot manner.

Introduction

Biomass resources have attracted much attention because they can serve as a sustainable source of renewable fuels and chemicals in a carbon-neutral fashion.[1-3] Lignocellulosic biomass, the most abundant woody biomass, is mainly composed of monosaccharides in the form of cellulose, hemicellulose, and lignin.[4,5] Conversion of xylose, a pentose derived from hemicellulose, into value-added chemicals such as ethanol, xylitol, furfural, furfuryl alcohol, levulinic acid, and γ-valerolactone is one of reactions worth conducting in biorefinery. Especially, furfurals have been extensively focused on fabrications of the practical uses of biomass resources because they have great potentials as non-petroleum building blocks in the production of fine chemicals, polymers, and phamaceuticals.[5-9]

Moreau et al. have reported the synthesis of furfural from xylose in good selectivity (90-95%) over solid acid catalysts such as H-mordenite and H-Y faujasite.[10] Furthermore dehydration of xylose to furfural is examined using various solid acid catalysts like Nafion 117,[11] ion-exchange resins,[12] sulfated zirconia,[13] porous niobium silicates,[14] sulfonic acid modified mesoporous shell silica bead,[15] and zeolite-based catalysts.[16-21] However, these reactions were performed at high temperature (>423 K).

In advanced researches, it was demonstrated that furfurals was effectively formed from aldoses such as glucose, xylose, and arabinose in a one-pot manner involving isomerization of aldose into ketose catalyzed by solid base hydrotalcite and successive dehydration of ketose into the corresponding furfurals by Brønsted acid Amberlyst-15 at 373 K.[22-24] Binder et al.[25] and Suzuki et al.[26] have reported the conversion of xylose into furfural under a mild condition (373 K) using $CrCl_2$ with LiBr and SO_4^{2-}/SnO_2. These reports proposed that Lewis acid of $CrCl_3$ or SnO_2 promoted isomerization of xylose (aldopentose) to xylulose (ketopentose), and then co-existing Brønsted acid catalyzed the further dehydration to furfural.

Many researchers reported that furfural derivatives obtained by C-C bond formation such as aldol condensation can be converted into chemicals and biofuel alkanes.[27-32] The Knoevenagel condensation, a C-C bond formation of carbonyl compounds (aldehyde and ketones) with active methylene compounds, of furfural can also provide value-added furfural derivatives. Soliman et al. demonstrated that (2-furanylmethylene) malononitrile (**2**, in Scheme 1), a Knoevenagel product of furfural with malononitrile, is expected as a semiconducting organic material such as photovoltaic devices fabrication.[33]

Mg-Al hydrotalcite (HT; $[Mg^{2+}{}_{1-x}Al^{3+}{}_{x}(OH)_2]^{x+}\ A^{n-}{}_{x/n}\cdot mH_2O$) is the most well-known layered double hydroxides (LDHs) which is composed of brucite-like positively charged two-dimensional sheets and interlayer anions A^{n-} such as carbonate and hydroxide. HT is generally used as a Brønsted base catalyst for epoxidation,[34,35] transesterification,[36] aldol condensation,[37,38] and the Knoevenagel reaction.[39-41] Although HT is known as an effective support,[42-47] it have been rarely used for the synthesis of furfural from pentoses and the Knoevenagel condensation of furfural.

Herein, I report (1) the Knoevenagel condensation of furfural using HT as a solid base catalyst and (2) a direct synthesis of (2-furanylmethylene)malononitrile from xylose using various metal supported HTs (M/HTs) and solid acid Amberlyst-15 catalysts in a one-pot manner (Scheme 1). Though there were many previous reports about the Knoevenagel condensation of various aldehyde over HT catalyst such as benzaldehyde,[39-41] salicylaldehyde,[39] 4-methylbenzaldehyde,[39] and so on, this is the first report about the application of HT for the Knoevenagel condensation of furfural and *in situ* formed furfural from xylose and arabinose.

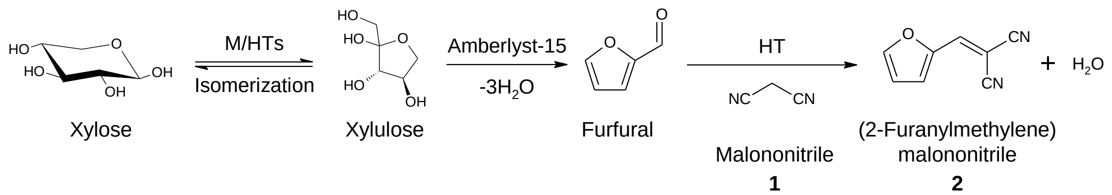

Scheme 1 One-pot synthesis of (2-furanylmethylene)malononitrile from xylose.

Experimental

Materials and synthesis of M/HTs catalyst

Mg-Al hydrotalcite (HT) (AD500NS; Mg/Al = 3.1, MgO 38.1%, Al_2O_3 15.7%, CO_2 8.1%) were purchased from Tomita Pharmaceutical Co., Ltd.. Stannic chloride pentahydrate ($SnCl_4\cdot5H_2O$), chromium chloride hexahydrate ($CrCl_3\cdot6H_2O$), lanthanum chloride heptahydrate

($LaCl_3 \cdot 7H_2O$), ferric chloride hexahydrate ($FeCl_3 \cdot 6H_2O$), zirconium oxychloride octahydrate ($ZrCl_2O \cdot 8H_2O$), and nickel chloride hexahydrate ($NiCl_2 \cdot 6H_2O$) were supplied by Wako Pure Chemical Ind., Ltd. Co. whereas copper chloride dihydrate ($CuCl_2 \cdot 2H_2O$) and *N*,*N*-dimethylformamide (DMF) were served from Kanto Chem. Co. Ltd..

The metal supported hydrotalcites (M/HTs) were prepared by an impregnation method (adsorption) using HT and an aqueous solution of various metal chlorides: each metal chloride was dissolved in 100 mL of water, then 2 g of HT was added. The metal content was adjusted to 9 wt% in theory. After stirred at 353 K for 24 h, the obtained paste was filtered, washed with 2L of distilled water, and then dried at 383 K for overnight.

Reactions

All reactions were performed in a Schlenk tube attached with a reflex condenser under an N_2 flow (30 mL min^{-1}). The reaction was typically performed using 0.1-0.2 g of solid base HT and/or 0.1 g of solid acid Amberlyst-15 in 3 mL of DMF at 373-393 K. For the Knoevenagel condensation reaction ofTh furfural, 1 mmol of furfural and 1.2 eq. of active methylene compounds were used. The yields of the Knoevenagel products were calculated on the basis of furfural. One-pot synthesis of furfural derivatives from pentoses was carried out *via* a two-step reaction without catalyst separation: Step 1) the one-pot conversion of pentoses into furfural using solid acid and base catalysts, and Step 2) the reaction mixture after the Step 1 was cooled down to room temperature without stirring, then donor compound was added, thereafter, the following Knoevenagel condensation was conducted under vigorous stirring. The yields of furfural and furfural derivatives were calculated on the basis of xylose.

Recyclability tests of Cr/HT and Amberlyst-15 for the one-pot synthesis of (2-furanylmethylene)malononitrile from xylose was consumed as follows: After the reaction, catalysts were collected and washed with DMF and water for several times, and then reused for the next reaction.

All products were analyzed by a GC-FID (SHIMADZU, GC-2014) equipped with a non-polar column (Agilent, DB-1).

Characterizations

X-ray diffraction (XRD) patterns were collected on a SmartLab (Rigaku) using a Cu Kα X-ray source (40 kV, 30 mA). XRD patterns were compared with a data base in the international centre for diffraction data (ICDD). Nitrogen adsorption measurements were carried out to determine the BET (Brunauer-Emmett-Teller) specific surface area. The measurements were conducted at 77 K on a Belsorp-max (BEL. Japan, Inc.). X-ray photoelectron spectroscopy (XPS) analyses were performed with a Kratos AXIS-URTRA DLD (SHIMADZU) using a monochromatic Al Kα source (10 mA, 15 kV). The binding energies were calibrated with C 1s level (284.5 eV) as the internal standard. X-ray absorption spectra in Cr *K*-edge were recorded at a BL5S1 of Aichi Synchrotron Radiation Research Center (2nd period, 2013). All samples were grained and pressed to a pellet (Ø = 10 mm). The energy for Cr *K*-edge XAFS spectra were adjusted at the edges of Cu foil (8.9800 keV). Double Si(111) single crystals were used for division of energy. The obtained spectra were analyzed with the REX2000 software (ver. 2.5.92, Rigaku).

Results and discuttion

The Knoevenagel condensation of furfural

Preliminary, I examined the Knoevenagel condensation of furfural over the base HT catalyst with various active methylene compounds of malononitrile (**1**), ethyl cyanoacetate (**3**), diethylmalonate (**5**) or propionaldehyde (**7**). These results were shown in Table 1. The Knoevenagel condensation of furfural with malononitrile (**1**) was successfully performed over HT catalyst; it afforded (2-furanylmethylene)malononitrile (**2**) in >99% yield (entry 1). The typical solid base catalysts of MgO, $Mg(OH)_2$, CaO and $NaHCO_3$ also showed good or less activity for the reaction but HT catalyst exhibited the best catalytic activity among them (entries 2-6). Thus, HT was further applied to the Knoevenagel condensation of furfural with various active methylene compounds of **3**, **5** and **7**. In the reaction of furfural with **3** (entry 7), the HT catalyst gave 93% conversion of furfural and 73% yield of ethyl-(2E)-2-cyano-3-(2-furyl)-

acrylate (**4**). On the other hand, in the reaction with **5**, the corresponding diethyl 2-furfuryliden malonate (**6**) was obtained only a 22% yield (entry 8) because of low acidic strength of **5** (*p*Ka ~ 13). However, when the amount of HT was increased to 0.2 g, the reaction was promoted and yielded **6** with 41% (entry 8b). The HT catalyst also showed a good activity for the reaction of **7** and furfural; it afforded 3-(2-furyl)-2-methylacrolein (**8**) with 71% yield in 1 h (entry 9b). From these results, it was indicated that the HT exhibited a good activity for the Knoevenagel condensation of furfural with various active methylene compounds such as nitrile, aldehyde and ester.

Table 1 The Knoevenagel condensation of furfural with various active methylene compounds.[a]

Entry	Donor	Product	Catalyst	Time	Conversion of furfural /%	Yield of product /%
1	1 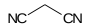	2 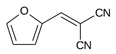	HT	15 min	>99	>99
2			MgO	15 min	>99	83
3			$Mg(OH)_2$	15 min	>99	83
4			CaO	15 min	>99	1
5			$NaHCO_3$	15 min	99	64
6			—	15 min	26	15
7	3 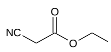	4 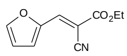	HT	1 h	93	73
8[c]	5 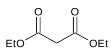	6 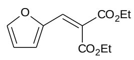	HT	18 h	54, 79[b]	22, 41[b]
9	7 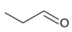	8 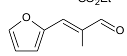	HT	1 h	57, 84[b]	52, 71[b]

[a]*Reaction conditions*: furfural (1 mmol), donor (1.2 mmol), catalyst (0.1 g, 0.2 g[b]), DMF (3 mL), temp. (373 K, 393 K[c]), N_2 flow (30 mLmin^{-1}). [b]*Reaction conditions*: furfural (1 mmol), donor (1.2 mmol), catalyst (0.2 g), DMF (3 mL), temp. (373 K), N_2 flow (30 mL min^{-1}). [c]*Reaction conditions*: furfural (1 mmol), donor (1.2 mmol), catalyst (0.1 g), DMF (3 mL), temp. (393 K), N_2 flow (30 mL min^{-1}).

One-pot synthesis of furfural derivatives from xylose

In the next stage, the one-pot synthesis of furfural derivatives from xylose using solid acid Amberlyst-15 and base HT was attempted. The results are shown in Table 2. A combined use of Amberlyst-15 and HT gave 21% yield for the one-pot synthesis of **2** from xylose (entry

1). In the reaction with **3** or **5**, 7% or 4% yield of **4** or **6** was formed with 14% and 12% yield of furfural intermediate, respectively (entries 2 and 3). On the other hand, when active methylene compounds (**7**) were used for one-pot synthesis, no Knoevenagel product was observed (entry 4); nevertheless the donor conversion was high. Even though the used catalysts of HT and Amberlyst-15 were removed after the Step 1 and fresh base HT catalyst was added for a further Knoevenagel condensation reaction with **7**, the Knoevenagel product (**8**) was not obtained (entry 4d). These results suggested that no activity in the one-pot synthesis of **8** was resulted in the degradation of HT during Step 1. Because the donor of **7** was aldehyde type, one of the active functional groups, the reaction between donor **7** and xylose, xylulose and/or some degradation products would occurred preferentially, and the successive Knoevenagel condensation was prohibited. Arabinose, a structural isomer of xylose, was also examined as substrate for one-pot synthesis of **2**. In the case of arabinose, a combined use of HT and Amberlyst-15 gave 17% of **2** (entry 5).

Table 2 One-pot synthesis of furfural derivatives from pentoses.[a]

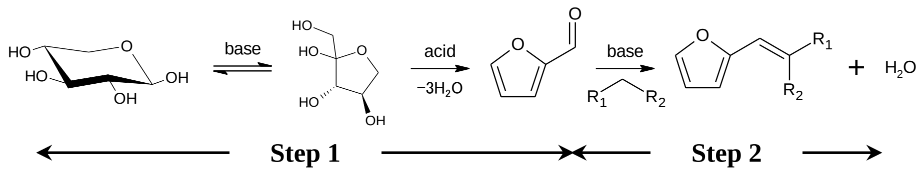

Entry	Donor	Product	Conv. of donor /%	Yield /%	
				furfural	Product
1	1	2	60	0	21
2	3	4	18	14	7
3[b]	5	6	48	12	4
4	7	8	98, 90[d]	19, 12[d]	0, 0[d]
5[c]	1	2	57	0	17

[a]*Reaction conditions*: Step 1) xylose (0.67 mmol), HT (0.2 g), Amberlyst-15 (0.1 g), DMF (3 mL), 373 K, 3 h, N_2 flow (30 mL min^{-1}). Step 2) After the Step 1, the reaction mixture was cooled down to room temperature without stirring. Then 0.8 mmol of donor was added and restarted the reaction. 1 h, N_2 flow (30 mL min^{-1}). [b]393 K, Step 2 (18 h). [c]Arabinose (0.67 mmol) was used as the substrate. [d]After the Step 1, catalysts were removed and fresh HT was added for Step 2.

In order to elucidate the reaction pathway, time-course of the one-pot synthesis of **2** from xylose was monitored (Figure 1). In the Step 1 (conversion of xylose toward furfural), furfural yield gradually increased with increasing reaction time. This step depend on the reactions of isomerization of xylose to xylulose and further dehydration of xylulose to furfural reported in our previous report.[22] After the addition of **1**, furfural was immediately consumed, and the product **2** was formed (Step 2). Furfural intermediate was consumed completely for 1 h of the Step 2. These results clearly indicate that the one-pot reaction involves three elemental reactions; (i) isomerization of xylose into xylulose catalyzed by solid base HT, (ii) dehydration of xylulose into furfural by solid Brønsted acid Amberlyst-15, and (iii) the Knoevenagel condensation of furfural by solid base HT to yield the corresponding Knoevenagel products.

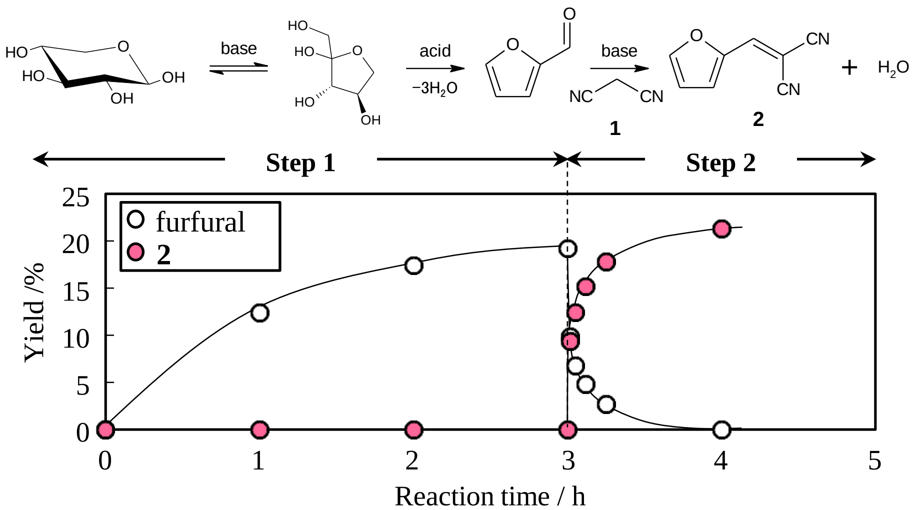

Figure 1 Time-cause of the one-pot synthesis of (2-furanylmethylene) malononitrile (**2**) from xylose. *Reaction conditions*: Step 1) xylose (0.67 mmol), HT (0.2 g), Amberlyst-15 (0.1 g), DMF (3 mL), 373 K, N_2 flow (30 mL min^{-1}). Step 2) After the step 1, the reaction mixture was cooled down to room temperature without stirring. Then 0.8 mmol of **1** was added and restarted the reaction.

Catalytic performances and structural properties of metal supported hydrotalcites (M/HTs)

Isomerization of aldopentose into ketopentose is a static reaction whereas following dehydration of ketopentoses and Knoevenagel condensation are one-way reactions in the one-pot synthesis of furfural derivatives from aldopentoses. Because the yield of intermediate furfural was limited at ~20% from xylose over bare HT and Amberlyst-15 catalysts, the following yield of **2** could not reach above that value. Thus, enhancement of the former isomerization reaction is a crucial point for the one-pot synthesis of furan derivatives. In order to increase the yield of the Knoevenagel product in one-pot synthesis from aldopentoses, various metal supported HTs (M/HTs) catalysts were prepared and applied for the one-pot reaction. Cr, Sn, Zr, Ni, La, Fe and Cu were selected as the metal species for promoting the isomerization reaction.

Figure 2(A) shows the results for one-pot synthesis of **2** from xylose using Amberlyst-15 and various M/HTs. Remarkably, the combined use of Amberlyst-15 and Cr/HT or Sn/HT resulted in 44% and 34% yield of **2**, respectively. The pairs of Amberlyst-15 and Cr/HT or Sn/HT showed better catalytic activities than that of Amberlyst-15 and Zr/HT, Ni/HT or La/HT catalysts. The activities of Fe/HT and Cu/HT were lower than bare HT. Moreover, though bare HT produced only **2** as a furfural product, some of M/HTs gave not only **2** but also intermediate furfural in one-pot synthesis. These results suggested that M/HTs possessed smaller number of base sites than HT itself. In fact, when I applied the Cr/HT for the Knoevenagel condensation of furfural with **1** under the same reaction condition as entry 1 in Table 1, it showed 97% conversion of furfural and 97% yield for **2**. These values were slightly less than the case of bare HT (>99%; Table 1, entry 1). The one-pot synthesis from arabinose was also examined with a highly active Cr/HT and Sn/HT catalyst (Figure 2(B)). These Amberlyst-15 and Cr/HT or Sn/HT gave 42% and 34% yields of **2**, respectively. From these results, it was demonstrated that Cr/HT and Sn/HT effectively increased the activity for one-pot synthesis of **2** from aldopentoses such as xylose and arabinose in comparison of bare HT.

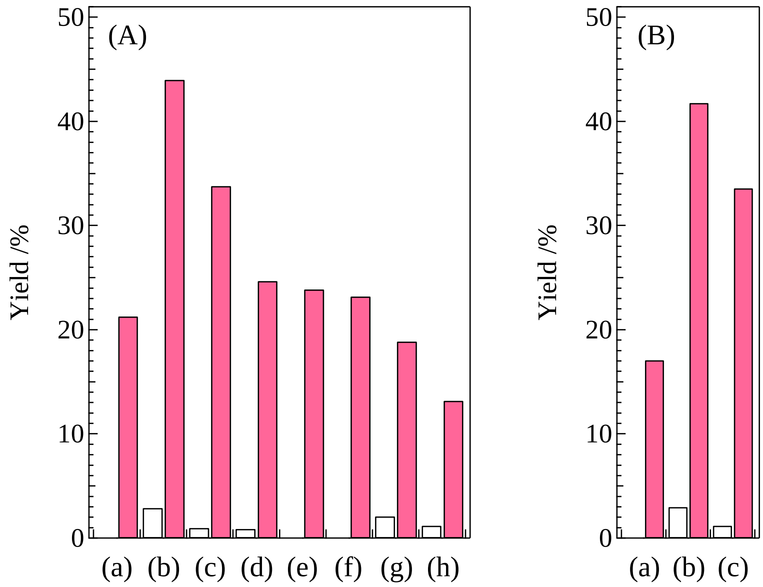

Figure 2 Yields of (■) (2-furanylmethylene)malononitrile (**2**) and (□) furfural in the one-pot transformation of (A) xylose and (B) arabinose with a combined use of Amberlyst-15 and (a) HT or various M/HTs (M: (b) Cr, (c) Sn, (d) Zr, (e) Ni, (f) La, (g) Fe, and (h) Cu) catalysts. *Reaction conditions*: Step 1) pentoses (0.67 mmol), M/HT (0.2 g), Amberlyst-15 (0.1 g), DMF (3 mL), 373 K, 500 rpm, 3 h, N_2 flow (30 mL min^{-1}). Step 2) After the Step 1, the reaction mixture was cooled down to room temperature without stirring. Then 0.8 mmol of donor was added and restarted the reaction. 373 K, 500 rpm, 1 h, N_2 flow (30 mL min^{-1}).

The reaction mixture obtained after a one-pot formation of **2** from xylose using the Cr/HT and Amberlyst-15 was filtered, and then the filtrate was analysed by ICP-AES to check the amount of eluted Cr species. No leached Cr was observed in the solution (below the detection limit of1 ppb). However, in the reuse experiments, the yield of **2** was gradually decreased with increase of the amount of furfural intermediate (Figure 3). The yield of **2** (black) gradually decreased from 44% to 28% (for 2nd run) and 20% (for 3rd run). In contrast, the yield of furfural (white), an intermediate of one-pot synthesis of **2**, increased from 3% to 7% (for 2nd and 3rd runs). These results clearly showed that step 2, the Knoevenagel condensation of furfural catalyzed by base, became slower in reuse runs. In the same time, color of the Cr/HT was changed from green to dark-brown before and after the reaction. Thus, I supposed that some of base sites of Cr/HT became covered by the adsorbents of intermediate and/or other by-products, and those caused decrease of catalytic activity for the further one-pot reactions. It is notable that even though Cr/HT and Amberlyst-15 in second reaction gave a decrease to 27% of furfurals yield, which is higher value in comparison with 21% for the pair of fresh HT and Amberlyst-15.

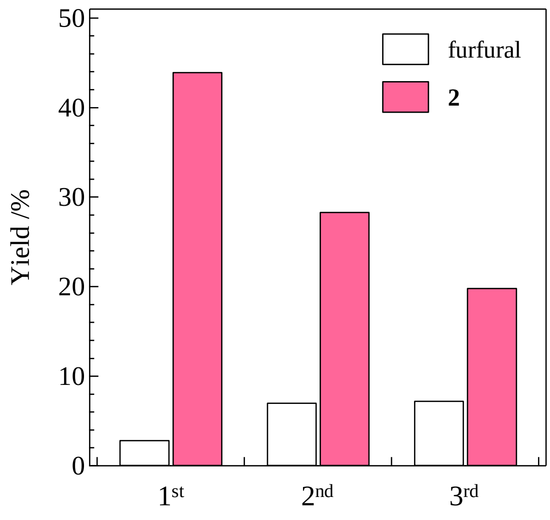

Figure 3 Recyclability of Cr/HT and Amberlyst-15 for the one-pot synthesis of **2** from xylose. *Reaction conditions*: Step 1) xylose (0.67 mmol), Cr/HT (0.2 g), Amberlyst-15 (0.1 g), DMF (3 mL), 373 K, N_2 flow (30 mL min^{-1}). Step 2) After the step 1, the reaction mixture was cooled down to room temperature without stirring. Then 0.8 mmol of malononitrile (**1**) was added, and the following reaction was started.

XRD patterns of various M/HTs and original HT as a reference were examined (Figure 4). All prepared M/HTs had a layered double hydroxide (LDH) structure of HT origin. The XRD patterns of Cr/HT, Sn/HT, Zr/HT, Ni/HT and Fe/HT had no other peaks. Since the reflection peaks attributed to LDH structure were same with the original HT, the supported metal species were widely dispersed on HT surface in the cases of them. By contrast, La/HT and Cu/HT showed another peak which was different from LDH structure. These peaks were similar to that of La(OH)(NO_3) like or $LaAlO_3$ structure and $CuAlO_2$, respectively.

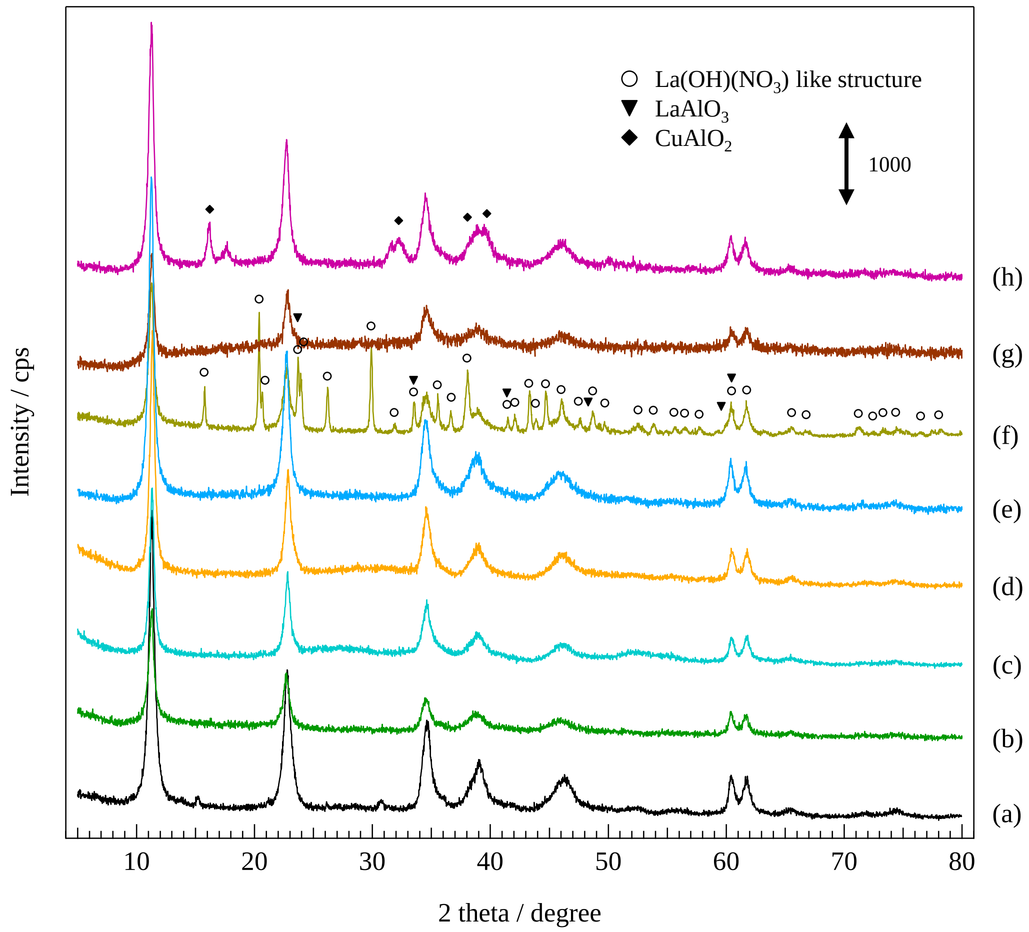

Figure 4 XRD patterns of HT and various M/HTs; (a) bare HT, (b) Cr/HT, (c) Sn/HT, (d) Zr/HT, (e) Ni/HT, (f) La/HT, (g) Fe/HT and (h) Cu/HT.

BET specific surface areas of M/HTs were also listed in Table 3. By supporting Cr, Sn, Zr or Fe onto HT, the surface area increased up to 2 - 3 times comparing from parent HT (45 m^2 g^{-1}), and Cr/HT showed the highest value (130 m^2 g^{-1}). Nevertheless Fe/HT also has high surface area (124 m^2 g^{-1}), its activity was not high (19% yield of **2** as mentioned in Figure 2(A)). It seemed that the surface area of catalyst scarcely impacted on the one-pot synthesis of furfurals from pentoses but the kinds of supported metal played a significant role for their catalytic activity in the one-pot reaction.

Table 3. Structural properties and activities for one-pot synthesis of **2** from xylose and/or arabinose.

Entry	M/HTs	Yield[a] /%		$S_{BET}{}^{c}$ / m^2 g^{-1}
		furfural	**2**	
1	HT	0, 0[b]	21, 17[b]	45
2	Cr/HT	3, 3[b]	44, 42[b]	130
3	Sn/HT	1, 1[b]	34, 34[b]	95
4	Zr/HT	1	25	89
5	Ni/HT	0	24	53
6	La/HT	0	23	46
7	Fe/HT	2	19	124
8	Cu/HT	1	13	62

[a]Yield for one-pot synthesis of **2** from xylose and/or arabinose. *Reaction conditions*: Step 1) xylose (0.67 mmol), M/HTs (0.2 g), Amberlyst-15 (0.1 g), DMF (3 mL), 373 K, N_2 flow (30 mL min^{-1}). Step 2) After the step 1, the reaction mixture was cooled down to room temperature without stirring. Then 0.8 mmol of **1** was added and restarted the reaction. [b]Arabinose (0.67 mmol) was used as the substrate. [c]BET surface area.

To determine the oxidation states of highly active Cr/HT and Sn/HT, XPS experiment was conducted. The XPS analysis of Cr $2p_{3/2}$ showed a peak at 576.5 eV which was assigned to the Cr_2O_3[48] whereas the XPS analysis of Sn $3d_{5/2}$ showed a peak at 486.0 eV corresponding to the SnO and/or SnO_2.[49] Presence of the Cr_2O_3 in Cr/HT was also supported by Cr *K*-edge XANES analysis (Figure 5). These Cr and Sn oxides were conventionally well-known as the strong Lewis acid. Therefore, I suggested that the combined use of Lewis acid derived from supported metal and base site on HT support facilitated the isomerization step of aldopentoses into ketopentoses, and which achieved their high activities.

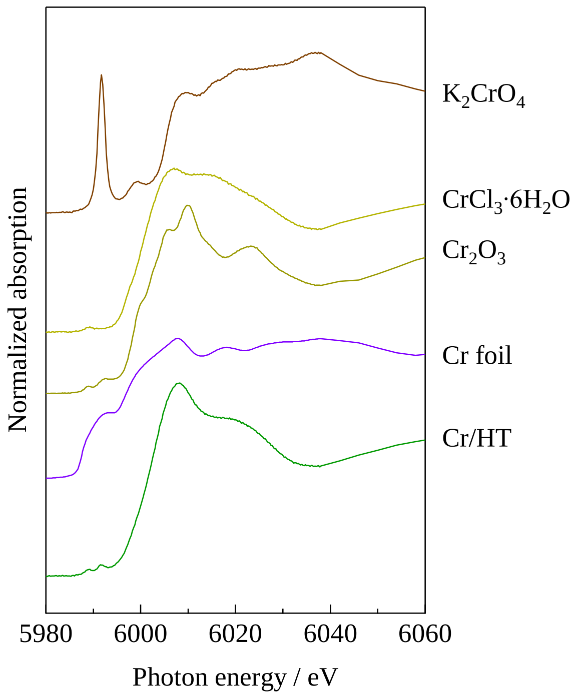

Figure 5 Cr *K*-edge XANES spectra of reference samples and Cr/HT.

Generally, the acidic properties of solid catalysts were investigated using pyridine adsorbed FT-IR technique; however, the large bands for –OH groups derived from water molecules in HT structure concealed the small bands from adsorbed pyridine species; *i.e.* the pyridine-IR spectra could not use for the Cr/HT to check the Lewis acidity. The Lewis acidity of the Cr/HT is verified by the catalytic activity for Meerwein-Ponndorf-Verley (MPV) reaction of furfural in 2-propanol toward furfuryl alcohol (FA) (Table 4). It has been known that the Lewis acid sites are able to catalyze the MPV hydride transfer reaction.[50-53] As shown in entry 3, a typical Lewis acid γ-Al_2O_3 showed high catalytic activity for the MPV reduction of furfural while the reaction did not proceed at all in the case of Brønsted acid Amberlyst-15 or blank test (entries 4 and 5). These results clearly suggested that this reaction was promoted by Lewis acid sites. In the presence of base HT, although the conversion of furfural was low, a little FA product was observed (entry 2). This seemed that one of a local location of HT surface composed by the metal oxide structure such as Mg-O-Al and which might catalyze the MPV reduction as the Lewis acid sites (though it was tiny amounts of). Nevertheless, the Cr/HT showed a much higher catalytic activity than the bare HT with 33% yield of FA. In addition, the selectivity of FA also increased up to 81% from 63%. These results strongly indicated that the dispersed Cr_2O_3 species can promote the MPV hydride transfer reaction more effectively than bare HT as Lewis acid; *i.e.* Cr/HT possessed not only Brønsted base sites of HT but also Lewis acid sites of Cr_2O_3, and they cooperatively proceeded the isomerization reaction of aldopentoses into ketopentoses in the one-pot reaction.

Table 4 MPV reduction of furfural by various solid catalysts.[a]

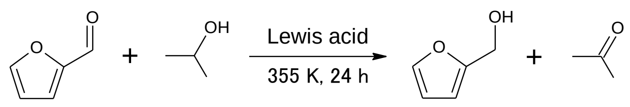

furfural 2-propanol furfuryl alcohol (FA) acetone

Entry	Catalyst	Conversion /%	Yield of FA /%	Selectivity of FA /%
1	Cr/HT	40	33	81
2	HT	14	9	63
3	γ-Al_2O_3	80	74	93
4	Amberlyst-15	34	0	0
5	—	10	0	0

[a]*Reaction conditions*: furfural (1.3 mmol), 2-propanol (83 mmol), catalyst (0.1 g), 355 K, 24 h, 500 rpm.

Role of dispersed Cr_2O_3 on hydrotalcites

In order to evaluate the role of Cr_2O_3 on HT, the one-pot synthesis of furfural from xylose *via* the isomerization of xylose into xylulose and dehydration of xylulose into furfural in various combination with HT, Cr/HT, Cr_2O_3 and/or Amberlyst-15 catalysts were examined as shown in Table 5. The use of Amberlyst-15 alone gave poor furfural yield (4%) (entry 6) because Amberlyst-15 cannot promote the isomerization of xylose into xylulose under such a low temperature (373 K). Besides, in the presence of HT, no production of furfural was observed (entry 8). This means that HT is not effective for dehydration of pentoses. An efficient production of furfural was obtained in the combined use of Amberlyst-15 and Cr/HT with 36% yield (entry 1) which was a much higher value than the Amberlyst-15 and bare HT (19%) (entry 4)¶. Because the furfural synthesis from xylose scarcely proceeded by Cr/HT (entry 7), it was clearly shown that the Cr/HT was not effective for direct dehydration of xylose but it could promote the isomerization of xylose into xylulose more than original HT. The physical mixture

Table 5 One-pot synthesis of furfural from xylose.[a]

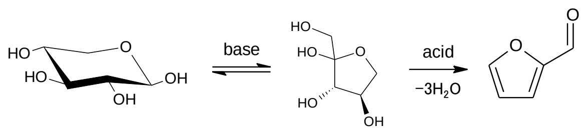

Entry	Catalyst A	Catalyst B	Yield /%
1	Cr/HT	Amberlyst-15	36
2	HT + γ-Al_2O_3[b]	Amberlyst-15	26
3	HT + Cr_2O_3[c]	Amberlyst-15	21
4	HT	Amberlyst-15	19
5	Cr_2O_3	Amberlyst-15	4
6	—	Amberlyst-15	4
7	Cr/HT	—	1
8	HT	—	0
9	Cr_2O_3	—	0

[a]*Reaction conditions*: xylose (0.67 mmol), catalyst A (0.2 g), [b]HT (0.174 g) + γ-Al_2O_3 (0.026 g), [c]HT (0.174 g) + Cr_2O_3 (0.026 g), catalyst B (0.1 g), DMF (3 mL), 373 K, 3 h, N_2 flow.

of HT, Amberlyst-15, and Cr_2O_3 was also tested for the one-pot reaction, and it showed a little improvement of furfural yield to 21% in comparison with 19% for the pair of HT and Amberlyst-15 (entries 3 and 4). In addition, when γ-Al_2O_3 possessing the higher activity in Lewis acid reaction of MPV reduction was used in instead of Cr_2O_3, the one-pot furfural synthesis was slightly promoted; 26% yield of furfural was obtained (entry 2). However, these activities were less than the combined use of Cr/HT and Amberlyst-15 (36%, entry 1). These results strongly suggested that the coexistence of Brønsted base HT and Lewis acid Cr_2O_3 or γ-Al_2O_3 is effective for the one-pot synthesis of furfural from xylose, and the Cr_2O_3 species well-dispersed on HT surface (Cr/HT) is the best structure for promoting their correlations (entries 1-3). It is noted that neither use of bulk Cr_2O_3 nor combined use of bulk Cr_2O_3 and Amberlyst-15 were ineffective for the one-pot synthesis of furfural from xylose (entries 5 and 9). These results indicated that the bulk Cr_2O_3 has no activity for both isomerization of aldopentoses into ketopentoses and dehydration of pentoses into furfural, however dispersed Cr_2O_3 species can act as promoter for the isomerization step catalyzed by HT base site (entry 1).

Reaction mechanism

Finally, the reaction mechanism of direct synthesis of furfural from xylose using Cr/HT and Amberlyst-15 is considered. It has known that the isomerization of aldose into ketose is catalyzed by both Lewis acid and base through hydride shift[54,55] and proton shift,[56,57] respectively. For instance, glucose (aldohexose) conversion into 5-hydroxymethylfurfural through the intermediate formation of fructose (ketohexose) using Lewis acidic $CrCl_2$ is reported by Pidko et al..[54] The initial attack by chromium (II) chloride to O1 results the glucopyranose ring opening. The reactive metal chloride is able to directly coordinate the substrate at the O1H site. Formation of the coordination complex with glucose initiates the isomerization reaction involving the transient formation of binuclear Cr complexes that substantially stabilizes the activated anionic sugar intermediates.[54] Ekeberg et al. reported that the isomerization of aldoses into ketoses catalyzed by base pyridine proceeds *via* the Lobry de Bruyn-Alberda van Ekenstein transformation.[56,57] It is generally agreed that the Lobry de Bruyn-Alberda van Ekenstein transformation proceeds *via* an enediol intermediate.[58] Despite being a too weak base to remove the proton from O1, pyridine is a good proton acceptor and cause polarisation of the O-H bond. It increased negative charges on O1, and which facilitates the ring opening. A proton shift will lead to a pseudo-cyclic 1,2-enediol intermediate.[57]

Based on these references, I propose the isomerization of xylose (aldopentose) into xylulose (ketopentose) over the Cr/HT catalyst as described in Figure 6, which proceeds *via* ring-opening reaction and Lobry de Bruyn-Alberda van Ekenstein aldos-ketose transformations. Lewis acidic sites of dispersed Cr_2O_3 itself possibly catalyze the isomerization of aldose into ketose *via* the direct hydride shift mechanism;[54,55] however, in the case of isomerization over the Cr/HT, it is proposed that the main active site would not be the Lewis acid Cr_2O_3 sites but the Brønsted base site on HT since the dispersed Cr_2O_3 species supported on various metal oxides exhibited less activities than the Cr/HT (Figure 7). The reaction is initiated by the direct coordination of xylose with the Lewis acidic Cr_2O_3 center (Cr_2O_3···O1, (A)). This increases positive charge on O1, and bond strength between O1 and O1H became weaker. Then the HT base site facilitates the deprotonation of the O1H, and xylopyranose is transformed to open-xylose (B). The C2H of open-xylose, an α-proton of carbonyl, is easily deprotonated by HT base (C). The generated 1,2-endiol (enolate) intermediate would form the coordination complex with Lewis acidic Cr_2O_3 on HT, and then open-xylulose is constituted by a proton shift

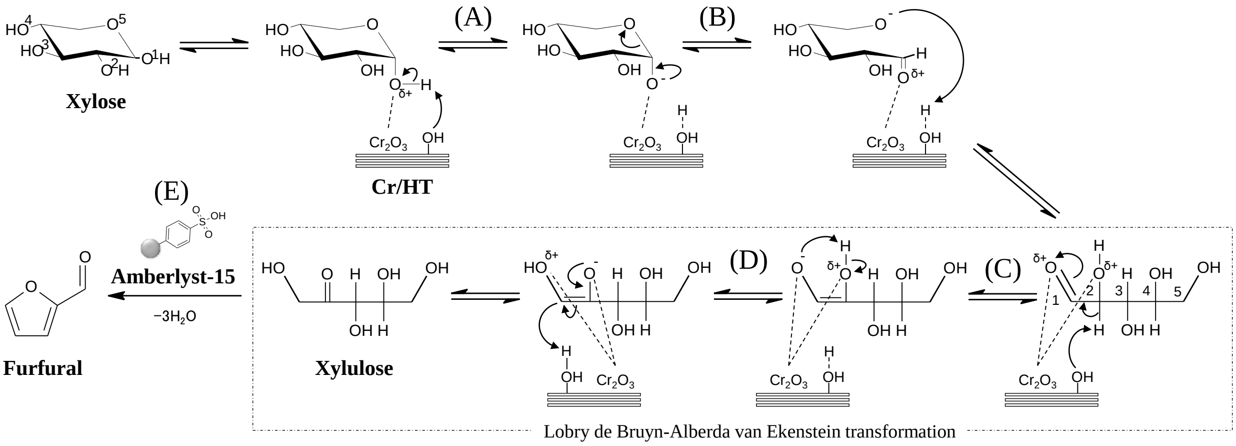

Figure 6 Proposed reaction path of direct synthesis of furfural from xylose using Cr/HT and Amberlyst-15.

from O2 to O1 (D) and protonation of C1H. Then, the generated xylulose will be dehydrated to furfural by Brønsted acid Amberlyst-15 (E). In our developed study, combined use of Cr/HT and Amberlyst-15 can provide catalytic reaction system which Lewis and Brønsted acid, and Brønsted base active sites act concertedly, and achieved the one-pot synthesis of furfural derivatives from xylose and arabinose.

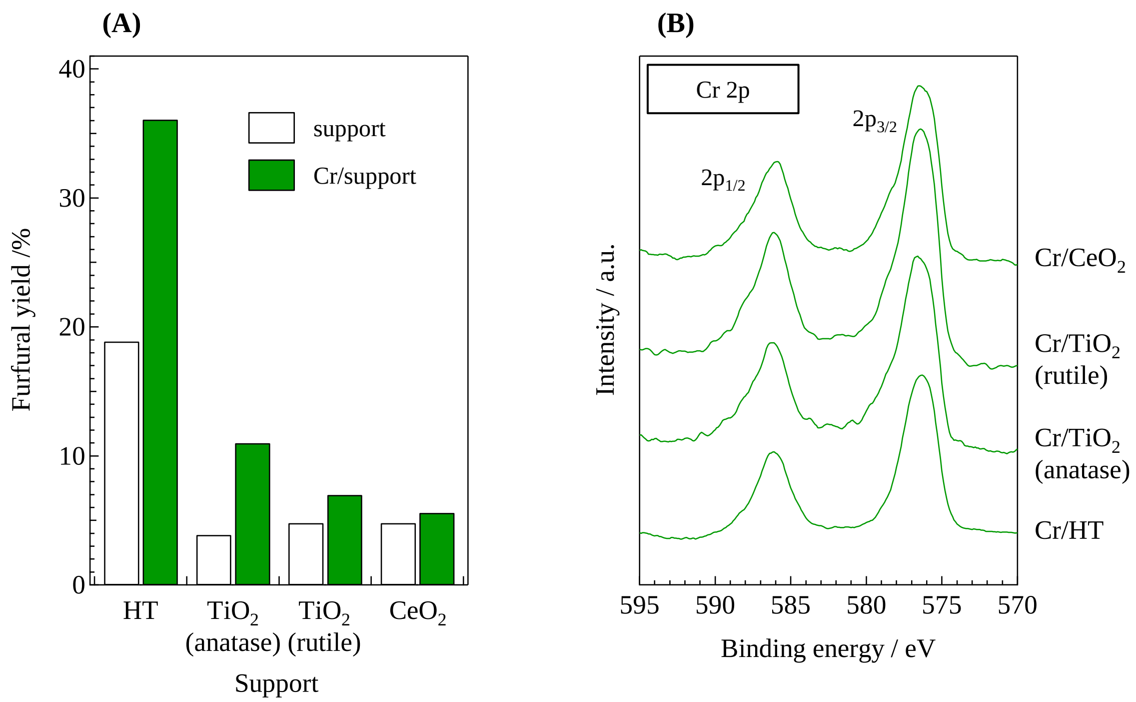

Figure 7 (A) Furfural yields for one-pot conversion of xylose using Cr-supported various metal oxides and Amberlyst-15, and (B) Cr 2p XPS spectra of the Cr-supported various metal oxides. **Reaction conditions*: xylose (0.67 mmol), support or Cr/support (0.2 g), Amberlyst-15 (0.1 g), DMF 3 mL, 373 K, 3 h, N_2 flow.

Conclusions

As a solid base catalyst, hydrotalcite (HT) showed good activity for the Knoevenagel condensation of furfural with various active methylene compounds such as nitrile, aldehyde, and ester. Direct synthesis of (2-furanylmethylene)malononitrile from pentoses *via* the (i) isomerization, (ii) dehydration, and (iii) the Knoevenagel condensation proceeded in one-pot manner by using heterogeneous acid Amberlyst-15 and base HT. Cr/HT was found to be an excellent catalyst for the one-pot synthesis of (2-furanylmethylene)malononitrile with 44% yield. The oxidation state of Cr species on Cr/HT is similar to that of Cr_2O_3 which is known as strong Lewis acid. I suggested that the combined use of dispersed Cr_2O_3 as Lewis acid and Brønsted base sites of HT facilitated the isomerization step of aldopentoses into ketopentoses, and achieved a good activity.

References

1 G. W. Huber, J. N. Chheda, C. J. Barrett, J. A. Dumesic, *Science*, 2005, **308**, 1446.

2 R. Karinen, K. Vilonen, M. Niemelá, *ChemSusChem*, 2011, **4**, 1002.

3 P. Gallezot, *Chem. Soc. Rev.*, 2012, **41**, 1538.

4 G. W. Huber, S. Iborra, A. Corma, *Chem. Rev.*, 2006, **106**, 4044.

5 J. N. Chheda, G. W. Huber, J. A. Dumesic, *Amgew. Chem. Int. Ed.*, 2007, **46**, 7164.

6 C. H. Zhou, X. Xia, C. X. Lin, D. S. Tong, J. Beltramini, *Chem. Soc. Rev.*, 2011, **40**, 5588.

7 J. J. Bozell, G. R. Petersen, *Green Chem.*, 2010, **12**, 539.

8 B. Danon, G. Marcotullio, W. de Jong, *Green Chem.*, 2014, **16**, 39.

9 G. W. Huber, A. Corma, *Angew. Chem. Int. Ed.*, 2007, **46**, 7184.

10 C. Moreau, R. Durand, D. Peyron, J. Duhamet, P. Rivalier, *Ind. Crops Prod.*, 1998, **7**, 95.

11 E. Lam, E. Majid, A. C. W. Leung, J. H. Chong, K. A. Mahmoud, J. H. T. Luong, *ChemSusChem*, 2011, **4**, 535.

12 D. Mercadier, L. Rigal, A. Gaset, J.-P. Gorrichon, *J. Chem. Technol. Biotechnol.*, 1981, **31**, 503.

13 A. S. Dias, S. Lima, M. Pillinger, A. A. Valente, *Catal. Lett.*, 2007, **114**, 151.

14 A. S. Dias, S. Lima, P. Brandão, M. Pillinger, J. Rocha, A. A. Valente, *Catal. Lett.*, 2006,

108, 179.

15 G. H. Jeong, E. G. Kim, S. B. Kim, E. D. Park, S. W. Kim, *Micropor. Mesopor. Mater.*, 2011, **144**, 134.

16 A. S. Dias, M. Pillinger, A. A. Valente, *Appl. Catal. A: Gen.*, 2005, **285**, 126.

17 A. S. Dias, S. Lima, D. Carriazo, V. Rives, M. Pillinger, A. A. Valente, *J. Catal.*, 2006, **244**, 230.

18 S. Lima, M. Pillinger, A. A. Valente, *Catal. Commun.*, 2008, **9**, 2144.

19 R. O'Neill, M. N. Ahmad, L. Vanoye, F. Aiouache, *Ind. Eng. Chem. Res.*, 2009, **48**, 4300.

20 S. Lima, M. M. Antunes, A. Fernandes, M. Pillinger, F. Ribeiro, A. A. Valente, *Appl. Catal. A: Gen.*, 2010, **388**, 141.

21 S. Lima, A. Fernandes, M. M. Antunes, M. Pillinger, F. Ribeiro, A. A. Valente, *Catal. Lett.*, 2010, **135**, 41.

22 A. Takagaki, M. Ohara, S. Nishimura, K. Ebitani, *Chem. Lett.*, 2010, **39**, 838.

23 J. Tuteja, S. Nishimura, K. Ebitani, *Bull. Chem. Soc. Jpn*, 2012, **3**, 275.

24 A. Takagaki, M. Ohara, S. Nishimura, K. Ebitani, *Chem. Commun.*, 2009, 6276.

25 J. B. Binder, J. J. Blank, A. V. Cefali, R. T. Raines, *ChemSusChem*, 2010, **3**, 1268.

26 T. Suzuki, T. Yokoi, R. Otomo, J. N. Kondo, T. Tatsumi, *Appl. Catal. A: Gen.*, 2011, **408**, 117.

27 G. W. Huber, J. N. Chheda, C. J. Barrett, J. A. Dumesic, *Science*, 2005, **308**, 1446.

28 J. N. Chheda, J. A. Dumesic, *Catal. Today*, 2007, **123**, 59.

29 L. Faba, E. Díaz, S. Ordóñez, *ChemSusChem*, 2013, **6**, 463.

30 R. M. West, Z. Y. Liu, M. Peter, J. A. Dumesic, *ChemSusChem*, 2008, **1**, 417.

31 J. O. Metzger, *Angew. Chem. Int. Ed.*, 2006, **45**, 696.

32 R. Xing, A. V. Subrahmanyam, H. Olcay, W. Qi, G. P. van Walsum, H. Pendse, G. W. Huber, *Green Ghem.*, 2010, **12**, 1933.

33 H. S. Soliman, Kh. M. Eid, H. A. M. Ali, M. A. M. El-Mansy, S. M. Atef, *Spectrochim. Acta A: Molec. Biomolec. Spectra.*, 2013, **105**, 545.

34 K. Yamaguchi, K. Mori, T. Mizugaki, K. Ebitani, K. Kaneda, *J. Org. Chem.*, 2000, **65**, 6897.

35 T. Honma, N. Nakajo, T. Mizugaki, K. Ebitani, K. Kaneda, *Tetrahedron Lett.*, 2002, **43**, 6229.

36 E. Li, Z. P. Xu, V. Rudolph, *Appl. Catal. B*, 2009, **88**, 42.

37 Z. An, W. Zhang, H. Shi, J. He, *J. Catal.*, 2006, **241**, 319.

38 H. C. Greenwell, P. J. Holliman, W. Jones, B. V. Velasco, *Catal. Today*, 2006, **114**, 397.

39 M. L. Kantam, B. M. Choudary, Ch. V. Reddy, K. K. Rao, F. Figueras, *Chem. Commun.*, 1998, 1033.

40 E. Angelescu, O. D. Pavel, R. Bîrjega, R. Zăvoianu, G. Costentin, M. Che, *Appl. Catal. A: Gen.*, 2006, **308**, 13.

41 M. J. Climent, A. Corma, S. Iborra, K. Epping, A. Velty, *J. Catal.*, 2004, **225**, 316.

42 T. Mitsudome, A. Noujima, T. Mizugaki, K. Jitsukawa, K. Kaneda, *Green Chem.*, 2009, **11**, 793.

43 T. Mitsudome, A. Noujima, T. Mizugaki, K. Jitsukawa, K. Kaneda, *Adv. Synth. Catal.*, 2009, **351**, 1890.

44 T. Mitsudome, A. Noujima, Y. Mikami, T. Mizugaki, K. Jitsukawa, K. Kaneda, *Angew. Chem. Int. Ed.*, 2010, **49**, 5545.

45 A. Takagaki, M. Takahashi, S. Nishimura, K. Ebitani, *ACS Catal.*, 2011, **1**, 1562.

46 S. Nishimura, Y. Yakita, M. Katayama, K. Higashimine, K. Ebitani, *Catal. Sci. Technol.*, 2013, **3**, 351.

47 S. Nishimura, A. Takagaki, K. Ebitani, *Green Chem.*, 2013, **15**, 2026.

48 P. Keller, H-H. Strehblow, *Corros. Sci.*, 2004, **46**, 1939.

49 A. Virnovskaia, S. Jørgensen, J. Hafizovic, Ø. Prytz, E. Kleimenov, M. Hävecker, H. Bluhm, A. Knop-Gericke, R. Schlögl, U. Olsbye, *Surf. Sci.*, 2007, **601**, 30.

50 L. Bui, H. Luo, W. R. Gunther, Y. Román-Leshkov, *Angew. Chem. Int. Ed.*, 2013, **52**, 8022.

51 Y. Zhu, G. Chuah, S. Jaenicke, *J. Catal.*, 2004, **227**, 1.

52 C. Jiménez-Sanchidrián, J. M. Hidalgo, J. R. Ruiz, *Appl. Catal. A: Gen.*, 2006, **303**, 23.

53 A. B. Merlo, V. Vetere, J. F. Ruggera, M. L. Casella, *Catal. Comun.*, 2009, **10**, 1665.

54 E. A. Pidko, V. Degirmenci, E. J. M. Hensen, *ChemCatChem*, 2012, **4**, 1263.

55 Y. Román-Leshkov, M. Moliner, J. A. Labinger, M. E. Davis, *Angew. Chem. Int. Ed.*, 2010, 49, 8954.

56 D. Ekeberg, S. Morgenlie, Y. Stenstrøm, *Carbohdr. Res.*, 2005, **340**, 373.

57 D. Ekeberg, S. Morgenlie, Y. Stenstrøm, *Carbohdr. Res.*, 2007, **342**, 1992.

58 S. J. Angyal, *Top. Curr. Chem.*, 2001, **215**, 1.

Chapter 2-2

One-pot Synthesis of Furfural from Xylose using Al_2O_3—Ni-Al Layered Double Hydroxide Acid-Base Bi-functional Catalyst and Sulfonated Resin

Abstract

Furfural was effectively synthesized from xylose in a one-pot manner by a combined use of Ni^{2+}-modified γ-Al_2O_3 (Al_2O_3–Ni-Al layered double hydroxide (LDH)) and sulfonated resin (Amberlyst-15) at 373 K (46% yield). The addition of Ni^{2+} onto γ-Al_2O_3 generated the bi-functional site of Lewis acid γ-Al_2O_3 and Brønsted base Ni-Al LDH at close boundary, and these would facilitate the xylose isomerization into xylulose and/or ribulose to afford the good yield of furfural after successive dehydration of generated ketopentoses on Amberlyst-15.

Introduction

Conversion of biomass resources into value-added chemicals/fuels has been accepted as one of the important reactions to utilize renewable resources.[1-3] Cellulose and hemicellulose, the major component of lignocellulosic biomass, are the most abundant compounds which are mainly composed of monosaccharides.[4,5] Cellulose and hemicellulose can be converted into monosaccharides such as glucose and xylose by the hydrolysis over activated carbons.[6-9] Therefore, the successive chemical conversion of saccharides into value-added chemicals such as furans, sugar alcohols, levulinic acid, and γ-valerolactone have attracted much attention as one of the reactions worth conducting in biorefineries.

Furfural, a dehydration product of pentoses such as xylose and arabinose, has a great potential as non-petroleum building blocks in the production of polymers, pharmaceuticals, biofuels, and fine chemicals.[5,10-13] Conventionally, dehydration of xylose into furfural was examined using various solid acid catalysts such as sulfated zirconia,[14] porous niobium silicate,[15] sulfonic acid modified mesoporous shell silica beads,[16] propylsulfonic SBA-15,[17] and zeolite-based catalysts.[18-21] However, due to the stability of xylose, these direct dehydrations need high reaction temperatures (>423 K).

To overcome this problem, one approach merging the isomerization of xylose (aldose) into unstable xylulose (ketose) before the dehydration was generated.[22,23] Dehydration of xylose *via* aldose-ketose isomerization over Lewis acid catalysts under a mild condition (373 K) has been reported by Binder *et al*.[23] and Suzuki *et al*.[24] using $CrCl_2$ with LiBr and SO_4^{2-}/SnO_2, respectively. As a different expedient, I have demonstrated that a combined use of Brønsted solid base Mg-Al layered double hydroxide (Mg-Al LDH) and Brønsted solid acid Amberlyst-15 efficiently afforded furfural from xylose in a one-pot manner. This reaction involves aldose-ketose isomerization by base LDH and successive dehydration of ketose by acid Amberlyst-15.[22] As advanced research studies, the bi-functional Cr/Mg-Al LDH surface, which consists of LDH originated Brønsted base sites and Lewis acid sites on the dispersed Cr_2O_3, was found to be an more excellent isomerization catalyst than bare Mg-Al LDH, where the pair of Brønsted base and Lewis acid effectively promotes the aldose-ketose isomerization.[25]

Herein, I focused on the modification of typical solid Lewis acid γ-Al_2O_3 with M^{2+} ion additions. It is known that M^{2+} species from aqueous solution onto γ-Al_2O_3 can generate M^{2+}-Al^{3+} LDH-type compounds,[26] thus, the addition of M^{2+} onto γ-Al_2O_3 would easily generate bi-functional Lewis acid γ-Al_2O_3 − Brønsted base M-Al LDH sites. I investigated modification effects owing to the additive M^{2+} ions onto γ-Al_2O_3 in the one-pot synthesis of furfural from xylose with Amberlyst-15 (Scheme 1). The characterizations on crystal structure, crystallite size, and surface area of the M^{2+}-modified Al_2O_3 are demonstrated. The Lewis acidity is estimated by the Meerwein–Ponndorf–Verley (MPV) reduction of furfural toward furfuryl alcohol in 2-propanol.

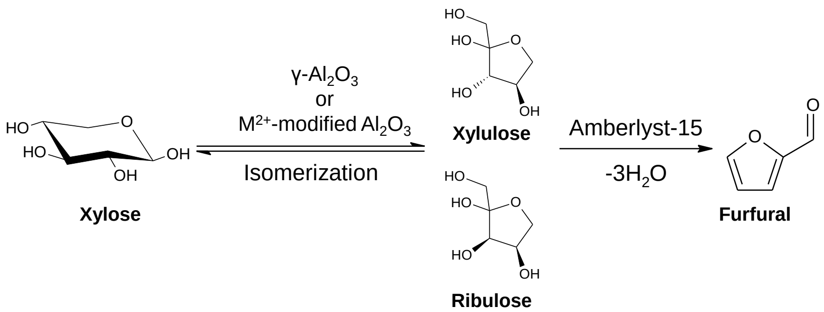

Scheme 1 Possible reaction path for furfural synthesis *via* aldose-ketose isomerization over γ-Al_2O_3 based catalyst and successive dehydration on Amberlyst-15.

Experimental

Materials and synthesis of M^{2+}-modified Al_2O_3

γ-Al_2O_3 (JRC-ALO-8) was obtained from the Catalysis Society of Japan. Magnesium nitrate hexahydrate ($Mg(NO_3)_2{\cdot}6H_2O$), cobalt nitrate hexahydrate ($Co(NO_3)_2{\cdot}6H_2O$), nickel nitrate hexahydrate ($Ni(NO_3)_2{\cdot}6H_2O$), cupper nitrate trihydrate ($Cu(NO_3)_2{\cdot}3H_2O$), zinc nitrate hexahydrate ($Zn(NO_3)_2{\cdot}6H_2O$), and 2-propanol were purchased from Wako pure Chemical Ind., Ltd. *N*,*N*-dimethylformamide (DMF) and xylose were obtained from Kanto Chem. Co. Ltd. Amberlyst-15 and furfural were supplied by Sigma-Aldrich Co., Ltd. and Acros Organics, respectively.

A series of M^{2+}-modified Al_2O_3 were prepared by an impregnation method (adsorption) of γ-Al_2O_3 with urea and an aqueous solution of various metal nitrates: each metal nitrate was dissolved in 50 mL of ultra pure water (Smart 2 Pure, Nikko Hansen Co. Ltd; 18.2 MΩ・cm), and then 1 g of urea and 1 g of γ-Al_2O_3 were added. The modified M^{2+}/Al^{3+} atomic ratio was adjusted to 0.05. After stirring at 353 K for 24 h, the obtained paste was filtered, washed with ultra pure water, and then dried at 383 K overnight.

Reactions

The one-pot synthesis of furfural from xylose was performed in a Schlenk tube attached to a reflex condenser. Thereafter 0.67 mmol xylose, 0.2 g of metal-modified Al_2O_3 and Amberlyst-15 were charged into reactor, and then which was purged by nitrogen gas (30 $mL \cdot min^{-1}$) for 20 min. Finally, 3 mL of *N*,*N*-dimethylformamide (DMF) was added into the reactor using syringe, and the reactor was heated at 373 K.

The Meerwein–Ponndorf–Verley (MPV) reduction of furfural in 2-propanol toward furfuryl alcohol was performed in 50 mL of pear-shaped flask attached to a reflex condenser. 1.3 mmol furfural, 83 mmol 2-propanol (6.4 mL) and 0.1 g of catalysts were charged into the reactor, and then heated at 355 K for 1 h. Products were analyzed using a GC-FID (SHIMADZU GC-2014) equipped with a non-polar column (Agilent, DB-1) or HPLC (Waters 515) with RSPak KC-811 column (Shodex).

The back titration experiment

The back titration experiment was performed using 10 mM benzoic acid / DMF solution and 10 mM NaOH aq. as adsorption reagent and titration standard solution, respectively. 10 mL of adsorption reagent and 0.1 g of γ-Al_2O_3 or Ni^{2+}-modified -Al_2O_3 were sealed in 20 mL of screw tube, and then stirred for 10 min. Thereafter, the sample was removed by Millex-LG Syringe Filter (pore size: 0.20 μm), and then few drops of phenolphthalein aq. was added as indicator. Finally, 4 mL of sample liquid was titrated with NaOH aq. until the liquid color changes to pale red. Basic site amount was estimated using the difference between the initial amount of benzoic acid and the titrated NaOH amount. Basic site density was calculated by dividing the basic site amount by the BET specific surface area.

Results and discuttion

Preliminarily, I investigated the activity of combined use of γ-Al_2O_3 and Amberlyst-15 for xylose transformation. The time courses are shown in Fig.1. The use of γ-Al_2O_3 alone hardly gave furfural at 373 K, whereas furfural was efficiently produced with the combined use of γ-Al_2O_3 and Amberlyst-15. In the latter case, the yield of furfural increased with time, and it

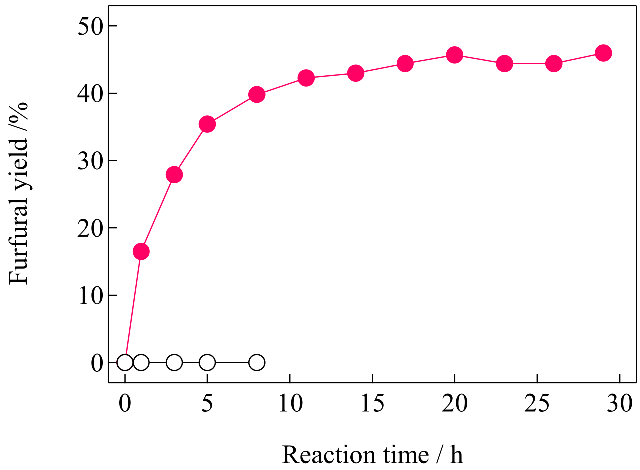

Figure 1 Time course of furfural yield from xylose on γ-Al_2O_3 (○) and combined use of γ-Al_2O_3 and Amberlyst-15 (●). *Reaction conditions*: xylose (0.67 mmol), γ-Al_2O_3 (0.2 g), Amberlyst-15 (0.1 g), DMF (3 mL), 373 K, 500 rpm, N_2 flow (30 mL·min^{-1}).

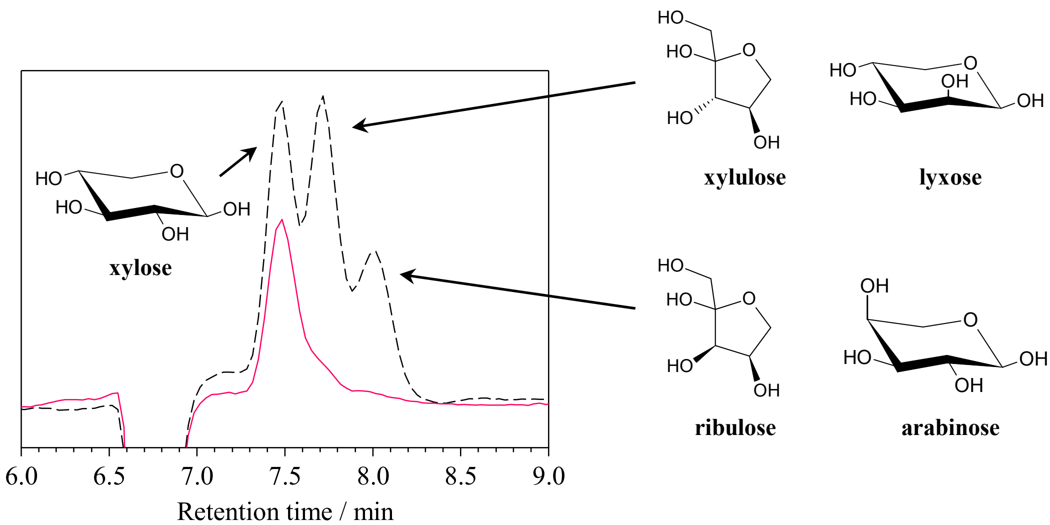

Figure 2 HPLC chart of transformation of xylose using γ-Al_2O_3 (dashed line) and combined use of γ-Al_2O_3 and Amberlyst-15 (solid line). *Reaction conditions*: xylose (0.67 mmol), γ-Al_2O_3 (0.2 g), Amberlyst-15 (0.1 g), *N*,*N*-dimethylformamide (3 mL), 373 K, 8 h, 500 rpm, N_2 flow (30 mL·min^{-1}).

became constant at around 45% at above 17 h of the reaction. It is noteworthy that this value was higher than that in previous reports performed at 373 K using solid catalysts.[22,24] The HPLC chart of reaction mixture at 8 h is shown in Figure 2. In the presence of γ-Al_2O_3 alone, three peaks were observed at retention time of 7.5 min, 7.7 min, and 8.0 min, which could be assigned to the xylose, xylulose and lyxose, and ribulose and arabinose, respectively. These results indicated that γ-Al_2O_3 promoted the isomerization of xylose towards such pentoses, significantly. In the case of combined use with Amberlyst-15, very few amounts of such pentoses were detected. Since Ambetlyst-15 is ineffective for dehydration of aldopentoses such as xylose and arabinose below at 373 K,[22,25,27] the reaction path of one-pot synthesis of furfural from xylose is proposed as follows: At first, γ-Al_2O_3 promoted the isomerization of xylose toward xylulose, lyxose, ribulose, and/or arabinose, thereafter, Amberlyst-15 effectively dehydrated xylulose and ribulose toward furfural.

In the next stage, I prepared various M^{2+}-modified Al_2O_3 catalysts (M^{2+}/Al^{3+} atomic ratio = 0.05) and evaluated their catalytic performance and structural properties. The XRD patterns of various M^{2+}-modified Al_2O_3 and bare γ-Al_2O_3 are shown in Figure 3. All prepared M^{2+}-modified Al_2O_3 possessed the γ-Al_2O_3 phase. Interestingly, XRD patterns of LDH structure were also observed in the cases of Mg^{2+}, Co^{2+}, Ni^{2+}, and Zn^{2+}-modified Al_2O_3.

Table 1 summarizes the catalytic activities for one-pot synthesis of furfural from xylose using M^{2+}-modified Al_2O_3 and Amberlyst-15. Catalytic activity of M^{2+}-modified Al_2O_3 for the MPV reduction was estimated on the basis of initial rate for the hydrogenation of furfural. BET specific surface areas of M^{2+}-modified Al_2O_3 are also listed in Table 1. It remarkably indicated that the pairs of Ni^{2+}-modified Al_2O_3 and Amberlyst-15 showed better catalytic activities for furfural synthesis than that of γ- Al_2O_3 and Amberlyst-15. Because the BET surface areas of M^{2+}-modified Al_2O_3 were almost same values (136 ~ 158 $m^2 \cdot g^{-1}$), no significant correlation between catalytic activity for furfural synthesis and surface area were expected in these catalysts.

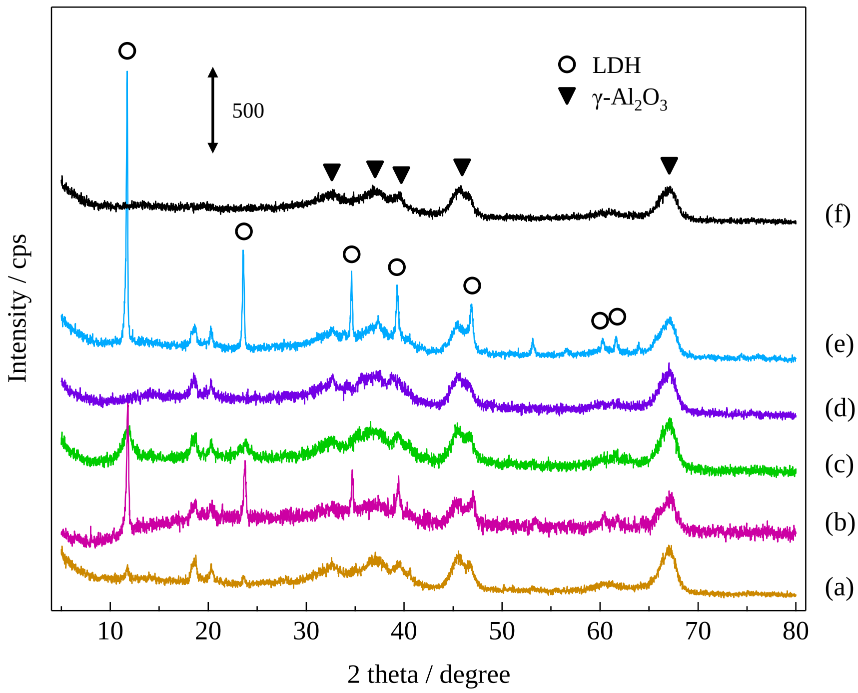

Figure 3 XRD patterns of γ-Al_2O_3 and various M^{2+}-modified Al_2O_3; (a) Mg^{2+}-modified Al_2O_3, (b) Co^{2+}-modified Al_2O_3, (c) Ni^{2+}-modified Al_2O_3, (d) Cu^{2+}-modified Al_2O_3, (e) Zn^{2+}-modified Al_2O_3 and (f) γ-Al_2O_3.

Table 1 Catalytic activities and surface area of M^{2+}-modified Al_2O_3.

Modified metal ion	Furfural yield^{a,b} /%	Initial rate for furfural synthesis^{a,c} / mmol·g^{-1}·h^{-1}	Initial rate for MPV reduction^{d} / mmol·g^{-1}·h^{-1}	S_{BET}^{e} / m^2·g^{-1}
Mg^{2+}	38	0.36	2.32	154
Co^{2+}	37	0.30	2.22	155
Ni^{2+}	46	0.45	2.25	158
Cu^{2+}	25	0.21	0.47	153
Zn^{2+}	33	0.32	1.82	136
-	40	0.37	2.92	193

^{a}*Reaction conditions*: xylose (0.67 mmol), M^{2+}-modified Al_2O_3 (0.2 g), Amberlyst-15 (0.1 g), DMF (3 mL), 373 K, N_2 flow (30 mL·min^{-1}). ^{b}8 h. ^{c}1 h. ^{d}*Reaction conditions:* furfural (1.3 mmol), 2-propanol (83 mmol), M^{2+}-modified Al_2O_3 (0.1 g), 355 K, 1 h. ^{e}BET specific surface area.

In contrast, the good correlation was observed between the catalytic activities of γ-Al_2O_3 and Mg^{2+}, Co^{2+}, Cu^{2+}, and Zn^{2+}-modified Al_2O_3 for furfural synthesis and MPV reduction, as shown in Figure 4 (open circle); the activity for furfural synthesis increased with increasing the activity for MPV reduction. Román-Leshkow *et al.* have reported that the isomerization of aldose into ketose over Lewis acid catalyst, such as tin-containing zeolite, proceeded *via* MPV reduction under hydride shift mechanism.[28] Therefore, it would be determined that the Lewis acidity is one of the important factor in M^{2+}-modified Al_2O_3 catalysts. In fact, a linear trend (R^2 = 0.90) was assigned in Figure 4 except for only the case of Ni^{2+}-modified Al_2O_3 (close circle); *i.e.* the initial rate for furfural production of Ni^{2+}-modified Al_2O_3 is faster than Mg^{2+}, or Co^{2+}-modified Al_2O_3 whereas MPV reduction occurs with almost the same rate. This result suggested that the improvement of activity for furfural synthesis in Ni^{2+}-modified Al_2O_3 catalyst was hardly explained on Lewis acidity alone. Indeed, the activity for MPV reduction on Ni^{2+}-modified Al_2O_3 (2.25 mmol·g^{-1}·h^{-1}) was slower than that on γ-Al_2O_3 (2.92 mmol·g^{-1}·h^{-1}).[29] Thus, effects of generated Ni-Al LDH need to be considered.

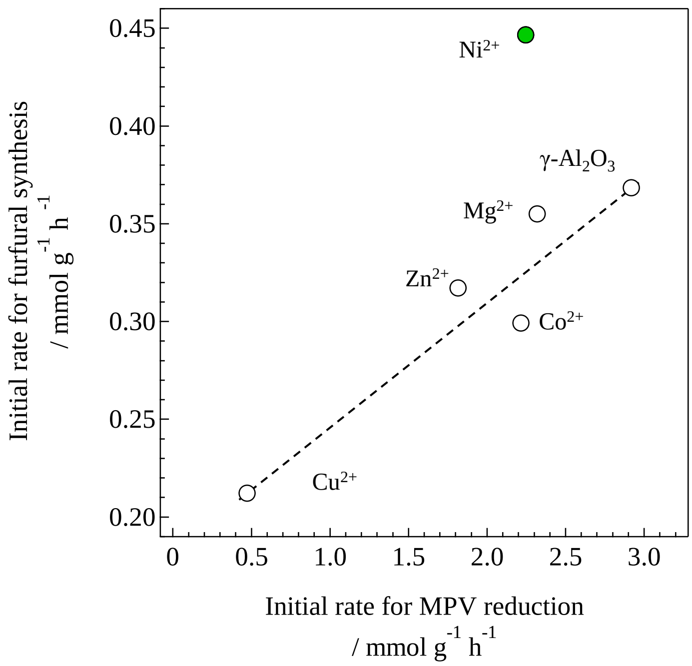

Figure 4 Correlation of activities for MPV reduction and furfural synthesis over various M^{2+}-modified Al_2O_3 catalysts.

To discuss about singularity of Ni^{2+} modification, basic density of Ni^{2+}-modified Al_2O_3 and crystallite size of generated Ni-Al LDH on γ-Al_2O_3 were investigated. An increase of base density of Ni^{2+}-modifies Al_2O_3 (0.71 nm^{-2}) from γ-Al_2O_3 (0.59 nm^{-2}) owing to generation of Ni-Al LDH on γ-Al_2O_3 was determined by titration experiment using benzoic acid and N_2 adsorption. Interestingly, it was observed that the generated LDH (003) plane crystallite size over Ni^{2+}-modified Al_2O_3 was obviously the smallest (7 nm) in comparison to Mg^{2+}-modified Al_2O_3 (25 nm), Co^{2+}-modified Al_2O_3 (33 nm), and Zn^{2+}-modified Al_2O_3 (43 nm) (Figure 5). These suggested the possibility that xylose is successfully converted using coexistence of small basic Ni-Al LDH with γ-Al_2O_3.

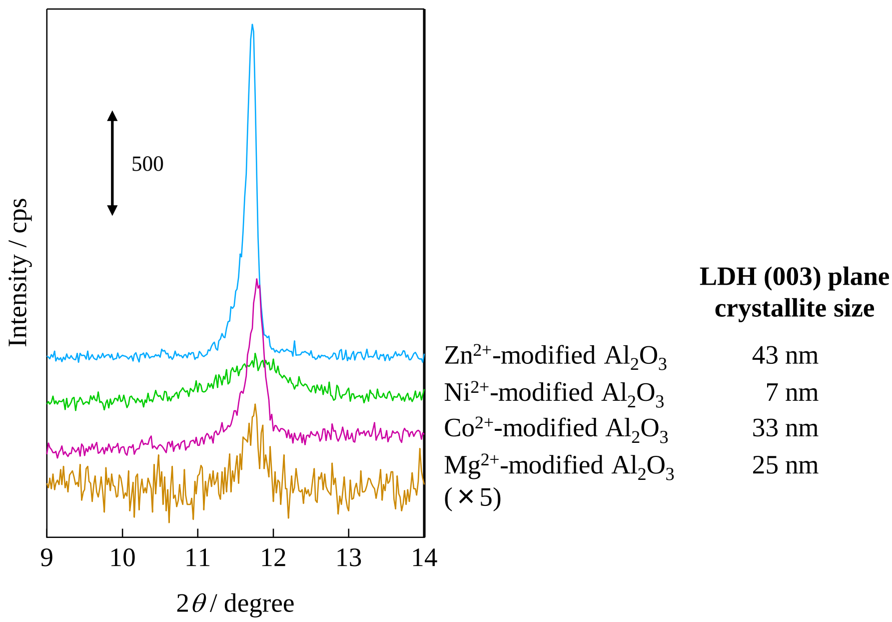

Figure 5 LDH (003) plane XRD peaks of Mg^{2+}, Co^{2+}, Ni^{2+}, and Zn^{2+}-modified Al_2O_3. The LDH (003) plane crystallite size of Mg^{2+}, Co^{2+}, Ni^{2+}, and Zn^{2+}-modified Al_2O_3 were calculated by the Scherrer equation; $D_{hkl} = K\lambda/\beta\cos\theta$ (K: Scherrer number (0.9), λ: incident ray wavelength (0.1542 nm), β: peak width at half height (rad), θ: Bragg angle, the error to measure the width at half height is 0.04°, D_{003} calculation error is about ±8%).

To verify this hypothesis, I prepared the physically- mixed catalyst of small Ni-Al LDH (5 nm) and γ-Al_2O_3 following to the estimation; *viz.* the weight ratio of Ni-Al LDH and γ-Al_2O_3 in the Ni^{2+}-modified Al_2O_3 is to be 0.16 by the XRD peak intensities for Ni-Al LDH (003) and γ-Al_2O_3 (440) plane (Figure 6). The Ni/Al atomic ratio calculated based on the Ni-Al LDH/γ-Al_2O_3 ratio of 0.16 is 0.052 that is almost identical with Ni^{2+}-modified Al_2O_3. Then obtained physical-mixed catalyst was applied to furfural synthesis with Amberlyst-15. Initial rate of the physically-mixed catalyst (0.34 mmol·g^{-1}·h^{-1}) is almost similar to that of bare γ-Al_2O_3 and significantly smaller than Ni^{2+}-modified Al_2O_3 (0.45 mmol·g^{-1}·h^{-1}). Furthermore, when the physical mixture of γ-Al_2O_3 and Ni-Al LDH was applied to the MPV reduction, the initial rate

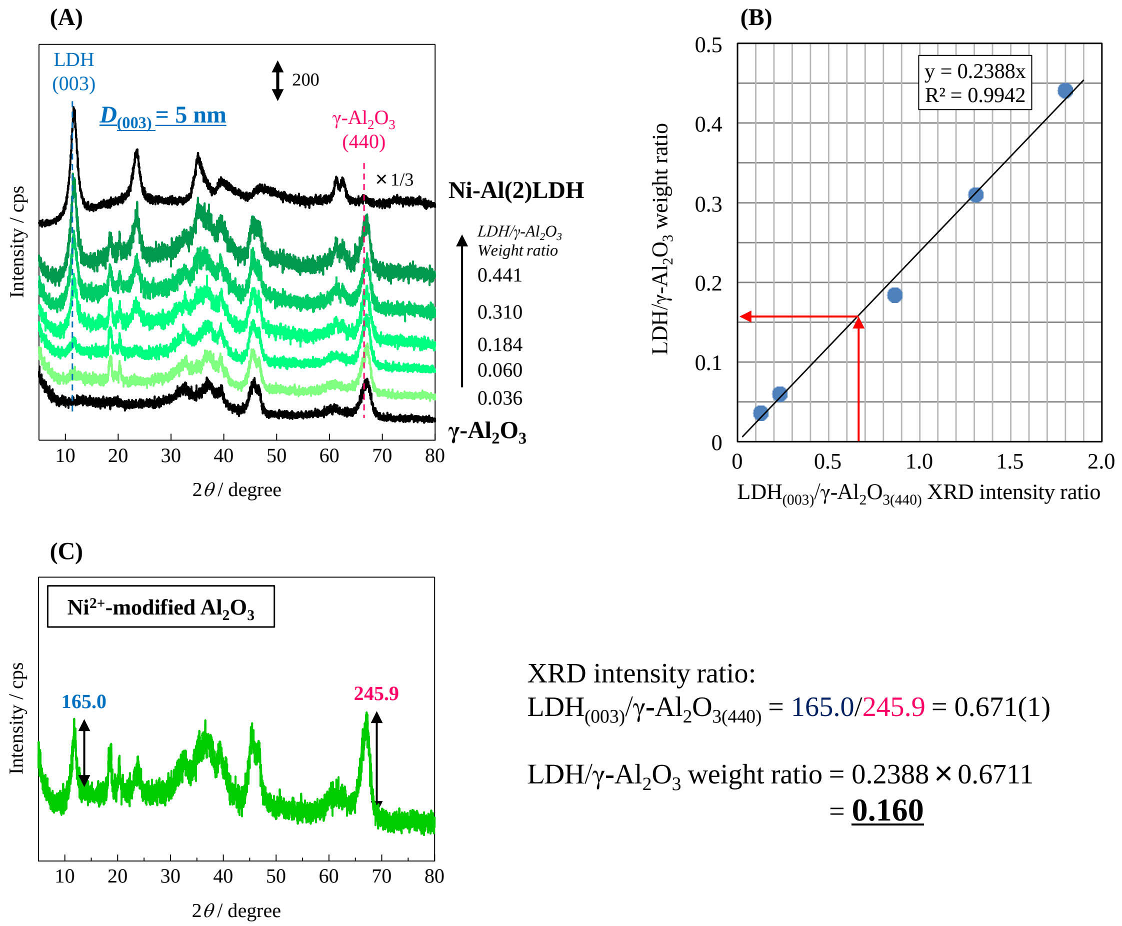

Figure 6 Estimation of Ni-Al LDH/γ-Al_2O_3 weight ratio of Ni^{2+}-modified Al_2O_3. (A) XRD patterns of bare γ-Al_2O_3, Ni-Al LDH, and physical mixture of γ-Al_2O_3 and Ni-Al LDH with various weight ratios. (B) Plot of XRD intensity ratio of LDH (003) plane and γ-Al_2O_3 (440) plane vs LDH/γ-Al_2O_3 weight ratio. (C) XRD pattern of Ni^{2+}-modified Al_2O_3 and intensities for LDH (003) plane and γ-Al_2O_3 (440) plane.

for furfuryl alcohol was 2.22 mmol·g^{-1}·h^{-1}, which was similar to that of Ni^{2+}-modified Al_2O_3 (2.25 mmol·g^{-1}·h^{-1}). Therefore, the enhanced activity for xylose conversion of the Ni^{2+}-modified Al_2O_3 could not be explained in terms of the Lewis acidity nor simple coexistence of fine Ni-Al LDH and γ-Al_2O_3.

Figure 7 shows TEM images of γ-Al_2O_3 and Ni^{2+}-modified Al_2O_3. Ni^{2+}-modified Al_2O_3 possess a morphology in which acicular γ-Al_2O_3 and flat plate Ni-Al LDH were well mixed uniformly. Caillerie *et al.* have reported that the breaking of Al-O bonds of γ-Al_2O_3 can be promoted by Ni^{2+} or Co^{2+} ions at neutral pH, thus the adsorption of Co^{2+} or Ni^{2+} complexes from aqueous solution onto γ-Al_2O_3 can generate Ni-Al and Co-Al hydrotalcite-type compounds *via* three simultaneous phenomena at the oxide/water interface; the adsorption of ions, the alumina dissolution, and the co-precipitation of M^{2+} with Al^{3+} ions extracted from support.[26] Accordingly, I considered that Ni^{2+}-modified Al_2O_3 possess boundaries between Al_2O_3 and LDH more abundantly than simple mixture of γ-Al_2O_3 and Ni-Al LDH. In addition, since the crystallite size of Ni-Al LDH in Ni^{2+}-modified Al_2O_3 was exceedingly smaller than that of Mg^{2+}, Co^{2+}, and

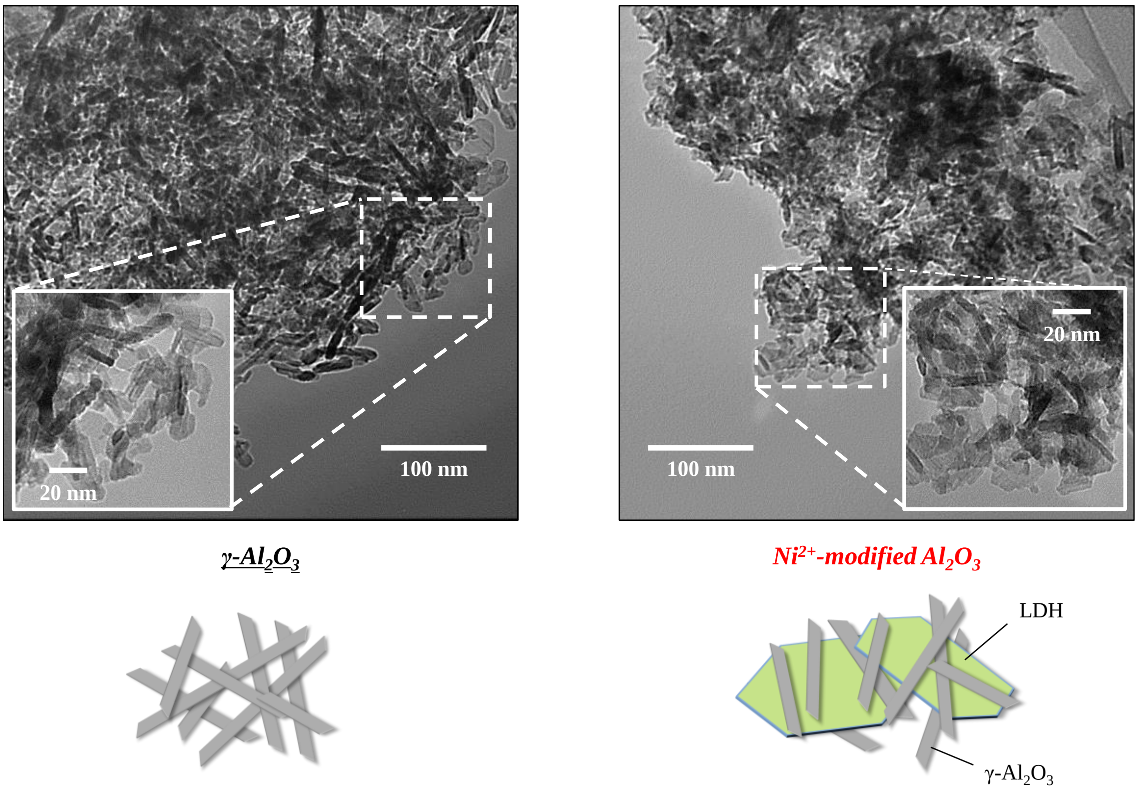

Figure 7 TEM images of γ-Al_2O_3 and Ni^{2+}-modified Al_2O_3 and their structural models.

Zn^{2+}- modified Al_2O_3, the Ni^{2+}-modified Al_2O_3 would possess a lot of close boundaries compared to other M^{2+}-modified Al_2O_3. Therefore, I suggested that the close boundaries between γ-Al_2O_3 and Ni-Al LDH facilitated the isomerization step of xylose into xylulose as bifunctional Lewis acid - Brønsted base active sites.

Next, I investigated the effect of Ni loading amount in the Ni^{2+}-modified Al_2O_3 catalysts. As shown in Figure 8, the XRD intensities of the Ni-Al LDH peaks were increased in accordance with the Ni/Al atomic ratio from 0.03 to 0.13, while all prepared Ni^{2+}-modified Al_2O_3 retained the original γ-Al_2O_3 structure. Furfural yield in the one-pot transformation of xylose over a combined use of Amberlyst-15 and Ni^{2+}-modified Al_2O_3 with various Ni/Al atomic ratios are shown in Figure 8 and Table 2. Specific surface areas of Ni^{2+}-modified Al_2O_3 catalysts are summarized in Table 2, and are almost identical regardless of a Ni/Al atomic ratio. All prepared Ni^{2+}-modified Al_2O_3 showed higher catalytic activity than bare γ-Al_2O_3.

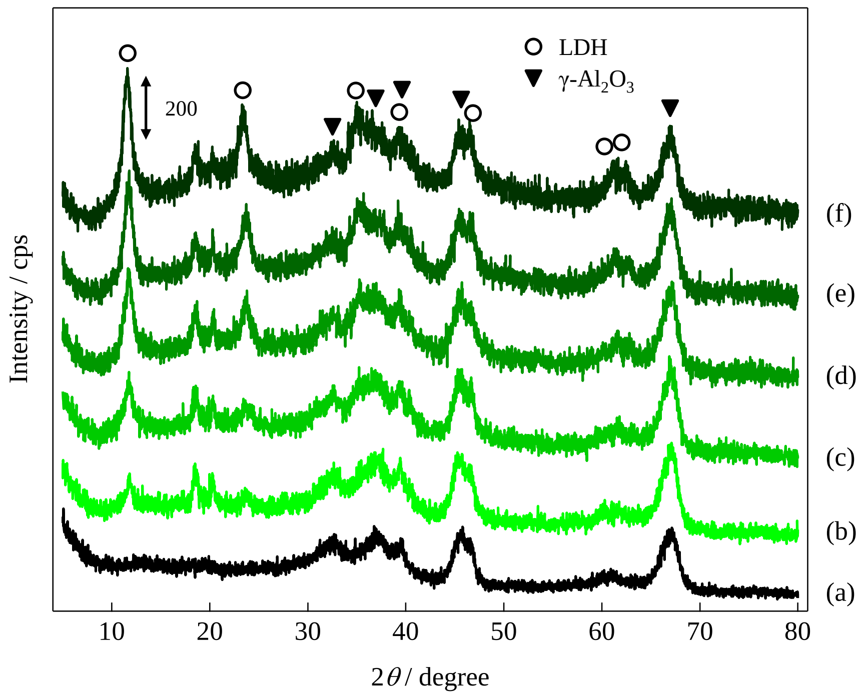

Figure 8 XRD patterns of (a) γ-Al_2O_3 and Ni^{2+}-modified Al_2O_3 with various Ni/Al atomic ratio of (b) 0.03, (c) 0.05, (d) 0.07, (e) 0.09 and (f) 0.13.

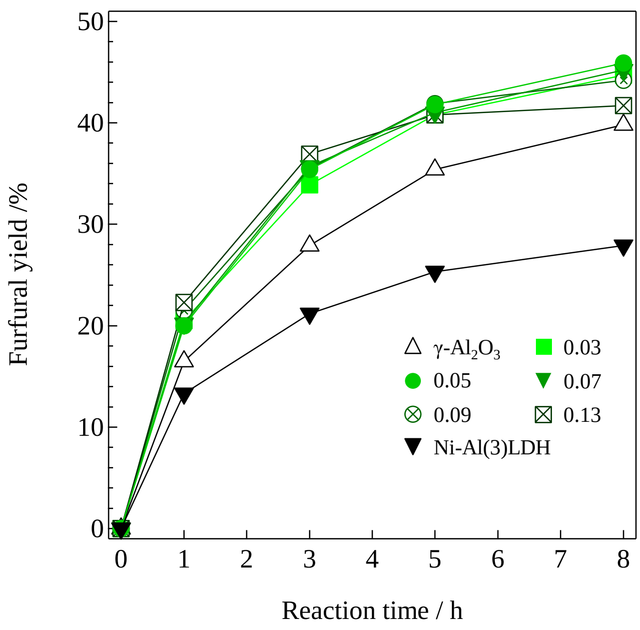

Figure 9 Time cause of one-pot synthesis of furfural from xylose over combined use of Amberlyst-15 and Ni^{2+}-modified Al_2O_3 with various Ni/Al atomic ratio. *Reaction conditions*: xylose (0.67 mmol), Ni^{2+}-modified Al_2O_3 (0.2 g), Amberlyst-15 (0.1 g), DMF (3 mL), 373 K, N_2 flow (30 mL·min^{-1}).

Table 2 Furfural yield in the one-pot transformation of xylose and surface area of Ni^{2+}-modified Al_2O_3 with various Ni/Al atomic ratio.

Catalyst	Furfural yield^a /%				$S_{BET}{}^b$ / m^2 g^{-1}
	1 h	3 h	5 h	8 h	
γ-Al_2O_3	17	28	35	40	174
Ni^{2+}-modifiedAl_2O_3(0.03)	21	34	41	45	151
Ni^{2+}-modifiedAl_2O_3(0.05)	20	35	42	46	146
Ni^{2+}-modifiedAl_2O_3(0.07)	20	36	41	45	151
Ni^{2+}-modifiedAl_2O_3(0.09)	22	36	42	44	151
Ni^{2+}-modifiedAl_2O_3(0.13)	22	37	41	42	155
Ni-Al(3)LDH	13	21	25	28	100

^{a}*Reaction conditions*: xylose (0.67 mmol), Ni^{2+}-modified Al_2O_3 (0.2 g), Amberlyst-15 (0.1 g), DMF (3 mL), 373 K, N_2 flow (30 mL·min^{-1}). ^{b}BET specific surface area.

Interestingly, although Ni^{2+}-modified Al_2O_3 composed of lower Ni/Al atomic ratio from 0.03 to 0.07 gave similar furfural yield, those composed of higher Ni/Al atomic ratio of 0.09 and 0.13 showed different trend; Ni^{2+}-modified Al_2O_3 -(0.09) and -(0.13) achieved slightly higher furfural yield in a short reaction time, whereas the increases of yield from 5 h to 8 h were lower than others. Moreover, when I compared the activity of γ-Al_2O_3 and Ni-Al(3)LDH, it is clearly observed that the increase of furfural yield over Ni-Al(3)LDH promptly becomes moderate, indicating Ni-Al(3)LDH is easier to be deactivated than γ-Al_2O_3. Therefore, I infer that the Ni^{2+}-modified Al_2O_3 -(0.09) and -(0.13), which would possess abundant Ni-Al LDH crystal and cross boundary between LDH and γ-Al_2O_3, showed higher activity in a short reaction time, however it promptly be deactivated.

The effect of calcination in Ni^{2+}-modified Al_2O_3(0.05) was investigated. Figure 10 and 11 showed XRD patterns of calcined Ni^{2+}-modified Al_2O_3(0.05), and time cause of furfural yield in the one-pot transformation of xylose over a combined use of Amberlyst-15 and calcined Ni^{2+}-modified Al_2O_3(0.05), respectively. After the calcination at 523 K, the XRD patterns derived from the LDH structure decreased because of dehydration of the interlayer water. All LDH originated XPD peaks disappeared at calcination temperature of >623 K, and only the γ-Al_2O_3 originated peaks were observed. Catalytic activities for the furfural synthesis over the combined uses of Amberlyst-15 and the calcined Ni^{2+}-modified Al_2O_3(0.05) decreased in accordance with calcination temperature, and were lower than γ-Al_2O_3 calcined at 723 K. These results strongly supported that the coexistence of LDH crystal and γ-Al_2O_3 is one of the crucial factors to develop the bifunctional Lewis acid - Brønsted base active sites at the close boundaries between γ-Al_2O_3 and Ni-Al LDH.

Finally, it was noted that the combined use of Ni^{2+}-modified Al_2O_3 and Amberlyst-15 yielded 46% furfural from xylose in 8 h, though the pair of bare γ-Al_2O_3 and Amberlyst-15 needed 17 h (45%).

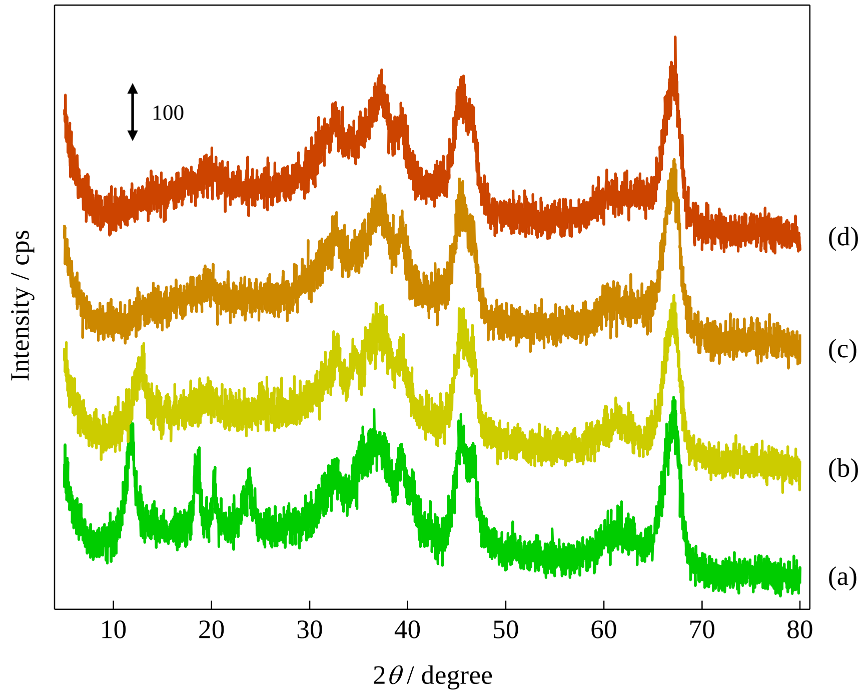

Figure 10 XRD patterns of Ni^{2+}-modified Al_2O_3(0.05) calcined at various temperature. (a) non calcined, (b) 523 K, (c) 623 K, (d) 723 K. (b)-(d) were first pre-calcined at 473 K for 1 h (rewarming rate: 10 K min^{-1}), then calcined at ordered temperature for 5 h (rewarming rate: 5 K min^{-1}).

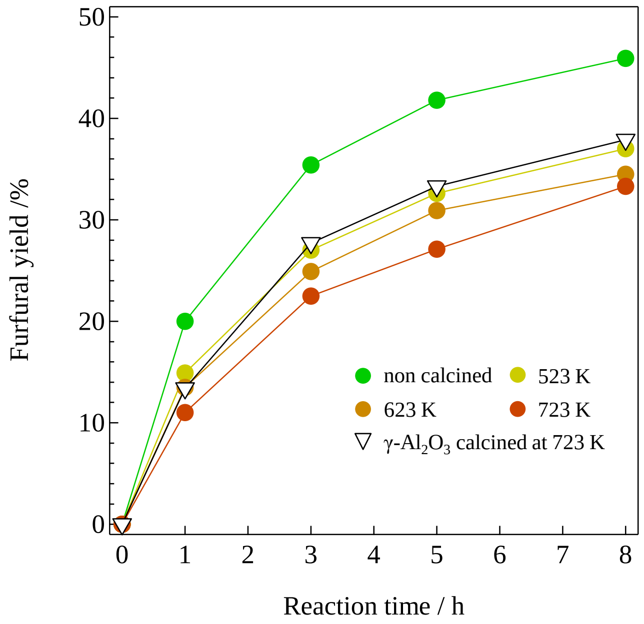

Figure 11 Time cause of one-pot synthesis of furfural from xylose over combined use of Amberlyst-15 and calcined Ni^{2+}-modified Al_2O_3 at various temperature. *Reaction conditions*: xylose (0.67 mmol), Ni^{2+}-modified Al_2O_3 (0.2 g), Amberlyst-15 (0.1 g), DMF (3 mL), 373 K, N_2 flow (30 mL·min^{-1}).

Conclusions

In conclusion of this chapter, one-pot synthesis of furfural from xylose efficiently proceeded by a combined use of Ni^{2+}-modified Al_2O_3, which contains fine Ni-Al layered double hydroxide (LDH) crystal, and Amberlyst-15. The close boundaries between Lewis acid γ-Al_2O_3 and Brønsted base Ni-Al LDH facilitated the isomerization of xylose into xylulose and ribulose, which is dehydrated into furfural catalyzed by Brønsted acid Amberlyst-15.

References

1 G. W. Huber, J. N. Chheda, C. J. Barrett, J. A. Dumesic, *Science*, 2005, **308**, 1446.

2 R. Karinen, K. Vilonen and M. Niemelá, *ChemSusChem*, 2011, **4**, 1002.

3 P. Gallezot, *Chem. Soc. Rev.*, 2012, **41**, 1538.

4 G. W. Huber, S, Iborra and A. Corma, *Chem. Rev.*, 2006, **106**, 4044.

5 J. N. Chheda, G. W. Huber, and J. A. Dumesic, *Angew. Chem. Int. Ed.*, 2007, **40**, 7164.

6 S. Suganuma, K. Nakajima, M. Kitano, D. Yamaguchi, H. Kato, S. Hayashi and M. Hara, *J. Am. Chem. Soc.*, 2008, **130**, 12787.

7 A. Onda, T. Ochi and K. Yanagisawa, *Green Chem.*, 2008, **10**, 1033.

8 H. Kobayashi, T. Komanoya, K. Hara and A. Fukuoka, *ChemSusChem*, 2010, **3**, 440.

9 T. Komanoya, H. Kobayashi, K. Hara, W.-J. Chun and A. Fukuoka, *Appl. Catal. A: General*, 2011, **407**, 188.

10 C. H. Zhou, X. Xia, C. X. Lin, D. S. Tong and J. Beltramini, *Chem. Soc. Rev.*, 2011, **40**, 5588.

11 H. Choudhary, S. Nishimura and K. Ebitani, *Chem. Lett.*, 2012, **41**, 409.

12 B. Danon, G. Marcotullio and W. de Jong, *Green Chem.*, 2014, **16**, 39.

13 G. W. Huber and A. Corma, *Angew. Chem. Int. Ed.*, 2007, **46**, 7184.

14 A. S. Dias, S. Lima, M. Pillinger and A. A. Valente, *Catal. Lett.*, 2007, **114**, 151.

15 A. S. Dias, S. Lima, P. Brandão, M. Pillinger, J. Rocha and A. A. Valente, *Catal. Lett.*, 2006, **108**, 179.

16 G. H. Jeong, E. G. Kim, S. B. Kim, E. D. Park and S. W. Kim, *Microporous Mesoporous Mater.*, 2011, **144**, 134.

17 I. Agirrezabal-Telleria, J. Requies, M. B. Güemez and P. L. Arias, *Appl. Catal. B. Environ.*, 2014, **145**, 34.

18 A. S. Dias, M. Pillinger and A. A. Valente, *Appl. Catal., A*, 2005, **285**, 126.

19 S. Lima, M. Pillinger and A. A. Valente, *Catal. Commun*, 2008, **9**, 2144.

20 R. O'Neill, M. N. Ahmad, L. Vanoye and F. Aiouache, *Ind. Eng. Chem. Res.*, 2009, **48**, 4300.

21 S. Lima, A. Fernandes, M. M. Antunes, M. Pillinger, F. Ribeiro and A. A. Valente, *Catal. Lett.*, 2010, **135**, 41.

22 A. Takagaki, M. Ohara, S. Nishimura and K. Ebitani, *Chem. Lett.*, 2010, **39**, 838.

23 J. B. Binder, J. J. Blank, A. V. Cefali and R. T. Raines, *ChemSusChem*, 2010, **3**, 1268.

24 T. Suzuki, T. Yokoi, R. Otomo, J. N. Kondo and T. Tatsumi, *Appl. Catal. A: Gen.*, 2011, **408**, 117.

25 M. Shirotori, S. Nishimura and K. Ebitani, *Catal. Sci. Technol.*, 2014, **4**, 971.

26 J. B. d'Espinose de la Caillerie, M. Kermarec and O. Clause, *J. Am. Chem. Soc.*, 1995, **117**, 11471.

27 J. Tuteja, S. Nishimura and K. Ebitani, *Bull. Chem. Soc. Jpn.*, 2012, **3**, 275.

28 Y. Román-Leshkov, M. Moliner, J. A. Labinger, and M. E. Davis, *Angew. Chem. Int. Ed.*, 2010, **49**, 8954.

29 Lewis acid amount of Ni^{2+}-modified Al_2O_3 was tentetively estimated to be 63 $\mu mol\cdot g^{-1}$ on the basis of the initial rates for MPV reduction and Lewis acid value of γ-Al_2O_3 (JRC-ALO-8) (82 $\mu mol\cdot g^{-1}$) reported in ref. 30.

30 T. Kitano, T. Shishido, K. Teramura, and T. Tanaka, *J. Phys. Chem. C*, 2012, **116**, 11615.

Chapter 3

Genesis of a Bi-functional Acid-Base Site on a Cr-supported Layered Double Hydroxide Catalyst Surface for One-pot Synthesis of Furfural from Xylose with Solid Acid Catalyst

Abstract

A Cr-supported Mg–Al layered double hydroxide (Cr/Mg–Al LDH) comprised bi-functional Lewis acid–Brønsted base active sites on the catalyst surface at close boundaries between Cr^{3+} oxide and Mg–Al LDH. These enabled efficient aldose–ketose isomerization. The combined use of solid Brønsted acid Amberlyst-15 and bi-functional acid–base Cr/Mg–Al LDH exhibits higher activity for one-pot transformation of xylose into furfural via aldose–ketose isomerization and successive dehydration under mild conditions than those exhibited by basic bare Mg–Al LDH, substituted Mg–Cr LDH, and Lewis acidic Cr^{3+} supported catalysts with Amberlyst-15. The correlation between the activity and the Cr loading amount for Mg–Al LDH was evaluated using several characterization techniques and MPV reduction as a model reaction for Lewis acidity investigation. The results show the following: (1) the monomer of Lewis acidic Cr^{3+} oxide is supported on the Mg–Al LDH surface below 1 wt%. (2) Thereafter, Cr^{3+} species form small Lewis acidic Cr^{3+} oxide dimers and/or trimers up to 5 wt%. Then, they cover the Mg–Al LDH surface to generate highly active bifunctional Lewis acid–Brønsted base sites. (3) Above 5 wt%, the excess Cr^{3+} species generate inert Mg–Cr and/or Mg–Al–Cr LDH-like composites. They are deposited on some active sites, leading to decreased activity. The results show that furfural yields vary significantly in accordance with Cr loadings and that the 5 wt%

Cr/Mg–Al LDH achieved the highest value (59% yield, 18 h) because the most effective interaction between the Lewis acidic Cr^{3+} oxide and the Mg–Al LDH basic site is observed at 5 wt% Cr loading.

Introduction

Mg-Al layered double hydroxide (Mg-Al LDH; $[Mg_{1-x}^{2+}Al_x^{3+}(OH)_2]^{x+}A_{x/n}^{n-}\cdot mH_2O$), a well-known layered clay mineral, possesses Brønsted base sites as adsorbed carbonate and hydroxide ions at its surface of brucite-like positive charged two-dimensional sheets. LDH has been widely used as solid base catalyst and support for metal catalysts such as Ru, Pd, Ag, Au, and Pt.[1-7] As a Brønsted base solid catalyst, LDH shows catalytic activity for various organic reactions such as Knoevenagel condensation,[8-11] epoxidation,[12-13] transesterification,[14] and aldol condensation[15-16] as well as aldose–ketose isomerization.[11, 17-19]

Conversion of biomass resources into value-added chemicals and fuels has attracted much attention because such materials can serve as sustainable non-petroleum building blocks in biorefineries.[20-23] Lignocellulosic biomass, a renewable carbon source composed mainly of cellulose, hemicellulose, and lignin, is known as the most abundant woody biomass.[24-26] The hydrolysis of cellulose and hemicellulose into monosaccharides such as glucose and xylose, the first step in biorefinery operations, has been demonstrated with enzyme and chemical catalysts such as soluble mineral acids and solid acids,[27-28] acidic carbons,[29-32] sulfonated carbons,[33-35] and biomass-derived carbon-based catalyst.[36]

The successive conversion of glucose and xylose into furans such as 5-(hydroxymethyl)furfural and furfural has been emphasized because they have great potential as non-petroleum substrates in production of polymers, pharmaceuticals, biofuels, and fine chemicals.[19, 25-26, 37-38] Because this reaction proceeds trimolecular dehydration, Brønsted acid catalysts such as sulfonated zirconia,[39] porous niobium silicates,[40] sulfonic acid modified mesoporous shell silica beads,[41] arenesulfonic SBA-15,[42] and zeolite-based catalysts[43-46] have conventionally been applied at high reaction temperatures (>423 K).

As advanced research studies, many researchers have recently reported two-step transformations of monosaccharides into furans *via* aldose–ketose isomerization and dehydration of ketose. A benefit of this two-step reaction path is that it reduces the energy used for dehydration. For example, the reported activation barrier of xylose (aldopentose) is approximately 30–32 kcal/mol,[47-48] whereas that of xylulose (ketopentose) was calculated as 23.1 kcal/mol.[49] In fact, in this two-step reaction system, the reaction temperature can be reduced to 373 K with 29–56% yield of furfural.[18, 50-51] However, because aldose–ketose isomerization is an equilibrium rate-determining reaction and because the subsequent dehydration of ketopentose is a one-way reaction in a two-step system, discovery of a highly active catalyst surface in aldose–ketose isomerization has been the crucial factor for additional activation. Both Lewis acid sites and base sites are active, respectively, for aldose–ketose isomerization *via* hydride shift and proton shift reaction.[52] Binder *et al.*[50] and Suzuki *et al.*[51] have respectively demonstrated two-step dehydration of xylose into furfural composed of isomerization over Lewis acid site and successive dehydration over Brønsted acid site under mild conditions (373 K) using $CrCl_2$ with LiBr and SO_4^{2-}/SnO_2.

Our earlier studies have demonstrated that furfural can be formed effectively from xylose in a one-pot manner involving aldose–ketose isomerization over Mg-Al LDH *via* proton shift of pentose and successive dehydration of xylulose into furfural over Brønsted acid Amberlyst-15 at 373 K.[18] This catalytic system also shows activity in direct synthesis of furfural derivatives such as (2-furanylmethylene)malononitrile (FMM), known as a semiconducting organic material for photovoltaic device fabrication,[53] from xylose in a one-pot manner *via* successive Knoevenagel condensation by base site of Mg-Al LDH. As advanced research studies, I have reported that the Cr-supported Mg-Al LDH catalyst (Cr/Mg-Al LDH), which is composed of Mg-Al LDH carrier and immobilized Cr^{3+} oxide onto LDH surface, showed higher activity to aldose–ketose isomerization as a bi-functional Lewis acid – Brønsted base catalyst than bare Mg-Al LDH.[11] Furthermore, I have demonstrated a similar strategy in the presence of a different family of bi-functional Lewis acid – Brønsted base Ni^{2+}-modified Al_2O_3 catalyst.[54] The bi-functional Lewis acid – Brønsted base site might act as a highly effective active site for aldose–ketose isomerization. Nevertheless, the detailed local structure of the bi-functional site, the optimized surface structure, and the method for preparing the optimum bi-functional Lewis acid – Brønsted base catalyst for aldose–ketose isomerization remain open questions.

This chapter describes the genesis of a bi-functional Lewis acid – Brønsted base site on Cr/Mg-Al LDH for one-pot transformation of xylose into furfurals. This study was conducted to elucidate the origin of specific high activity for xylose isomerization over the bi-functional acid–base site. A detailed local structure of surface Cr cation species with various Cr loadings was proposed from physicochemical measurements taken using XPS, XAS, ESR, and DTA. I revealed the significance of a bi-functional Lewis acid – Brønsted base site on Cr/Mg-Al LDH generated at close boundaries between small clusters of Cr^{3+} oxide and LDH base sites by comparing catalytic activity with other Cr-supported catalysts and MPV reduction of furfural as a model reaction to evaluate Lewis acidity.

Experimental

Materials and synthesis of catalysts

Mg-Al LDH (AD500NS; Mg/Al = 3.1, MgO 38.1%, Al_2O_3 15.7%, CO_2 8.1%) was purchased from Tomita Pharmaceutical Co., Ltd. $CrCl_3{\cdot}6H_2O$, $MgCl_2{\cdot}6H_2O$, AlOOH (boehmite), CeO_2, and 2-propanol were supplied by Wako Pure Chemical Industries Ltd. *N*,*N*-dimethylformamide, xylose, and TiO_2 (rutile) were obtained from Kanto Chemical Co. Inc., whereas TiO_2 (anatase) and γ-Al_2O_3 (JRC-ALO-8) were supplied respectively by Tokyo Chemical Industry Co. Ltd. and the Catalysis Society of Japan. Amberlyst-15 was purchased from Sigma-Aldrich Corp. Furfural and malononitrile were obtained from Acros Organics BVBA.

Cr/Mg-Al LDHs were prepared using an impregnation method (adsorption) with Mg-Al LDH and an aqueous solution of $CrCl_3{\cdot}6H_2O$: $CrCl_3{\cdot}6H_2O$ was dissolved in 100 mL of distilled water. Then 2 g of Mg-Al LDH was added. After stirring at 353 K for 24 h, the obtained greenish paste was filtered and washed with 2 L of distilled water. Then it was dried overnight at 383 K.

Mg-Cr LDH (Mg/Cr = 3) was prepared by co-precipitation. An aqueous solution of $MgCl_2{\cdot}6H_2O$ and $CrCl_3{\cdot}6H_2O$ ($[M^{2+}] + [M^{3+}]$ = 1 M, 40 mL) and an aqueous NaOH solution (1.0 M) were dropped slowly into an aqueous solution of Na_2CO_3 (1.5 M, 40 mL) with stirring at room temperature and pH 10.0. Then the resulting solution was stirred at 338 K for 6 h. The obtained paste was filtered, washed with 2 L of distilled water, and then dried at 383 K overnight.

Cr-supported SiO_2, CeO_2, TiO_2(rutile), TiO_2(anatase), AlOOH, and γ-Al_2O_3 (Cr: 9 wt%) were prepared by an impregnation method (adsorption) using various supports and an aqueous solution of $CrCl_3{\cdot}6H_2O$ and urea: $CrCl_3{\cdot}6H_2O$ was dissolved in 50 mL of distilled water; then 1 g of support and 2 g of urea were added. After stirring at 353 K for 24 h, the obtained paste was filtered, washed with 2 L of distilled water, and then dried at 383 K overnight.

Characterizations

X-ray diffraction patterns (XRD) were collected on a SmartLab (Rigaku) using a Cu Kα X-ray source (40 kV, 30 mA). Nitrogen adsorption measurements were taken to ascertain the BET specific surface area. Measurements were taken at 77 K (BELSORP-max; BEL Japan, Inc.). X-ray photoelectron spectroscopy (XPS) analyses were performed (Kratos AXIS-URTRA DLD; Shimadzu Corp.) using a monochromatic Al Kα source (10 mA, 15 kV). The binding energies were calibrated with C 1s level (284.5 eV) as the internal standard. X-ray absorption spectra (XAS) in Cr K-edge were recorded at room temperature using double Si(111) single-crystal monochromator at the BL-9C station of KEK-PF, Japan (Proposal No. 2013G586). The obtained spectra were analyzed using software (ver. 2.5.92REX2000; Rigaku Corp.). Solid state Electron spin resonance (ESR) spectra were produced (JES-FA200; JEOL) at X-band frequency with a 100 kHz modulation frequency, 1 mW microwave power, and 0.6 mT modulation width. Spectra were recorded at 103 K. Differential thermal analysis (DTA) curves were corrected on a Thermo plus EVO2 (Rigaku Corp.) with a rewarming rate of 10°C min^{-1} in air. Transmission electron microscopy (TEM) images were taken (H-7100; Hitachi Co. Ltd.) at 100 kV. Diffuse reflectance UV-vis spectroscopy (DR UV-vis) spectra were collected on a U-3900H (Hitachi) at wavelength of 220-800 nm with a scan rate of 120 nm min^{-1}. α-Cr_2O_3, $Cr(OH)_3 \cdot nH_2O$ and $CrCl_3 \cdot 6H_2O$ were diluted 10 times with $BaSO_4$.

Reactions

One-pot synthesis of furfural from xylose was performed in a Schlenk tube attached to a reflex condenser under an N_2 flow (30 mL min^{-1}). The reaction was typically performed using 0.67 mmol of xylose, 0.2 g of Cr-LDHs or Mg-Al LDH, 0.1 g of Amberlyst-15 and 3 mL of *N*,*N*-dimethylformamide at 373 K.

One-pot synthesis of FMM from xylose, which consists of furfural synthesis and successive Knoevenagel condensation was conducted *via* a two-step reaction without catalyst separation: after furfural synthesis, the reaction mixture was cooled to room temperature without stirring, then 0.8 mmol of malononitrile was added; thereafter, the following

Knoevenagel condensation was conducted under stirring at 373 K. The yields of furfural and FMM were calculated based on xylose.

Meerwein–Ponndorf–Verley (MPV) reduction of furfural in 2-propanol toward furfuryl alcohol was performed in 50 mL of a pear-shaped flask attached to a reflex condenser. After 1.3 mmol furfural, 83 mmol 2-propanol (6.4 mL), and 0.1 g of catalysts were charged into the reactor, they were heated at 355 K.

Products obtained from one-pot synthesis of furfural and FMM from xylose, and from MPV reduction were analyzed using GC-FID (GC-2014; Shimadzu Corp.) equipped with a non-polar column (DB-1; Agilent Technologies Inc.), whereas isomerization of xylose was analyzed using HPLC (515; Waters Corp.) with a column (RSPak KC-811; Shodex, Showa Denko K.K.). The HPLC analysis conditions were set as 0.1 wt% H_3PO_4 aq. eluent, 1.0 mL min^{-1} flow rate, and 323 K column temperature.

Results and discuttion

Effect of Cr species location

Preliminarily, I prepared Cr-LDHs with different location of Cr species. Then I investigated their catalytic performance and structural properties. The substituted type Mg-Cr LDH had a typical LDH structure. The supported type 9wt%Cr/Mg-Al LDH retained the original Mg-Al LDH structure ascertained from XRD measurements (Figure 1(A)). This result indicates that, the Cr species are mainly supported on Mg-Al LDH surface as small clusters in the case of 9wt%Cr/Mg-Al LDH. The XPS analyses of Cr/Mg-Al LDH and Mg-Cr LDH revealed Cr $2p_{2/3}$ peaks at 576.5 eV and 577.0 eV, respectively corresponding to the Cr^{3+} oxide and hydroxide[55] (Figure 1(B)). X-ray absorption near-edge structure (XANES) features of both Cr-LDHs in Cr *K*-edge XAS were similar to those of Cr^{3+} compounds. Moreover, because strong pre-edge peaks at around 5992 eV attributed to tetrahedral Cr species were observed only slightly in prepared Cr-LDHs, the Cr species in those Cr-LDHs are expected to exist only as octahedral compounds (Figure 1(C)). From these results, the following structural properties of

Cr-LDHs were inferred: The small octahedral cluster of Cr^{3+} oxide species is present on the Mg-Al LDH surface in the case of Cr/Mg-Al LDH, whereas $Cr(OH)_3$ constituted the LDH octahedral hydroxide layers with $Mg(OH)_2$ in the case of Mg-Cr LDH.

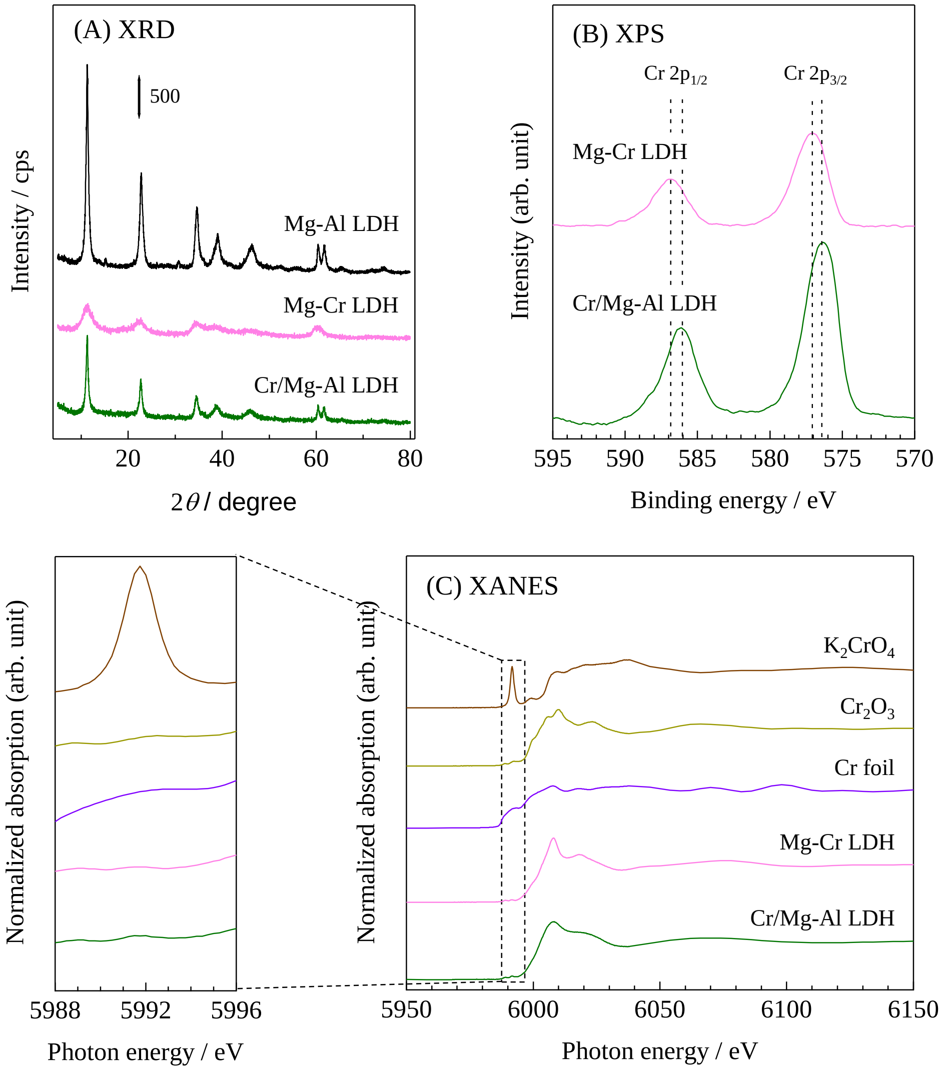

Figure 1 (A) XRD patterns, (B) Cr 2p XPS, and (c) Cr *K*-edge XANES of 9wt%Cr/Mg-Al LDH and Mg-Cr LDH (Mg/Cr = 3).

Table 1 presents the results of furfural yield in one-pot dehydration of xylose using the pair of Amberlyst-15 and supported type Cr/Mg-Al LDH, the substituted type Mg-Cr LDH, or the physical mixture of Mg-Al LDH and Cr_2O_3. The combined use of Amberlyst-15 and bare

Mg-Al LDH, and blank test (just loading Amberlyst-15) were also tested. The table shows that just loading Amberlyst-15 was unsuitable for direct dehydration of xylose to furfural. The combined use of Amberlyst-15 and bare Mg-Al LDH gave 19% yield of furfural with ~30% selectivity and ~70% xylose conversion. The substituted type Mg-Cr LDH or the physical mixed type Mg-Al LDH + Cr_2O_3 system showed similar yield to that of bare Mg-Al LDH. Therefore, implementation of Cr^{3+} species or physical mixing of bulk Cr_2O_3 is unsuitable for xylose transformation. Higher performance was observed in the case of supported type Cr/Mg-Al LDH catalyst with 36% yield of furfural, ~40% selectivity of furfural, and ~85% xylose conversion. Isomerized pentoses selectivity was ~30%, and no other products were detected by GC-FID and HPLC. The combined use of Cr/Mg-Al LDH and Amberlyst-15 achieved 59% yield of furfural from xylose after optimization of Cr loading amount and reaction time (*vide infra*). These results demonstrate clearly that supporting the trivalent Cr species onto LDH surface is more effective than substitution or physical mixing.

Table 1 Activities of combined use of Cr-LDHs and Amberlyst-15 for one-pot synthesis of furfural from xylose.[a]

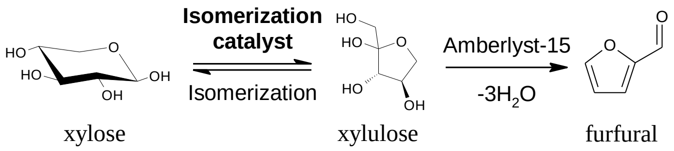

entry	isomerization catalyst	yield of furfural /%
1	Cr/Mg-Al LDH	36,[b] 59[c]
2	Mg-Cr LDH[d]	24
3	Mg-Al LDH + Cr_2O_3[e]	21
4	Mg-Al LDH	19
5	—	4

[a]*Reaction conditions*: xylose (0.67 mmol), isomerization catalyst (0.2 g), Amberlyst-15 (0.1 g), *N*,*N*-dimethylformamide (3 mL), 373 K, 3 h, N_2 flow (30 mL min^{-1}). [b]Cr (9 wt%). [c]Cr (5 wt%), 18 h. [d]Mg/Cr = 3. [e]Mg-Al LDH (0.174 g) + Cr_2O_3 (0.026 g).

To investigate the effect of Cr^{3+} loading onto Mg-Al LDH on the activity for xylose isomerization, I examined the transformation of xylose over Cr/Mg-Al LDH and bare Mg-Al LDH in the absence of Amberlyst-15. The retention times for detected compounds were, respectively, 7.5, 7.7, and 8 .0 min for xylose, xylulose and lyxose, for ribulose, and for arabinose (Figure 2). The supported type Cr/Mg-Al LDH exhibited higher xylose conversion and isomerized pentose selectivity, as shown in the obtained HPLC charts (Figure 2) and exhibited rough calculated values (Table 2). These results suggest that the immobilization of Cr species on Mg-Al LDH surface affected not only promotion of the reaction rate but also suppression of side reactions, such as oligomerization or decomposition.

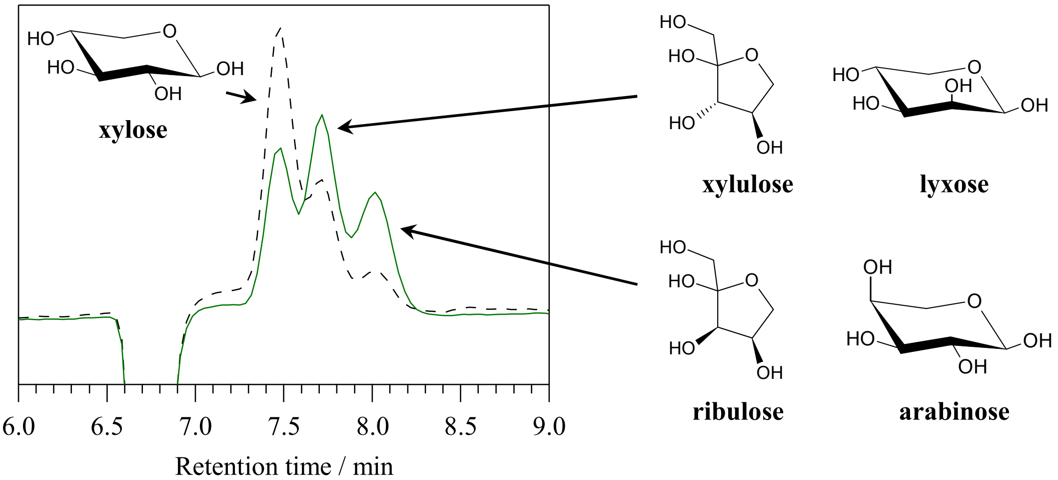

Figure 2 HPLC chart of transformation of xylose using Mg-Al LDH (dashed line) and 9wt%Cr/Mg-Al LDH (solid line). *Reaction conditions*: xylose (0.67 mmol), catalyst (0.2 g), *N*,*N*-dimethylformamide (3 mL), 373 K, 3 h, 500 rpm, and N_2 flow (30 mL min^{-1}).

Table 2 Rough calculated conversion and selectivity values for isomerization of xylose over Mg-Al LDH and 9wt%Cr/Mg-Al LDH.

Catalyst	Conversion of xylose /%	Selectivity for isomerized pentoses /%
9wt%Cr/Mg-Al LDH	~80	~55
Mg-Al LDH	~60	~30

[a]*Reaction conditions*: xylose (0.67 mmol), isomerization catalyst (0.2 g), Amberlyst-15 (0.1 g), *N*,*N*-dimethylformamide (3 mL), 373 K, 3 h, N_2 flow (30 mL min^{-1}). [b]Cr (9 wt%). [c]Cr (5 wt%), 18 h. [d]Mg/Cr = 3. [e]Mg-Al LDH (0.174 g) + Cr_2O_3 (0.026 g).

Table 3 presents the Lewis acidity of various Cr-LDHs as its catalytic activity for the MPV reduction of furfural in 2-propanol toward furfuryl alcohol, a typical hydride shift reaction catalyzed by a Lewis acid such as γ-Al_2O_3 (entry 5).[11] It is noted that solid base catalysts, such as MgO and CaO, have also been reported affording high activity in the MPV reduction.[56-59] However, these typical solid base catalysts usually required a pretreatment with high temperature to generate the basic O^{2-} anion because these Lewis base sites are easily poisoned by CO_2 and H_2O in the atmosphere.[60] In fact, un-pretreated MgO showed no activity for the MPV reduction (entry 7). Accordingly, the catalytic performance for MPV reduction in this reaction conditions should be mainly influenced by the Lewis acidity. Our earlier study demonstrated that Cr/Mg-Al LDH exhibited higher activity to the MPV reduction than bare Mg-Al LDH, as shown in entries 1 and 2. Therefore, I compared the activities of supported type Cr/Mg-Al LDH with substituted type Mg-Cr LDH in the MPV reduction. As shown in entry 3, the activity of Mg-Cr LDH resembled that of bare Mg-Al LDH. It was much lower than Cr/Mg-Al LDH. These results suggest that supporting Cr^{3+} species onto the Mg-Al LDH surface is suitable to provide Lewis acidity rather than substituting Cr^{3+} species in Mg-Cr LDH. They

Table 3 Activities of Cr-LDHs for MPV reduction of furfural.[a]

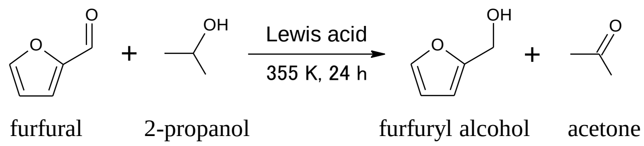

entry	catalyst	yield of furfuryl alcohol /%
1	Cr/Mg-Al LDH[b]	33
2	Mg-Al LDH	9
3	Mg-Cr LDH[c]	7
4	Cr_2O_3	trace
5	γ-Al_2O_3	74
6	Amberlyst-15	0
7	MgO	0

[a]*Reaction conditions*: furfural (1.3 mmol), 2-propanol (83 mmol), catalyst (0.1 g), 355 K, 24 h. [b]Cr (9 wt%). [c]Mg/Cr = 3.

also suggest that the Cr/Mg-Al LDH surface consisted of LDH-originated Brønsted base sites and supported Cr^{3+}-originated Lewis acid sites. Cr/Mg-Al LDH showed higher activity for furfural production from xylose than bare Mg-Al or Mg-Cr LDH surface, which is composed mainly of Brønsted base sites. Therefore, the Brønsted base – Lewis acid bi-functional Cr/Mg-Al LDH surface might function more efficiently for xylose conversion. Moreover, because this MPV reduction was only slightly promoted over the bulk Cr_2O_3 surface (entry 4), dispersion of Cr^{3+} species is expected to play an important role in generating Lewis acidity.

Effect of support

To evaluate the bi-functional Lewis acid – Brønsted base surface, various Cr^{3+} supported catalysts (Cr/Support) were prepared to assess its catalytic activities for MPV reduction and one-pot synthesis of furfural from xylose in the presence of Amberlyst-15. As Cr^{3+} supports, SiO_2, CeO_2, TiO_2(rutile), TiO_2(anatase), AlOOH, and γ-Al_2O_3 were selected in addition to Mg-Al LDH. The Cr content was adjusted to 9 wt%. The XPS analysis results suggested that the oxidation states of Cr species on CeO_2, TiO_2(rutile), TiO_2(anatase), AlOOH, and γ-Al_2O_3 were Cr^{3+} oxides, and that of Cr/SiO_2 was Cr^{3+} hydroxide[55] (Figure 3). All Cr^{3+} supported catalysts retained their original respective support structures, as determined using XRD (Figure 4).

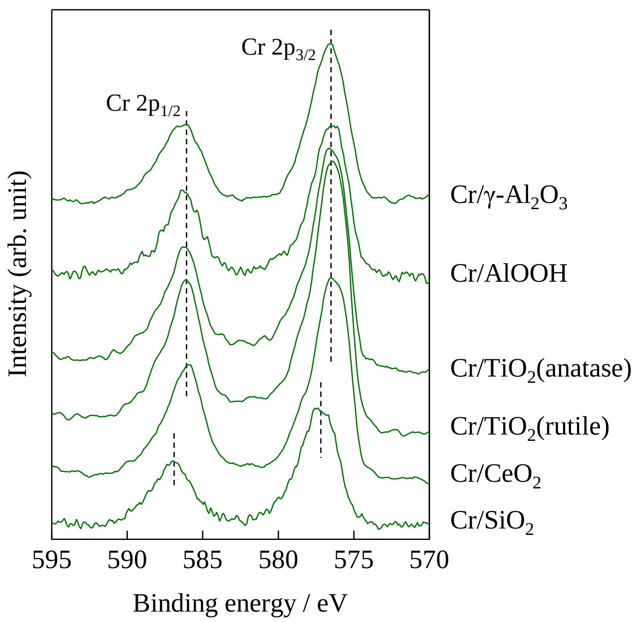

Figure 3 Cr 2p XPS of various Cr supported catalysts with 9 wt% Cr loading.

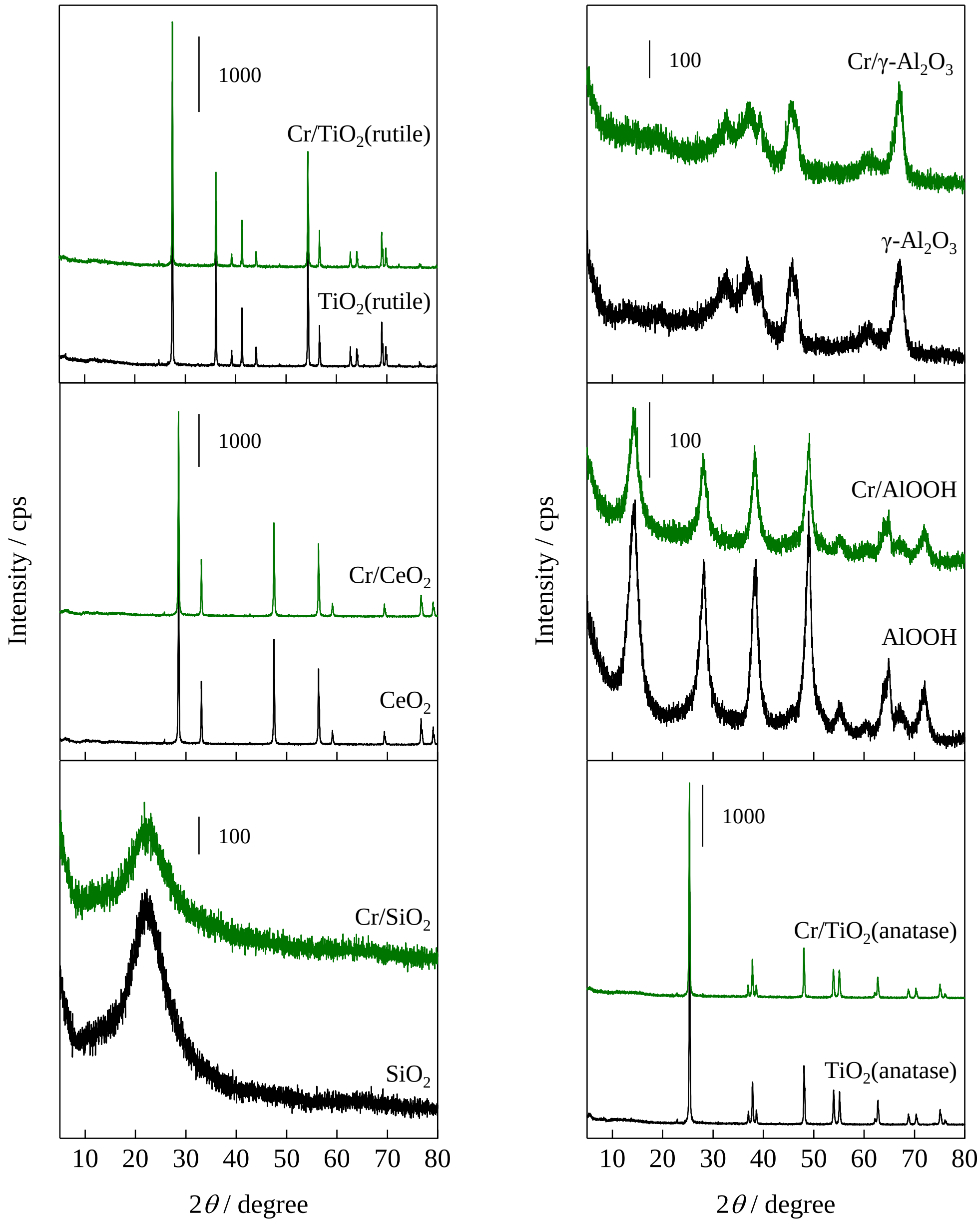

Figure 4 XRD patterns of various supports and Cr supported catalysts with 9 wt% Cr loading.

Lewis acidities evaluated as activity for the MPV reduction over bare supports and Cr supported catalysts are presented in Figure 5. The use of bare SiO_2, CeO_2, TiO_2(rutile), and TiO_2(anatase) gave furfuryl alcohol only slightly. Nevertheless, furfuryl alcohol production was observed over Cr supported SiO_2, CeO_2, TiO_2(rutile), and TiO_2(anatase). Therefore, I infer that the impregnation of Cr^{3+} onto these supports, which themselves possess no active Lewis acidic site for MPV reduction, causes generation of Lewis acidity. Furthermore, increasing Lewis acidity by Cr^{3+} support was observed for Lewis acidic AlOOH and γ-Al_2O_3 which showed medium or high activity for MPV reduction even support itself. These results show clearly that supported Cr^{3+} species can act as a Lewis acid site and can promote MPV reduction irrespective of the support.

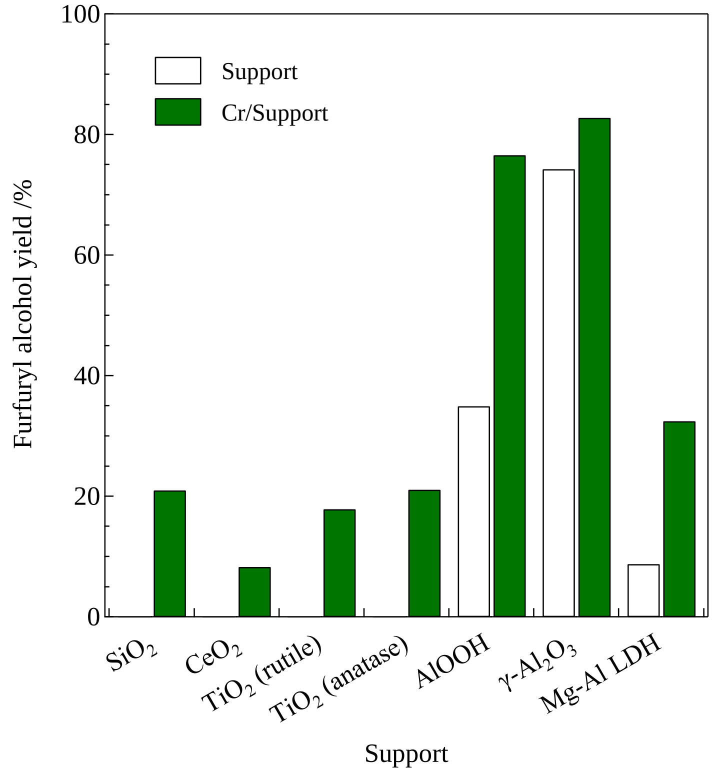

Figure 5 Activities of various supports and Cr/Support catalysts for MPV reduction.
Reaction conditions: furfural (1.3 mmol), 2-propanol (83 mmol), catalyst (0.1 g), 355 K, 24 h, amount of Cr (9 wt%).

Figure 6 presents the furfural yield from xylose by combined use of Amberlyst-15 and bare or Cr^{3+} supported catalysts. In the case of combined use of Amberlyst-15 and bare SiO_2, CeO_2, TiO_2(rutile), and TiO_2(anatase), which are inactive for MPV reduction, gave poor furfural yield. Furfural amounts obtained using those catalysts were similar to that of Amberlyst-15 alone (approx. 5%). Therefore, these supports seemed to possess no active sites effective for xylose conversion. However, Cr supported SiO_2, CeO_2, TiO_2(rutile), and TiO_2(anatase) showed better activities than bare supports. These results suggest that Cr^{3+} species itself can convert xylose as Lewis acid sites. Efficient production of furfural was observed with combined use of Amberlyst-15 and Lewis acidic AlOOH, γ-Al_2O_3, or Brønsted basic Mg-Al LDH. Increasing furfural production amounts by Cr^{3+} support was also observed for those active supports.

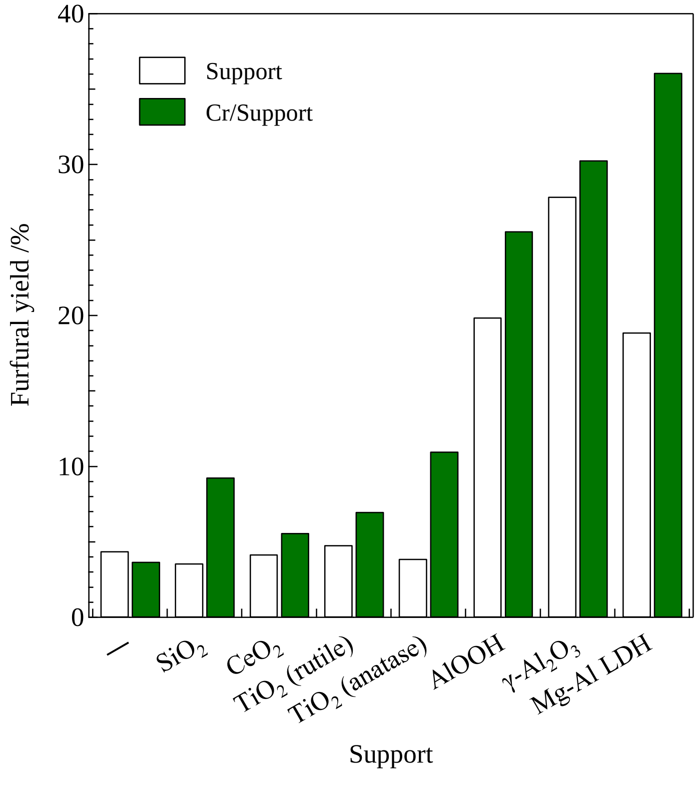

Figure 6 Activities of combined use of various supports or Cr/Supports as isomerization catalysts and Amberlyst-15 for one-pot synthesis of furfural from xylose. *Reaction conditions*: xylose (0.67 mmol), isomerization catalyst (0.2 g), Amberlyst-15 (0.1 g), *N*,*N*-dimethylformamide (3 mL), 373 K, 3 h, N_2 flow (30 mL min^{-1}), amount of Cr (9 wt%).

Román-Leshkov *et al.* have reported that aldoses are isomerized into ketoses, which can be dehydrated into furfural by Brønsted acid site, *via* intermolecular MPV reduction over Lewis acid site.[52] I therefore expect that Lewis acidity directly affects the furfural production amount. Figure 7(A) portrays correlation between Lewis acidity of various Cr^{3+} supported catalysts as furfuryl alcohol yield in the MPV reduction and furfural yield in one-pot dehydration of xylose by combined use of Amberlyst-15 and various Cr^{3+} supported catalysts. Actually, good linearity was found: R^2 = 0.99. Nevertheless, Cr/Mg-Al LDH alone did not fit this trend. It showed high activity to furfural synthesis in spite of its Lewis acidity. Given simply, this was apparently true because of the Brønsted basicity of Mg-Al LDH. In the case of Cr/Mg-Al LDH, the furfural yield is affected not only by Lewis acidity originated Cr^{3+} species but also by Brønsted basicity originated Mg-Al LDH. Therefore, if this specifically high activity occurred because of the simple coexistence of Brønsted base site of Mg-Al LDH, these plots show linearity when these were modified to differences of catalytic activities between Cr/Support and Support itself.

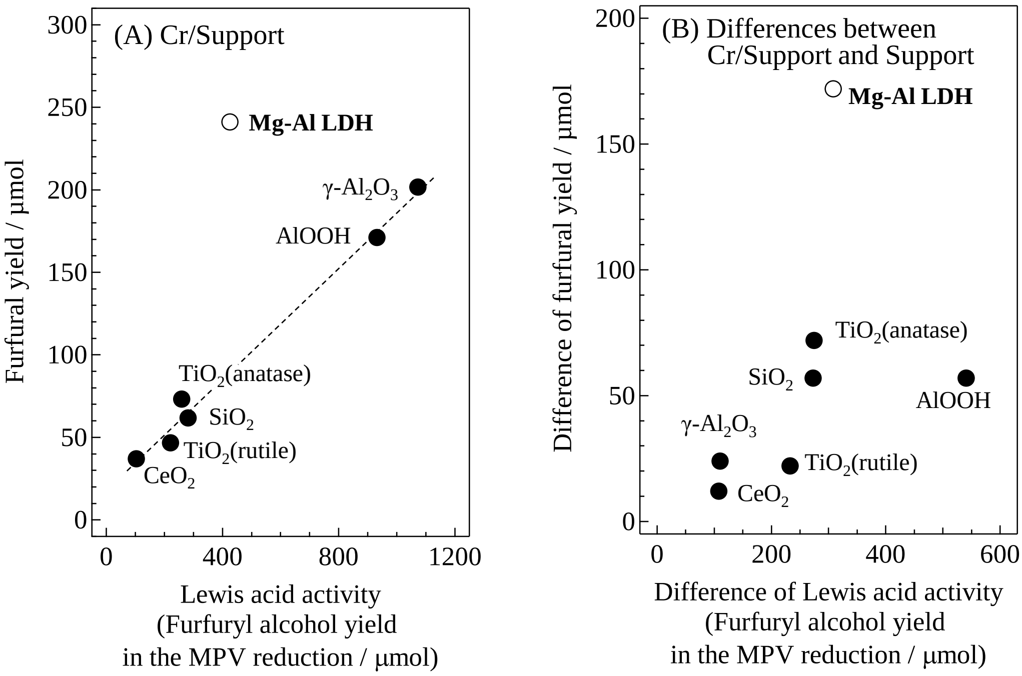

Figure 7 Correlations between catalytic activity for MPV reduction and furfural synthesis over (A) Cr/Supports, and (b) differences of yield between Cr/Support and the support itself ([Yield over Cr/Support](μmol) – [Yield over Support](μmol)). Amount of Cr (9 wt%).

However, even when modifying these plots to differences of yields between Cr/Support and the support itself ([Yield over Cr/Support] – [Yield over Support]), the Cr/Mg-Al LDH system showed a significantly higher furfural yield than that suggested by the tendency shown by other Cr^{3+} supported catalysts (Figure 7(B)). This result shows clearly that combination of Lewis acidic Cr^{3+} oxide and Brønsted basic Mg-Al LDH exhibited a significant effect on xylose isomerization. Our previous reports confirmed that the combined use of Amberlyst-15 and physical mixture of γ-Al_2O_3 + Mg-Al LDH, a pair of a typical Lewis acid and Brønsted base, showed lower activity to one-pot synthesis of furfural from xylose than the combined use of Amberlyst-15 and Cr/Mg-Al LDH.[11] Moreover, the combined use of Amberlyst-15 and Ni^{2+}-modified Al_2O_3, which possess close boundaries between Lewis acid γ-Al_2O_3 and Brønsted base fine Ni-Al LDH, facilitated the synthesis of furfural from xylose more efficiently than Amberlyst-15 and a physical mixture of γ-Al_2O_3 and Ni-Al LDH.[54] Therefore, I suggest that the close boundaries between Cr^{3+} oxide and Mg-Al LDH acted as bi-functional Lewis acid – Brønsted base sites (Figure 7(A)), facilitating aldose–ketose isomerization from xylose into ketopentoses.

Reaction mechanism

The reaction mechanism for the aldose–ketose isomerization of xylose into xylulose is discussed. Some reports describe two reaction paths from aldose to ketose: a hydride shift mechanism *via* intermolecular MPV reduction catalyzed by Lewis acid such as Sn-Beta,[52] $CrCl_2$ or $CrCl_3$,[50, 61]; and a proton shift mechanism *via* Lobry de Bruyn-Alberda van Ekenstein transformation catalyzed by a base site.[52, 62-63] The rate determining step in both reaction paths is considered to be a hydride/proton shift reaction of deprot-O2-open-aldose (an activated ring opening aldose formed by deprotonation at O2H)[61] or 1,2-endiol(enolate) intermediate[63] (Figures 5(B) & 5(C)). Pidko *et al.* demonstrated that glucose (aldohexose) isomerization toward fructose (ketohexose) was facilitated using Lewis acidic $CrCl_2$ in dialkylimidazolium chloride ionic liquids. They have also described the role of Cr^{2+} ion based on DFT-computed reaction energy diagrams. Two Cr^{2+} ions make coordination with activated sugar intermediate. In the resulting deprot-O2-open-glucose···×2Cr complex, the carbonyl O1 moiety bridges two

Cr ions with one of Cr^{2+} additionally coordinating to the anionic O2 group. Interaction with the two metal cations substantially stabilized the anionic reaction intermediates involved in the H shift reaction.[61] Ekeberg *et al.* reported that the reaction rate of the Lobry de Bruyn-Alberda van Ekenstein transformation of aldose to ketose in boiling pyridine was increased strongly by the addition of aluminum oxide. In this catalytic system, the base pyridine is regarded as the main active site. The catalytic effect of aluminum oxide is presumably attributable to adsorption on the surface and stabilization of the enediol intermediate produced by the rate-determining proton shift step by base, thereby lowering the energy of the transition state.[63]

Based on these reports, I propose the possible aldose–ketose isomerization mechanism over bare Mg-Al LDH and Cr/Mg-Al LDH as shown in Figure 8. In the case of bare Mg-Al LDH, at first the deprotonation of C2H of the open-xylose, an α-proton of carbonyl, by the basic site generates unstable 1,2-endiol(enolate) intermediate. Then successive rate-determining proton shifts from O2 to O1 and protonation of C1H occur to form open-xylulose (Figure 8(B)). However, in the case of Cr/Mg-Al LDH (Figure 8(C)), Lewis acid Cr^{3+} oxides make coordination with O1 and O2(H) of open-xylose, which increases positive charges on C2H and O2H. At the close boundaries between Cr^{3+} oxide and Mg-Al LDH, the bi-functional Lewis acid – Brønsted basic sites, the C2H is deprotonated by Brønsted base sites. Also, the isomerization reaction proceeds in the same proton shift process as bare Mg-Al LDH. Unstable 1,2-endiol(enolate) intermediate is expected to be generated as the coordination complex with Lewis acid Cr^{3+} oxide in this case. Therefore, the transition state energy is decreased and the reaction rate is increased compared to that proceeding over bare Mg-Al LDH. Moreover, even at Lewis acid Cr^{3+} oxide, which is not adjacent to the base site, O2H of coordination complex of open-xylose with Cr^{3+} oxide can be deprotonated. A successive intermolecular MPV hydride shift reaction would occur to form open ketopentoses in the same process as Lewis acidic Cr supported SiO_2, CeO_2, TiO_2(rutile), TiO_2(anatase), AlOOH, or γ-Al_2O_3.

Accordingly, I propose that the bi-functional Lewis acid – Brønsted basic sites constructed on Cr/Mg-Al LDH enhance the proton shift mechanism as a main reaction path, and propose that the parts of isolated Cr^{3+} oxides on Cr/Mg-Al LDH proceed by the hydride shift mechanism as a side reaction path. Therefore, such complementary isomerization paths of xylose into ketopentoses over Cr/Mg-Al LDH serve successively higher activity rather than bare Mg-Al LDH and other Cr supported catalysts, leading to high yield for the one-pot formation of furfural.

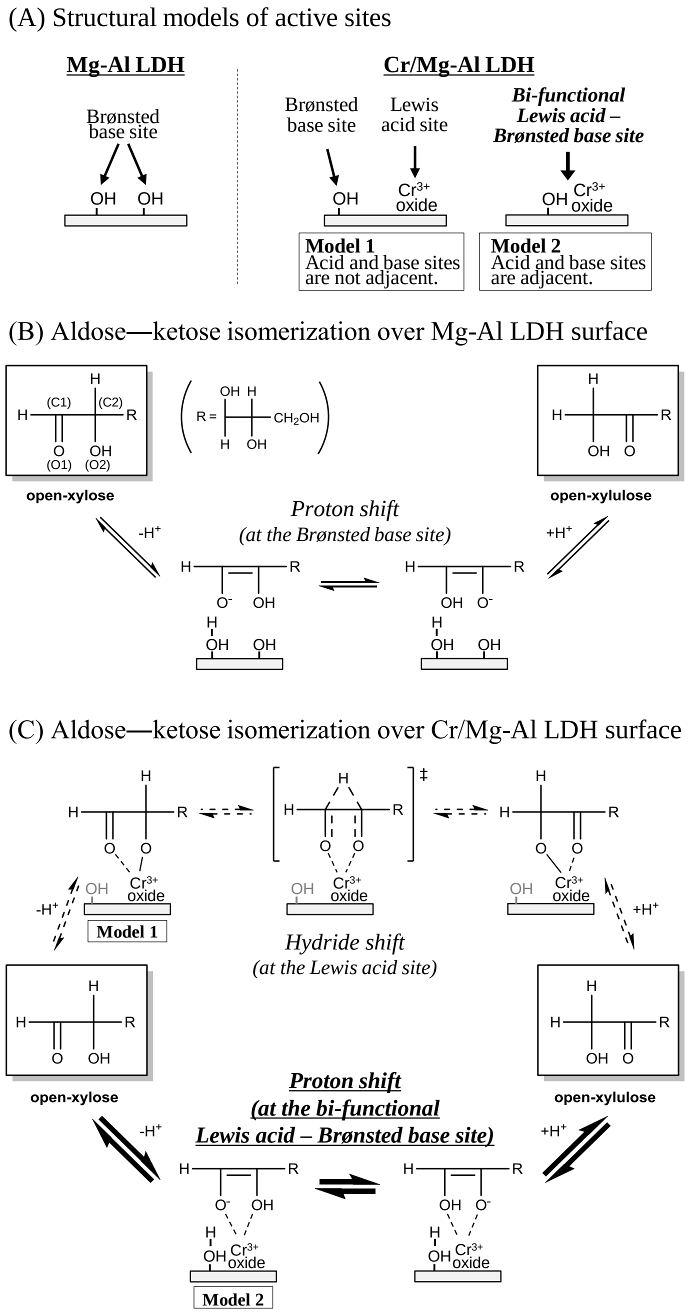

Figure 8 (A) Structural models of active sites on Mg-Al LDH and Cr/Mg-Al LDH surfaces, and the proposed reaction mechanism for aldose–ketose isomerization over (B) Mg-Al LDH and (C) Cr/Mg-Al LDH.

Effect of the loading amount in Cr supported Mg-Al LDHs

Results show that the loading amount of Cr^{3+} oxide also strongly affects catalytic activity and structural properties in Cr/Mg-Al LDH (*vide infra*). First, the crystal properties of Mg-Al LDH support, electronic states, and local structural properties of Cr species on Cr/Mg-Al LDHs with various Cr loading amounts were evaluated using XRD, XPS, XAS, DTA, and ESR measurements. The XPS analysis of all Cr/Mg-Al LDHs exhibited a Cr $2p_{2/3}$ peak at around 576.5 eV corresponding to the Cr^{3+} oxide. The normalized XPS spectra were almost identical at all Cr loading amounts (Figure 9). No significant change of diffraction patterns in accordance with the Cr amount was found using XRD measurements (Figure 10). Even for 15wt%Cr/Mg-Al LDH, only LDH originated XRD patterns were observed. No other Cr^{3+} originated structure such as crystalline α-Cr_2O_3 was detected. Lattice parameters *a* and *c*, which are calculated respectively from (003) and (110) plane diffraction peaks, were almost comparable irrespective of Cr loading amounts, as shown in Figure 11.

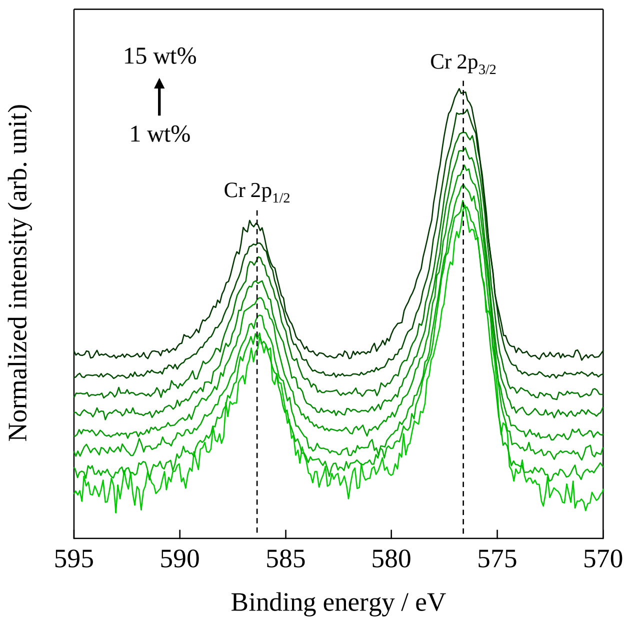

Figure 9 Normalized Cr 2p XPS of Cr/Mg-Al LDHs with various Cr loadings.

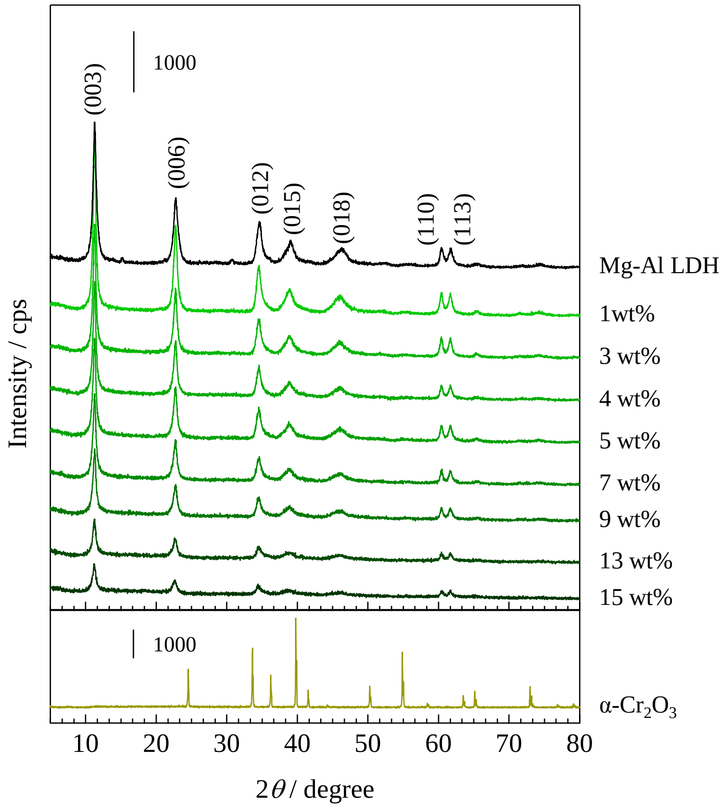

Figure 10 XRD patterns of Cr/Mg-Al LDHs with various Cr loadings.

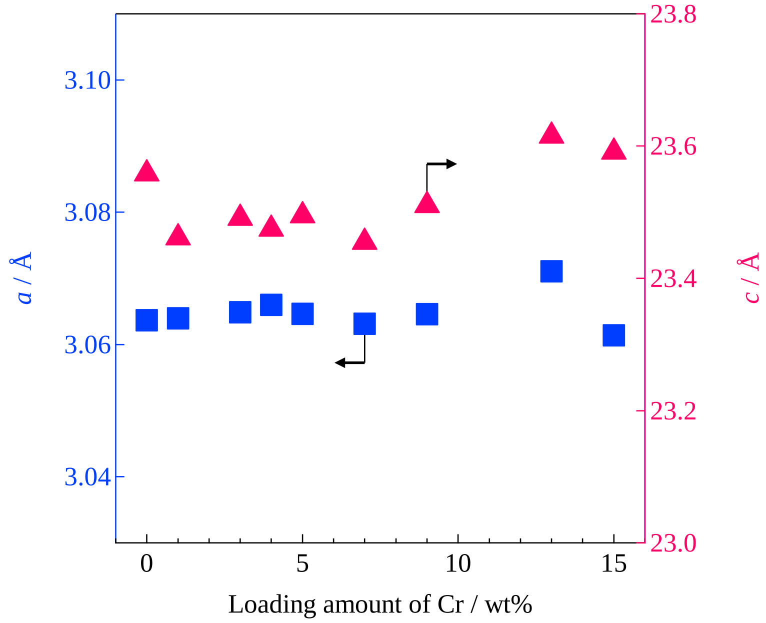

Figure 11 Lattice parameter *a* and *c* of Cr/Mg-Al LDHs with various Cr loadings.

Figure 12 shows Cr *K*-edge XANES spectra of various Cr/Mg-Al LDHs and Mg-Cr LDH, amorphous $Cr(OH)_3{\cdot}nH_2O$, and crystalline α-Cr_2O_3 as Cr^{3+} references. All XANES of Cr/Mg-Al LDHs showed Cr^{3+}-originated main peak and some small pre-edge peaks at around 5988–5994 eV. These pre-edges are attributed to distorted octahedral Cr^{3+} of 1s to 3d(2g), 1s to3d(e2g),[64-65] and metal–metal transitions.[65-66] Overall XANES shapes of Cr/Mg-Al LDHs appeared to be intermediate of Mg-Cr LDH and $Cr(OH)_3{\cdot}nH_2O$. It is interesting that only 1wt%Cr/Mg-Al LDH showed a sharp XANES spectral shape in comparison to others, which is more similar to Mg-Cr LDH than $Cr(OH)_3{\cdot}nH_2O$. The 3–15wt%Cr/Mg-Al LDHs shape resembled amorphous $Cr(OH)_3{\cdot}nH_2O$ more than it resembled that of Mg-Cr LDH.

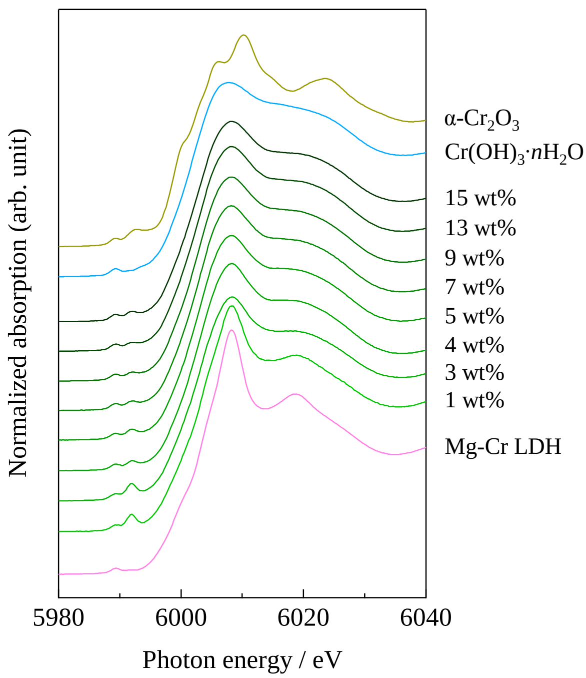

Figure 12 Cr *K*-edge XANES of reference samples and Cr/Mg-Al LDHs with various Cr loadings.

A similar trend was observed from Cr *K*-edge k^3-weighted extended X-ray absorption fine structure (EXAFS) spectra of Cr/Mg-Al LDHs with various Cr loadings (Figure 13(A)). For 3–15 wt%, although the EXAFS spectra were only slightly varied in the region above 9 $Å^{-1}$, the overall shapes in oscillation were almost identical. Whereas, the articulate difference in 1 wt% was observed in the oscillation region around 5.5 and 8.5 $Å^{-1}$. Moreover, the respective

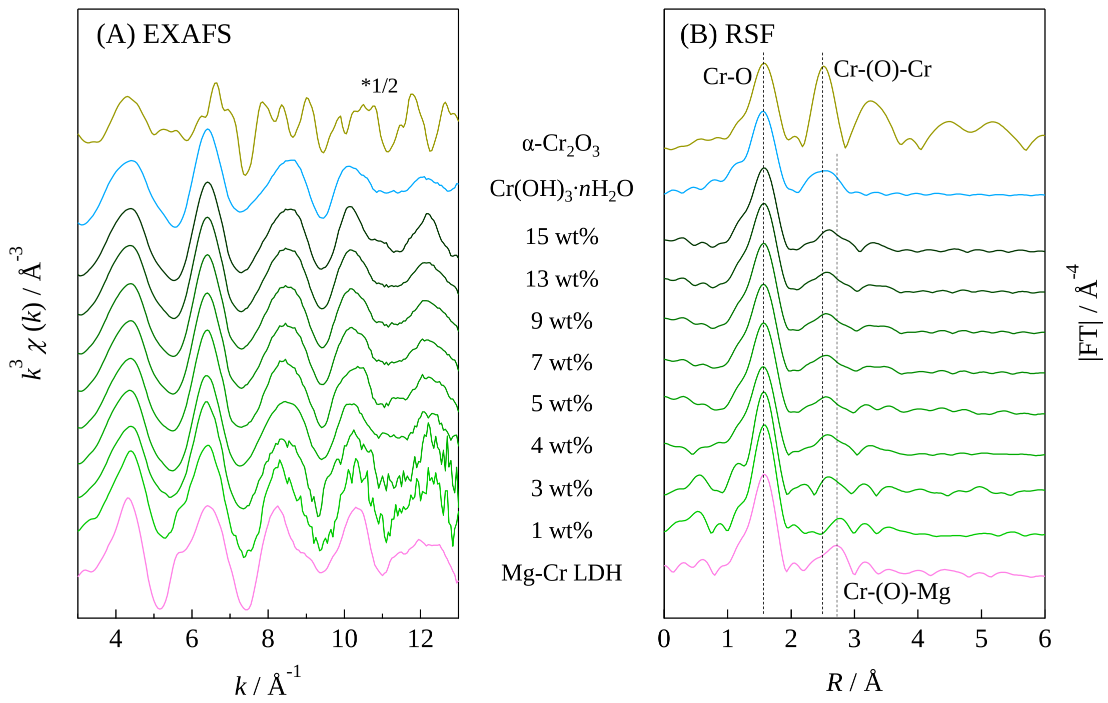

Figure 13 Cr K-edge XANES of reference samples and Cr/Mg-Al LDHs with various Cr loadings.

shapes in oscillation of 3–15 wt% and 1 wt% were similar to those of amorphous $Cr(OH)_3 \cdot nH_2O$ and Mg-Cr LDH. These results suggest that the Cr^{3+} species were trapped at first by peripheral defect sites of two-dimensional Mg-Al hydroxide sheets to form substituted Mg-Cr LDH like structure. Subsequently, they adsorbed onto LDH flat plane surface to generate a Cr^{3+} oxide monomer or cluster that has $Cr(OH)_3 \cdot nH_2O$-like amorphous structure. The diffuse reflectance UV-visible (DR UV-vis) spectra of bulk Cr_2O_3, $Cr(OH)_3 \cdot nH_2O$, $CrCl_3 \cdot 6H_2O$, Mg-Cr LDH and Cr/Mg-Al LDH are presented in Figure 14. Clearly, the coordination environment of Cr^{3+} oxide on Mg-Al LDH is completely different with bulk Cr_2O_3, $Cr(OH)_3 \cdot nH_2O$, $CrCl_3 \cdot 6H_2O$, so that Cr^{3+} oxides

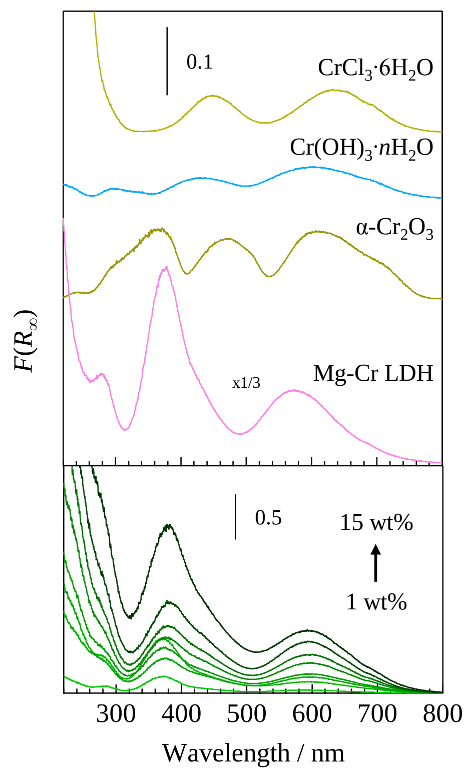

Figure 14 DR UV-vis spectra of Cr/Mg-Al LDH with various Cr loadings and α-Cr_2O_3, $Cr(OH)_3 \cdot nH_2O$, $CrCl_3 \cdot 6H_2O$ and Mg-Cr LDH as reference samples.

dispersed on Mg-Al LDH surface might form a monomer or cluster rather than the bulk structure of such a type. This point can be clarified by the radial structure function (RSF; Figure 13(B)). The RSFs (the phase shift was not corrected) of Cr/Mg-Al LDHs produced three peaks at 1.6, 2.5, and 2.8 Å. The first and second peaks were assigned respectively as first coordinated Cr-O and second coordinated Cr-(O)-Cr with 1.98 and 3.00 Å.[65] The third peak is expected to correspond to Cr-(O)-Mg by reference to RSF of Mg-Cr LDH with 3.07 Å

In the case of 1 wt%, the RSF showed two peaks corresponding to Cr-O and Cr-(O)-Mg. No Cr-(O)-Cr bond was observed. Above 3 wt%, the RSFs peak top at 2.5–2.8 Å shifted from 2.8 Å (Cr-(O)-Mg) to 2.5 Å (Cr-(O)-Cr) (Figure 15(A)). Then the amplitudes were little increased concomitantly with increasing Cr loading amount (Figure 15(B)). Curve-fitting analysis showed that the coordination numbers of Cr-(O)-Cr were about 1.2 (5 wt%) – 1.4 (15 wt%), indicating that Cr^{3+} oxide mainly formed a dimer or trimer.

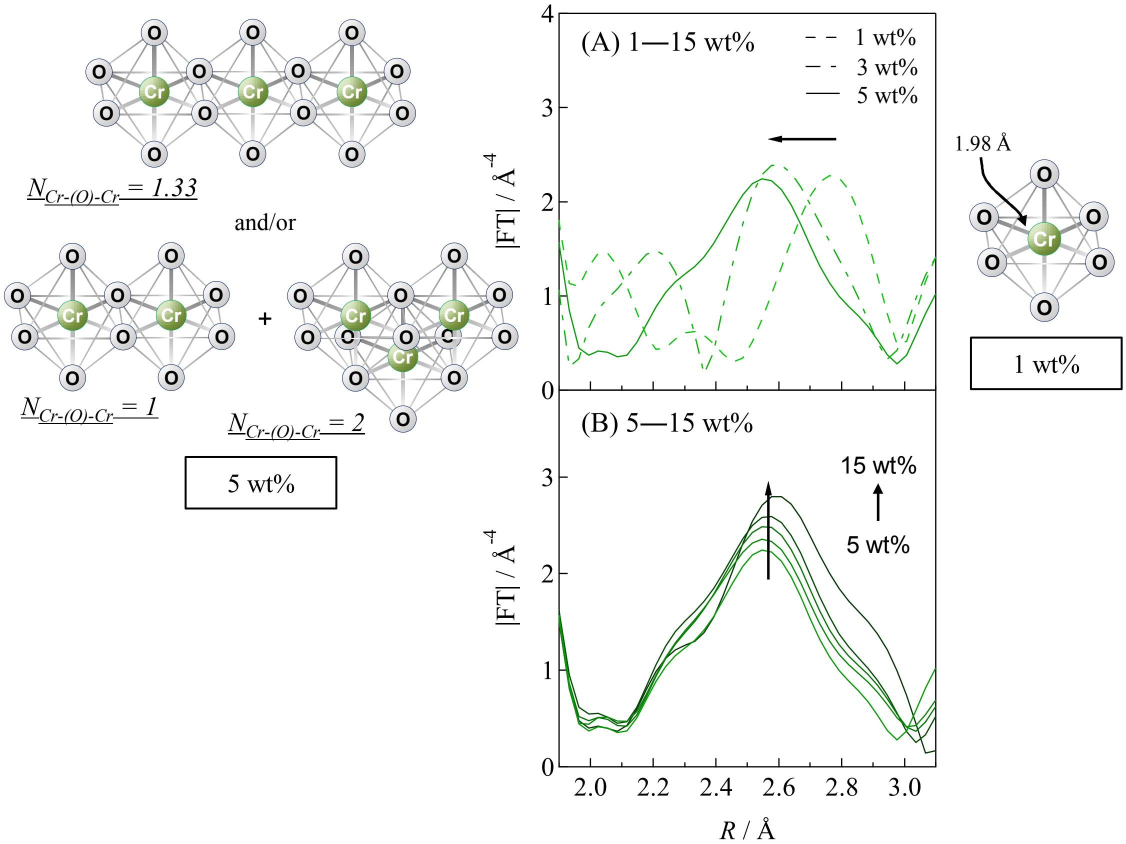

Figure 15 Fourier transforms of Cr *K*-edge k^3-weighted EXAFS of Cr/Mg-Al LDHs with various Cr loadings. (A) 1—5 wt% and (B) 5—15 wt%Cr/Mg-Al LDHs.

Figure 16(A) shows ESR spectra of Cr/Mg-Al LDHs with various Cr loadings recorded at 103 K. Main signals appeared at g = 2.02. Its amplitude increased in accordance with Cr loadings. It is particularly interesting that, in the case of 1 wt%, another signal was visible at g = 4.3 in normalized ESR spectra, as shown in Figure 16(b), whereas this signal was almost reduced in 3 wt%. Reportedly, three ESR responsiveness Cr species exist: (i) the γ-signal with g_{II} = 1.959 and $g_{\perp}$ = 1.978 corresponding to magnetically isolated axially symmetric Cr^{5+} surface species, (ii) the broad line that is visible at g' = 2, which is assigned to magnetically interacting Cr^{3+} ions in Cr_2O_3-like cluster (β-signal), and (iii) the broad line that appeared at g' = 4.3 assigned to magnetically isolated coordinatively unsaturated Cr^{3+} ions (δ-signal).[67] According to a previous report, the two signals appearing in Cr/Mg-Al LDHs at g = 2.02 and g = 4.3 were assigned respectively to Cr^{3+} originated β-signal and δ-signal. These results indicate that a part of Cr^{3+} species on the Mg-Al LDH exist as isolated Cr^{3+} monomer in the case of 1 wt%, and that it forms a Cr_2O_3-like Cr^{3+} cluster (not crystalline) in the cases of above 3 wt%. This result agrees well with XAS results.

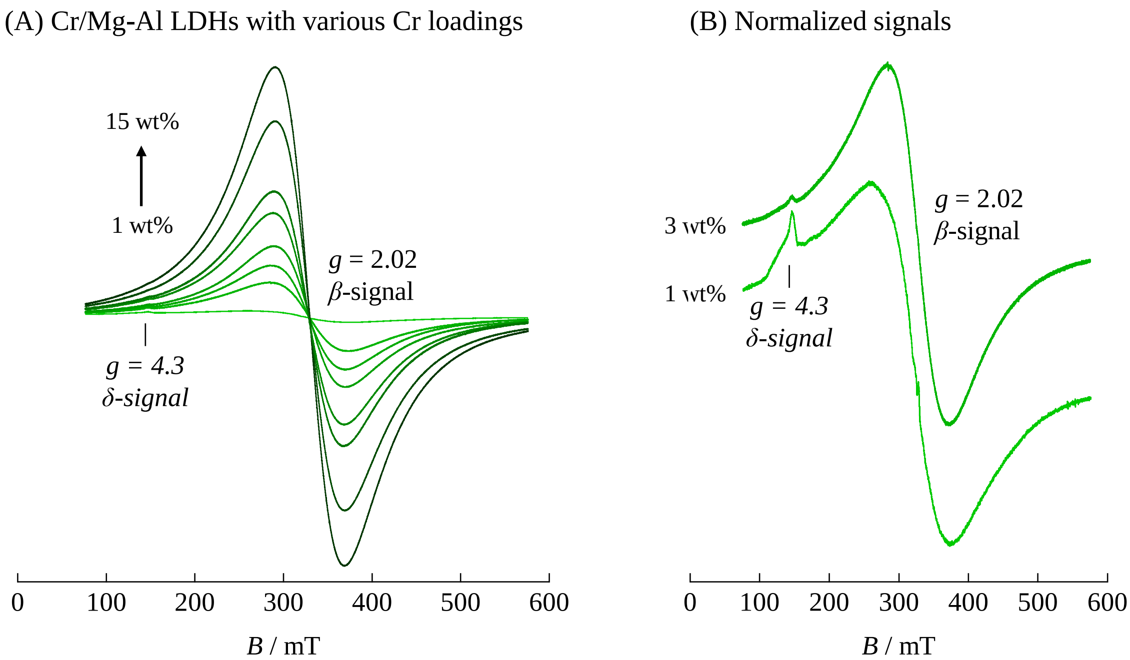

Figure 16 (A) ESR spectra of Cr/Mg-Al LDHs with various Cr loadings and (B) normalized spectra for 1 wt% and 3 wt% at 103 K.

A significant change in structural property of Mg-Al LDH support was observed in the DTA curves. Figure 17 shows DTA curves of Cr/Mg-Al LDHs with various Cr loadings. Dehydroxylation of layer hydroxide groups in Mg-Al-CO_3 LDH with Mg/Al = 3 is well known to occur at around 400 °C.[68] As demonstrated in the previous report, bare Mg-Al LDH showed an endothermic peak at 398 °C. The DTA curves of 1–4wt%Cr/Mg-Al LDHs were similar to those of Mg-Al LDH. Above 5 wt%, two shoulder peaks at around 355 °C and 415 °C are apparent. They increased in accordance with Cr loading. Figure 18 shows DTA peaks of various Cr^{3+} references with 15wt%Cr/Mg-Al LDH. Compared to the references, the extra endothermic peak at 355 °C was similar to that of Mg-Cr LDH with Mg/Cr = 5. Because an endothermic peak of Mg-Cr LDH with Mg/Cr = 3 is apparent at 402 °C, the peak at 355 °C is expected to originate from dehydroxylation of unstable Mg excess Mg-Cr composite hydroxide, such as $Mg_2Cr(OH)$. Another peak at 415 °C was only observed in the partially substituted Mg-Al-Cr LDH, indicating that this extra peak is attributed to dehydroxylation of MgAlCr(OH) site. These results suggest that Cr^{3+} species are dispersed mainly onto LDH surface up to 5 wt%. Then excess Cr^{3+} species generate Mg-Cr and/or Mg-Al-Cr LDH like composite structure above 5 wt%. Figure 19 portrays TEM images of bare Mg-Al LDH and Cr/Mg-Al LDH with various Cr loadings. LDH originated layered flat plane was observed in all samples. The morphology of Cr/Mg-Al LDH below 5 wt% was as smooth as that of bare Mg-Al LDH, although it became coarse above 5 wt%. Furthermore, no Cr^{3+} originated articulate particles were observed. Because no change in lattice parameter of Mg-Al LDH support with

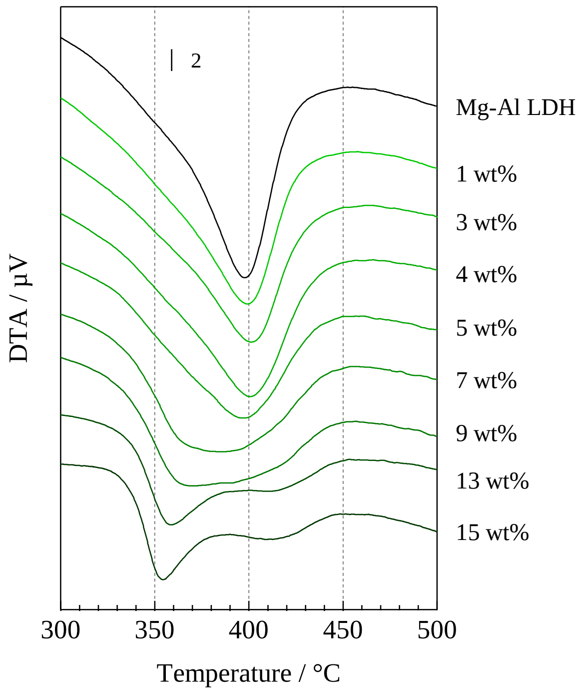

Figure 17 DTA profiles of Cr/Mg-Al LDHs with various Cr loadings.

various Cr loadings was observed, as shown in Figure 11, these results support that Cr^{3+} oxides were covering the LDH carrier as small size clusters up to 5 wt%, thereafter forming amorphous Mg-Cr and/or Mg-Al-Cr LDH-like composite at the surface of the Mg-Al LDH support.

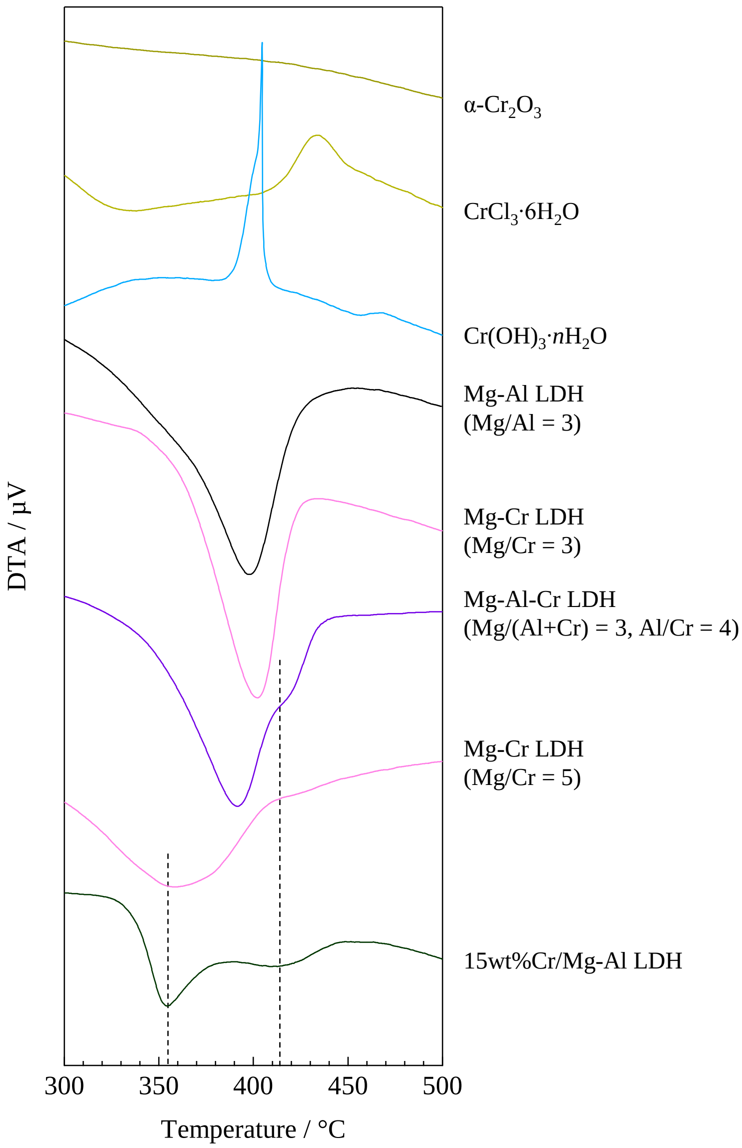

Figure 18 DTA of 15wt%Cr/Mg-Al LDH and Cr^{3+} references.

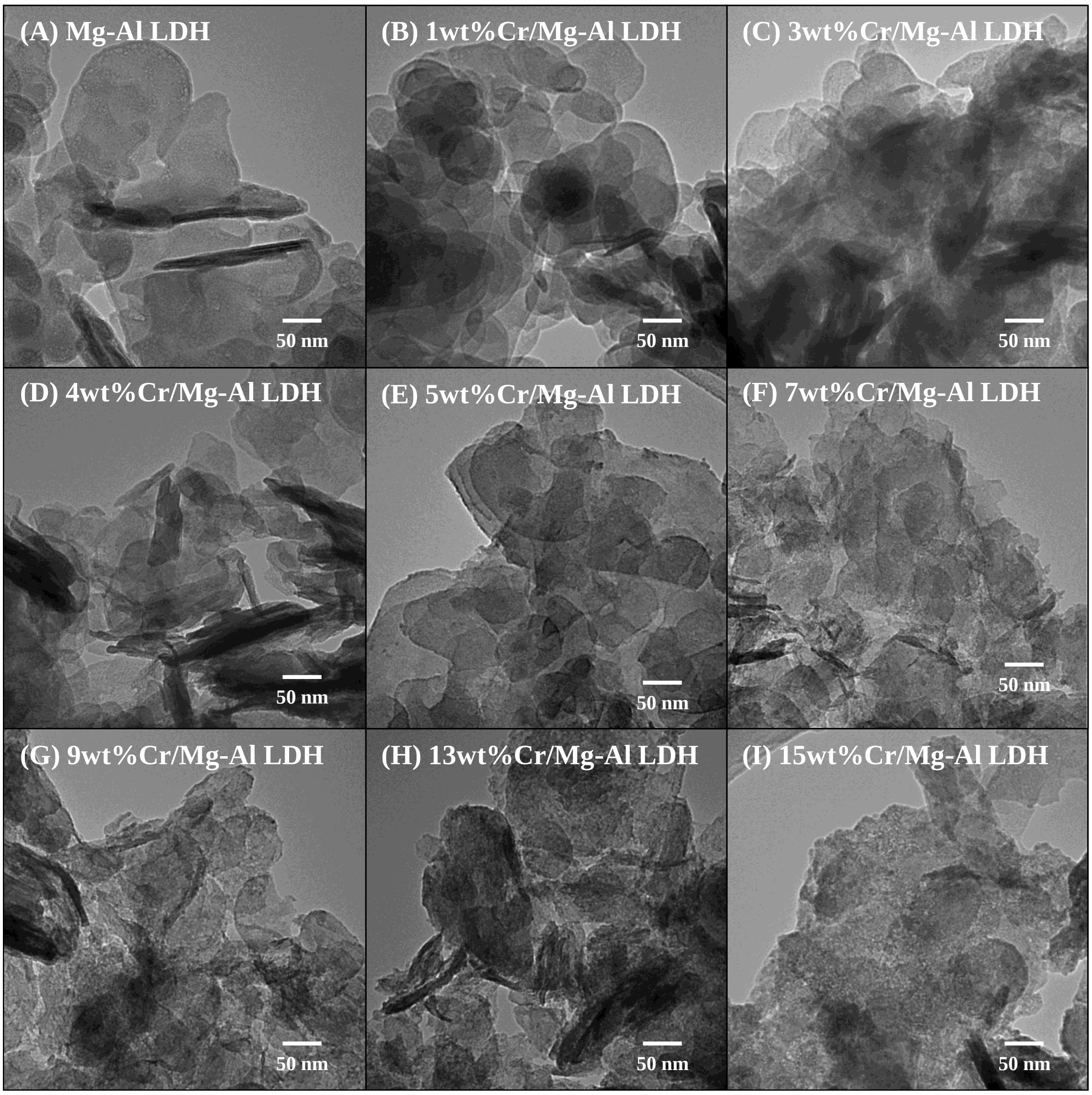

Figure 19 TEM images of Mg-Al LDH and Cr/Mg-Al LDHs with various Cr loadings: (A) Mg-Al LDH, (B) 1wt%-, (C) 3wt%-, (D) 4wt%-, (E) 5wt%-, (F) 7wt%- (G) 9wt%-, (H) 13wt%-, and (I) 15wt%Cr/Mg-Al LDH.

Based on the intensity of Cr 2p, Mg 2p and Al 2p XPS, the surface Cr/(Mg+Al) ratio was calculated as shown in Figure 20. The surface Cr/(Mg+Al) ratio was linearly increased in accordance with Cr loading up to 5 wt%. Thereafter, its increase became gradual. This result showed clearly that 5 wt% is a criterion that differentiates the character of Cr^{3+} species in Cr/Mg-Al LDH: most Cr^{3+}species are apparently supported on the Mg-Al LDH surface in the case of below 5 wt%, although a part of it substitutes brucite layer of LDH or forms Mg-Cr and/or Mg-Al-Cr composite.

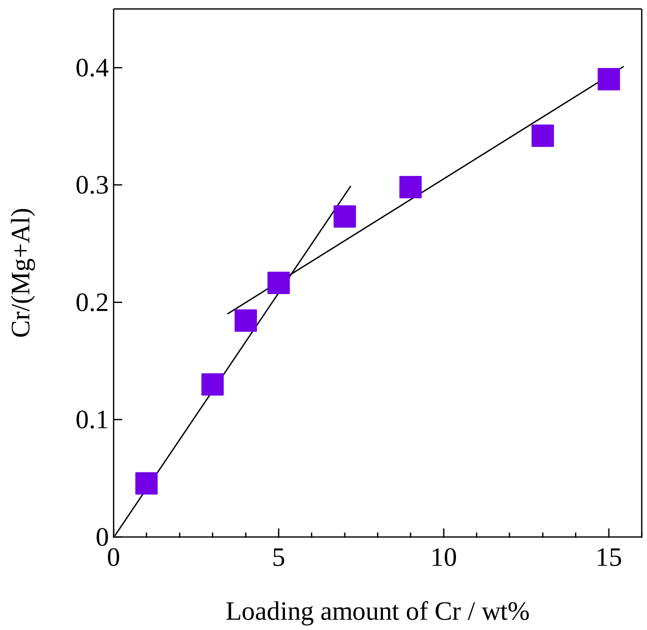

Figure 20 Atomic ratio of Cr/Mg-Al LDHs with various Cr loadings. Atomic ratios were calculated based on Cr 2p, Mg 2p and Al 2p XPS.

The specific surface areas (S_{BET}) of Cr/Mg-Al LDHs with various Cr loadings are presented in Table 4 and are shown in Figure 21. The Cr theoretical content, Cr content obtained by ICP-AES, surface area g(Mg-Al LDH)$^{-1}$ (S_0) calculated from S_{BET}, occupied area by Cr_2O_3 ($S_{occupied}$) calculated from Cr content, and theoretical coverage (θ) by Cr_2O_3 on Mg-Al LDH are listed in Table 4. To calculate S_0, $S_{occupied}$ and θ, I applied three assumptions: (i) all Cr^{3+} species exist as Cr_2O_3 octahedral, (ii) all Cr_2O_3 units have the same cross section, and (iii)

Table 4 Physical properties of Cr/Mg-Al LDHs with various Cr loadings.

Cr content				$S_{BET}{}^{c}$ / m^2 g^{-1}	$S_0{}^{d}$ / m^2	$S_{occupied}{}^{e}$ / m^2 g(cat)$^{-1}$	$S_{occupied}{}^{e}$ / m^2 g(Mg-Al LDH)$^{-1}$	θ^f /%
mmol g(Mg-Al LDH)$^{-1}$	wt% as Cr[a]	wt% as Cr[b]	wt% as Cr_2O_3[a]					
0	0	0	0	44.5	44.5	0	0	0
0.19	1	1.0	1.5	55.8	56.6	18.1	18.3	32.3
0.60	3	3.1	4.3	71.8	75.0	54.5	56.2	74.8
0.80	4	4.0	5.7	73.6	78.1	72.6	75.6	96.8
1.02	5	5.1	7.2	83.6	90.1	91.6	96.4	107
1.45	7	7.7	9.9	96.3	107	127	137	128
1.90	9	9.7	12.6	140	160	163	180	112
2.87	13	14.6	17.9	190	232	236	271	117
3.39	15	15.9	20.5	238	299	272	320	107

[a]Theoretical value. [b]Obtained by ICP-AES. [c]BET specific surface area. [d]Surface area of g(Mg-Al LDH)$^{-1}$ carrier. [e]Occupied area by Cr_2O_3 unit (0.16 nm^2). [f]Coverage of Cr_2O_3 on Mg-Al LDH.
Cross section of Cr_2O_3 unit on Mg-Al LDH was calculated as the cluster composed of two edge-sharing CrO_6 octahedral using the length of Cr-O (0.198 nm) obtained from EXAFS curve fitting.

the value of cross section is 0.16 nm^2 per Cr_2O_3. In the range of 0–5 wt%, S_{BET} was increased gradually from 44.5 to 83.6 m^2 g^{-1}. Thereafter, it increased rapidly and reached 238 m^2 g^{-1} (15 wt%). It is particularly interesting that S_0 showed the same trend with S_{BET}, indicating that the surface area of the LDH carrier itself is varied with Cr loading amount. Cr/Mg-Al LDHs were prepared in acidic $CrCl_3{\cdot}6H_2O$ aqueous solution with pH = 3–3.5. Therefore, this change of S_0 with Cr loadings is expected to be attributable to the dissolution and reprecipitation of LDH carrier with Cr^{3+} ion. It is noteworthy that simple treatment of Mg-Al LDH in aqueous hydrochloric solution of pH 3, the same pH with $CrCl_3{\cdot}6H_2O$ aqueous solution for preparation of 15 wt%Cr/Mg-Al LDH, did not strongly affect the increase of S_{BET} (52.4 m^2 g^{-1}). Because this change becomes prominent above 5 wt%, the point at which Mg-Al-Cr LDH composite begins to be generated, the amorphous Mg-Al-Cr composite might possess high surface area. Their generation might contribute to the improvement of S_{BET} and S_0. For 4–5 wt%, S_0 and $S_{occupied}$ were calculated respectively as 78.1–90.1 m^2 g^{-1} and 75.6–96.4 m^2 g(Mg-Al LDH)$^{-1}$. The theoretical θ at 4–5 wt% calculated from those values were 96.8–107%, indicating that most of the LDH surface was covered with a monolayer of Cr^{3+} oxide at 4–5 wt%.

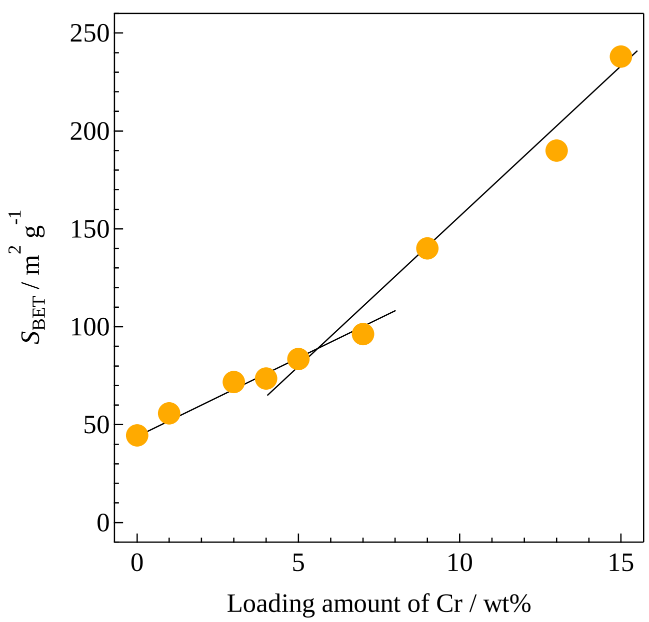

Figure 21 Specific surface area of Cr/Mg-Al LDHs with various Cr loadings.

Next, I investigated the effects of Cr loading amounts on catalytic activities. Figure 22(A) shows the correlation of furfural yield and Cr loading amounts in the one-pot synthesis of furfural from xylose using Amberlyst-15 and Cr/Mg-Al LDHs with various Cr loadings. Among the 0–15wt%Cr/Mg-Al LDH, 5wt%Cr/Mg-Al LDH catalyst showed the highest furfural yield (40%). Additionally, when those catalytic systems were applied to one-pot synthesis of FMM from xylose *via* successive Knoevenagel condensation of generated furfural with malononitrile, again 5wt%Cr/Mg-Al LDH showed the highest activity (49% yield with 94% selectivity, Figure 22(B)). Selectivity for FMM varied in accordance with the Cr amount: it decreased immediately for 0–5 wt% Cr loadings; thereafter the reduction rate became gradual. Our previous report

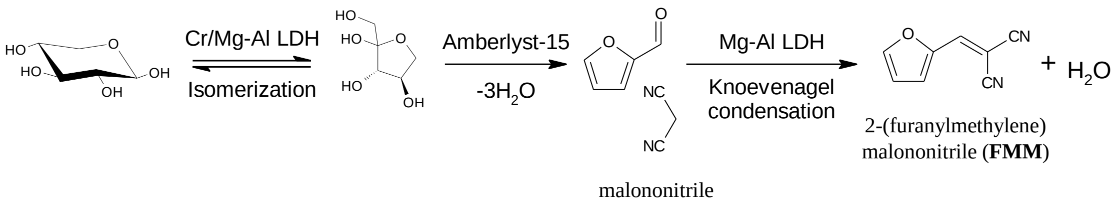

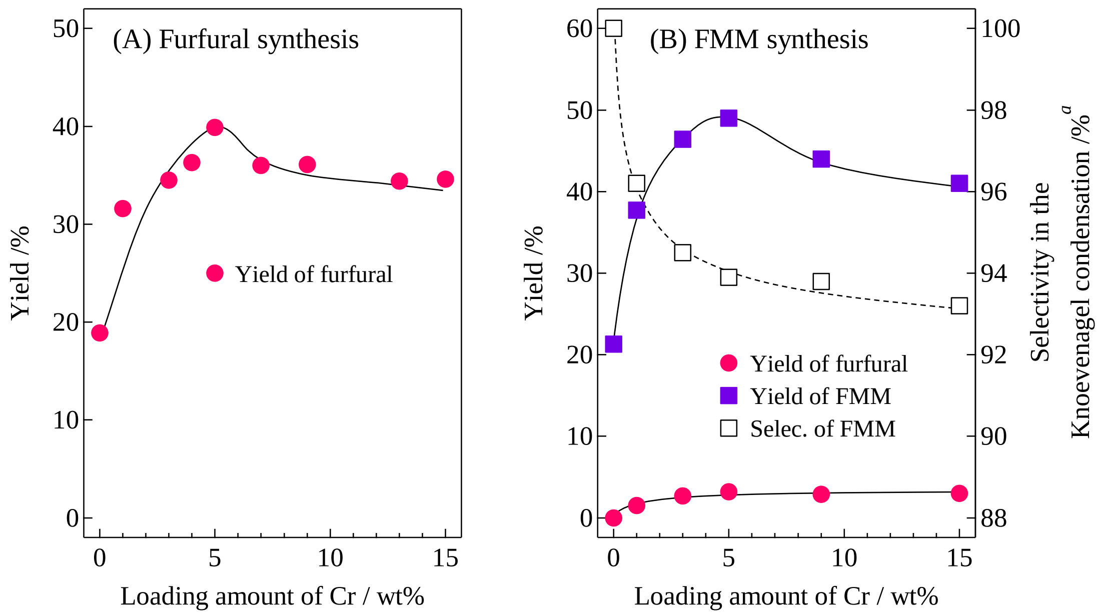

Figure 22 Activities of combined use of Amberlyst-15 and Cr/Mg-Al LDHs with various Cr loadings for one-pot transformation of xylose into (A) furfural and (b) FMM. *Reaction conditions*: (A) xylose (0.67 mmol), isomerization catalyst (0.2 g), Amberlyst-15 (0.1 g), *N*,*N*-dimethylformamide (3 mL), 373 K, 3 h, N_2 flow (30 mL min^{-1}). (B) after (a), the reaction mixture was cooled to room temperature without stirring. Then 0.8 mmol of malononitrile was added, and the reaction was restarted. 1 h, N_2 flow (30 mL min^{-1}). [a]Selectivity: $Yield_{FMM}/(Yield_{furfural} + Yield_{FMM}) \times 10^2$.

described that successive Knoevenagel condensation is catalyzed mainly by Brønsted base sites of Mg-Al LDH.[11] Therefore, this change in selectivity up to 5 wt% might occur because of the decrement of Mg-Al LDH-originated Brønsted base sites by Cr loading. Furthermore, above 5 wt%, generation of Mg-Cr and/or Mg-Al-Cr LDH-like composite might act as weak Brønsted base site to suppress the decrease of the reaction rate for Knoevenagel condensation. The absence of leaching of Cr after the reaction was confirmed by ICP-AES analysis, but the catalytic activity was reduced in the reuse experiments because of the adsorption of intermediate and other by-products onto the Cr/Mg-Al LDH.[11]

To elucidate the correlation between activities for xylose transformation and Lewis acidity in Cr/Mg-Al LDH system, I attempted to evaluate the activity derived from Lewis acidic sites on Cr/Mg-Al LDHs with various Cr loadings using the MPV reduction. Figure 23(A) shows that the simple increase in initial rate per weight of Cr/Mg-Al LDH by the increase in Cr loading amount was observed. Furthermore, when the initial rates for the MPV reduction were divided by specific surface area S_{BET}, a different trend was observed as shown in Figure 23(B): the initial rate per unit surface area of Cr/Mg-Al LDH increased linearly to 5 wt%. Then it decreased gradually. This change presumably occurs because of generation of the amorphous Mg-Cr and/or Mg-Al-Cr LDH-like composite (*vide supra*). Moreover, when the initial rates for the MPV reduction were divided by the total Cr loading amount to calculate the apparent turnover frequency (TOF), the 5 wt% was found as a criterion again, the Lewis acidity of Cr^{3+} species in Cr/Mg-Al LDH changes (Figure 23(C)). The TOFs of Cr species were almost equal for <5 wt%, but these values were decreased above 5 wt%. These facts indicate that Cr^{3+} oxide retained its Lewis acidity for <5 wt%, although a part of Cr^{3+} species which are forming Mg-Cr and/or Mg-Al-Cr LDH like composite cannot act efficiently as a Lewis acid site for >5 wt%.

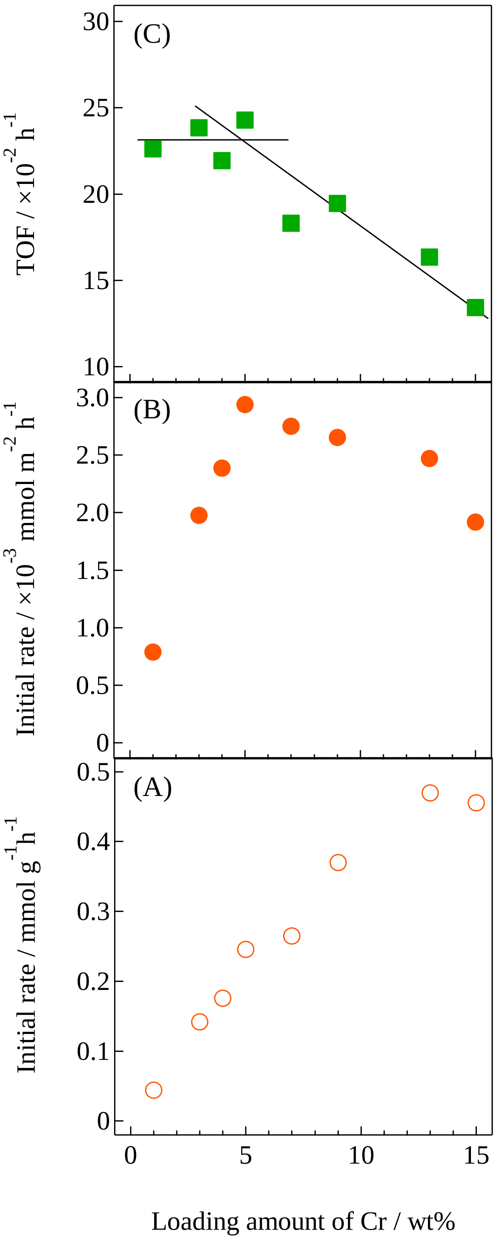

Figure 23 Lewis acidic activities of Cr/Mg-Al LDHs with various Cr loadings for the MPV reduction as (A) initial rate per unit weight of Cr/Mg-Al LDH, (B) initial rate per unit surface area of Cr/Mg-Al LDH and (C) apparent TOF of Cr species. *Reaction conditions*: furfural (1.3 mmol), 2-propanol (83 mmol), catalyst (0.1 g), 355 K, 1 h. TOF: Initial rate (mmol g^{-1} h^{-1}) / amount of Cr (mmol g^{-1}).

According to these results for characterizations and catalytic activities for Cr/Mg-Al LDHs with various Cr loadings, the 5 wt% Cr loading was found as the key point for the appearance of some characteristics: (1) Mg-Cr and/or Mg-Al-Cr LDH-like composite begins to be generated. (2) The LDH carrier is almost covered with a monolayer of Cr^{3+} oxide. (3) The activity for furfural synthesis is maximized. (4) The Lewis acid activity of Cr^{3+} species begins to decline. Kitano *et al.* reported that a Nb_2O_5, Ta_2O_5, MoO_3 or WO_3 monolayer or small cluster was generated on the Al_2O_3 carrier surface after calcination of Nb_2O_5, Ta_2O_5, MoO_3 or WO_3/Al_2O_3 at 1073–1223 K. These exhibited high thermal stable Brønsted acidity at the boundary of supported metal oxide monolayer domains.[69-72] For Nb_2O_5, Ta_2O_5 and MoO_3/Al_2O_3, when the supported metal oxide loading exceeded the amount necessary to form a two-dimensional metal oxide overlayer, inert Al-containing compounds such as $AlNbO_4$, $AlTaO_4$, and $Al_2Mo_3O_{12}$ were formed and were deposited on some Brønsted acid sites, thereby lowering the catalytic activity. Based on these reports, I infer the effect of Cr loading amount on the physical property and catalytic activity of Cr/Mg-Al LDH as follows. First, a part of a Cr^{3+} oxide monomer is trapped by peripheral defect sites of two-dimensional Mg-Al hydroxide sheets. Others are supported onto Mg-Al LDH surface in the case of the low Cr loading amount (>1 wt%). Second, the supported Cr^{3+} oxide forms a dimer or trimer cluster. It covers the Mg-Al LDH carrier surface up to 5 wt%. Because these Cr^{3+} monomers, dimers, and trimers act as Lewis acid sites, the cross boundaries between small Cr^{3+} clusters and the LDH surface form bi-functional Lewis acid – Brønsted base sites that are highly active sites for xylose isomerization. Third, when the Cr^{3+} loading exceeds the amount necessary to cover the Mg-Al LDH carrier (>5 wt%), excess Cr^{3+} species form non-Lewis acidic Mg-Cr and/or Mg-Al-Cr LDH-like composite and are deposit on some active Lewis acid – Brønsted base sites, thereby lowering the activity.

From these results, I infer that the 5 wt%Cr/Mg-Al LDH possesses the most effective interaction between Lewis acidic Cr^{3+} oxide and Mg-Al LDH basic site, giving superior catalytic activity for xylose conversion.

Homogeneous and heterogeneous catalytic dehydration of xylose to furfural at 373 K have been reported by some research groups. Binder *et al.* have demonstrated that 56% yield of furfural was observed by using 6 mol% $CrCl_2$ with LiBr in *N*,*N*-dimethylacetamide for 4 h.[50] Suzuki *et al.* have reported that heterogeneous SO_4^{2-}/SnO_2 catalyst afforded 26.6% yield of furfural for 48 h.[51] This reaction condition is more preferable because heterogeneous solid catalysts can be easily removed from solution after catalytic reaction, and they used only 50 mg catalyst against to 1 mmol of xylose. However, this system has a lower furfural yield relative to take a long reaction time. In this research, the combined use of 5 wt%Cr/Mg-Al LDH and Amberlyst-15 successfully converted xylose into furfural with 59% yield at 18 h reaction time (Figure 24). Although our catalytic system requires higher weight ratio for catalyst : xylose than Suzuki's report, this yield was the highest value among all those reported for previous studies conducted at 373 K.[11, 18, 50-51, 54] Additionally, this catalytic system showed high activity to direct synthesis of FMM from xylose *via* the successive Knoevenagel condensation of generated furfural with malononitrile. It performed 59% yield of FMM at 18 h of furfural synthesis from xylose and 5 h of successive Knoevenagel condensation in a one-pot manner.

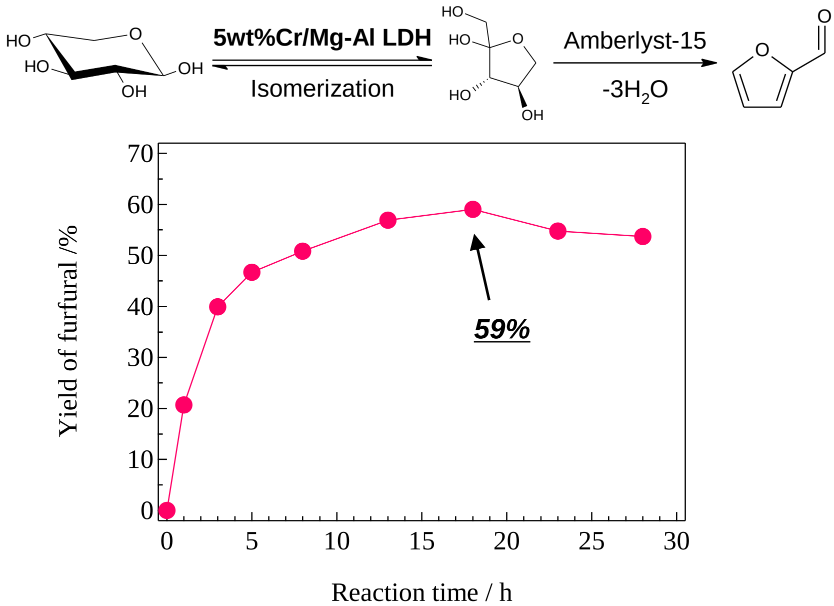

Figure 24 Time cause of furfural yield in the one-pot transformation of xylose using 5wt%Cr/Mg-Al LDH and Amberlyst-15. *Reaction conditions*: xylose (0.67 mmol), 5wt%Cr/Mg-Al LDH (0.2 g), Amberlyst-15 (0.1 g), *N*,*N*-dimethylformamide (3 mL), 373 K, 500 rpm, and N_2 flow (30 mL min^{-1}).

Conclusions

One-pot synthesis of furfural from xylose was performed successfully by the combined use of Brønsted acid Amberlyst-15 and bi-functional Lewis acid – Brønsted base Cr/Mg-Al LDH. The bi-functional Lewis acid – Brønsted base sites of Cr/Mg-Al LDH are expected to be generated at the cross boundaries between Lewis acidic Cr^{3+} oxide and Brønsted basic LDH surface. Xylose isomerization, the rate-determining step of the one-pot reaction, was promoted efficiently at the bi-functional Lewis acid – Brønsted base sites of Cr/Mg-Al LDH by proceeding proton shift reaction of the coordination complex of xylose with Lewis acid Cr^{3+} oxide, leading to higher furfural yield than basic bare Mg-Al LDH, substituted Mg-Cr LDH, and Lewis acidic other Cr supported catalysts. The surface structure and catalytic activities of Cr/Mg-Al LDH were varied with Cr loadings. The highest furfural and FMM yields were obtained by combined use of 5 wt%Cr/Mg-Al LDH and Amberlyst-15 with 59% yield at 373 K. XRD, XPS, XAS, ESR, DTA, N_2 adsorption measurement and MPV reduction revealed that (1) the monomer of Lewis acidic Cr^{3+} oxide is immobilized on the Mg-Al LDH surface below 1 wt%, (2) up to 5 wt%, Cr^{3+} species form Lewis acidic Cr^{3+} oxide dimer or trimer with covering Mg-Al LDH to generate highly active bi-functional Lewis acid – Brønsted base sites, (3) above 5 wt%, excess Cr^{3+} species form inert Mg-Cr and/or Mg-Al-Cr LDH-like composites and are deposited on some active bi-functional Lewis acid – Brønsted base sites, leading to lower activity. Therefore, I presume that the 5 wt%Cr/Mg-Al LDH surface that comprises LDH carrier and covering layer of Cr^{3+} oxide possesses the most effective interaction between Lewis acidic Cr^{3+} oxide and basic Mg-Al LDH surface to generate abundant bi-functional Lewis acid – Brønsted base sites, leading to the best catalytic activity. In the investigation of correlation between catalytic activity and structural properties of Cr/Mg-Al LDH with various Cr loadings, I elucidated the local structure and optimum preparation method of bi-functional Lewis acid – Brønsted base sites over LDH-based catalysts to propose a new technique to control acid–base bi-functional solid surfaces.

References

1 K. Kaneda, T. Yamashita, T. Matsushita, and K Ebitani, *J. Org. Chem.*, 1998, **63**, 1750.

2 N. Kakiuchi, Y. Maeda, T. Nishimura, and S. Uemura, *J. Org. Chem.*, 2001, **66**, 6620.

3 K. Motokura, D. Nishimura, K. Mori, T. Mizugaki, K. Ebitani, and K. Kaneda, *J. Am. Chem. Soc.*, 2004, **126**, 5662.

4 T. Mitsudome, Y. Mikami, H. Funai, T. Mizugaki, K. Jitsukawa, and K. Kaneda, *Angew. Chem. Int. Ed.*, 2008, **47**, 138.

5 W. Fang, Q. Zhang, J. Chen, W. Deng, and Y. Wang, *Chem. Commun.*, 2010, **46**, 1547.

6 A. Tsuji, K. T. V. Rao, S. Nishimura, A. Takagaki, and K. Ebitani, *ChemSusChem*, 2011, **4**, 542.

7 S. Nishimura, A. Takagaki, and K. Ebitani, *Green Chem.*, 2013, **15**, 2026.

8 M. L. Kantam, B. M. Choudary, C. V. Reddy, K. K. Rao, M. L. Kantam, B. M. Choudary, K. K. Rao, and F. Figueras, *Chem. Commun.*, 1998, 1033.

9 M. Climent, *J. Catal.*, 2004, **225**, 316.

10 E. Angelescu, O. D. Pavel, R. Bîrjega, R. Zăvoianu, G. Costentin, and M. Che, *Appl. Catal. A*, 2006, **308**, 13.

11 M. Shirotori, S. Nishimura, and K. Ebitani, *Catal. Sci. Technol.*, 2014, **4**, 971.

12 K. Yamaguchi, K. Mori, T. Mizugaki, K. Ebitani, and K. Kaneda, *J. Org. Chem.*, 2000, **65**, 6897.

13 T. Honma, M. Nakajo, T. Mizugaki, K. Ebitani, and K. Kaneda, *Tetrahedron Lett.*, 2002, **43**, 6229.

14 E. Li, Z. P. Xu, and V. Rudolph, *Appl. Catal.*, *B* 2009, **88**, 42.

15 Z. An, W. Zhang, H. Shi, and J. He, *J. Catal.*, 2006, **241**, 319.

16 H. C. Greenwell, P. J. Holliman, W. Jones, and B. V. Velasco, *Catal. Today*, 2006, **114**, 397.

17 M. Ohara, A. Takagaki, S. Nishimura, and K. Ebitani, *Appl. Catal. A*, 2010**, 383**, 149.

18 A. Takagaki, M. Ohara, S. Nishimura, and K. Ebitani, *Chem. Lett.*, 2010, **39**, 838.

19 A. Takagaki, M. Takahashi, S. Nishimura, and K. Ebitani, *ACS Catal.*, 2011, **1**, 1562.

20 G. W. Huber, J. N. Chheda, C. J. Barrett, and J. A. Dumesic, *Science*, 2005, **308**, 1446.

21 R. Karinen, K. Vilonen, and M. Niemelä, *ChemSusChem*, 2011, **4**, 1002.

22 P. Gallezot, *Chem. Soc. Rev.*, 2012, **41**, 1538.

23 C. O. Tuck, E. Pérez, I. T. Horváth, R. A. Sheldon, and M. Poliakoff, *Science*, 2012, **337**, 695.

24 G. W. Huber, S. Iborra, and A. Corma, *Chem. Rev.*, 2006, **106**, 4044.

25 J. N. Chheda, G. W. Huber, and J. A. Dumesic, *Angew. Chem. Int. Ed.*, 2007, **46**, 7164.

26 C. H. Zhou, X. Xia, C. X. Lin, D. S. Tong, and J. Beltramini, *Chem. Soc. Rev.*, 2011, **40**, 5588.

27 H. Kobayashi, and A. Fukuoka, *Green. Chem.*, 2013, **15**, 1740.

28 J. S. Luterbacher, D. M. Alonso, and J. A. Dumesic, *Green Chem.*, 2014, **16**, 4816.

29 H. Kobayashi, M. Yabushita, T. Komanoya, K. Hara, I. Fujita, and A. Fukuoka, *ACS Catal.*, 2013, **3**, 581.

30 P.-W. Chung, A. Charmot, O. A. Olatunji-Ojo, K. A. Durkin, and A. Katz, *ACS Catal.*, 2014, **4**, 302.

31 P.-W. Chung, M. Yabushita, A. T. To, Y. Bae, J. Jankolovits, H. Kobayashi, A. Fukuoka, and A. Katz, *ACS Catal.*, 2015, **5**, 6422.

32 A. T. To, P.-W. Chung, and A. Katz, *Angew. Chem. Int. Ed.*, 2015, **54**, 11050.

33 S. Suganuma, K. Nakajima, M. Kitano, D. Yamaguchi, H. Kato, S. Hayashi, and M. Hara, *J. Am. Chem. Soc.*, 2008, **130**, 12787.

34 X. Zhao, J. Wang, C. Chen, Y. Huang, A. Wang, T. Zhang, *Chem. Commun.*, 2014, **50**, 3439.

35 P. Dornath, H. J. Cho, A. Paulsen, P. Dauenhauer, and W. Fan, *Green Chem.*, 2015, **17**, 769.

36 H. Kobayashi, H. Kaiki, A. Shrotri, K. Techikawara, and A. Fukuoka, *Chem. Sci.*, 2016, **7**, 692.

37 H. Choudhary, S. Nishimura, and K. Ebitani, *Chem. Lett.*, 2012, **41**, 409.

38 B. Danon, G. Marcotullio, W. de Jong, *Green Chem.*, 2014, **16**, 39.

39 A. S. Dias, S. Lima, M. Pillinger, and A. A. Valente, *Catal. Lett.*, 2007, **114**, 151.

40 A. S. Dias, S. Lima, P. Brandão, M. Pillinger, J. Rocha, and A. A. Valente, *Catal. Lett.*, 2006, **108**, 179.

41 G. H. Jeong, E. G. Kim, S. B. Kim, E. D. Park, and S. W. Kim, *Microporous and Mesoporous Mater*., 2011, **144**, 134.

42 I. Agirrezabal-Telleria, J. Requies, M. B. Güemez, and P. L. Arias, *Appl. Catal. B*, 2014, **145**, 34.

43 A. S. Dias, M. Pillinger, and A. A. Valente, *Appl. Catal. A*, 2005, **285**, 126.

44 S. Lima, M. Pillinger, and A. Valente, *Catal. Commun.*, 2008, **9**, 2144.

45 R. O'Neill, M. N. Ahmad, L. Vanoye, and F. Aiouache, *Ind. Eng. Chem. Res.*, 2009, **48**, 4300.

46 S. Lima, A. Fernandes, M. M. Antunes, M. Pillinger, F. Ribeiro, and A. A. Valente, *Catal. Lett.*, 2010, **135**, 41.

47 R. Weingarten, J. Cho, J. Wm. Curtis Conner, and G. W. Huber, *Green Chem.*, 2010, **12**, 1423.

48 M. J. Climent, A. Corma, and S. Iborra, *Green Chem.*, 2011, **13**, 520.

49 V. Choudhary, S. I. Sandler, and D. G. Vlachos, *ACS Catal.*, 2012, **2**, 2022.

50 J. B. Binder, J. J. Blank, A. V. Cefali, and R. T. Raines, *ChemSusChem*, 2010, **3**, 1268.

51 T. Suzuki, T. Yokoi, R. Otomo, J. N. Kondo, and T. Tatsumi, *Appl. Catal. A*, 2011, **408**, 117.

52 Y. Roman-Leshkov, M. Moliner, J. A. Labinger, and M. E. Davis, *Angew. Chem. Int. Ed.*, 2010, **49**, 8954.

53 H. S. Soliman, M. Eid Kh, H. A. Ali, M. A. El-Mansy, and S. M. Atef, *Spectrochim. Acta A Mol. Biomol. Spectrosc.*, 2013, **105**, 545.

54 M. Shirotori, S. Nishimura, and K. Ebitani, *Chem. Lett.*, 2016, **45**, 194.

55 P. Keller, and H.-H. Strehblow, *Corros. Sci.*, 2004, **46**, 1939.

56 M. J. Gilkey, and B. Xu, *ACS Catalysis*, 2016, **6**, 1420.

57 M. A. Aramendía, V. Borau, C. Jiménez, J. M. Marinas, J. R. Ruiz, and F. J. Urbano, *Appl. Catal. A*, 2003, **255**, 301.M.

58 M. A. Aramendía, V. Borau., C. Jiménez, J. M. Marinas, J. R. Ruiz, and F. J. Urbano, *J. Mol. Catal. A*, 2001, **171**, 153.

59 M. A. Aramendía, V. Borau, C. Jiménez, J. M. Marinas, J. R. Ruiz, and F. J. Urbano, *J. Colloid. Interface Sci*., 2001, **238**, 385.

60 H. Hattori, *Appl. Catal. A*, 2001, **222**, 247.

61 E. A. Pidko, V. Degirmenci, and E. J. M. Hensen, *ChemCatChem*, 2012, **4**, 1263.

62 D. Ekeberg, S. Morgenlie, and Y. Stenstrom, *Carbohydr. Res.*, 2005, **340**, 373.

63 D. Ekeberg, S. Morgenlie, and Y. Stenstrom, *Carbohydr. Res.*, 2007, **342**, 1992.

64 S. G. Eeckhout, N. Bolfan-Casanova, C. McCammon, S. Klemme, and E. Amiguet, *Am. Mineral.*, 2007, **92**, 966.

65 N. Papassiopi, F. Pinakidou, M. Katsikini, G. S. Antipas, C. Christou, A. Xenidis, and E. C. Paloura, *Chemosphere*, 2014, **111**, 169.

66 J. Frommer, M. Nachtegaal, I. Czekaj, and R. Kretzschmar, *Am. Mineral.*, 2010, **95**, 1202.

67 Weckhuysen, B. M., *Chem. Commun.*, 2002, 97.

68 J. Zhang, Y. F. Xu, G. Qian, Z. P. Xu, C. Chen, and Q. Liu, *J. Phys. Chem. C*, 2010, **114**, 10768.

69 T. Kitano, S. Okazaki, T. Shishido, K. Teramura, and T. Tanaka, *Catal. Today*, 2012, **192**, 189.

70 T. Kitano, T. Shishido, K. Teramura, and T. Tanaka, *J. Phys. Chem. C*, 2012, **116**, 11615.

71 T. Kitano, S. Okazaki, T. Shishido, K. Teramura, and T. Tanaka, *J. Mol. Catal. A*, 2013, **371**, 21.

72 T. Kitano, T. Hayashi, T. Uesaka, T. Shishido, K. Teramura, and T. Tanaka, *ChemCatChem*, 2014, **6**, 2011.

Chapter 4

Development and Evaluation of Layered Double Hydroxide-based Catalysts Prepared with Coexistence of SiO_2 Spheres

Abstract

Fine-crystallized layered double hydroxides were prepared by co-precipitation method with coexistence of SiO_2 sphere (SiO_2@LDH), and these base catalysis and structural properties were investigated. As-prepared SiO_2@LDHs exhibited higher base catalysis for the Knoevenagel condensation than conventional LDHs prepared by co-precipitation method in absence of co-existence of SiO_2 sphere. Such increase in activity for base catalysis was also observed in various types of SiO_2@LDHs with different metal compositions (M^{2+}: Mg^{2+} or Ni^{2+}, M^{3+}: Al^{3+} or Ga^{3+}, M^{2+}/M^{3+}: 1 or 3). X-ray diffraction (XRD) measurement suggested that addition of SiO_2 induced the decrease in LDH crystallite size. The results of transmission electron microscopy – energy dispersive X-ray spectroscopy (TEM-EDS) and ^{29}Si cross polarization magic angle spinning nuclear magnetic resonance (^{29}Si CP-MAS NMR) on SiO_2@Mg-Al LDH suggested that the crystal of Mg-Al LDH is immobilized on SiO_2 surface through the Si-O-Al and Si-O-Mg covalent bonds. According to these results, I concluded that the co-precipitation method in the presence of colloidal spherical SiO_2 seeds, especially possessing 40 nm diameter, composed the highly-dispersed points of LDH crystal growth on SiO_2 surface, and which lead the generation of fine-crystallized highly active LDH nanocrystals.

Introduction

Layered double hydroxide (LDH) is one of well-known layered clay minerals which is composed of brucite-like two-dimensional sheets and interlayer anions. A chemical formal of LDH is generally denoted as $[M^{2+}_{1-x}M^{3+}_{x}(OH)_2]^{x+}A^{n-}_{x/n}\cdot mH_2O$, where $[M^{2+}_{1-x}M^{3+}_{x}(OH)_2]^{x+}$ corresponds to two-dimensional sheets consisting of octahedral M^{2+} and M^{3+} complex hydroxide layer. This hydroxide layer possesses positive charge derived from partially substituted M^{3+} ion. Interlayer anions A^{n-}, such as carbonate and hydroxide, and molecular water are inserted to interlayer of complex metal hydroxide layer resulting to compensate for the charge between sheets.[1-3] LDHs have been utilized as various functional materials because of these unique characters. As examples, LDHs can be used to anions removal, drug delivery system, and preparation of nano-scale organic/inorganic hybrid materials such as bio-composite and biosensor because LDHs possess anion-exchange ability: LDHs can intercalate inorganic anions,[1, 4-5] organic anions and organic molecules.[6-8]

Additionally, the LDH materials have been widely applied as unique hydrophilic solid base catalyst for variety types of organic reactions by many researchers in the world.[9-28] The identical anions which are adsorbed onto LDH surface, such as OH^- and HCO_3^-, are known to act as base sites. As a solid base catalyst, LDH materials have some unique characteristics described as follows; (*i*) the base properties are varied in accordance with the composition of metal hydroxide and type of interlayer anions, and (*ii*) LDHs can be transformed to Lewis acidic and basic bifunctional metal composite oxide by calcination. An enormous number of studies have been devoted to investigate these utility for various organic reactions such as aldol condensation,[14, 16, 23, 25] Knoevenagel condensation,[9, 12, 15, 24] epoxidation,[10-11, 20] transesterification,[13, 17, 26] and so on. Recently, LDHs have been also utilized to advanced environmental-friendly reactions such as biomass derived saccharides conversion[18-19, 21-22, 24, 27-28] and photocatalytic conversion of CO_2 in an aqueous solution.[29-31] However, generally the anions in the interlayer space cannot participate in these chemical reactions because the high charge density of the LDHs layers and the high content of anionic species and water molecules result in strong interlayer electrostatic interactions between the sheets.[3, 32] Therefore, not only the continuous studies for applications of highly active LDH-based solid catalysts but also the improvement of preparation method to upgrade the LDH derived-solid base catalyst have been envisaged.

To overcome this issue and to upgrade the LDH derived-solid base catalyst, two strategies have been proposed; one is the delamination of LDH nanosheets, and the other is the fine-crystallization of LDH crystallite. In 2000, Adachi *et al.* reported the method of delamination of LDHs using various anionic surfactants which will lead to a novel generation of LDH based materials in which total surface of the layered compound can be rendered accessible for chemical reactivity.[32] After that, several reports on delamination of LDHs[33-38] and method to prepare nano-hybrid materials composed of LDH nanosheets[39-43] has been presented. These methods are effective to utilize the flat plane of LDH nanosheets. Actually, various LDH nanosheets-based materials, which possess the laminated structure with other layered materials or metal nanoparticles, have been evaluated on their characteristics and utility as photo- and electro- catalysts.[39-40, 42] However, in order to improve the base catalysis of LDH itself, the delamination method seems to be insufficient, because the highly reactive sites of catalysts including LDHs are generally considered to be the edges and corners of the crystallites owing to the presence of low coordination state of atoms. As Roeffaers *et al.* reported, in the case of Li-Al LDH, transesterification occurs mainly at the {0001} plane where the basal surface of the LDH crystal, while, ester hydrolysis requires the OH^- ions at the $\{10\bar{1}0\}$ faces where the entrance of the galleries.[44] According to these previous reports, I believe that the both avoidance of *ab*-face stacking and fine-crystallization are required to maximize the base catalysis of LDH.

Immobilization of active species onto the support is one of the general methods to improve the catalytic property by avoidance of aggregation and excess growth of active species. Although the LDHs has often been used as a carrier to immobilize active species, I anticipated that the fine-crystallized LDHs can be prepared if the active LDHs can be immobilized onto the adequate carrier. To date, several nano-LDH materials which possess core-shell, yolk-shell or hollow-shell structure had been demonstrated.[45-50] A typical structure generally denoted as SiO_2@LDH is one of a hierarchical core-shell LDH material which promises strategy to avoid the *ab*-face stacking aggregation.[50] Two type procedures to prepare hierarchical SiO_2@LDH materials have been reported. Shao *et al.* demonstrated that core-shell, yolk-shell and hollow-shell SiO_2@LDH and SiO_2-coated Fe_3O_4 magnetite core-shell Fe_3O_4@SiO_2@LDH material can be obtained by layer-by-layer deposition process followed by *in situ* coating of AlOOH on SiO_2 (~340 nm) or Fe_3O_4@SiO_2 (~310 nm) core surface and successive growth of LDH crystals.[45-46] Using similar layer-by-layer method, Wang *et al.* prepared SiO_2@LDH nanoparticles over more small SiO_2 nanoparticles (~50 nm).[49] Another procedure is a simple method by using an *in situ* co-precipitation to directly deposit LDH precursors on the SiO_2 surface without any binder, reported by Chen *et al.*[47, 50] Advantages of Chen's reports are (*i*) the preparation method is very simple and easily handled and (*ii*) the size of SiO_2 spheres and the composition of LDH as well as the thickness of LDH layer can be controlled.

The LDH nanosheets derived materials, SiO_2@LDH nanoparticles and alkylcarboxylate-intercalated layered hydroxyl double salts, have been evaluated on their characteristics and utility as photo- and electro- catalysts,[39-40, 42] high active base catalyst for the Knoevenagel condensation[51] and epoxidation,[52] magnetic separation of proteins,[45] pseudocapacitance,[46] flame retardancy of epoxy resins[48] and adjuvant.[49] However, there are no reports on investigation of the improvement of base catalysis of LDH itself by fine-crystallization followed by *in situ* growth method of SiO_2@LDH nanoparticles.

The main subject of this research is the improvement of base catalysis of widely-used LDH material with unique strategy. Herein, I establish the small-crystallized LDH catalyst on SiO_2 nanoparticles and compare its base catalysis for the Knoevenagel condensation of benzaldehyde with conventional LDHs. A crystallite property, morphology and correlation between SiO_2 sphere and LDH were investigated by XRD, TEM-EDS and ^{29}Si CP-MAS NMR analytical methods. It is revealed that the coexistence of small SiO_2 sphere surfaces generate the starting points of LDH growth *via* Si-O-M covalent bond formation, leading to the fine-crystal LDH forming and enhancement of base catalysis for the Knoevenagel condensation.

Experimental

Materials and synthesis of catalysts

Tetraethyl orthosilicate (TEOS), triethanolamine (TEA) and benzaldehyde were purchased from Sigma-Aldrich Inc. Sodium carbonate (Na_2CO_3), sodium hydroxide (NaOH) and toluene were supplied by Kanto Chem. Co. Ltd. Cetyltrimethylammonium bromide (CTAB), aqueous solution of ammonium (25%), magnesium nitrate hexahydrate ($Mg(NO_3)_2{\cdot}6H_2O$), aluminium nitrate enneahydrate ($Al(NO_3)_3{\cdot}9H_2O$), nickel nitrate hexahydrate ($Ni(NO_3)_2{\cdot}6H_2O$), gallium nitrate *n*-hydrate ($Ga(NO_3)_3{\cdot}nH_2O$) and benzoic acid were obtained from Wako Pure Chemical Ind., Ltd. Co. Urea and ethyl cyanoacetate were purchased from Junsei Chemical Co., Ltd. and Tokyo Chemical Ind., Co., Ltd., respectively. The commercial Mg-Al(3)LDH (denoted as LDH(com.)) was obtained from Tomita Pharmaceutical Co., Ltd.

Spherical SiO_2(40nm) was prepared according to the previous reports.[49, 53] 96 mmol of TEA and 2 mL of TEOS were combined in a 200 mL of eggplant flask. The two-phase mixture was heated in an oil bath at 363 K for 20 min without stirring. When the mixture was taken out from the oil bath, 26.0 mL of an aqueous solution (2.8 wt%) of CTAB pre-heated at 333 K was immediately added as structure directing agent in a condensation process, and then continuously stirred for 24 h at room temperature. Thereafter, the resulting mixture was added in 50 mL of ethanol to obtain colloidal aqueous suspension. The obtained precipitate was centrifuged for 5 min at 4000 rpm. After decantation, the sediment was re-dispersed through vigorous stirring in 50 mL of an ethanolic solution of ammonium nitrate (20 g L^{-1}) and then refluxed for 1 h. This procedure was repeated three times. Then, the same operation was also performed with a solution of concentrated hydrochloric acid in ethanol (5 g L^{-1}) to replace the ammonium ions. The final sediment was washed with ethanol, and then dried *in vacuo*. The obtained spherical SiO_2 powder was calcined at 823 K under 1 L min^{-1} of air flow for 6 h.

Spherical SiO_2(250nm) was prepared using a modified literature method.[50] 13.5 mmol of TEOS was added to a mixed solution of 6.45 mL of ammonia (25 wt%), 23.55 mL of water and 50 mL of ethanol. The white suspension was stirred for 17 h at room temperature, and then centrifuged for 1 min at 4000 rpm. The obtained sediment was washed with ethanol, and then dried *in vacuo*. The resulting spherical SiO_2 powder was calcined at 823 K under 1 L min^{-1} of air flow for 6 h.

The $SiO_2(X)@M^{2+}$-$M^{3+}(Y)$LDH catalysts (X: desired size of spherical SiO_2; 40 nm or 250 nm, Y: M^{2+}/M^{3+} mol ratio; 1 or 3) were prepared *via* an *in situ* co-precipitation method according to a previous report.[50] Spherical SiO_2 particles with the desired size were dispersed in 20 mL of water using ultrasound treatment. After 30 min, the 0.96 mmol of Na_2CO_3 was added to the solution and a further 5 min of sonication was carried out. 19.2 mL of metal nitrates aqueous solution ($[M^{2+}] + [M^{3+}] = 0.075$ M) was slowly dropped into the above spherical SiO_2 dispersed solution under stirring at room temperature. The pH was maintained at 10.0 by an aqueous NaOH solution (1 M) during titration. The obtained suspension was stirred further 1 h. The resulting paste was filtered, washed with 1 L of water and ethanol, and then dried at 383 K overnight. The $Si/(M^{2+}+M^{3+})$ atomic ratios were basically adjusted to 0.50.

The M^{2+}-M^{3+}(3)LDH(CP) was synthesized by co-precipitation method. An aqueous solution of $M^{2+}(NO_3)_2 \cdot mH_2O$ and $M^{3+}(NO_3)_3 \cdot nH_2O$ ($M^{2+}/M^{3+} = 3$, $[M^{2+}] + [M^{3+}] = 0.075$ M, 19.2 mL) was slowly dropped into an aqueous Na_2CO_3 solution (0.048 M, 20 mL) with stirring at room temperature. The pH was kept to 10.0 by an aqueous NaOH solution (1 M) during titration. The obtained mixture was stirred further 1 h. The resulting paste was filtered, washed with 1 L of water and ethanol, and then dried at 383 K overnight. These LDHs are denoted as M^{2+}-$M^{3+}(Y)$LDH or LDH(CP).

The Mg-Al(3)LDH(U-CP) was prepared by urea co-precipitation method. 5.625 mmol of $Mg(NO_3)_2 \cdot 6H_2O$, 1.875 mmol of $Al(NO_3)_3 \cdot 9H_2O$ and 17.5 mmol of urea were dissolved in 500 mL of water, and then stirred at 373 K for 48 h. After cooling for 2 h, the obtained sediment was filtered, washed with 1.5 L of water and then dried at 333 K overnight. This LDH is denoted as LDH(U-CP).

Reaction

Knoevenagel condensation of benzaldehyde with ethyl cyanoacetate was performed in a 20 mL of Shlenk tube under an N_2 flow (30 mL min^{-1}). The reaction was typically performed using 1.0 mmol of benzaldehyde, 1.2 mmol of ethyl cyanoacetate, 10 mg of catalysts and 3 mL of toluene at 313 K. The obtained products were analysed using GC-FID (SHIMADZU GC-2014) equipped with a polar column (Agilent, DB-FFAP).

Characterizations

X-ray diffraction patterns (XRD) were collected on a SmartLab (Rigaku) using Cu $K\alpha$ X-ray source (40 kV, 30 mA). The LDH (003) and (110) crystallite sizes were calculated by the Scherrer equation; $D_{hkl} = K\lambda/(\beta\cos\theta)$ (K: Scherrer number (0.9), λ: incident ray wavelength (0.1542 nm), β: peak width at half height (rad), θ: Brag angle). ^{29}Si cross polarization magic angle spinning nuclear magnetic resonance (^{29}Si CP-MAS NMR) measurements were performed on a AVANCE III 500 MHz (Bruker) in a 4 mm ZrO_2 rotor. The spinning rate was 8 kHz. The ^{29}Si chemical shifts are referenced to hexamethyl cyclotrisiloxane (taken to be at δ = -9.6875 ppm). Scanning electron microscope (SEM) images were collected on a S-4500 (Hitachi). The sample powder was fixed onto a carbon tape and pretreated with a PtPd ion-sputter (Hitachi, E-1030) to reduce charge up issue. Transmission electron microscopy (TEM) images were taken using a H-7100 (Hitachi) at 100 kV. TEM-energy dispersive X-ray spectroscopy (TEM-EDS) elemental mapping was obtained by a JEM-ARM200F (JEOL) at 200 kV. N_2 adsorption measurements were carried out to determine the BET (Brunauer-Emmett-Teller) specific surface area for spherical SiO_2. The measurements were conducted at 77 K on a BELSORP-max (BEL Japan, Inc.). Inductively coupled plasma - atomic emission spectrometry (ICP-AES) was operated on the iCAP6300Duo (Thermo Fisher Sci.) to estimate the amount of precipitated $M(OH)_x$ and SiO_2 in SiO_2@LDHs.

Results and discussion

Synthesis and base catalysis evaluation of SiO_2(40nm)@M^{2+}-M^{3+}LDHs

Preliminarily, I prepared SiO_2(40nm)@LDHs with various combinations and composition ratios of metal hydroxide (Mg-Al, Ni-Al and Mg-Ga type LDH with M^{2+}/M^{3+} ratio of 1 or 3) in order to investigate the correlation between these base catalytic activities and structural properties. The particle diameter of spherical SiO_2(40nm) was confirmed by TEM observation as about 40 nm (Fig. 1(A)). SEM images suggested that SiO_2 spheres were uniformly distributed as shown in Fig. 1(B)). N_2 adsorption-desorption isotherm of spherical SiO_2(40nm) showed type IV isotherm (Fig. 2), and its specific surface area calculated by BET-theory was 1081 m^2 g^{-1}.

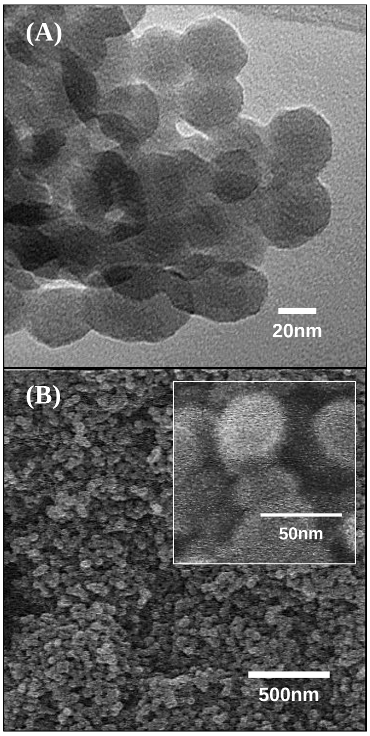

Figure 1 (A) TEM image and (B) SEM images of spherical SiO_2(40 nm).

Next, I synthesized various SiO_2(40nm)@M^{2+}-M^{3+} LDHs with M^{2+}/M^{3+} ratio of 3 by a co-precipitation with coexistence of obtained SiO_2(40nm) sphere. The actual ratios of $Si/(M^{2+}+M^{3+})$ and M^{2+}/M^{3+} in obtained materials were summarized in Table 1. The possibility of the residual sodium cation in the M^{2+}-M^{3+}(3) type LDHs were negligible in all M^{2+}-M^{3+}(3) type LDHs, evidenced by XPS (Fig. 3).

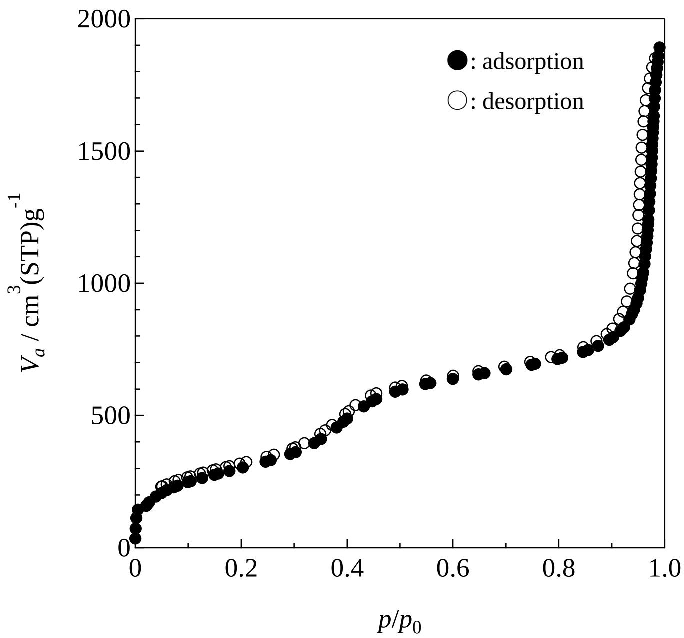

Figure 2 Nitrogen sorption isotherm of spherical SiO_2(40 nm).

Table 1 Chemical compositions of prepared M^{2+}-M^{3+}(3) type LDHs estimated by ICP-AES.

Catalyst		Si/(M^{2+}+M^{3+}) ratio		M^{2+}/M^{3+} ratio	
		Precursor	Obtained material	Precursor	Obtained material
Mg-Al(3)	LDH	—	—	3.0	2.8
	SiO_2@LDH	0.50	0.53	3.0	2.2
Ni-Al(3)	LDH	—	—	3.0	3.0
	SiO_2@LDH	0.50	0.44	3.0	3.1
Mg-Ga(3)	LDH	—	—	3.0	2.7
	SiO_2@LDH	0.50	0.56	3.0	2.3

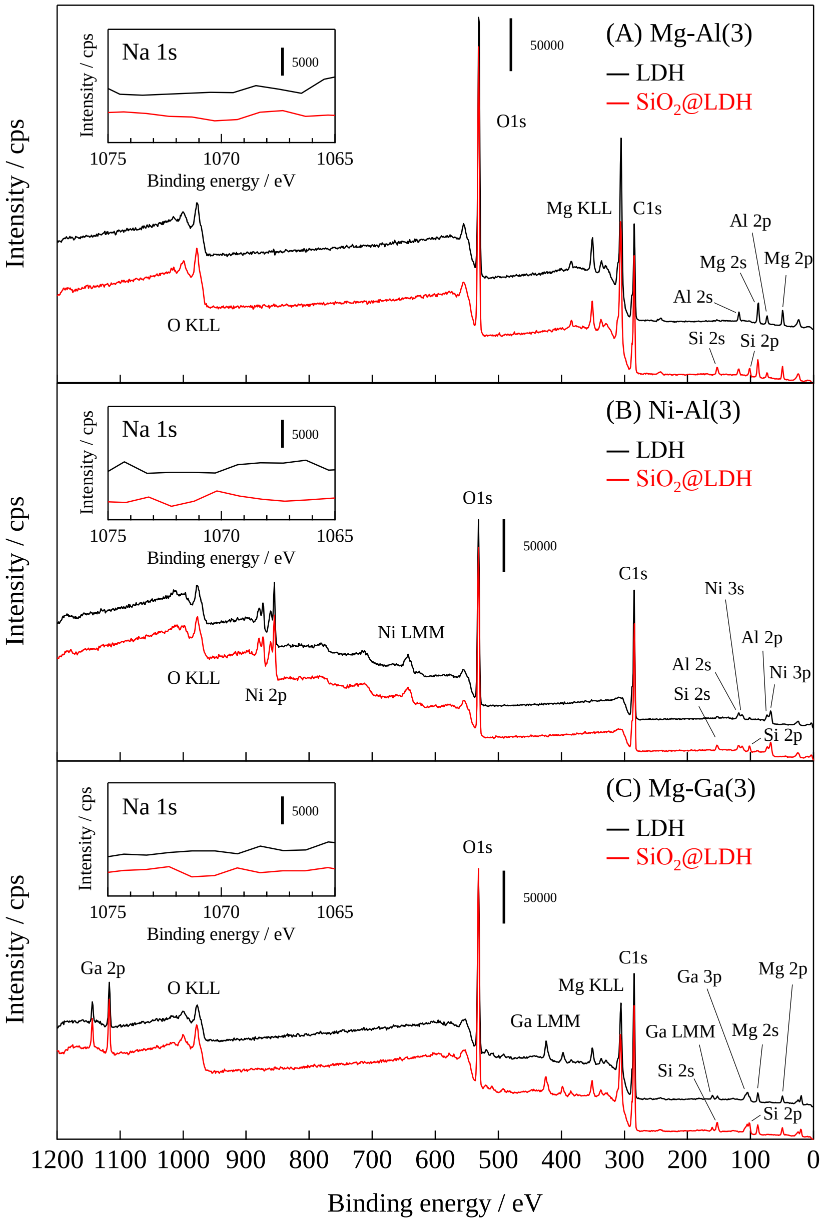

Figure 3 Survey XPS spectra of M^{2+}-M^{3+}(3)LDHs and SiO_2(40nm)@M^{2+}-M^{3+}(3)LDHs.

Fig. 4 shows time courses of benzaldehyde conversion in the Knoevenagel condensation of benzaldehyde with ethyl cyanoacetate over various M^{2+}-M^{3+}(3)LDHs and SiO_2(40nm)@M^{2+}-M^{3+}(3)LDHs. It was clearly shown that SiO_2(40nm)@M^{2+}-M^{3+}(3)LDHs efficiently mediated the Knoevenagel condensation than M^{2+}-M^{3+}(3)LDHs in all type LDHs. The reaction rates for the Knoevenagel condensation were calculated using reaction constant *k* which were estimated from the rate equation of pseudo first-order reaction, and summarized in Table 2. In the case of Mg-Al type LDH, the reaction rate for Mg-Al(3)LDH was 77 mmol g^{-1} h^{-1} whereas that of SiO_2(40nm)@Mg-Al(3)LDH was increased to 117 mmol g^{-1} h^{-1}. The increases of reaction rate by coexistence of spherical SiO_2(40nm) were more prominent in the case of Ni-Al and Mg-Ga type LDHs, and these values were respectively improved from 26 to 61 mmol g^{-1} h^{-1} and from 23 to 59 mmol g^{-1} h^{-1}. It is noted that the blank test and bare SiO_2(40nm) sphere gave no product for the Knoevenagel condensation. Thus, these results clearly indicate that co-existence of SiO_2 acts as a promoter for the base catalysis on LDHs.

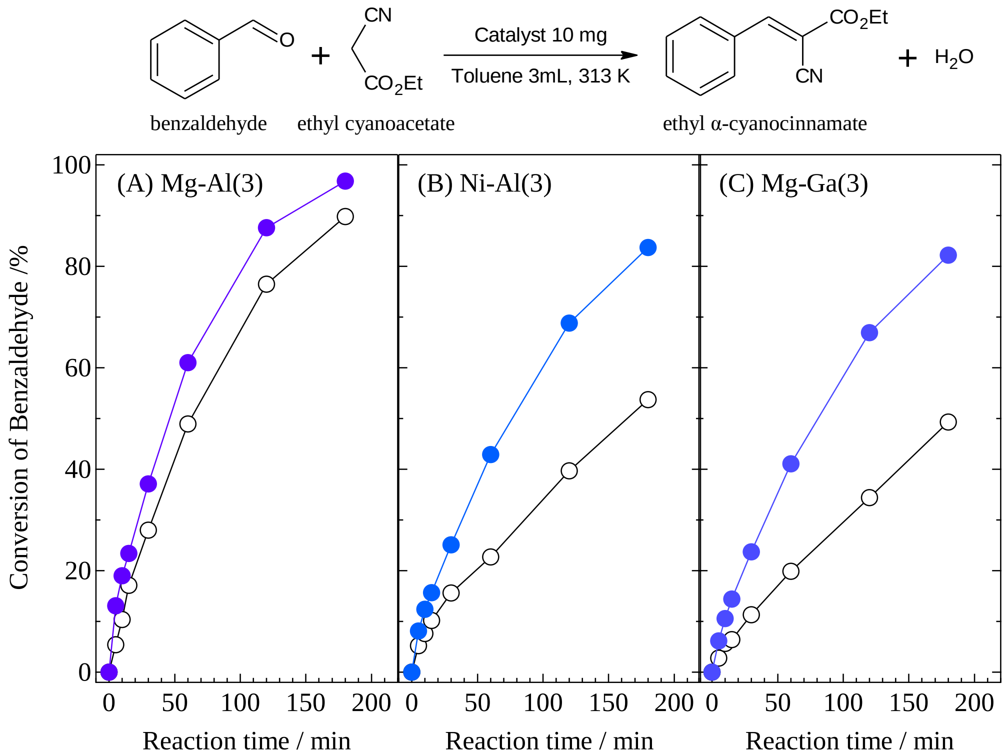

Figure 4 Activities of (○) M^{2+}-M^{3+}(3)LDH and (●) SiO_2(40nm)@ M^{2+}-M^{3+}(3)LDH with various metal compositions for the Knoevenagel condensation of benzaldehyde with ethyl cyanoacetate. *Reaction conditions*: benzaldehyde (1.0 mmol), ethyl cyanoacetate (1.2 mmol), catalyst (10 mg), toluene (3 mL), 313 K, N_2 flow (30 mL min^{-1}).

Table 2 Correlation between base activity and base property of M^{2+}-M^{3+}(3)LDHs and SiO_2(40nm)@M^{2+}-M^{3+}(3)LDHs.

Catalyst		Reaction rate[a] / mmol g^{-1} h^{-1}	Base amount[b] / mmol g^{-1}	$M(OH)_x$ amount[c] / mmol g^{-1}	Base/$M(OH)_x$[d] /%
Mg-Al(3)	LDH	76.9	0.45	12.16	3.7
	SiO_2@LDH	116.7	0.48	8.27	5.8
Ni-Al(3)	LDH	25.5	0.30	9.35	3.2
	SiO_2@LDH	60.6	0.44	7.12	6.2
Mg-Ga(3)	LDH	23.1	0.12	10.62	1.1
	SiO_2@LDH	58.8	0.37	7.52	4.9

[a]Reaction rate for the Knoevenagel condensation of benzaldehyde with ethyl cyanoacetate.
[b]Base amount calculated from poisoning test by benzoicacid titration.
[c]Total metal M^{2+} and M^{3+} hydroxide amount calculated by ICP-AES.
[d]Base amount per total metal hydroxide amount.

Fig. 5 showed XRD patterns of various M^{2+}-M^{3+}(3)LDHs and SiO_2(40nm)@M^{2+}-M^{3+}(3)LDHs. Clear reductions in the crystallinity by coexistence of spherical SiO_2(40nm) were observed in all type LDHs. Crystal properties obtained from XRD patterns are summarized in Table 3. The both crystallite sizes of stacking direction and plane direction, respectively denoted as *D*(003) and *D*(110) in SiO_2(40nm)@M^{2+}-M^{3+}(3)LDHs, were clearly smaller than those of M^{2+}-M^{3+}(3)LDHs, indicating coexistence of spherical SiO_2(40nm) inhibited the crystal growth of LDH in not only stacking direction but also plane direction. Since there were no significant change in the lattice parameter *a* and *c* between M^{2+}-M^{3+}(3)LDHs and SiO_2(40nm)@M^{2+}-M^{3+}(3)LDHs, the coexistence of spherical SiO_2(40nm) did not affect LDH unit structures. These results suggested that (*i*) coexistence of spherical SiO_2(40nm) inhibits the crystal growth of LDH, (*ii*) the obtained SiO_2(40nm)@M^{2+}-M^{3+}(3)LDHs possess higher activity for the basic Knoevenagel condensation than conventional M^{2+}-M^{3+}(3)LDHs, and (*iii*) those effects are similarly evolved in the cases of Mg-Al, Ni-Al and Mg-Ga type LDHs.

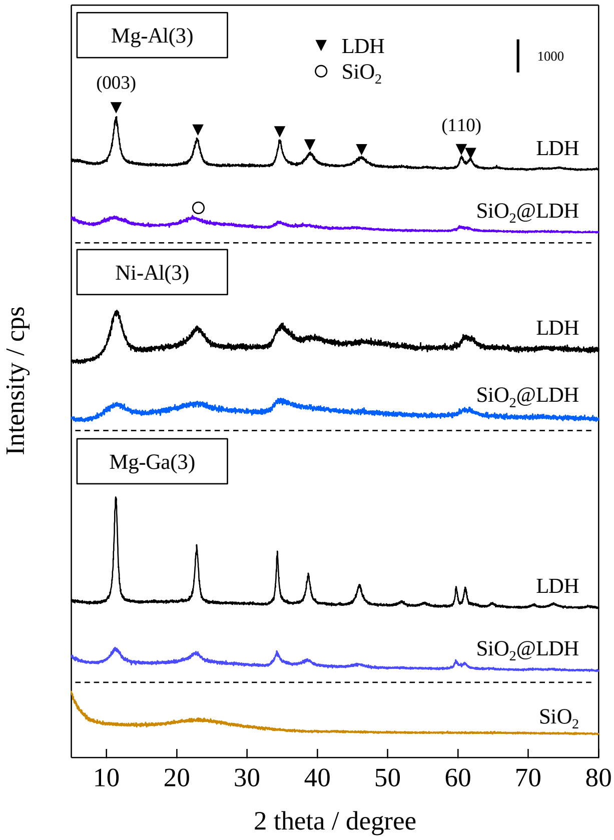

Figure 5 XRD patterns of M^{2+}-M^{3+}(3)LDHs and SiO_2(40nm)@M^{2+}-M^{3+}(3)LDHs.

Table 3 Crystal properties of M^{2+}-M^{3+}(3)LDHs and SiO_2(40nm)@M^{2+}-M^{3+}(3)LDHs.

Catalyst		Lattice parameter *c* / nm	Crystallite size (003)[a] / nm	Lattice parameter *a* / nm	Crystallite size (110)[a] / nm
Mg-Al(3)	LDH	2.33	7.6	0.31	13.4
	SiO_2@LDH	2.43	2.8	0.31	8.3
Ni-Al(3)	LDH	2.31	4.0	0.30	8.1
	SiO_2@LDH	2.35	2.4	0.30	4.1
Mg-Ga(3)	LDH	2.34	13.0	0.31	24.8
	SiO_2@LDH	2.34	4.7	0.31	14.0

[a]The crystallite sizes of LDHs were calculated by Scherrer equation; $D_{hkl} = K\lambda/\beta\cos\theta$ (K: Scherrer number (0.9), λ: incident ray wavelength (0.1542 nm), β: peak width at half height (rad)).

To evaluate versatility, I prepared M^{2+}-M^{3+}(1)LDHs and SiO_2(40nm)@M^{2+}-M^{3+}(1)LDHs, and then applied these catalysts to the Knoevenagel condensation. Because base activities of M^{2+}/M^{3+} = 1 type LDHs were much lower than M^{2+}/M^{3+} = 3, the Knoevenagel condensation was carried out using substrates with half scale. As shown in Fig. 6, SiO_2(40nm)@M^{2+}-M^{3+}(1)LDHs showed higher activity than conventional M^{2+}-M^{3+}(1)LDHs in all combinations of metal hydroxides. The reaction rates were increased by coexistence of spherical SiO_2(40nm), from 7.6 to 20 mmol g^{-1} h^{-1}, from 9.6 to 29 mmol g^{-1} h^{-1} and from 15 to 20 mmol g^{-1} h^{-1} in the case of Mg-Al, Ni-Al and Mg-Ga type LDHs, respectively. Reductions in the crystallinity by coexistence of spherical SiO_2(40nm) were also observed from XRD patterns as shown in Fig. 7. As same as M^{2+}-M^{3+}(3) type LDHs, the lattice parameter *c* are almost identical between

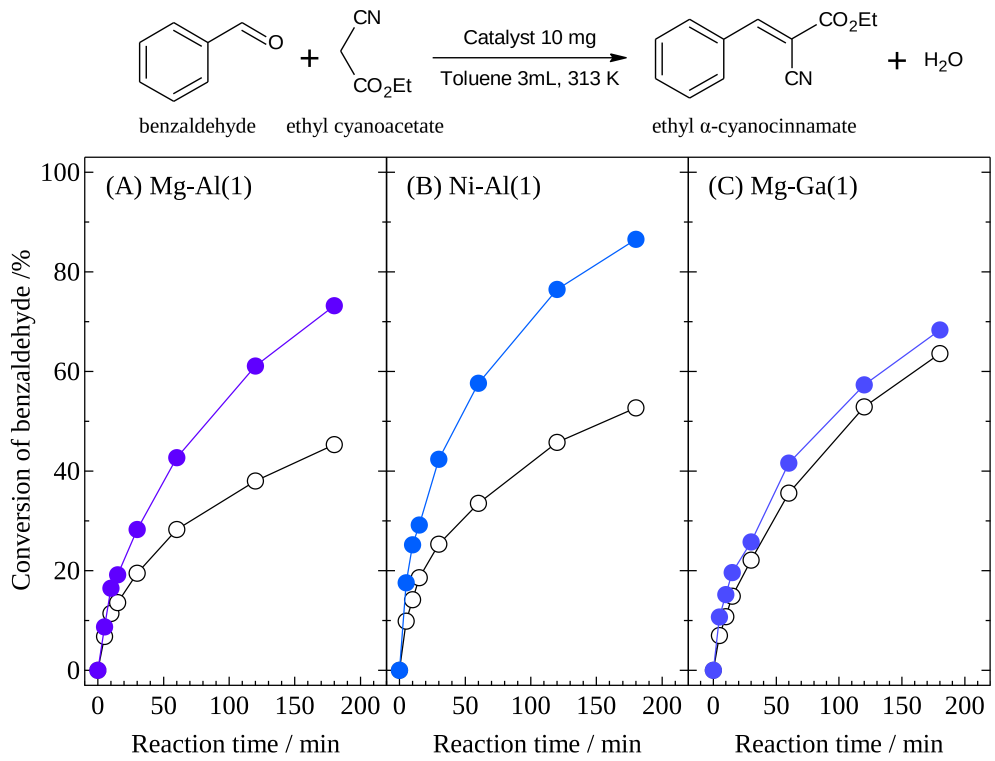

Figure 6 Activities of (○) M^{2+}-M^{3+}(1)LDH and (●) SiO_2(40nm)@ M^{2+}-M^{3+}(1)LDH with various metal compositions for the Knoevenagel condensation of benzaldehyde with ethyl cyanoacetate. *Reaction conditions*: benzaldehyde (0.5 mmol), ethyl cyanoacetate (0.6 mmol), catalyst (10 mg), toluene (3 mL), 313 K, N_2 flow (30 mL min^{-1}).

M^{2+}-M^{3+}(1)LDHs and SiO_2(40nm)@M^{2+}-M^{3+}(1)LDHs whereas LDH (003) plane crystallite sizes were reduced from 3.6 nm to 3.0 nm and from 9.7 nm to 3.4 nm in Mg-Al(1) and Mg-Ga(1) type LDHs, respectively. The reduction of crystallite size in plane direction is also observed in Mg-Al (1) and Mg-Ga(1) type LDHs whereas lattice parameter *a* does not change. The lattice parameter *c* and (003) plane crystallite size of SiO_2(40nm)@Ni-Al(1)LDH were hardly estimated because of the low intensity of diffraction peak. The lattice parameter *a* and (110) crystallite size of Ni-Al(1)LDH and SiO_2(40nm)@Ni-Al(1)LDH were also hardly estimated. These results indicated that the suppression of the crystal growth and increase of base activity were also observed in M^{2+}/M^{3+} = 1 type LDHs.

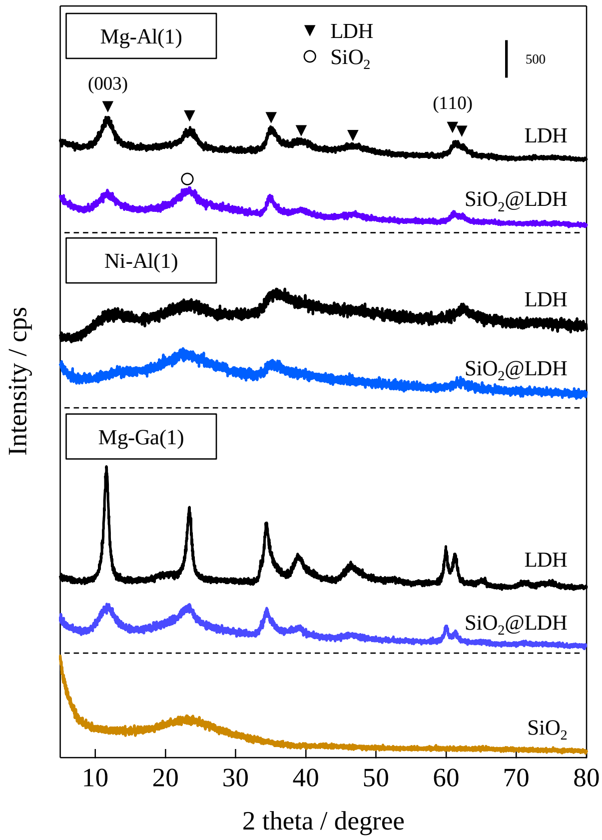

Figure 7 XRD patterns of M^{2+}-M^{3+}(1)LDHs and SiO_2(40nm)@M^{2+}-M^{3+}(1)LDHs.

Correlation between catalytic activity and base property

Next, I investigated the correlation between base activity and basicity of M^{2+}/M^{3+} = 3 type LDHs. Base amounts were estimated by the Knoevengel condensation in the presence of benzoic acid agent: *i.e.* because the benzoic acid interfered the basic sites of LDH for the Knoevenagel condensation, the correlation between the amounts of benzoic acid and product of ethyl α-cyanocinnamate showed a linear relationship leading to the base amount. Table 2 summarizes reaction rate for the Knoevenagel condensation and base amount of LDHs. Total divalent and trivalent metal hydroxide amount ($M(OH)_x$ amount) obtained from ICP-AES and base amount per total metal hydroxide amount (Base/$M(OH)_x$) are also listed in Table 2. Compared with conventional M^{2+}-M^{3+}(3)LDHs, $M(OH)_x$ values were *ca*. 24~32% reduced in SiO_2(40nm)@M^{2+}-M^{3+}(3)LDHs because of the coexistence of spherical SiO_2(40nm). On the other hand, the Base/$M(OH)_x$ ratios were 1.6~4.5 times increased by coexistence of spherical SiO_2(40nm). This suggests that coexistence of spherical SiO_2(40nm) plays crucial role to increase the number of hydroxide layers acting as surface base sites, and it would be contributed to the enhancement in the base catalysis for the Knoevenagel condensation in the cases of SiO_2(40nm)@M^{2+}-M^{3+}(3)LDHs.[61]

The morphology and interaction between SiO_2 and LDH in SiO_2(40nm)@Mg-Al(3)LDH were investigated by TEM and ^{29}Si CP-MAS NMR experiment. Fig. 8 showed TEM images of Mg-Al(3)LDH and SiO_2(40nm)@Mg-Al(3)LDH. The platen crystal size of SiO_2(40nm)@Mg-Al(3)LDH was smaller than that of Mg-Al(3)LDH. Besides, since SiO_2 spheres that should coexist in SiO_2(40nm)@Mg-Al(3)LDH was hardly observed in Fig. 8 (B), I applied EDS elemental mapping to SiO_2(40nm)@Mg-Al(3)LDH as shown in Fig. 9. It was confirmed that Mg and Al was uniformly dispersed in wide range whereas Si was prejudiced and

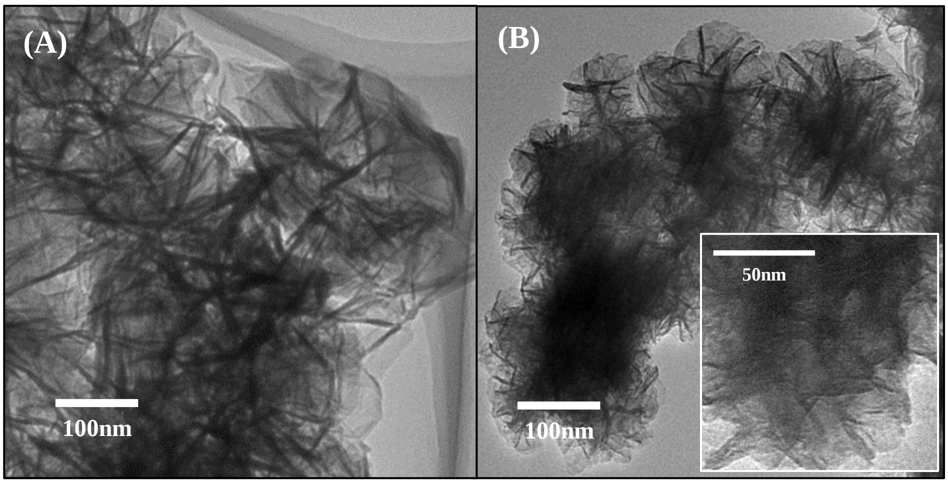

Figure 8 TEM images of (A) Mg-Al(3)LDH and (B) SiO_2(40nm)@Mg-Al(3)LDH.

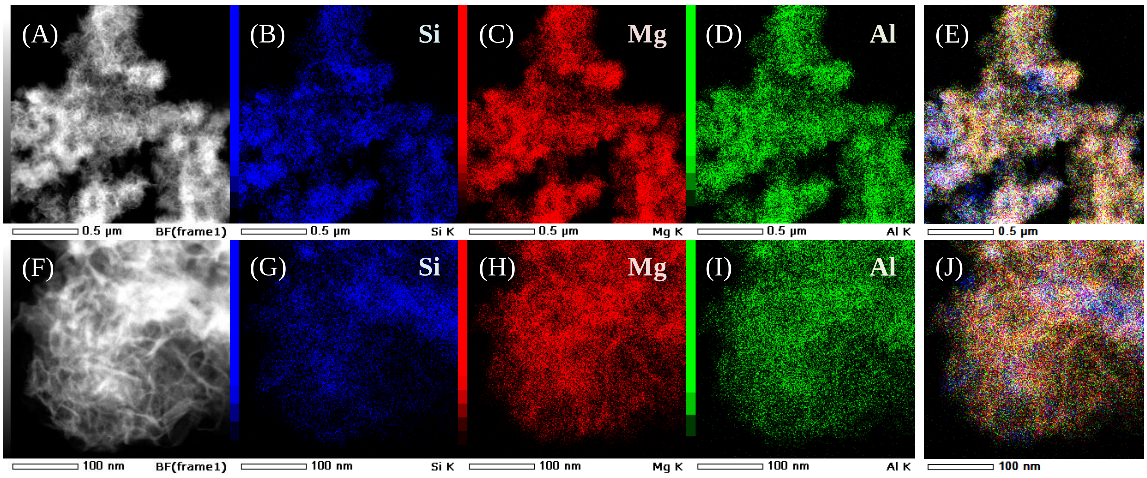

Figure 9 (A, F) Dark-field TEM images. Also shown are (B-E), (G-J) EDS mapping results of SiO_2@Mg-Al(3)LDH. (A-E): Low magnification visual field, and (F-J): high magnification visual field.

covered with Mg and Al to form SiO_2 core — LDH shell like structure (Fig. 9 (A)-(E)). Same trend was observed in high magnification visual fields (Fig. 9 (F)-(J)). Moreover, the shape of SiO_2 was not spherical but shapeless. These results suggested that spherical structure of SiO_2 was crumbled in the course of catalyst preparation, and was transferred to the shapeless structure. Because it is well known that SiO_2 is dissolved in basic condition, SiO_2(40nm) spheres possessing small high specific surface area would be partially dissolved and reprecipitated in the course of LDH crystal growth method. In fact, when I treated spherical SiO_2(40nm) in basic condition (pH = 10) for 1 h at room temperature, it formed shapeless structure (Fig. 10). To examine the actual morphology of

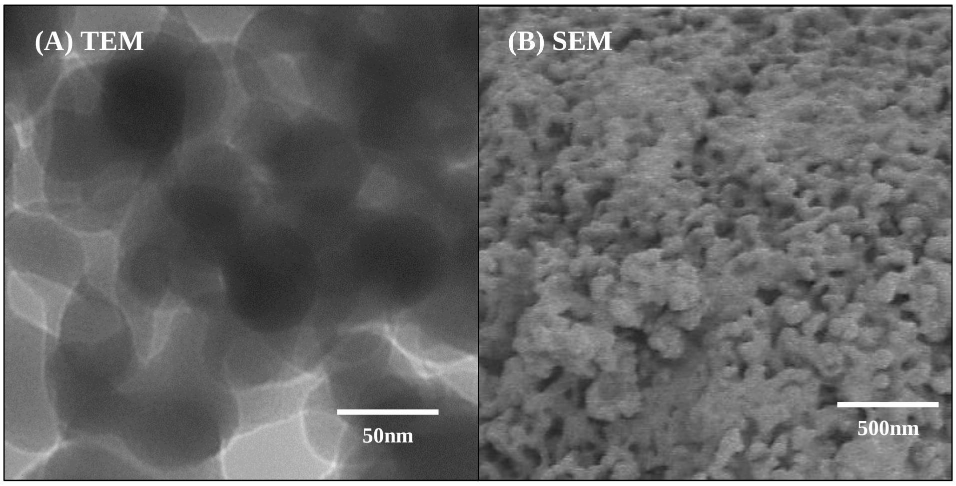

Figure 10 (A) TEM image and (B) SEM image of SiO_2(40nm) treated in basic condition (pH = 10) for 1 h.

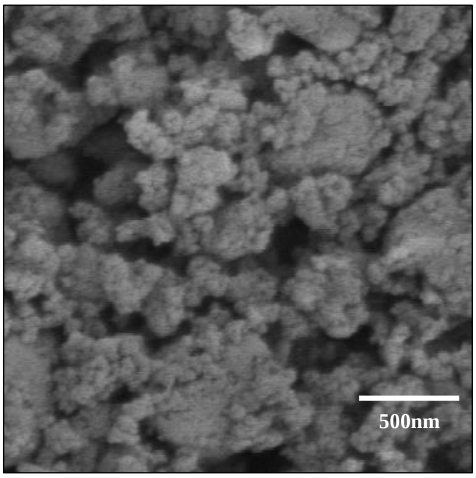

Figure 11 SEM image of SiO_2(40nm)@Mg-Al(3)LDH treated with HCl solution (1 M) after 0.5 h.

SiO_2 in the SiO_2(40nm)@Mg-Al(3)LDH, SEM images after treatment with 1 M HCl dissolving the LDH layers of SiO_2(40nm)@Mg-Al(3)LDH were monitored. As shown in Fig. 11, the presence of shapeless SiO_2 cores was also observed in the present catalyst.

Fig. 12 shows the ^{29}Si CP-MAS NMR spectra of spherical SiO_2 and SiO_2(40nm)@Mg-Al(3)LDH. Q^n designated the Si-centered tetrahedral structural species where Q refers to silicon atom and n denotes the number of bridging oxygens. The ^{29}Si CP-MAS NMR of spherical SiO_2(40nm) showed three peeks at -91, -100 and -109 ppm which respectively correspond to Q^2, Q^3 and Q^4.[54-56] On the other hand, SiO_2(40nm)@Mg-Al(3)LDH showed a broad resonance between -70 to -115 ppm, which can be deconvoluted into four peaks centered at -78, -85, -92 and -101 ppm. The peak at -78 ppm can be assigned to Q^0 and/or Q^1 species[55] generated because of dissolution and reprecipitation of SiO_2 sphere. Reportedly, Si-centered tetrahedral structure which possess Si-O-Al and Si-O-Mg bond gave some resonances between -73 to -105 ppm[50,

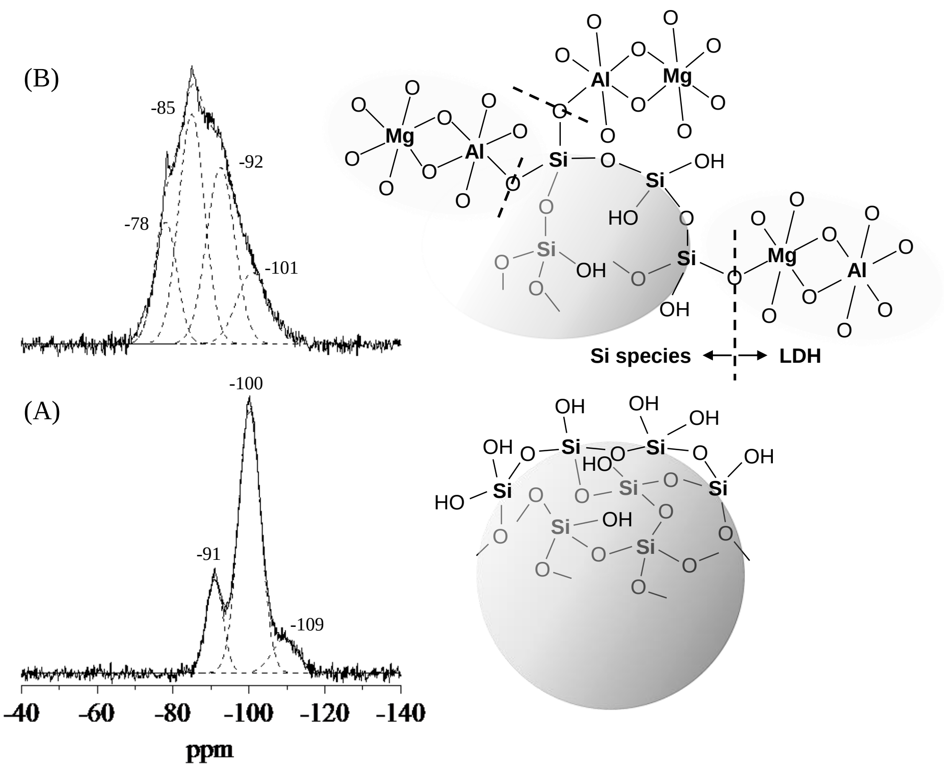

Figure 12 ^{29}Si CP-MAS NMR spectra of (A) spherical SiO_2(40nm) and (B) SiO_2(40nm)@Mg-Al(3)LDH.

Table 4 Assignments of ^{29}Si CP-MAS NMR peaks.

Assignment	δ / ppm	References
Q^4	-105 ~ -120	54-56
Q^4(1Al)	-99 ~ -105	49, 57, 59
Q^4(2Al)	-94 ~ -99	57
Q^4(3Al)	-89 ~ -94	57
Q^4(4Al)	-84 ~ -85	57
Q^3	-87 ~ -102	49, 54-56, 58, 59
Q^3(1Al)	-85 ~ -88	58
Q^3(2Al)	-81 ~ -84	58
Q^3(3Al)	-73	58
Q^3(1Mg)	-91 ~ -93	56, 60
Q^2	-73 ~ -93	54, 55
Q^2(1Mg)	-84	56, 60
Q^1	-68 ~ -83	55
Q^1(1Mg)	-70	56
Q^0	-60 ~ -82	55

[57-59] and -70 to -93 ppm,[56, 60] respectively, as described in Table 4. According to previous reports, the two signals appearing at -85 and -92 ppm were assigned respectively to Si-centered compound which has Si-O-Mg and/or Si-O-Al bonds as well as overlapping with Q^2. This strongly indicates that LDH sheets and SiO_2 do not interact only by electrostatic force but also the formation of Si-O-Al and Si-O-Mg covalent bonds. According to these results, the mechanism of generation of nano-crystallized Mg-Al LDH on SiO_2 spheres is predicted as follows: (*i*) a part of SiO_2 tetrahedral dissolves and reprecipitates (e.g. $2Q^n \leftrightarrow Q^{n+1} + Q^{n-1}$) in a basic mother solution, (*ii*) titrated Mg^{2+} and Al^{3+} ions in basic mother solution adsorb on unsaturated Si-O sites of SiO_2 surface, cause dispersion of starting points of LDH crystal growth, (*iii*) LDH nanosheets grow up from each dispersed points on SiO_2 to lead generation of small crystallite size LDH.

Evaluation of base catalysis on Mg-Al(3)LDHs with various crystallinities

To evaluate the correlation between crystalline of LDH and base catalysis on LDH or SiO_2@LDH, Mg-Al(3)LDH catalysts were prepared by various methods to assess these structural properties and catalytic activities for the Knoevenagel condensation. LDH(U-CP) and SiO_2(250nm)@LDH, synthesized respectively by an urea co-precipitation method and an *in situ* co-precipitation method with coexisting of SiO_2(250nm) spheres, were prepared in addition to LDH(CP) and SiO_2(40nm)@LDH. LDH(com.) purchased from Tomita Pharmaceutical Co., Ltd. was also evaluated its crystalline and base catalysis as a comparison.

Fig. 13 shows TEM images of five different Mg-Al(3)LDHs. LDH(U-CP) has well crystalline hexagonal structure. Orientations of most of LDH crystals in LDH(U-CP) and LDH(com.) are face up whereas these of SiO_2@LDHs and LDH(CP) are random, indicating the *ab*-face crystal sizes of LDH(U-CP) and LDH(com.) are bigger than LDH(CP). Moreover, the observed crystal size of SiO_2(40nm)@LDH was clearly smaller than that of SiO_2(250nm)@LDH, LDH(CP), and LDH(U-CP). SiO_2(250nm)@LDH possess a defined core-shell structure as well as result reported by Chen,[50] and its LDH crystal size was similar to that of LDH(CP).

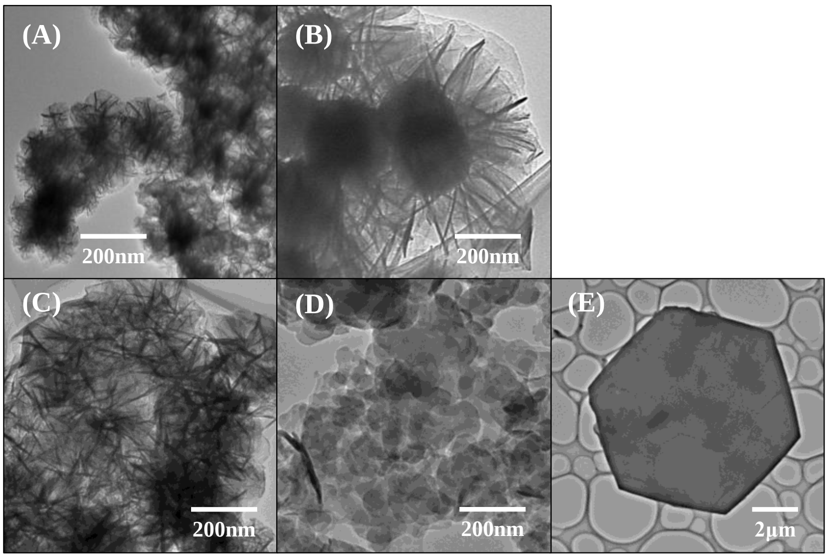

Figure 13 TEM image of various Mg-Al(3) type LDHs. (A)SiO_2(40nm)@LDH, (B) SiO_2(250nm)@LDH, (C) LDH(CP), (D) LDH(com.) and (E) LDH(U-CP).

Fig. 14 shows XRD patterns of various Mg-Al(3)LDHs. Lattice parameters and LDH (003) or (110) crystallite sizes are listed in Table 5. Similar diffraction patterns and lattice parameters were observed in all samples, indicating those LDHs composed of same LDH unit.

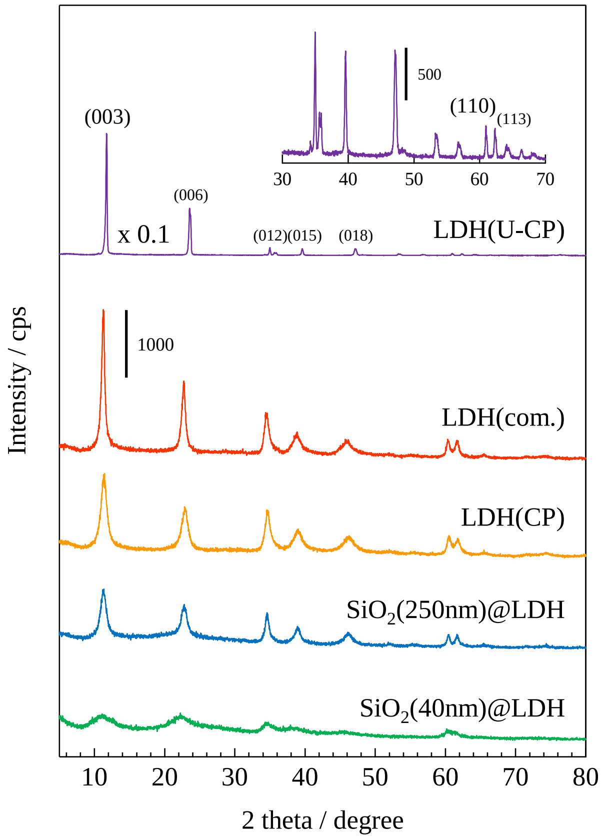

Figure 14 XRD patterns of various Mg-Al(3) type LDHs.

Table 5 Crystal properties of various Mg-Al(3)LDHs.

Type of Mg-Al(3)LDH	Lattice parameter *c* / nm	Crystallite size (003)[a] / nm	Lattice parameter *a* / nm	Crystallite size (110)[a] / nm
SiO_2(40nm)@LDH	2.43	2.8	0.31	8.3
SiO_2(250nm)@LDH	2.35	7.9	0.31	20.0
LDH(CP)	2.33	7.6	0.31	13.4
LDH(com.)	2.36	14.8	0.31	18.4
LDH(U-CP)	2.26	37.8	0.30	49.6

[a]The crystallite sizes of LDHs were calculated by Scherrer equation; $D_{hkl} = K\lambda/\beta\cos\theta$ (K: Scherrer number (0.9), λ: incident ray wavelength (0.1542 nm), β: peak width at half height (rad)).

The crystallite sizes of LDH(U-CP) and LDH(com.) were bigger than SiO_2@LDHs and LDH(CP), as expected by TEM images. Interestingly, crystallite size of SiO_2(40nm)@LDH was smaller than LDH(CP) whereas that of SiO_2(250nm)@LDH was little bigger than LDH(CP), indicating coexistence of spherical SiO_2(250nm) is not suitable for fine-crystallization of LDH. Fig 15 (A) shows ^{29}Si CP-MAS NMR spectra of SiO_2(250nm) sphere. Although the broad peak between -80 to -120 ppm could be deconvoluted into three peaks centered at -92, -101, and -110 ppm as well as SiO_2(40nm) sphere, ratios of these peaks in SiO_2(40nm) sphere and SiO_2(250nm) sphere were different as shown in Table 6; the ratio for Q^4, assigned to bridging saturation silicon, in SiO_2(250nm) sphere (25%) was higher than SiO_2(40nm) sphere (11%) whereas ratios for unsaturated silicon Q^3 and Q^2 in SiO_2(250nm) sphere was lower than SiO_2(40nm) sphere. Moreover, S_{BET} of SiO_2(250nm) sphere (50 m^2 g^{-1}) was much lower than SiO_2(40nm) sphere (1081 m^2 g^{-1}). These indicate that the surface of SiO_2(40nm) sphere possess more adsorption sites for Mg^{2+} and Al^{3+} ions than

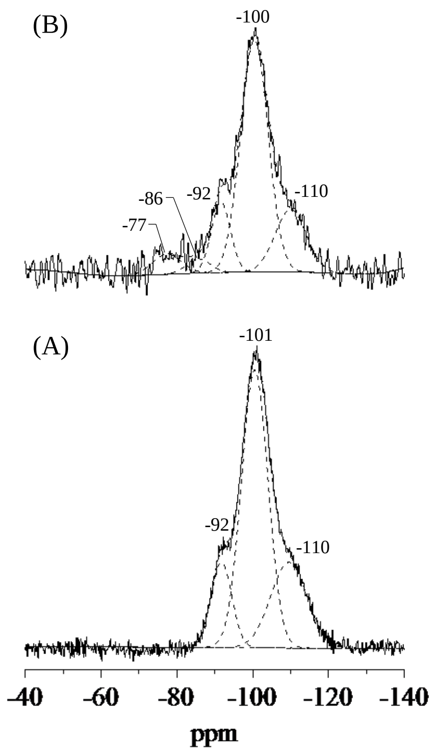

Figure 15 ^{29}Si CP-MAS NMR spectra of (A) spherical SiO_2(250nm) and (B) SiO_2(250nm)@Mg-Al(3)LDH.

SiO_2(250nm) sphere. In fact, the ratio for ^{29}Si CP-MAS NMR peak in SiO_2(250nm)@LDH (Fig. 15 (B)), the degree of interactions between the SiO_2 and the LDH crystal, was only ≤ 16% whereas that of SiO_2(40nm)@LDH was ≤ 68%. These results strongly suggest that the size and surface area of spherical SiO_2 are the crucial factors to generate a small crystallite size LDH because a small spherical SiO_2 which possess high surface area can be expected to be in contact with Mg^{2+} and Al^{3+} ions, leading to enhance the dispersion of starting points of LDH crystal growth.

Table 6 Surface area and silicon environments in the SiO_2 and SiO_2@LDH as determined by ^{29}Si CP-MAS NMR.

	S_{BET} / m_2 g^{-1}	Assignment	δ / ppm	Percentage /%
SiO_2(40nm) sphere	1081	Q^4	-109	11
		Q^3	-100	70
		Q^2	-91	19
SiO_2(40nm)@LDH	409	Q^3	-101	14
		Q^2 Q^4(3Al), Q^3(1Mg)	-92	*31*
		Q^4(4Al), Q^3(1Al), Q^2(1Mg)	-85	*37*
		Q^1 and/or Q^0	-78	17
SiO_2(250nm) sphere	50	Q^4	-110	25
		Q^3	-101	60
		Q^2	-92	14
SiO_2(250nm)@LDH	133	Q^4	-110	18
		Q^3	-100	60
		Q^2 Q^4(3Al), Q^3(1Mg)	-92	*13*
		Q^4(4Al), Q^3(1Al), Q^2(1Mg)	-86	*3*
		Q^1 and/or Q^0	-77	5

Catalytic activities for the Knoevenagel condensation are shown in Fig. 16 as time course of benzaldehyde conversion (Fig. 16 (A)) and reaction rate (Fig. 16 (B)), respectively. A high crystalline LDH(U-CP) hardly showed catalytic activity. Although LDH(com.) enhanced the Knoevenagel condensation, reaction rate was only 14 mmol g^{-1} h^{-1}. Remarkably, SiO_2(40nm)@LDH showed the highest activity with reaction rate of 117 mmol g^{-1} h^{-1} as previously described. Although SiO_2(250nm)@LDH resulted reaction rate of 60 mmol g^{-1} h^{-1}, its activity was little lower than LDH(CP) (77 mmol g^{-1} h^{-1}). This strongly suggests that catalytic activity is affected by not only morphologies of LDH catalysts (*ex.* SiO_2 core – LDH shell structure) but also LDH crystallite size. On the basis of ICP-AES results, I calculated the amount of LDH structure (wt%) in the various Mg-Al(3)LDHs as shown in Table 7. The reaction rate per each LDH structure was also plotted with both LDH(003) and LDH(110) crystallite sizes in Fig.17. These data clearly showed that the catalytic activity of obtained LDH

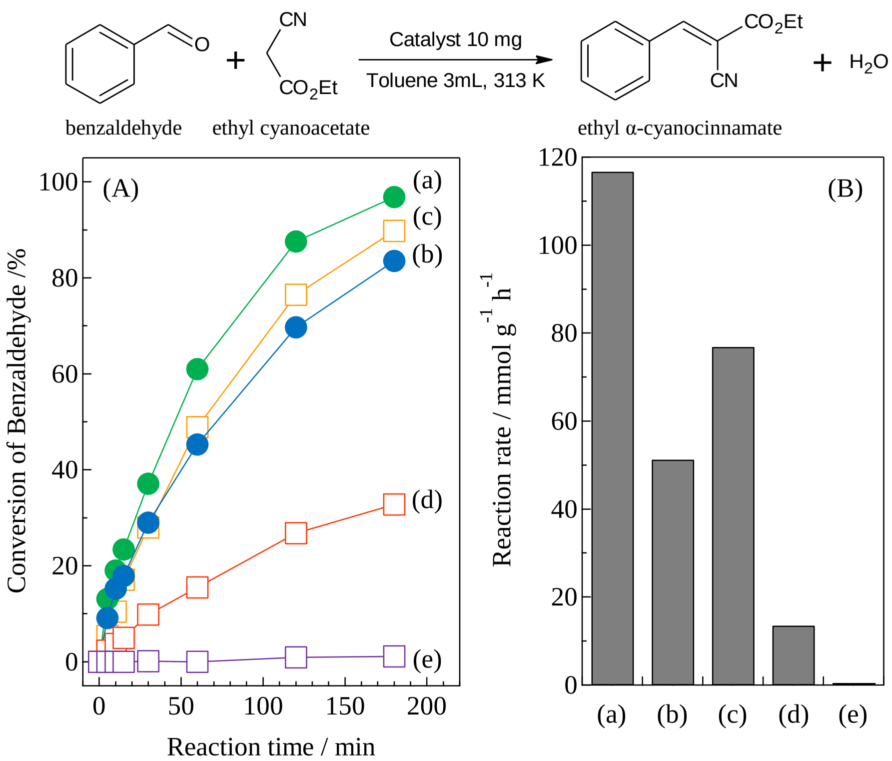

Figure 16 Activities of various Mg-Al(3) type LDHs (a) SiO_2(40nm)@LDH, (b) SiO_2(250nm)@LDH, (c) LDH(CP), (d) LDH(com.) and (e) LDH(U-CP) for the Knoevenagel condensation of benzaldehyde with ethyl cyanoacetate as (A) time cause and (B) reaction rate. *Reaction conditions*: benzaldehyde (1.0 mmol), ethyl cyanoacetate (1.2 mmol), catalyst (10 mg), toluene (3 mL), 313 K, N_2 flow (30 mL min^{-1}).

is drastically changed by the crystallite sizes, and this tendency became significant especially below crystallite sizes of 20 nm; the catalytic activity of LDH increased with decreasing of crystallite sizes. These results support that the fine-crystallization of LDH crystallite is a crucial factor to increase the base catalysis of LDH materials.

Table 7 Catalytic activity of the LDH in various Mg-Al(3)LDHs.

Type of Mg-Al(3)LDH	Amount of LDH[a] / wt%	Reaction rate[b] / mmol g(cat)$^{-1}$ h^{-1}	Reaction rate[b] / mmol g(LDH)$^{-1}$ h^{-1}
SiO_2(40nm)@LDH	73.6	116.7	158.4
SiO_2(250nm)@LDH	71.1	59.5	83.7
LDH(CP)	100	76.9	76.9
LDH(com.)	100	13.6	13.6
LDH(U-CP)	100	0.5	0.5

[a]The amount of LDH in the SiO_2@LDHs were calculated by ICP-AES with an assumption, that is all Mg-Al(3)LDHs are composed of only LDH structure or mixture of LDH and SiO_2.
[b]Reaction rate for the Knoevenagel condensation of benzaldehyde with ethyl cyanoacetate.

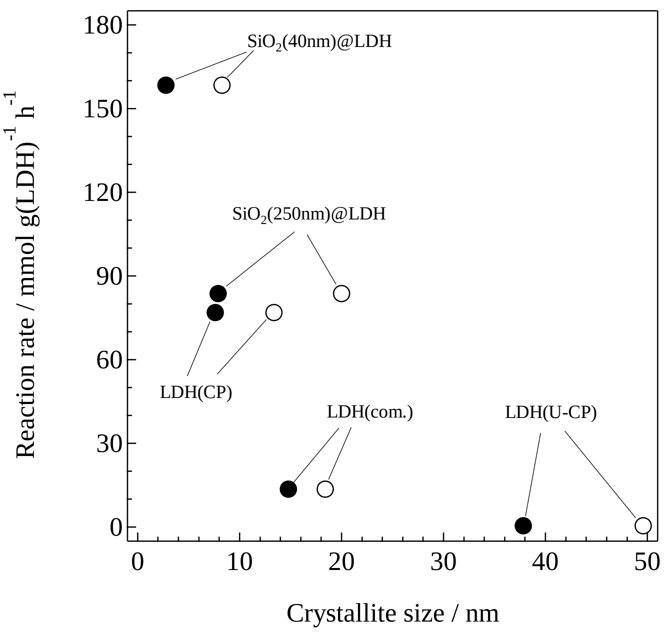

Figure 17 Correlation between the crystallite sizes (●: LDH(003) or ○: LDH(110) and the catalytic activity of LDH in the various Mg-Al(3)LDHs.

Base amounts and apparent TOF of each base sites (TOF_{base}) in various Mg-Al(3)LDHs are listed in Table 8. Base amount of SiO_2(250nm)@LDH estimated to 0.29 mmol g^{-1} is little lower than LDH(CP) whereas apparent TOF_{base} of both SiO_2(250nm)@LDH and LDH(CP) are similar. Because crystallite of SiO_2(250nm)@LDH is similar to that of LDH(CP), it is suggested that coexistence of SiO_2(250nm) results to just immobilize LDH crystal onto SiO_2 surface without avoiding the *ab*-face stacking, so that reaction rate was smaller than LDH(CP) whereas TOF_{base} was not changed. On the other hand, SiO_2(40nm)@LDH showed higher base amount and apparent TOF_{base} than LDH(CP), indicating effects of coexistence of SiO_2(40nm) is not only increase total base amount of LDH where the exchanged OH^- ions at the entrance of the galleries but also increase ratio of higher active site on LDH surface by fine-crystallization.

Table 8 Correlation between base activity and base property of various Mg-Al(3)LDHs.

Type of Mg-Al(3)LDH	Reaction rate[a] / mmol g^{-1} h^{-1}	Base amount[b] / mmol g^{-1}	TOF_{base} / h^{-1}
(a) SiO_2(40nm)@LDH	116.7	0.48	243
(b) SiO_2(250nm)@LDH	59.5	0.29	205
(c) LDH(CP)	76.9	0.45	171
(d) LDH(com.)	13.6	0.13	105
(e) LDH(U-CP)	0.5	n.d.	n.d.

[a]Reaction rate for the Knoevenagel condensation of benzaldehyde with ethyl cyanoacetate.
[b]Base amount calculated from poisoning test by benzoicacid titration.

Optimization of Si/(Mg+Al) ratio in SiO_2(40nm)@Mg-Al(3)LDH

Finally, I prepared SiO_2(40nm)@Mg-Al(3)LDHs with various SiO_2 loading amounts to reveal the optimized SiO_2(40nm)@Mg-Al(3)LDH structure. The correlation between Si/(Mg+Al) atomic ratio and base catalysis, structural properties of SiO_2(40nm)@Mg-Al LDHs were investigated. The Si/(Mg+Al) atomic ratio was varied from 0 to 0.50, and prepared catalysts are denoted as SiO_2(40nm)@(Z)LDH where Z is a Si/(Mg+Al) atomic ratio. The actual ratios of Si/(M^{2+}+M^{3+}) and M^{2+}/M^{3+} in obtained materials were summarized in Table 9.

Table 9 Chemical compositions of prepared various SiO_2(40nm)@(Z)Mg-Al(3)LDHs estimated by ICP-AES.

	Si/(M^{2+}+M^{3+}) ratio		M^{2+}/M^{3+} ratio	
	Precursor	Obtained material	Precursor	Obtained material
LDH(CP)	—	—	3.0	2.8
SiO_2(40nm)@(0.13)LDH	0.13	0.14	3.0	2.5
SiO_2(40nm)@(0.17)LDH	0.17	0.18	3.0	2.6
SiO_2(40nm)@(0.25)LDH	0.25	0.28	3.0	2.5
SiO_2(40nm)@(0.50)LDH	0.50	0.53	3.0	2.2

Fig. 18 shows the catalytic activity for the Knoevenagel condensation over SiO_2(40nm)@(Z)LDHs as (A) time cause of benzaldehyde conversion and (B) reaction rate. Among various Si/(Mg+Al) atomic ratio from 0 to 0.50, 0.17 was found to be the best catalyst with reaction rate of 171.1 mmol g^{-1} h^{-1}. This reaction rate is 2.2 times higher than conventional LDH(CP) (Si/(Mg+Al) = 0).

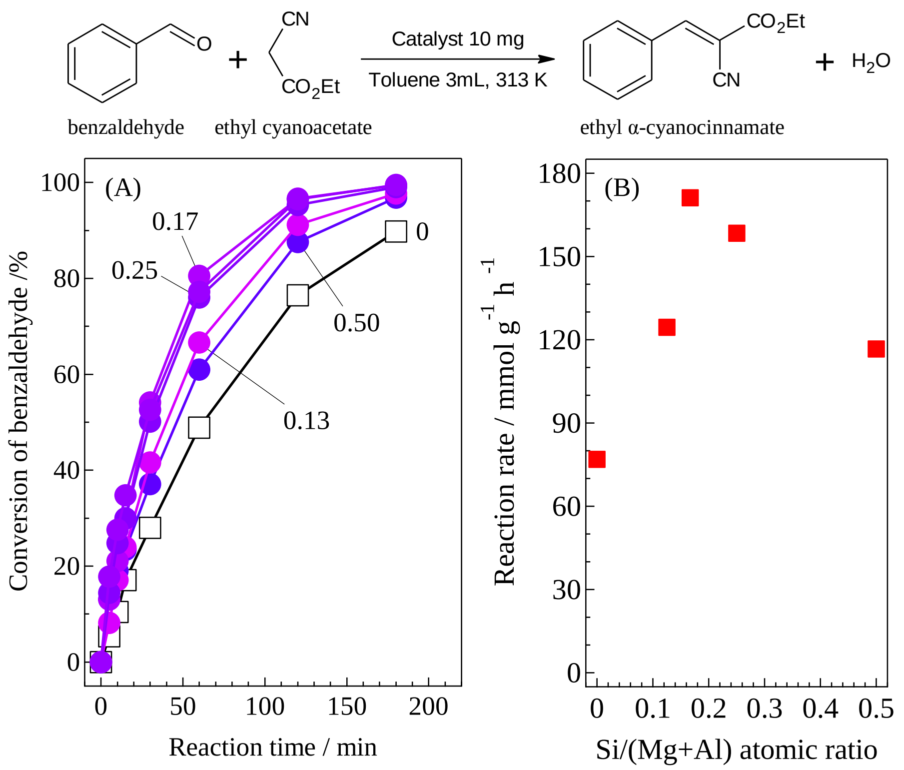

Figure 18 Activities for the Knoevenagel condensation of benzaldehyde with ethyl cyanoacetate as (A) time cause and (B) reaction rate over the SiO_2(40nm)@LDHs with various Si/(Mg+Al) atomic ratio. *Reaction conditions*: benzaldehyde (1.0 mmol), ethyl cyanoacetate (1.2 mmol), catalyst (10 mg), toluene (3 mL), 313 K, N_2 flow (30 mL min^{-1}). Number in (A) denotes Si/(Mg+Al) atomic ratio.

The XRD patterns and crystal properties of SiO_2(40nm)@(Z)LDHs are shown in Fig. 19 and Table 10, respectively. All prepared catalysts showed LDH originated diffraction pattern. The intensity of LDH originated peaks are decreased in accordance with Si loading amount whereas that of amorphous SiO_2 is slightly increase. The lattice parameters *a* and *c*, respectively calculated from LDH (003) and (110) diffraction peaks, are almost identical between Si/(Mg+Al) atomic ratio of 0 ~ 0.50. This result clearly indicate that these SiO_2(40nm)@(Z)LDHs have a same LDH crystal unit. On the other hand, the crystallite size of LDH is definitely affected by Si/(Mg+Al) atomic ratio. The crystallite size of *D*(003) is reduced in accordance with Si loading amount. The crystallite size of *D*(110) is almost identical in the region between Si/(Mg+Al) ratio of 0 ~ 0.13, whereas it is reduced from *ca*. 13 to 8 nm when a Si/(Mg+Al) ratio increased. These results suggested that in the case of lower Si/(Mg+Al) atomic ratio (< 0.13), the LDH crystal is immobilized onto the SiO_2 surface to inhibit *ab*-face stacking without reducing the plane crystallite size. This seems because of less number of starting points of LDH crystal growth; *i.e.* the amount of metal constituting one crystal did not change compared with LDH(CP). Actually, the proportion for the ^{29}Si CP-MAS NMR peaks attributed to Si-O-Mg and Si-O-Al bonds on the SiO_2(40nm)@(0.13)LDH is only ≤ 40% whereas that of SiO_2(40nm)@(0.17)LDH is ≤ 61%, as shown in Fig. 20 and Table 11. Thus, I infer that the number of Si-O-Mg and Si-O-Al bonds on the SiO_2 surface deeply affected to reduce the crystallite size of not only the stacking direction but also the plane direction in the case of below Si/(Mg+Al) < 0.17 ~ 0.25.

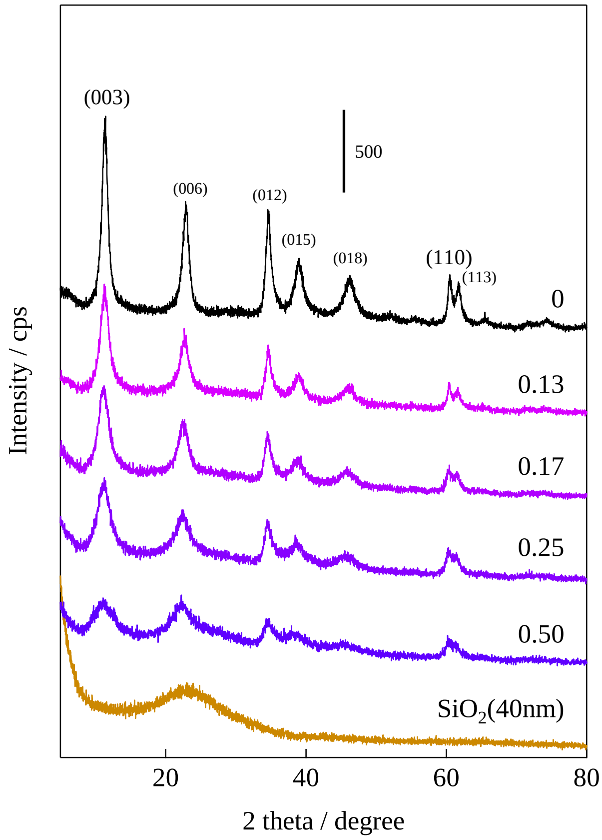

Figure 19 XRD patterns of various SiO_2(40nm)@(Z)Mg-Al(3) type LDHs where Z is a Si/(Mg+Al) atomic ratio.

Table 10 Crystal properties of various SiO_2(40nm)@(Z)Mg-Al(3)LDHs.

Si/(Mg+Al) atomic ratio	Lattice parameter *c* / nm	Crystallite size (003)[a] / nm	Lattice parameter *a* / nm	Crystallite size (110)[a] / nm
0	2.33	7.6	0.31	13.4
0.13	2.32	5.2	0.31	13.7
0.17	2.36	4.5	0.31	10.3
0.25	2.38	3.7	0.31	8.0
0.50	2.43	2.8	0.31	8.3

[a]The crystallite sizes of LDHs were calculated by Scherrer equation; $D_{hkl} = K\lambda/\beta\cos\theta$ (K: Scherrer number (0.9), λ: incident ray wavelength (0.1542 nm), β: peak width at half height (rad)).

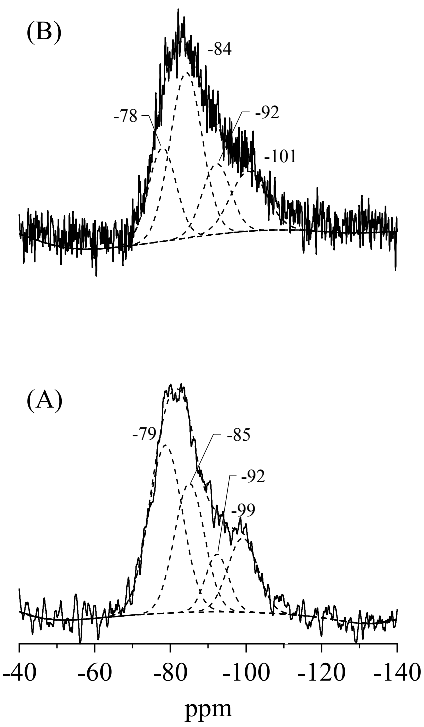

Figure 20 ^{29}Si CP-MAS NMR spectra of (A) SiO_2(40nm)@(0.13)LDH and (B) SiO_2(40nm)@(0.17)LDH.

Table 11 Surface area and silicon environments in the SiO_2 and SiO_2@LDH as determined by ^{29}Si CP-MAS NMR.

	Assignment	δ / ppm	Percentage /%
SiO_2(40nm)@(0.17)LDH	Q^3	-100	18
	Q^2 Q^4(3Al), Q^3(1Mg)	-92	*17*
	Q^4(4Al), Q^3(1Al), Q^2(1Mg)	-85	*44*
	Q^1 and/or Q^0	-78	21
SiO_2(40nm)@(0.13)LDH	Q^3	-99	17
	Q^2 Q^4(3Al), Q^3(1Mg)	-92	*10*
	Q^4(4Al), Q^3(1Al), Q^2(1Mg)	-85	*30*
	Q^1 and/or Q^0	-79	43

The correlation between base amount and catalytic activity for the Knoevenagel condensation over SiO_2(40nm)@(Z)LDHs are summarized in Table 12. Although the base amount of SiO_2(40nm)@(0.13)LDH was lower than LDH(CP), reaction rate and apparent TOF per base site for SiO_2(40nm)@(0.13)LDH are higher than those of LDH(CP). Because the *D*(003) of SiO_2(40nm)@(0.13)LDH was smaller than LDH(CP) whereas *D*(110) of SiO_2(40nm)@(0.13)LDH and LDH(CP) are almost identical as shown in Table 10, these indicated that the immobilization of LDH crystal onto SiO_2 with inhibiting the *ab*-face stacking leading to increase the number of highly active base sites located on the surface LDH layer. Above the Si/(Mg+Al) atomic ratio of 0.13, a base amount increased in accordance with Si/(Mg+Al) ratio from 0.32 to 0.49 mmol g^{-1}. Besides, the activity was maximized at Si/(Mg+Al) ratio of 0.17 with the reaction rate of 171.1 mmol $g(cat)^{-1}$ h^{-1}. Interestingly, the reaction rate per obtained LDH phase and TOF_{base} were also maximized at Si/(Mg+Al) ratio of 0.17 with the reaction rate of 193.6 mmol $g(LDH)^{-1}$ h^{-1} and TOF_{base} of 450 h^{-1}. Above Si/(Mg+Al) ratio of 0.17, both reaction rate per LDH phase and TOF_{base} were decreased to 158.4 mmol $g(LDH)^{-1}$ h^{-1} and 238 h^{-1} at Si/(Mg+Al) ratio of 0.50, respectively. These strongly indicate that the Si/(Mg+Al) atomic ratio affects to not only LDH crystallite size and base amount but also the type of base sites and these fraction.

Because the LDH crystallite size of SiO_2(40nm)@(0.50)LDH is at least smaller than that of SiO_2(40nm)@(0.17)LDH, the base catalysis of SiO_2(40nm)@(0.50)LDH should be better than that of SiO_2(40nm)@(0.17)LDH if the base catalysis is influenced by the crystallite size. ^{29}Si CP-MAS NMR spectra showed that the proportion of terminal Si-OH species assigned as Q^0 and/or Q^1 decreased in accordance with Si/(Mg+Al) atomic ratio as shown in Tables 6 and 11, indicating at first a surface Si-O-Si bond is cleaved to generate terminal Si-OH species and then these act as cross-link point with Mg and Al ions. Thus, when there are the excess free terminal Si-OH species in the solution after the generation of SiO_2@LDH, these excess Si-OH species cover the LDH crystal to make Si-O-Mg and Si-O-Al covalent bonds. Although the base amount is increased even the region from SiO_2(40nm)@(0.13)LDH to SiO_2(40nm)@(0.50)LDH, this phenomenon might be not occurred on the inferior base sites located at a flat plane of LDH.

Table 12 Activity for the Knoevenagel condensation and base amount of SiO_2(40nm)@(Z)LDHs

	Amount of LDH[a] / wt%	Reaction rate[b]		Base amount[c] / mmol g^{-1}	TOF_{base} / h^{-1}
		mmol $g(cat)^{-1}$ h^{-1}	mmol $g(LDH)^{-1}$ h^{-1}		
LDH(CP)	100	76.9	76.9	0.42	183
SiO_2(40nm)@(0.13)LDH	90.8	124.5	137.0	0.32	389
SiO_2(40nm)@(0.17)LDH	88.3	171.1	193.6	0.38	450
SiO_2(40nm)@(0.25)LDH	82.9	158.4	191.0	0.40	396
SiO_2(40nm)@(0.50)LDH	73.6	116.7	158.4	0.49	238

[a]The amount of LDH in the SiO_2(40nm)@(Z)LDHs were calculated by ICP-AES with an assumption, that is all SiO_2(40nm)@(Z)LDHs are composed of mixture of LDH and SiO_2.

[b]Reaction rate for the Knoevenagel condensation of benzaldehyde with ethyl cyanoacetate.

[c]Base amount calculated from poisoning test by benzoicacid titration.

However, the decrease of TOF_{base} strongly suggested that the high active base sites are poisoned by Si species in the case of higher Si/(Mg+Al) atomic ratio.

The dark-field TEM images and results of EDS elemental mapping of SiO_2(40nm)@(Z)LDHs are shown in Fig. 21. In the case of lower Si/(Mg+Al) atomic ratio such as 0.13 and 0.17, the LDH crystal is generated with covering the SiO_2 phase to form SiO_2 core — LDH shell like structure as shown in Fig. 21 (A)-(J). Besides, it was observed that the boundary between SiO_2 phase and LDH phase become ambiguous accordance with the increase of Si/(Mg+Al) atomic ratio (Fig. 21 (K)-(T)). These indicate that at first the LDH crystal grow up from the SiO_2 surface to generate the immobilized SiO_2 core — LDH shell structure and if

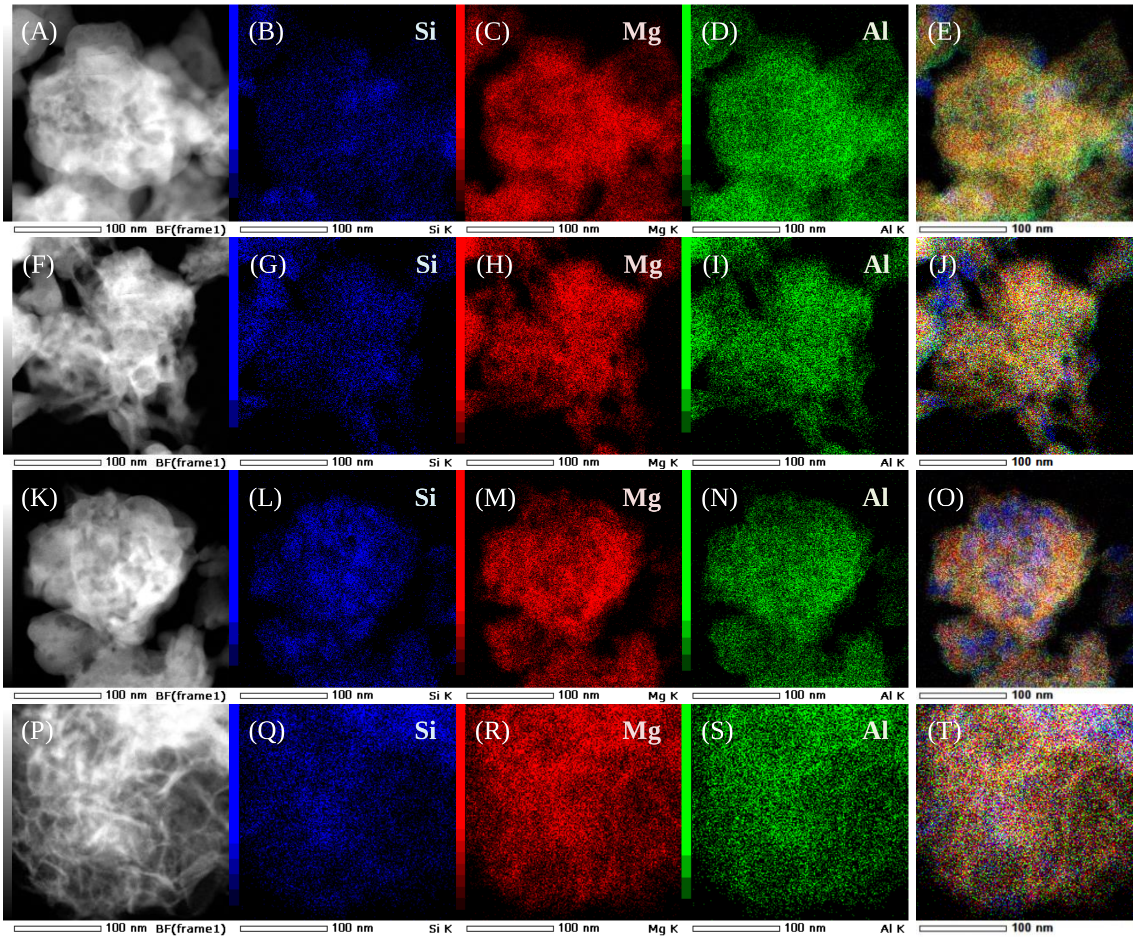

Figure 21 (A, F, K, P) Dark-field TEM images of SiO_2(40nm)@Mg-Al(3)LDHs with various Si/(Mg+Al) atomic ratio: (A) 0.13, (F) 0.17, (K) 0.25 and (P) 0.50. Also shown are (B-E), (G-J), (L-O), (Q-T) EDS mapping results of SiO_2(40nm)@Mg-Al(3)LDHs with various Si/(Mg+Al) atomic ratio.

there are the excess dissolved SiO_2 species possessing a free terminal Si-OH group, then these make Si-O-Mg and Si-O-Al covalent bonds with LDH crystal to cover the LDH shell.

Accordingly, I infer the correlation between Si/(Mg+Al) atomic ratio and base catalysis of prepared SiO_2(40nm)@(Z)LDHs as shown in Fig. 22. (i) Below Si/(Mg+Al) atomic ratio of 0.13, the LDH crystal is just immobilized onto SiO_2 surface with inhibiting the *ab*-face stacking, and the exposed corner and edge located at the surface layer act as the highly active base sites. (ii) The fine crystallization occurs not only in the stacking direction but also in the plane direction to increase the amount of base sites, especially base site with high activity up to Si/(Mg+Al) atomic ratio of 0.17. (iii) Above a Si/(Mg+Al) atomic ratio of 0.17, excess terminal Si-OH species covered the highly active base sites to make Si-O-Mg and Si-O-Al covalent bonds, thereby lowering the activity.

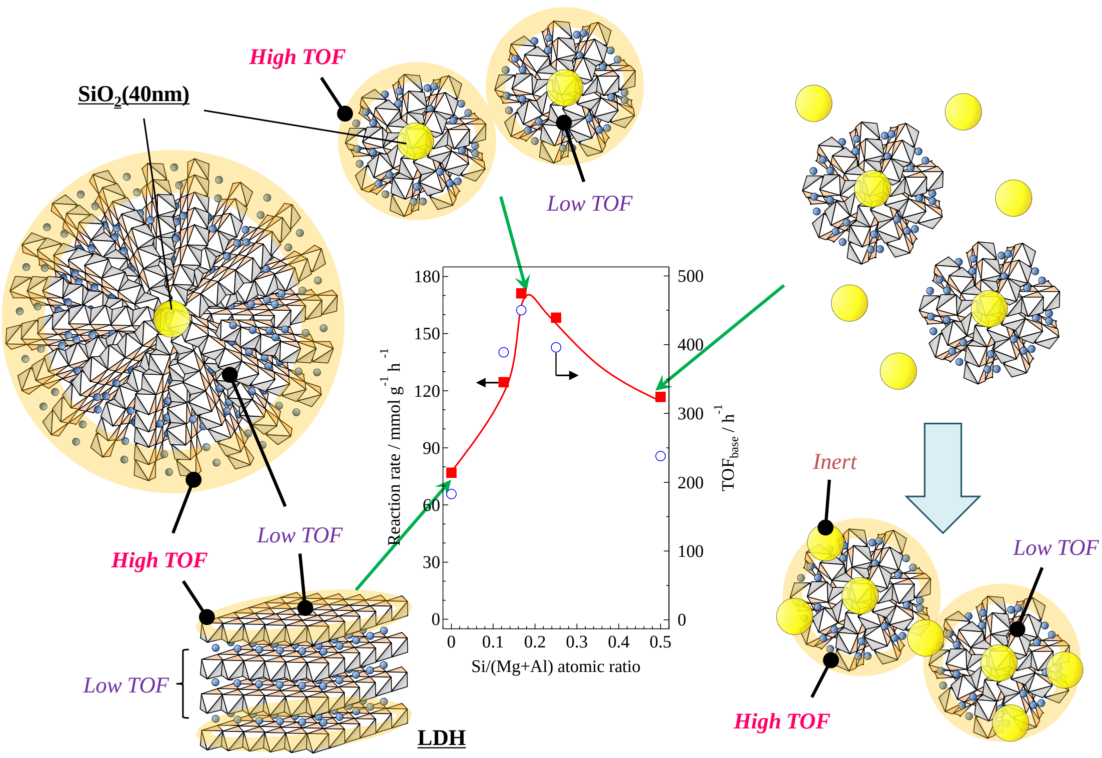

Figure 22 Structural models and activities for the Knoevenagel condensation of SiO_2(40nm)@Mg-Al(3)LDHs with various Si/(Mg+Al) atomic ratio. Although actually SiO_2 exist with shapeless structure, they are described with spherical structure in the models for easy image to the correlation between SiO_2 and LDH.

Conclusions

Highly active SiO_2(40nm)@LDH catalysts were synthesized by co-precipitation method with coexistence of small SiO_2 sphere whose particle size of *ca.* 40 nm. The results of XRD suggested that the crystallite sizes of SiO_2(40nm)@LDHs were smaller than conventional LDHs prepared by co-precipitation method without coexistence of SiO_2 sphere, whereas the lattice parameters of LDH crystal were hardly changed. All SiO_2(40nm)@LDHs showed higher catalytic activity for the Knoevenagel condensation of benzaldehyde and ethyl cyanoacetate than conventional LDHs regardless of metal compositions and ratios. Detailed characterizations on SiO_2(40nm)@Mg-Al LDH using TEM-EDS and ^{29}Si CP-MAS NMR revealed that SiO_2(40nm)@Mg-Al(3)LDH forms SiO_2 core ─ LDH shell like structure with Si-O-Al and Si-O-Mg covalent bonds, indicating LDH crystal is immobilized on SiO_2 surface. Compared to various type of Mg-Al(3)LDHs, SiO_2(40nm)@Mg-Al(3)LDH has the smallest LDH crystallite and it shows the highest catalytic activity among all. On the other hand, SiO_2(250nm)@Mg-Al(3)LDH which possesses similar size of LDH crystallite with Mg-Al(3)LDH(CP) shows lower catalytic activity than Mg-Al(3)LDH. I concluded that co-precipitation method with coexistence of spherical SiO_2(40nm), which has high surface area and can easily serve Si-O sites, causes dispersion of starting points of LDH crystal growth on SiO_2 surface to lead generation of fine-crystallized highly active LDH nanocrystal. After the optimization of Si/(Mg+Al) atomic ratio in SiO_2(40nm)@Mg-Al(3)LDHs, the Si/(Mg+Al) atomic ratio of 0.17 was found to be the best catalyst with the reaction rate of 171.1 mmol g^{-1} h^{-1}.

References

1. S. Miyata, *Clays and Clay Minerals*, 1980, **28**, 50-56.
2. P. J. Sideris, U. G. Nielsen, Z. Gan and C. P. Grey, *Science*, 2008, **321,** 113-117.
3. S. Nishimura, A. Takagaki and K. Ebitani, *Green Chem.*, 2013, **15**, 2026-2042.
4. N. Iyi, T. Matsumoto, Y. Kaneko and K. Kitamura, *Chem. Mater.*, 2004, **16**, 2926-2932.

5. Y. F. Lung, Y. S. Sun, C. K. Lin, J. Y. Uan and H. H. Huang, *Sci. Rep.*, 2016, **6**, 32458.
6. J.-H. Choy, S.-Y. Kwak, J.-S. Park, Y.-J. Jeong and J. Portier, *J. Am. Chem. Soc.*, 1999, **121**, 1399-1400.
7. S. Aisawa, H. Hirahara, K. Ishiyama, W. Ogasawara, Y. Umetsu and E. Narita, *J. Solid State Chem.*, 2003, **174**, 342-348.
8. J. H. Lee, S. W. Rhee and D.-Y. Jung, *Chem. Mater.*, 2004, **16**, 3774-3779.
9. M. L. Kantam, B. M. Choudary, C. V. Reddy, K. K. Rao and F. Figueras, *Chem. Commun.*, 1998, 1033-1034.
10. K. Yamaguchi, K. Mori, T. Mizugaki, K. Ebitani and K. Kaneda, *J. Org. Chem.*, 2000, **65**, 6897-6903.
11. T. Honma, M. Nakajo, T. Mizugaki, K. Ebitani and K. Kaneda, *Tetrahedron Lett.*, 2002, **43**, 6229-6232.
12. M. J. Climent, A. Corma, S. Iborra, K. Epping and A. Velty, *J. Catal.*, 2004, **225**, 316-326.
13. M. Fuming, P. Zhi and L. Guangxing, *Org. Process Res. Dev.*, 2004, **8**, 372-375.
14. Z. An, W. Zhang, H. Shi and J. He, *J. Catal.*, 2006, **241**, 319-327.
15. E. Angelescu, O. D. Pavel, R. Bîrjega, R. Zăvoianu, G. Costentin and M. Che, *Appl. Catal. A.*, 2006, **308**, 13-18.
16. H. C. Greenwell, P. J. Holliman, W. Jones and B. V. Velasco, *Catal. Today*, 2006, **114**, 397-402.
17. E. Li, Z. P. Xu and V. Rudolph, *Appl. Catal. B*, 2009, **88**, 42-49.
18. M. Ohara, A. Takagaki, S. Nishimura and K. Ebitani, *Appl. Catal. A*, 2010, **383**, 149-155.
19. A. Takagaki, M. Ohara, S. Nishimura and K. Ebitani, *Chem. Lett.*, 2010, **39**, 838-840.
20. O. D. Pavel, B. Cojocaru, E. Angelescu and V. I. Pârvulescu, *Appl. Catal. A*, 2011, **403**, 83-90.
21. A. Takagaki, M. Takahashi, S. Nishimura and K. Ebitani, *ACS Catal.*, 2011, **1**, 1562-1565.
22. J. Tuteja, S. Nishimura and K. Ebitani, *Bull. Chem. Soc. Jpn.*, 2012, **85**, 275-281.
23. L. Hora, V. Kelbichová, O. Kikhtyanin, O. Bortnovskiy and D. Kubička, *Catal. Today*, 2014, **223**, 138-147.
24. M. Shirotori, S. Nishimura and K. Ebitani, *Catal. Sci. Technol.*, 2014, **4**, 971-978.

25. D.-G. Crivoi, R.-A. Miranda, E. Finocchio, J. Llorca, G. Ramis, J. E. Sueiras, A. M. Segarra and F. Medina, *Appl. Catal. A*, 2016, **519**, 116-129.

26. J. Nowicki, J. Lach, M. Organek and E. Sabura, *Appl. Catal. A*, 2016, **524**, 17-24.

27. M. Shirotori, S. Nishimura and K. Ebitani, *Chem. Lett.*, 2016, **45**, 194-196.

28. M. Shirotori, S. Nishimura and K. Ebitani, *Catal. Sci. Technol.*, 2016, **6**, 8200-8211.

29. K. Teramura, S. Iguchi, Y. Mizuno, T. Shishido and T. Tanaka, *Angew. Chem. Int. Ed.*, 2012, **51**, 8008-8011.

30. S. Iguchi, K. Teramura, S. Hosokawa and T. Tanaka, *Catal. Today*, 2015, **251**, 140-144.

31. S. Iguchi, S. Kikkawa, K. Teramura, S. Hosokawa and T. Tanaka, *Phys. Chem. Chem. Phys.*, 2016, **18**, 13811-13819.

32. M. Adachi-Pagano, C. Forano and J.-P. Besse, *Chem. Commun.*, 2000, 91-92.

33. E. Gardner, K. M. Huntoon and T. J. Pinnavaia, *Adv. Mater.*, 2001, **13**, 1263-1266.

34. S. O'Leary, D. O'Hare and G. Seeley, *Chem. Commun.*, 2002, 1506-1507.

35. T. Hibino, *Chem. Mater.*, 2004, **16**, 5482-5488.

36. W. Chen, L. Feng and B. Qu, *Chem. Mater.*, 2004, **16**, 368-370.

37. Z. Liu, R. Ma, M. Osada, N. Iyi, Y. Ebina, K. Takada and T. Sasaki, *J. Am. Chem. Soc.*, 2006, **128**, 4872-4880.

38. H. Kang, Y. Shu, Z. Li, B. Guan, S. Peng, Y. Huang and R. Liu, *Carbohydr. Polym.*, 2014, **100**, 158-165.

39. J. L. Gunjakar, T. W. Kim, H. N. Kim, I. Y. Kim and S. J. Hwang, *J. Am. Chem. Soc.*, 2011, **133**, 14998-15007.

40. J. Zhao, X. Kong, W. Shi, M. Shao, J. Han, M. Wei, D. G. Evansa and X. Duan, *J. Mater. Chem.*, 2011, **21**, 13926-13933.

41. W. Shi, R. Liang, S. Xu, Y. Wang, C. Luo, M. Darwish and S. K. Smoukov, *J. Phys. Chem. C*, 2015, **119**, 13215-13223.

42. C. Zhang, J. Zhao, L. Zhou, Z. Li, M. Shao and M. Wei, *J. Mater. Chem. A*, 2016, **4**, 11516-11523.

43. G. Zhu, Y. Long, H. Ren, Y. Zhou, L. Zhang, Z. Shi, F. K. Shehzad and H. M. Asif, *J. Phys. Chem. C*, 2016, **120**, 22549-22557.

44. M. B. Roeffaers, B. F. Sels, I. H. Uji, F. C. De Schryver, P. A. Jacobs, D. E. De Vos and J. Hofkens, *Nature*, 2006, **439**, 572-575.

45. M. Shao, F. Ning, J. Zhao, M. Wei, D. G. Evans and X. Duan, *J. Am. Chem. Soc.*, 2012, **134**, 1071-1077.

46. M. Shao, F. Ning, Y. Zhao, J. Zhao, M. Wei, D. G. Evans and X. Duan, *Chem. Mater.*, 2012, **24**, 1192-1197.

47. C. Chen, P. Wang, T.-T. Lim, L. Liu, S. Liu and R. Xu, *J. Mater. Chem. A*, 2013, **1**, 3877-3880.

48. S. D. Jiang, Z. M. Bai, G. Tang, L. Song, A. A. Stec, T. R. Hull, Y. Hu and W. Z. Hu, *ACS Appl. Mater. Interfaces*, 2014, **6**, 14076-14086.

49. J. Wang, R. Zhu, B. Gao, B. Wu, K. Li, X. Sun, H. Liu and S. Wang, *Biomaterials*, 2014, **35**, 466-478.

50. C. Chen, R. Felton, J. C. Buffet and D. O'Hare, *Chem. Commun.*, 2015, **51**, 3462-3465.

51. T. Hara, J. Kurihara, N. Ichikuni and S. Shimazu, *Chem. Lett.*, 2010, **39**, 304-305.

52. T. Hara, J. Kurihara, N. Ichikuni and S. Shimazu, *Catal. Sci. Technol.*, 2015, **5**, 578-583.

53. J. Kobler, K. Möller and T. Bein, *ACS Nano*, 2008, **2**, 791-799.

54. P. N. Gunawidjaja, M. A. Holland, G. Mountjoy, D. M. Pickup, R. J. Newport and M. E. Smith, *Solid State Nucl. Magn. Reson.*, 2003, **23**, 88-106.

55. A. M. B. Silva, C. M. Queiroz, S. Agathopoulos, R. N. Correia, M. H. V. Fernandes and J. M. Oliveira, *J. Mol. Struct.*, 2011, **986**, 16-21.

56. M. Lewandowski, G. S. Babu, M. Vezzoli, M. D. Jones, R. E. Owen, D. Mattia, P. Plucinski, E. Mikolajska, A. Ochenduszko and D. C. Apperley, *Catal. Commun.*, 2014, **49**, 25-28.

57. E. Lippmaa, M. Magi, A. Samoson, M. Tarmak and G. Engelbardt, *J. Am. Chem. Soc.*, 1981, **103**, 4992-4996.

58. J. Sanz and J. M. Serratosa, *J. Am. Chem. Soc.*, 1984, **106**, 4790-4793.

59. P. P. Man, M. J. Peltre and D. Barthomeuf, *J. Chem. Soc., Faraday Trans.*, 1990, **86**, 1599-1602.

60. J.-B. d'Espinose de la Caillerie, M. Kermarec and O. Clause, *J. Phys. Chem.*, 1995, **99**, 17273-17281.

61. The BET specific surface area values of SiO_2(40nm)@Mg-Al(3)LDH and Mg-Al(3)LDH were 409 m^2 $g(cat)^{-1}$ and 150 m^2 $g(LDH)^{-1}$, respectively. On the basis of Si content in SiO_2(40nm)@Mg-Al(3)LDH (12.3 wt%, ICP-AES), the specific

surface area of Mg-Al(3)LDH itself prepared on SiO_2(40nm) surface tentatively calculated to be above 168 m^2 $g(LDH)^{-1}$, which was higher value than Mg-Al(3)LDH prepared without SiO_2 seeds.

Summary

In this doctoral thesis, I broadly succeeded in development of two kinds of layered double hydroxide (LDH)-based functionalized catalysts, bifunctional acid-base LDH and immobilized fine crystalline LDH, and summarized the results of these catalytic activity and structural properties.

Chapter 1 overviewed current situation of solid acid-base catalyst and its application for various chemical reactions especially focused on biomass transformations. I also introduced characteristic, function, application, advantage and disadvantage for LDH as a base catalyst. From this overview, I proposed possible strategies for development of novel functionalized LDH-based solid catalysts to improve the utility of LDH.

In Chapter 2, preliminary I studied the base catalysis of conventional Mg-Al LDH catalyst for the Knoevenagel condensation of furfural with various active methylene compounds. I found that conventional Mg-Al LDH shows higher activity for the Knoevenagel condensation than typical solid base such as MgO and CaO. In the next stage, physical mixing solid acid-base catalytic system composed from Mg-Al LDH and Amberlyst-15 was applied to the one-pot synthesis of furfural derivatives from pentoses. I found that direct synthesis of furfural derivatives from pentoses are proceeded over physical mixing acid-base catalytic system, and time-cause investigation indicated that the one-pot reaction involves three elemental reactions; (i) isomerization of xylose into xylulose over solid base Mg-Al LDH, (ii) dehydration of xylulose into furfural by solid Brønsted acid Amberlyst-15, and (iii) the Knoevenagel condensation of furfural by solid base Mg-Al LDH. Several metal supported Mg-Al LDH catalysts were prepared and evaluated these activity for one-pot synthesis of furfural and (2-furanylmethylene)malononitrile, a Knoevenagel product of furfural with malononitrile, from xylose with Amberlyst-15. Among all, Cr supported catalyst (Cr/Mg-Al LDH) was found to be the best catalyst with 36% and 44% yield in furfural synthesis and FMM synthesis, respectively.

Various characterization results suggested that Cr species are supported on the Brønsted basic Mg-Al LDH surface as Lewis acidic Cr^{3+} oxide. In addition, Cr/Mg-Al LDH showed higher activity to xylose transformation than physical mixing of Mg-Al LDH and γ-Al_2O_3 as typical solid Brønsted base and Lewis acid, respectively. Thus, I considered that joining Lewis acid site and Brønsted base site is the key factor to increase activity. I also prepared γ-Al_2O_3-based bifunctional Lewis acid-Brønsted base catalyst by adding of M^{2+} onto γ-Al_2O_3. Obtained M^{2+}-modifies Al_2O_3 catalyst where M^{2+} is Mg^{2+}, Co^{2+}, Ni^{2+} and Zn^{2+} had not only γ-Al_2O_3 crystal phase but also LDH crystal phase. I found that activity for furfural synthesis from xylose over M^{2+}-modified Al_2O_3 are affected by only Lewis acidity while only Ni^{2+}-modified Al_2O_3 showed high activity to furfural synthesis in spite of its Lewis acidity. Crystallite studies based on XRD revealed that the crystallite size of generated LDH on Ni^{2+}-modified Al_2O_3 was obviously the smallest in comparison to other M^{2+}-modified Al_2O_3, indicating Ni^{2+}-modified Al_2O_3 would possess a lot of close boundaries between Lewis acidic γ-Al_2O_3 and Brønsted basic LDH compared to other M^{2+}-modified Al_2O_3 to lead high activity. Based on these results, I suggested that the close boundaries between Cr^{3+} oxide and Mg-Al LDH, and γ-Al_2O_3 and small crystalline Ni-Al LDH facilitated the xylose isomerization as Lewis acid-Brønsted base bifunctional sites.

On the other hand, the discoveries in Chapter 2 give me a new research issue that is “how can I design the optimum bi-functional Lewis acid-Brønsted base site on surface of one catalyst?” Therefore in Chapter 3, I described the detailed local structure of the bifunctional acid-base site and the optimized surface structure on the Cr/Mg-Al LDH. The catalytic activity of Cr/Mg-Al LDH for one-pot synthesis of furfural from xylose with solid acid was strongly affected by Cr loading amount. Among 0-15 wt%Cr/Mg-Al LDH, 5 wt%Cr/Mg-Al LDH showed the highest activity with 36% of furfural yield (373 K, 3 h). XRD, XPS, XAS, ESR, DTA and N_2 adsorption measurement revealed that the local structure of Cr species were varied with Cr loading amount; (i) below 1 wt%, a part of a Lewis acidic Cr^{3+} oxide monomer is trapped by peripheral defect sites of Mg-Al hydroxide layer, and others are immobilized onto LDH surface, (ii) Lewis acidic Cr^{3+} oxide dimer or trimer is generated on the LDH surface with covering LDH surface up to 5 wt%, (iii) above 5wt%, excess Cr^{3+} species form Mg-Cr and/or Mg-Al-Cr LDH-like composite. Lewis acid activity was also investigated using MPV reduction, the results suggested that Cr^{3+} oxide monomer and cluster retained its Lewis acidity for <5wt%, whereas a part of Cr^{3+} species which are forming Mg-Cr and/or Mg-Al-Cr LDH-like composite lost its Lewis acidity. I concluded that the 5 wt%Cr/Mg-Al LDH surface which is covered by monolayer of Lewis acidic Cr^{3+} oxide clusters possesses the most effective interaction between Lewis acidic Cr^{3+} oxide and Brønsted basic Mg-Al LDH surface to generate abundant bifunctional sites, leading to the best catalytic activity. The combined use of 5 wt%Cr/Mg-Al LDH and Amberlyst-15 achieved 59% yield of furfural at 18 h of reaction time. This yield was the highest value among all those reported for previous studies conducted at 373 K.

Description of Chapter 4 is the development of various fine-crystallized LDH catalysts and base catalysis of prepared LDHs for the Knoevenagel condensation. Fine-crystallized M^{2+}-M^{3+} LDHs (M^{2+}: Mg^{2+} or Ni^{2+}, M^{3+}:Al^{3+} or Ga^{3+}) were prepared by co-precipitation method with coexistence of SiO_2 nano-sphere whose particle size is *ca.* 40 nm. XRD exhibited that the crystallite sizes of obtained SiO_2@LDHs were smaller than LDHs prepared by conventional co-precipitation method regardless of compositions and M^{2+}/M^{3+} atomic ratios. All SiO_2@LDHs showed higher activity for the Knoevenagel condensation than conventional LDHs. The detailed investigation on generation mechanism of fine-crystallized LDH and interaction between SiO_2 and LDH was conducted using SiO_2@Mg-Al(3)LDH. The results of TEM-EDS and ^{29}Si CP-MAS NMR revealed that (i) a part of Si-O-Si bond cleaves in basic mother solution to generate unsaturated Si-O site at SiO_2 surface, (ii) titrated Mg^{2+} and Al^{3+} ions are trapped by unsaturated Si-O site with forming Si-O-Mg and Si-O-Al covalent bonds to result dispersion of Mg^{2+} and Al^{3+} to SiO_2 surface and (iii) LDH nanosheets grow up from each dispersed Mg^{2+} and Al^{3+} on SiO_2 surface to lead generation of fine-crystallized LDH with avoiding the *ab*-face stacking. Interestingly, although the coexistence of SiO_2 sphere with particle size of 250 nm also synthesized the immobilized SiO_2@LDH, it was not effective for both generation of fine-crystallized LDH and increase of base catalysis because of small amount of surface Si-O site on SiO_2 sphere. This result strongly suggested that not only the immobilization of LDH on

SiO_2 surface but also the number of surface Si-O site as a trapping point of metal cations are important. I concluded that the *in-situ* growth of LDH crystal on SiO_2 sphere with particle size of 40 nm is effective for preparation of fine-crystallized SiO_2@LDH which possesses higher base catalysis than conventional LDH.

In conclusion, I discovered the preparation methods of the LDH-based highly functionalized solid catalysts such as Lewis acid-Brønsted base bifunctional catalysts and fine-crystallized LDH catalysts. I demonstrated that the multifunctional solid catalytic system composed of bifunctional Lewis acid-Brønsted base LDH-based catalysts (Cr/Mg-Al LDH or Ni^{2+}-modified Al_2O_3) and Brønsted acid sulfonic resin (Amberlyst-15) effectively catalyzed one-pot synthesis of pentoses to furfurals. Studies on genesis of bifunctional acid-base site on Cr/Mg-Al LDH revealed that bifunctional acid-base sites are generated at cross boundaries between Lewis acidic Cr^{3+} oxide and Brønsted basic LDH surface. In addition, I found that bifunctional catalysis is maximized when Cr^{3+} species form Lewis acidic Cr^{3+} oxide cluster with covering LDH surface. I also suggested that coexistence of nano-SiO_2 sphere in preparation stage enable the generation of fine-crystallized LDH with highly base catalysis.

As scopes, I describe the further possible development of novel LDH-based catalysts based on this doctoral thesis as follows;

Bi-functional acid-base catalyst. I revealed that the immobilization of Lewis acidic Cr^{3+} oxide onto Brønsted basic Mg-Al LDH generates the bi-functional acid-base sites at the cross boundaries. This discovery can be applied to design the various bi-functional LDH-based catalysts by altering the immobilized active species or type and morphology of LDH carrier. Although I successfully prepared the bi-functional Lewis acid–Brønsted base Cr/Mg-Al LDH catalysts which show the high activity for the xylose isomerization, it does not mean that the Cr/Mg-Al LDH is the best catalyst for all chemical reactions catalyzed by bi-functional acid-base site. The chemical reactions that proceeds on the solid surface is very complicated, and is strongly affected not only by the type of active site, such as base, acid and bi-functional acid-base, but also by the strength, density, dispersibility and local structure of active sites including the distance between acid and base sites. We must continue to explore the catalyst surface suitable for each chemical reaction. This doctoral thesis gives knowledge about the local structure of the bi-functional site and optimum surface structure on the metal oxide supported LDH catalysts to aid the development the family of LDH-based bi-functional catalysts.

Immobilized fine-crystallized LDH catalyst. I established that the coexistence with small SiO_2 sphere in a co-precipitation method generate the immobilized fine-crystallized LDH catalyst with highly active base catalysis. I also demonstrated that this technique could be applied to various LDHs with different metal compositions. Therefore, this discovery has a potential to promote most conventional chemical reactions using LDH as a base catalyst. Moreover, since the role of SiO_2 sphere is only immobilization of LDH crystal, removal of excess SiO_2 by washing with basic solution can be expected to further enhance the catalytic activity per weight. On the other hand, SiO_2 is well known as the support that can be immobilized organic functional species to generate various active sites such as Brønsted acid, Lewis acid and Lewis base sites. Therefore, the modification of SiO_2 sphere may allow the development of novel multifunctional SiO_2@LDH-based catalysts for multistep reactions.

These works described in this doctoral thesis give catalytic science new strategies to design the multi-functionalized supported catalysts and to increase the original function of the layered catalysts for the development of noble modern organic synthesis including biomass-derived saccharides transformations.

List of Publications

Chapter 2.

1. **Mahiro Shirotori**, Shun Nishimura and Kohki Ebitani
   One-pot synthesis of furfural derivatives from pentoses using solid acid and base catalyst
   Catalysis Science & Technology, 2014, **4**, 971-978.

2. **Mahiro Shirotori**, Shun Nishimura and Kohki Ebitani
   One-pot Synthesis of Furfural from Xylose using Al_2O_3—Ni-Al Layered Double Hydroxide Acid-Base Bi-functional Catalyst and Sulfonated Resin
   Chemistry Letters, 2016, **45**, 194-196.

Chapter 3.

3. **Mahiro Shirotori**, Shun Nishimura and Kohki Ebitani
   Genesis of bi-functional acid-base site on a Cr-supported layered double hydroxide catalyst surface for one-pot synthesis of furfurals from xylose with a solid acid catalyst
   Catalysis Science & Technology, 2016, **6**, 8200-8211. [Selected as the inside front cover]

Chapter 4.

4. **Mahiro Shirotori**, Shun Nishimura and Kohki Ebitani
   Fine-crystallized LDHs prepared with SiO_2 sphere as highly active solid base catalyst
   Journal of Materials Chemistry A, in press.

5. **Mahiro Shirotori**, Shun Nishimura and Kohki Ebitani
   Effect of SiO_2 amount on Heterogeneous Base Catalysis of SiO_2@Mg-Al LDH
   To be submitted.

List of international conferences

1 **Mahiro Shirotori**, Shun Nishimura and Kohki Ebitani
"One-pot Synthesis of Furfural Derivatives from Pentoses Using Solid Acid and Base Catalyst"
7th International Symposium on Acid-Base Catalysis (ABC-7), Tokyo, Japan, 2013.5.13. [Poster]

2 **Mahiro Shirotori**, Shun Nishimura and Kohki Ebitani
"One-pot Synthesis of (2-Furanylmethylene)malononitrile from Pentoses"
14th Japan-Korea Symposium on Catalysis, Nagoya, Japan, 2013.7.1. [Poster]

3 **Mahiro Shirotori**, Shun Nishimura and Kohki Ebitani
"Bifunctional Acid-Base Cr-containing Layered Double Hydroxides Promoted One-pot Transformation of Xylose"
15th Korea-Japan Symposium on Catalysis, Tokyo, Japan, 2015.5.26. [Oral-Young]

4 Kohki Ebitani, Jaya Tuteja, Hemant Choudhary, Pham Anh Son, **Mahiro Shirotori** and Shun Nishimura
"Synthesis of Value-added Chemicals from Biomass-derived Materials using Heterogeneous Catalytic Systems"
IISc-JAIST Joint Workshop on Functional Inorganic and Organic Materials, Ishikawa, Japan, 2016.2.7. [Oral](invited)

5 **Mahiro Shirotori**, Shun Nishimura and Kohki Ebitani
"Correlation between Catalytic Activity and Surface Structure of Cr supported Layered Double Hydroxide for One-pot Transformation of Xylose into Furfurals"
IISc-JAIST Joint Workshop on Functional Inorganic and Organic Materials, Ishikawa, Japan, 2016.2.7. [Poster]

6 **Mahiro Shirotori**, Shun Nishimura and Kohki Ebitani
"Effect of Cr Loading Amount in the Cr/Mg-Al Layered Double Hydroxide Mediated One-pot Transformation of Xylose to Furfural"
9th International Conference on Environmental Catalysis (ICEC), Newcastle, Australia, 2016.7.13. [Oral]